12-2013

Unified Model of Charge Transport in Insulating Polymeric Materials

Alec Sim
Utah State University

UNIFIED MODEL OF CHARGE TRANSPORT

IN INSULATING POLYMERIC MATERIALS

by

Alec Sim

A dissertation submitted in partial fulfillment
of the requirements for the degree

of

DOCTOR OF PHILOSOPHY

in

Physics

Approved:

_____	_____
Dr. John Robert Dennison Major Professor	Dr. D. Mark Riffe Committee Member
_____	_____
Dr. Jan J. Sojka Committee Member	Dr. Timothy E. Doyle Committee Member
_____	_____
Dr. Charles Swenson Committee Member	Dr. Mark R. McLellan Vice President for Research and Dean of the School of Graduate Studies

UTAH STATE UNIVERSITY
Logan, Utah

2013

ABSTRACT

Unified Model of Charge Transport in Insulating Polymeric Materials

by

Alec Sim, Doctor of Philosophy

Utah State University, 2013

Major Professor: Dr. JR Dennison
Department: Physics

Presented here is a detailed study of electron transport in highly disordered insulating materials (HDIM). Since HDIMs do not lend themselves to a lattice construct, the question arises: How can we describe their electron transport behavior in a consistent theoretical framework? In this work, a large group of experiments, theories, and physical models are coalesced into a single formalism to better address this difficult question. We find that a simple set of macroscopic transport equations—cast in a new formalism—provides an excellent framework in which to consider a wide array of experimentally observed behaviors. It is shown that carrier transport in HDIMs is governed by the transport equations that relate the density of localized states (DOS) within the band gap and the occupation of these states through thermal and quantum interactions. The discussion is facilitated by considering a small set of simple DOS models. This microscopic picture gives rise to a clear understanding of the macroscopic carrier transport in HDIMs. We conclude with a discussion of the application of this theoretical formalism to four specific types of experimental measurements employed by the Utah State University space environments effects Materials Physics Group.

(292 pages)

PUBLIC ABSTRACT

Unified Model of Charge Transport in Insulating Polymeric Materials

Alec Sim, Doctor of Philosophy

Utah State University, 2013

Charge transport, charging, and subsequent electrostatic discharge due to interactions with the space environment are primary concerns of spacecraft designers. Developing a physical understanding of the interactions of charge with the multitude of materials that spacecraft are composed of is a critical step in understanding and mitigating both short-term and long-term spacecraft degradation. In particular, the study of charge transport in highly insulating materials is critical as they store charge longer, with higher capacity, and with greater destructive capability than other materials.

The Utah State University Materials Physics Group, with the funding of the NASA James Webb Space Telescope project and Rocky Mountain Space Consortium, have developed a complete and consistent theoretical model that predicts short-term and long-term storage capabilities based on physical material parameters. This model is applicable across a wide range of experimental systems designed to test specific behaviors that characterize charging phenomena.

Modeling and understanding the complex relationships between the spacecraft and its surroundings are fundamentally based on detailed knowledge of how individual materials store and transport charge. The ability to better understand these effects will help make exploring the edges of the universe more stable, reliable, and economic.

ACKNOWLEDGMENTS

Dr. J.R. Dennison is a talented, dedicated, and very patient advisor, whose effort and love of his work, students, and community is, without question, a model for us all. To say that I have learned a lot from him is not enough, I have not the words. To say that he is patient when students travel the difficult road that is graduate school is not enough. In life there are those journeys that can only be had with a guide; thank you, J.R.

Thanks to the faculty and staff of USU without whose many hours of teaching, listening, and patience, this work would not have been completed. In particular, I would like to thank Dr. Riffe for many interesting arguments and grammatical discussions, Sharon Pappas, Judy Larsen, and Karalee Ransom whose shoulders bore many a difficulty and always bought sunshine no matter the time of year. Finally, I would like to thank the committee for drudging though the first drafts of this work.

To my parents, Mike Sim and Kathy Gilbert, thank you for all the help and positive thoughts over the many long years it took for me to become the person I am. To my grandparents, Bob and Mary Long—both of whom passed during my years of school—I cannot offer any words to you, for I finished too late. I pray you can see the outcome of your love from Heaven; I love you and miss you.

To my friends, Lane Vance, Justin Dekany, Josh Hodges, and Eric Barnett, no words need be said but thank you. To the USU MPG, you know who you are and you are fantastic at what you do. Thank you for copious amounts of data upon which to test the ideas laid down in this dissertation.

To my son, Gavin Maxwell Sim, as of the completion of this document you are nine years old. I hope you will read this someday and understand the choices I made, the difficulties endured, and know I love you more than anything in the world. Thank you because you are my son.

The effort and dedication required to create a document such as this cannot be put into words. I do not mean that it is an especially good or bad book. It is like many other books, the outpouring of knowledge of one flavor or another in an attempt to contribute to this world. If this has been accomplished, and this work is found useful, then it is grand indeed.

Alec Sim

CONTENTS

Page

LIST OF TABLES

LIST OF FIGURES

NOMENCLATURE

a = average nearest neighbor trap separation or TAH hopping distance [L]

a_B = Bohr radius [L]

A = area [L^2]

A_{beam} = cross-sectional area of electron beam [L^2]

B = general constant

b_r = capture cross section for holes, recombination centers [L^2]

b_t = capture cross section for trapping centers [L^2]

c = speed of light [LT^{-1}]

C = general constant

C_{Euler} = Euler's constant [unitless]

C_{tot}^{i} = ratio of total trapped carriers to those trapped at a particular level i [unitless]

d = sample thickness or depth [L]

D = absorbed radiation dose [EM^{-1}]

$\dot{D}$ = absorbed radiation dose rate [$EM^{-1}T^{-1}$]

D_E = Einstein diffusion coefficient [ETM^{-1}]

d_{eff} =effective sample depth; penetration depth for contact electrode injection, SCLC convention [L]

D_n = Fick's diffusion coefficient for electrons [$ET^{-1}M^{-1}$]

D_o = unspecified diffusion coefficient [$ET^{-1}M^{-1}$]

ε = energy [E]

ε_b = incident beam energy [E]

ε_{CB} = energy of the conduction band edge [E]

ε_{CF} = energy difference between top of conduction band and the steady-state Fermi level [E]

ε_d^i = demarcation energy; may be a function of time, temperature or both, $\varepsilon_d(t,T)$. i represents the DOS type: c for constant, e for exponential, G for Gaussian, l for linear, p for power, and t for single trap level delta function [E]

ε_F = Fermi energy [E]

ε_f = Fermi level or chemical potential [E]

ε_f^0 = equilibrium Fermi level [E]

ε_{gap} = energy width of band gap [E]

ε_{gnd} = ground state energy [E]

ε_{high} = energy high in the energy gap of a DOS [E]

ε_{HOMO} = energy of the highest occupied molecular orbital [E]

ε_i = energy level of a single localized state [E]

ε_d^i = energy of the demarcation line; *d* stands for demarcation; *i* represents the DOS type: *e* for exponential, G for Gaussian, etc. [E]

ε_F^i = energy of the Fermi level; *i* represents the DOS type: *e* for exponential, G for Gaussian, etc. [E]

ε_t^i = transport band energy; *t* stands for transport; *i* represents the DOS type: *e* for exponential, G for Gaussian, etc. [E]

ε_{ij} = energy between sites *i* and *j* [E]

ε_{ion} = energy for activation of ionic conduction [E]

ε_{low} = energy low in the energy gap of a DOS [E]

ε_{LUMO} = energy of the lowest unoccupied molecular orbital [E]

ε_{mean} = mean energy at the center of the energy distribution for a DOS [E]

ε_{ME} = mobility edge energy [E]

ε_p = energy distribution of a power DOS, gives scale to the energetic distribution of the DOS [E]

ε_t = energy level of the transport band, where *t* stands for transport [E]

ε_{trap} = DOS energy level of a single set of trapped states, delta function type [E]

ε_{VB} = energy of the top of the valence band, usually set to zero [E]

ε_o = energy difference between bottom of conduction band and the Fermi level [E]

$\langle\varepsilon_\infty\rangle$ = energy of the center of the charge distribution in a Gaussian DOS; also the QFL [E]

ε_0^i = energy scale for a given DOS; *i* represents the DOS type: *c* for constant, *e* for exponential, *G* for Gaussian, *l* for linear, *p* for power, and *t* for single trap level delta function [E]

$erf(x)$ = the error function [unitless]

$F(z)$ = electric field as a function of distance, may also be a function of energy and time [$EQ^{-1}L^{-1}$]

$F(t)$ = time-dependent evolution of carriers in the DOS [unitless]

$f_i(\varepsilon, t)$ = mean occupation number; i is given by subscripts FD for Fermi-Dirac and MB for Maxwell-Boltzmann distributions [unitless]

$\mathbb{F}$ = force, where a subscript denotes the type of force if necessary [MLT^{-2}]

f_{AB} = probability of transition occurrence from state A to B [unitless]

F_{eff} = effective electric field [unitless]

F_{ESD} = electrostatic breakdown field strength [$EQ^{-1}L^{-1}$]

f_{FD} = Fermi-Dirac distribution function, usually a function of energy [unitless]

F_{PF} = electric field at which PF behavior becomes important [$EQ^{-1}L^{-1}$]

f_{rad} = flux density of incident radiation [NL^{-3}]

$F_s(t)$ = time-dependent electric field at the surface of the insulator [$EQ^{-1}L^{-1}$]

$F_t(t)$ = time-dependent electric field produced by the trapped charge distribution [$EQ^{-1}L^{-1}$]

F_{TAH} = thermally activated hopping reduced E-field scaling factor [$EQ^{-1}L^{-1}$]

F_{VRH} = variable range hopping reduced E-field scaling factor [$EQ^{-1}L^{-1}$]

F_0 = applied electric field [$EQ^{-1}L^{-1}$]

G = generation rate of carriers [$NL^{-3}T^{-1}$]

g_e = degeneracy factor arising from a degenerate set of energy levels in a trapping center [unitless]

G_{ex} = electron generation density; the *ex* refers to an external source [$NL^{-3}T^{-1}$]

h = Planck constant [ETL^{-1}]

$\mathcal{H}$ = Hamiltonian [E]

i = index or subscript indicator [unitless]

I = current [QT^{-1}]

J = current density [$QT^{-1}L^{-2}$]

j = index or subscript indicator [unitless]

J_b = current density of the incident electron beam [$QT^{-1}L^{-2}$]

$J_c(t)$ = conduction current density as a function of time $[QT^{-1}L^{-2}]$

$J_d(t)$ = displacement current density as a function of time $[QT^{-1}L^{-2}]$

J_D(t) = diffusion current density as a function of time $[QT^{-1}L^{-2}]$

$J_{disp}(t)$ = dispersion current density as a function of time $[QT^{-1}L^{-2}]$

$J_{inj}(t)$ = injected current density as a function of time $[QT^{-1}L^{-2}]$

$J_{Leak}(t)$ = leakage current density as a function of time $[QT^{-1}L^{-2}]$

$J_{meas}(t)$ = current density as a function of time measured at the rear electrode $[QT^{-1}L^{-2}]$

$J_p(t)$ = polarization current density as a function of time $[QT^{-1}L^{-2}]$

J_{p0} = maximum (initial) polarization current density as a function of time $[QT^{-1}L^{-2}]$

$J_p^{\downarrow}(t)$ = decrease in polarization current density as a function of time $[QT^{-1}L^{-2}]$

$J_p^{\uparrow}(t)$ = increase in polarization current density as a function of time $[QT^{-1}L^{-2}]$

$J_s(t)$ = surface injection current density at the surface that enters the sample as a function of time $[QT^{-1}L^{-2}]$

J_{sat} = equilibrium saturation current density that exits the sample at the rear electrode $[QT^{-1}L^{-2}]$

J_{sd} = steady state current density as measured at the rear electrode, not to be confused with surface injection current density or time-dependent current density $[QT^{-1}L^{-2}]$

J_{tot}(t) = total current density as a function of time $[QT^{-1}L^{-2}]$

J_0 = initial current density $[QT^{-1}L^{-2}]$

k = wave vector $[L^{-1}]$

K(z_p) = number of electrons deposited per unit time per unit volume, where z_p is the penetration depth $[NE^{-1}L^{-3}]$

k_b = Boltzmann constant $[EK^{-1}]$

$\hat{m}$ = coordination number [unitless]

m_e* = electron effective mass $[M]$

m_h* = hole effective mass $[M]$

$N(\varepsilon)$ = density of localized states per unit energy per unit volume $[NE^{-1}L^{-3}]$

N_A = number of participating particles at site A [unitless]

N_B = number of participating particles at site B [unitless]

n_e = density of free carriers per unit volume $[NL^{-3}]$

$n_e(\varepsilon, t)$ = density of free carriers per unit energy per unit volume $[NL^{-3}]$

N_e = total density of electron conduction states within k_bT of the CB per unit volume $[NL^{-3}]$

$\tilde{n}_e(s)$ = Laplace transform of the change in the density of electrons $[NL^{-3}T^{-1}]$

N_{inj} = total density of injected carriers $[NL^{-3}]$

$n_h(t)$ = density of immobile holes per unit volume $[NL^{-3}]$

$n_{RIC}(\varepsilon, t)$ = density of thermally or RIC generated carriers per unit energy per unit volume $[NE^{-1}L^{-3}]$

n_t = density of trapped carriers per unit volume, not the total $[NL^{-3}]$

$n_t(\varepsilon, t)$ = density of trapped carriers (occupied trap states) per unit energy per unit volume $[NE^{-1}L^{-3}]$

N_t = total density of (available) localized states per unit volume; (not a trapped carrier), $N_t = \int N(\varepsilon)d\varepsilon$ $[NL^{-3}]$

$n_{tot}(z,t)$ = total density of carriers per unit volume as a function of spatial position and time $[NL^{-3}]$

N_v = total density of valence states per unit volume $[NL^{-3}]$p = a constant, usually a power [unitless]

P = polarization density $[QL^{-4}EM^{-1}T^2]$

P_{ion} = probability for ionic transition from one vacancy to another [unitless]

q_i = charge per carrier, where *i* is the type of carrier: e = electron, h = hole, ex = exciton, etc. $[Q]$

Q_{inj} = injected charge per unit area $[QL^{-2}]$

$Q_{accumulated}$ = accumulated charge $[Q]$

r = radius to some point P in the sample or in space $[L]$

R = range of a carrier; this can apply to the range of an incident particle penetrating into a material or the range of an electron as it hops from one localized state to the next, typically a mean value $[L]$

R_c = electron capture radius $[L]$

R_{ij} = location of the j^{th} atom with respect to the i^{th} atom; also the range between localized states $[L]$

s = Laplace integration variable $[T^{-1}]$

$S(r,t)$ = volume charge rate density creation term; has dimensions of [$L^{-3}T^{-1}$]

s_c = capture cross section of conduction electrons by fixed holes [L^2]

t = time [T]

T = temperature [K]

T_A = TAH reduced-temperature scaling factor [K]

$\acute{T}_{bend}$ = difficulty with which electric field-dependent changes can be made in the energetic structure of the DOS; modification of the effective temperature [K]

T_c = critical transition temperature between hopping and TAH transport [K]

T_{eff} = effective temperature; it may depend on many quantities, e.g., field, time, sample temperature [K]

T_F = effective temperature with field dependence [K]

T_{low} = temperature at which the conductivity losses its temperature dependence hopping becomes important [K]

$t_{transit}$ = time for drifting carriers to travel from one electrode to another [T]

t_τ = transit time, time for carriers to cross the sample thickness d [T]

T_V = variable range hopping reduced temperature scaling factor [K]

T_0 = characteristic dispersion of states in a given DOS; always coupled with k_b to give energy [K]

T_0^i = characteristic dispersion of states in a given DOS; i represent DOS type: e for exponential, l for linear, G for Gaussian [K]

V = volume [L^{-3}]

V = electric potential [EQ^{-1}]

v_A = velocity of carriers at some site A [LT^{-1}]

V_{app} = externally applied voltage [EQ^{-1}]

V_c = critical potential below which no transport occurs [EQ^{-1}]

v_e = velocity of electron [LT^{-1}]

v_i = velocity of object I [LT^{-1}]

$\langle V_{jk} \rangle$ = average potential between two states j and k [EQ^{-1}]

v_{rms} = root mean squared velocity $[LT^{-1}]$

$V_s(z,t)$ = surface potential $[EQ^{-1}]$ v_T = thermal velocity of carrier $[LT^{-1}]$

V_{TFL} = voltage at which trap filled limit occurs; an onset voltage $[EQ^{-1}]$

V_Ω = transition voltage from Ohmic to SCLC behavior $[EQ^{-1}]$

V_0 = initial potential $[EQ^{-1}]$

W = width of energetic distribution of potential wells; band width, in a density of states $[E]$

W_j = energy of the j^{th} hop from some other localized state $[E]$

y(x) = a function of x $[L]$

z = spatial coordinate with unit vector $\hat{z}$, generally used to represent a position into a sample $[L]$

Z_{center} = atomic number $[N]$

z_p = penetration depth of carriers into a sample also called the range; see range, R $[L]$

Z_V = complex function of β_V used in VRH theory [unitless]

α = dispersion parameter, T/T_0 [unitless]

α_{AB} = interaction coefficient between two states A and B $[L^3T\ N^{-1}]$

α_i = polarizability for a given process denoted by *i*: c for space charge, e for electronic, h for hopping, *i* for atomic, o orientation, tot for total $[Q^2M^{-1}T^2]$

α_{er} = interaction coefficient between CB and holes $[L^3T\ N^{-1}]$

α_{et} = interaction coefficient between CB and trapped states $[L^3T\ N^{-1}]$

α_{te} = interaction coefficient between trapped states and CB $[L^3T\ N^{-1}]$

α_{tr} = interaction coefficient between trapped states and holes $[L^3T\ N^{-1}]$

α_{tt} = interaction coefficient between trapped states and trap states at the transport energy $[L^3T\ N^{-1}]$

β_A = ratio of field energy to thermal energy for thermally activated hopping conductivity [unitless]

β_{PF} = Poole-Frenkle factor [unitless]

β_V = ratio of field energy to thermal energy for variable range hopping conductivity [unitless]

Γ = gamma function

Δ = $(1+\alpha)^{-1}$ parameter used in TOF and RIC to describe power law behavior [unitless]

δ = some perturbing energy, a small shift in energy $[E]$

$\delta\varepsilon_{PF}$ = change in energy due to Poole-Frenkle effect $[E]$

$\acute{\Delta}\delta\varepsilon_{PF}$ = Poole-Frenkle energy change $[E]$

δ_{yield} = secondary electron yield coefficient $[N]$

$\Delta\varepsilon_{trap}$ = high field correction to energy depth of a set of trap states $[E]$

ΔG = Gibb's free energy $[E]$

ΔH = enthalpy $[EN^{-1}]$

$\Delta\mathcal{H}$ = energy separation of states $[E]$

$\Delta\mathcal{H}_{hop}$ = energy separation between the trapped charge distribution and the transport band for hopping conductivity $[E]$

Δn_e = number of photo-excited carriers in CB $[N]$

Δx_{ij} = hopping distance between two sites, *i* and *j* $[L]$

ϵ_r = relative permittivity of material $[unitless]$

ϵ_0 = permittivity of free space $[Q^2L^{-3}M^{-1}T^2]$

η = real space decay constant of the localized wave function for a given state (also called localization length) $[L]$

η_{yield} = backscattered yield for secondary electron emission [unitless]

$\theta(\varepsilon)$ = SCLC correction factor caused by the presence of a DOS [unitless]

$\theta(z - z_0)$ = Heaviside step function at the spatial point z_0 [unitless]

λ_m = mean-free path of carriers in a material $[L]$

μ_i = carrier mobility, where *i* is the type of carrier: e = electron, etc. $[L^2T^{-1}E^{-1}Q]$

μ_e = trap-free mobility of an electron in the conduction band $[L^2T^{-1}E^{-1}Q]$

μ_{low} = estimate of diffusion limited mobility at or below the recombination limited temperature $[L^2T^{-1}E^{-1}Q]$

μ_{trap} = trap-reduced mobility $[L^2T^{-1}E^{-1}Q]$

$\langle\mu(t)\rangle$ = time-averaged mobility $[L^2T^{-1}E^{-1}Q]$

$v_{et}(\varepsilon)$ = probability of carrier trapping per unit time as a function of energy $[T^{-1}]$

$v_{er}(\varepsilon)$ = probability of electron hole recombination per unit time as a function of energy $[T^{-1}]$

v_{ij} = hopping rate between sites *i* and *j* $[T^{-1}]$

ν_{ion} = frequency of escape attempts for an ion in ionic conduction $[T^{-1}]$

$v_{te}(\varepsilon)$ = probability that an electron will escape from trap per unit time as a function of energy; also called the frequency factor in many applications $[T^{-1}]$

v_{TAH} = hopping frequency for thermally activated hopping conductivity $[T^{-1}]$

$v_{th}(\varepsilon)$ = probability of a trapped election to recombine with a hole per unit time $[T^{-1}]$

v_{VRH} = hopping attack frequency for variable range hopping conductivity $[T^{-1}]$

v_0 = frequency of carrier escapes $[T^{-1}]$

ρ = resistivity of a material $[ETQ^{-2}L]$

ρ_b = bound charge density $[QL^{-3}]$

ρ_f = free charge density $[QL^{-3}]$

ρ_m = mass density $[ML^{-3}]$

ρ_{tot} = total charge density $[QL^{-3}]$

$\rho_{tot}(z,t)$ = total charge density at position z and time t $[QL^{-3}]$

σ = conductivity $[Q^2L^{-3}T^{-1}E^{-1}]$

$\sum$ = unitless spatial disorder parameter [unitless]

$\sigma_{initial}$ = initial total electron yield before charge accumulation [unitless]

σ_d = drift conductivity $[Q^2L^{-3}T^{-1}E^{-1}]$

σ_{diff} = diffusive conductivity $[Q^2L^{-3}T^{-1}E^{-1}]$

σ_{total} = total conductivity $[Q^2L^{-3}T^{-1}E^{-1}]$

σ_{inital} = initial uncharged yield $[unitless]$

σ_P = polarization conductivity $[Q^2L^{-3}T^{-1}E^{-1}]$

σ_{TAH} = thermally activated hopping (TAH) conductivity $[Q^2L^{-3}T^{-1}E^{-1}]$

σ_{TAHo} = thermally activated hopping reduced conductivity scaling factor $[Q^2L^{-3}T^{-1}E^{-1}]$

σ_{Tot} = total conductivity; i.e., the sum of conductivities $[Q^2L^{-3}T^{-1}E^{-1}]$

σ_{VRH} = variable range hopping (VRH) conductivity $[Q^2L^{-3}T^{-1}E^{-1}]$

σ_{VRHo} = variable range hopping reduced conductivity scaling factor $[Q^2L^{-3}T^{-1}E^{-1}]$

σ_{VRH}^{i} = variable rage hopping conductivity for an *i* type DOS: *e* for exponential, G for Gaussian, etc. $[Q^2L^{-3}T^{-1}E^{-1}]$

σ_{VRH}^{C-low} = low field variable range hopping conductivity for a constant DOS $[Q^2L^{-3}T^{-1}E^{-1}]$

σ_{VRH}^{C-High} = high field variable range hopping conductivity for a constant DOS $[Q^2L^{-3}T^{-1}E^{-1}]$

τ = characteristic onset time for current decay to occur $[T]$

τ_{CB} = lifetime of a carrier in the conduction band without trapping $[T]$

τ_d = relaxation time of SCLC carriers between electrodes $[T]$

τ_{et} = electron lifetime in CB with trapping $[T]$

$\tau^{i}{}_{seg}$ = segregation time for a DOS of type *i*: *e* for exponential, G for Gaussian, etc. $[T]$

$\tau^{C,F}{}_{seg}$ = segregation time for a constant DOS with electric field dependence $[T]$

τ_T^i = thermalization time, τ_T, for a DOS of type *i*: *e* for exponential, G for Gaussian, etc. $[T]$

τ_{trap} = lifetime of a carrier in a trapped state $[T]$

Υ = unitless function defined by a transcendental equation [unitless]

ϕ_{eff} = effective barrier height $[E]$

φ = material work function or energy barrier at metal-insulator interface $[E]$

χ = dielectric susceptibility [unitless]

ACRONYMS AND ABBREVIATIONS

AC = Alternating Current

BG = Band Gap

CB = Conduction Band

CVC = Constant Voltage Conductivity

DC = Direct Current

DE = Demarcation Energy

DFL = Dark Fermi Limit

DOS = Density of States

ESD = Electrostatic Discharge

FD = Fermi Dirac

FL = Fermi Level

HDIM = Highly Disordered Insulating Material

HDPE = High Density Polyethylene

HOMO = Highest Occupied Molecular Orbital

LDPE = Low Density Polyethylene

LUMO = Lowest Unoccupied Molecular Orbital

MAR = Miller and Abrahams hopping Rate

MPG = Material Physics Group

MT = Multiple Trapping

PEA = Pulsed Electro-Acoustic

PF = Poole-Frenkle

PI = Polyimide (Kapton^{TM})

QFL = Quasi-Fermi Level

RIC = Radiation Induced Conductivity

SCC = Spacecraft Charging

SCLC = Space Charge Limited Current

SEE = Secondary Electron Emission

SVP = Surface Voltage Probe

TAH = Thermally Activated Hopping

TB = Transport Band

TE = Transport Energy

TOF = Time of Flight

TSC = Thermally Stimulated Current

USU = Utah State University

VB = Valence Band

VRH = Variable Range Hopping

XLPE = Crosslinked Polyethylene

CHAPTER 1

INTRODUCTION

This dissertation represents a comprehensive theoretical study of the basic physical principles of electron transport in Highly Disordered Insulating Materials (HDIM). The study of electron transport in HDIM requires a fundamentally different approach from materials that have long-range order and use conventional band theory, one which focuses on electron transport via localized trap states and the resultant understanding of the spatial and energetic distributions of trapped states, their occupancy, and transitions. The primary focus of the physics addressed in this dissertation is the electronic structure of highly disordered insulating materials that lack any substantial long-range order, and their electrical response under charge injection. Ashcroft's and Merman's classic text on solid state physics mentions the concept of disordered material many times, but refers to amorphous materials only four times, and does not address the issues associated with electron transport in HDIM. Largely this is so because Bloch's theorem and the concomitant theoretical simplification from periodic potentials in the Schrodinger equation are insufficient to describe disordered transport phenomena, except as a perturbation on the theory of ordered materials. There are many types of disordered materials, all of which fall into three categories defined by the material's ability to conduct charge: conducting, semiconducting, and insulators. Testing by Utah State University's (USU) Material Physics Group (MPG) is driven by the problems associated with spacecraft charging on insulating material surfaces; thus, problems associated with charge transport in such materials is of key interest. It is the goal of this dissertation to present a first order, single carrier, theoretical framework that brings the many experimental systems used by the USU MPG together in a single nomenclature with an emphasis on HDIMs. The HDIM is an extreme example of disorder, and as such, requires a different approach to charge transport theory that emphasizes charge carrier transport via localized states with spatial and energetic distributions of trap states, their occupation, and transitions between the localized states and transport states. In order to present a complete discussion of the true nature of the problems faced, a discussion of the fundamental macroscopic quantities involved in charge conduction must be introduced, connected to the microscopic nature, and then applied to many different experimental outcomes.

The conductivity of a material is the key transport parameter in determining how deposited charge will redistribute throughout the system, how rapidly charge imbalances will dissipate, and what equilibrium potential will be established under given environmental conditions (Dennison *et al.*, 2009d). Further, the conductivity connects the physical make up of a material with the number of available carriers, carrier type(s), and the mobility of charge within the material. It is the low charge mobility of insulators that causes charge to accumulate where deposited, preventing uniform redistribution of charge and creating differential local potentials. Careful experimental investigations can develop an understanding of the contribution of carrier types, carrier density, and their mobility. As will be shown, this reduced mobility is ultimately due to the disordered nature of the material.

The primary goal of this dissertation is to unify both the experimental and theoretical basis of the charge transport models and the related phenomena in HDIMs used in spacecraft design. The accumulation and decay of charge in HDIMs is governed by the rate at which charge can escape once deposited in the material. *This dissertation then, is about the physics of carriers trapped in HDIMs and their subsequent release.*

1.1. Theoretical Framework of Dissertation

This dissertation represents a completed comprehensive study of the physical underpinnings of many response phenomena in the context of different experimental systems for changes in temperature, applied field, energy dose and dose rate, electrical breakdown threshold, and time. While this work leaves a great deal to be explained, its primary goal is accomplished. This goal is the unification of many theoretical concepts into a single formalism that allows for a consistent progression for modeling future experimental studies in HDIMs, while providing a physically based set of analytical and numerical models for current USU MPG experiments.

The development of common theory, common nomenclature, and application of this formalism to the specific nature of spacecraft charging is the primary goal of this dissertation. Currently, the set of theoretical ideas needed to comprehensively describe the phenomena seen across an array of spacecraft charging experiments (see Fig. 1.1) must be drawn from a number of other related fields. Recently, it has become clear that all of these behaviors may be described in a single theoretical formalism (Montanari and

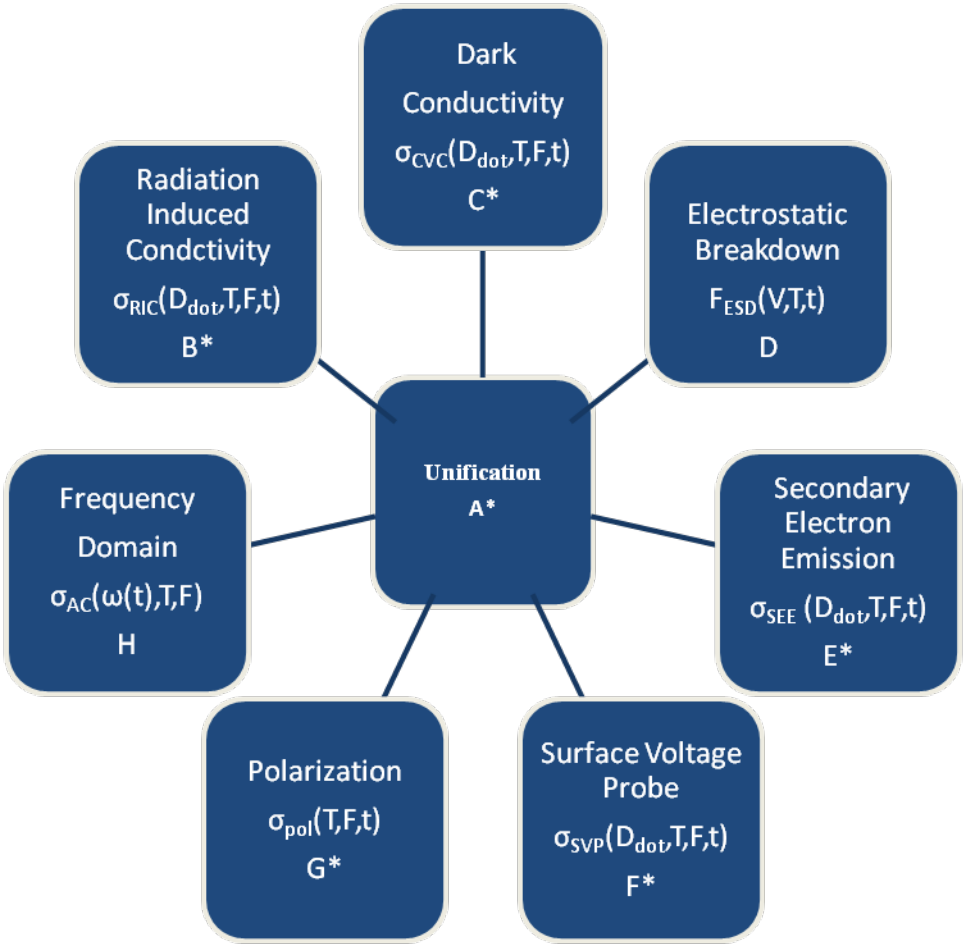

FIG 1.1. Materials Physics Group experimental organization diagram and conduction mechanisms. Each box represents a specific conduction mechanism associated with a specific set of experimentally measured parameters. (A) Model unification (Sim, 2010). (B) RIC = Radiation Induced Conductivity (Guthrie, 2013). (C) DCC = Dark Current Conductivity (Brunson, 2009; Dekany and Dennison, 2009). (D) ESD = Electrostatic Breakdown (Sim, 2010). (E) SEE = Secondary Electron Emission (Hoffmann, 2010). (F) SVP = Small Voltage Probe (Hodges, 2009). (G) POL= Impulse polarization studies (Brunson, 2009). (H) FD = Frequency domain polarization studies.

Morshuis, 2005; Teyssedre and Laurent, 2005; Dennison *et al*., 2009a; Brunson, 2009; Novikov *et al*., 2009; Griseri, 2009). In fact, the majority of the theoretical machinery needed to describe the physics and resulting phenomena was developed at Bell Labs and other semiconductor research facilities for an array of solid state applications; xerography is a primary example. As a result, the divergent nomenclature—and consequently the ideas surrounding much of the phenomena studied—is difficult to follow; perplexing terms with multiple and confusing meanings, such as time of flight, space charge, electrostatic discharge, and current decay are good examples. Further, it has often been the case that necessary work has been done

without publication (or publication in English), thus obscuring necessary information to understand the models. While many excellent texts have been written on the subject of dielectric studies (e.g., Sessler, 1987; Fothergill, 1998; Kao, 2004; Baranovskii and Rubel, 2006), they are often incomplete and are not geared specifically toward spacecraft applications.

This dissertation is a first step in bringing together a vast set of ideas in a common language to provide an interpretation for application to a specific set of real-world results and specific experimental tests. This goal is accomplished by assembling knowledge from a large spectrum of disciplines covering nearly every conceivable motivation (regarding charge interaction in solid materials) in a single formalism, which allows for the study of electron transport in materials across many experimental systems. The intricate relationships between spacecraft insulators and their surroundings are fundamentally based on a detailed knowledge of how individual materials store and transport charge. The key to mitigating these effects is an understanding of the time required to dissipate harmful charge imbalances on and within the material used in spacecraft construction. Figure 1.2 gives an estimation of the safety zones associated with charge decay times and their corresponding resistivities (Brunson, 2009; Hodges, 2013). In a simple parallel capacitor geometry, the charge decay time is linearly proportional to the resistivity of the material, which is a function of electric field, F, incident dose rate, $\dot{D}$, time, t, and material temperature, T: $\tau \propto \rho(F, \dot{D}, t, T)$. In discussions of material properties in this dissertation, we refer to the conductivity, σ, as the fundamental measure of charge transport, where the resistivity (often used in the spacecraft chagrining literature) is related to the conductivity by $\sigma(F, \dot{D}, t, T) = \rho(F, \dot{D}, t, T)^{-1}$. The conductivity results from the mobility of charge carriers, which is a measure of the ability of charge to move within the material**.** From a spacecraft operations perspective, the times of interest range from seconds to decades, with corresponding conductivities from $\sim 10^{-12}\ (\Omega\ cm)^{-1}$ to $10^{-22}\ (\Omega\ cm)^{-1}$ for HDIM.

1.2. Scope of Dissertation

Work in spacecraft charging covers a broad range of interests including the space environment, spacecraft potential studies, solar cell sustainability, control systems damage, and human exposure and viability studies (Garrett, 1981; Novikov, 1999; Molinie, 2005; Novikov *et al.*, 2006, 2009; Griseri, 2009). Thus, it is critical to understand where contributions can be made and what their impact is. Figure 1.3

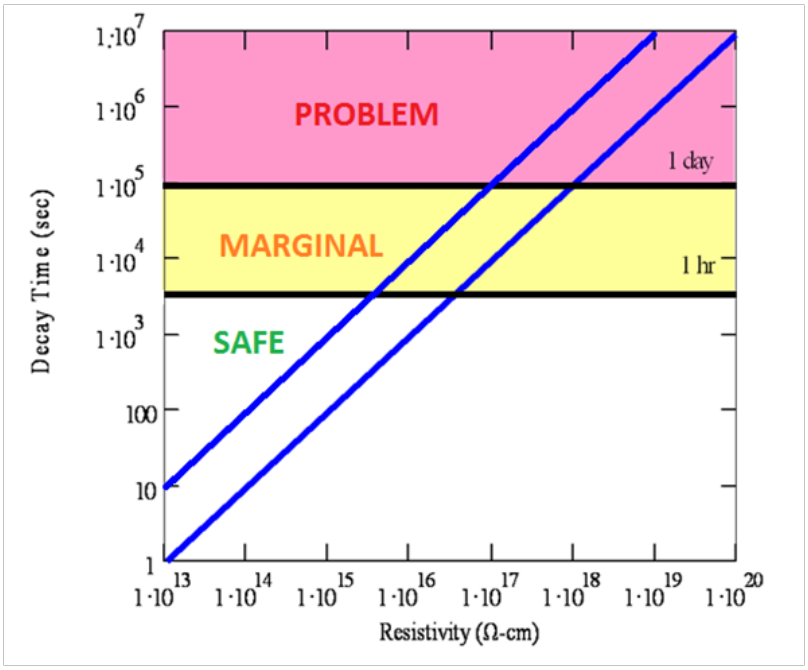

FIG 1.2. Relationship between charge decay time and sample resistivity, $\rho = \epsilon_0 \epsilon_r \tau$. Blue lines represent the extremes in dielectric constants of (ε_r=1 and ε_r=10) typical for spacecraft insulators (Brunson, 2009).

gives a graphical overview of the community and the USU MPGs current areas of interest. The three classes, in which all spacecraft charging research may be categorized, are given at the top and the collective results of the process are shown at the bottom. The reader should keep in mind that each of these boxes represents a wide field of interest and that here, only the contribution of the USU MPG has been expanded (in blue). The contributions made by this dissertation are highlighted in yellow under the heading Mathematical Models and Programs. The outcome of the spacecraft interactions figure is identified in the bottom two boxes of Fig. 1.3, labeled: (*i*) methods for predicting the spacecraft reliability and performance time, and (*ii*) recommendations for the spacecraft protection from radiation effects. While the direct testing and characterization of specific materials provides the ultimate measuring stick, such testing is time consuming and costly. The ability to predict these outcomes from a set of reliable models is critical to the spacecraft community. A great deal of research has been done on many different types of materials in other disciplines, for example, power line insulation degradation. This database provides a repository of knowledge upon which to test models and subsidize the current spacecraft materials characterization. This dissertation brings together these many sources and models in a single formalism.

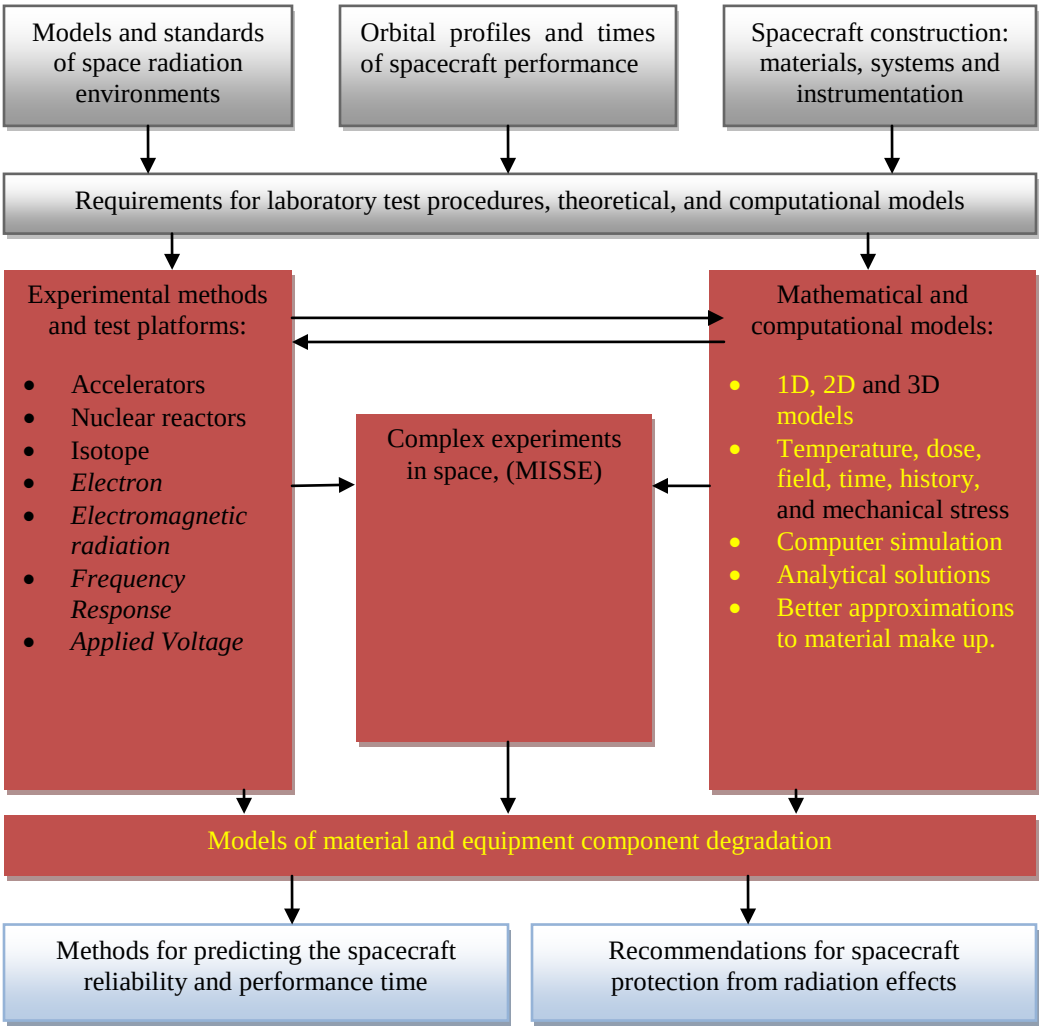

FIG 1.3. Organization of spacecraft interaction effects. The areas where the USU MPG has made major contributions are highlighted regions in red. The areas where this dissertation has made major contributions are yellow highlighted text. Diagram adapted from Zatekin *et al.* (2008).

Spacecraft in orbit are exposed to intense plasma environments and high energy particles, which provide the mechanism by which charge is injected, scattered, and removed leading to large variations in spacecraft potential. Charging to high potentials can lead to satellite material modifications, degraded instrumentation performance, or induced systems failures (Leach and Alexander, 1995), as well as creating potential safety hazards (Hastings and Garrett, 1996; Mandell *et al.*, 2001; Griseri *et al.*, 2005; Novikov *et al.*, 2009). The ubiquity of highly disordered insulating materials (HDIMs) in the design of spacecraft and many other technology components places special emphasis on understanding and modeling the electrical properties of the insulators. Detailed study of experimental data and physical models are critical for

anticipating and minimizing potentially damaging charging phenomena (Hastings and Garrett, 1996; Dennison *et al.*, 2006b; Garrett *et al.*, 2007; Ferguson, 2012). Developing a better understanding of the physics of insulating materials, increasing the versatility and reliability of charge transport models, and expanding the database of information for the electronic properties of insulating materials can assist spacecraft designers in accommodation and mitigating these harmful effects (Hastings and Garrett, 1996; Dennison *et al.*, 2006b).

There are many ways to study the electrical response of HDIMs: particle beam injection; contacts (both metallic and semiconducting); or internal charge excitation due to radiation and polarization, either by a changing contact potential or field. Each of the experimental systems developed at USU has been designed to test specific material behavior. Figure 1.1 shows the relationship of these experimental systems to the theoretical developments presented in this dissertation and their dependence on conductivity. In each of these applications, the USU MPG has implemented theoretical models to describe the observed behavior. These models essentially address six test configurations as depicted in Figs. 1.4(a) and 1.4(b). The illustrations in Fig. 1.4(a) are for electron beam irradiated configurations. The three illustrations show an increasing beam energy that results in either (i) a dusting of electrons on the surface, (ii) deposition of charge internal to the material, or (iii) complete penetration through the material. These three configurations are implemented in two MPG experimental systems: (i) the secondary electron emission (SEE) chamber (Hoffmann, 2010) with its associated surface voltage probe (SVP) (Hodges, 2013), and (ii) the radiation induced conductivity (RIC) chamber (Dennison *et al.*, 2009c). Each of these experimental methods provides a slightly different perspective on the trap filling dynamics, induced conductivity, injection method, and ratio of injected to escaping electrons across a huge energy scale (a few eV to $\sim 10^7$ eV).

The illustrations in Fig. 1.4(b) show experimental systems that use a parallel metallic contact plate configuration. In Fig. 1.4 (b) (i), a simple step function (very-long duration pulse) is applied and the response studied, as is done in the constant voltage conductivity (CVC) chamber (Swaminathan, 2004). This approach gives information on the polarization, trapping, and space charge injection using sensitive electrometers and well-characterized measurement conditions. Figure 1.4(b) (ii), with a series of incremental step increases in applied voltage, is used for the study of electrostatic breakdown (ESD). This

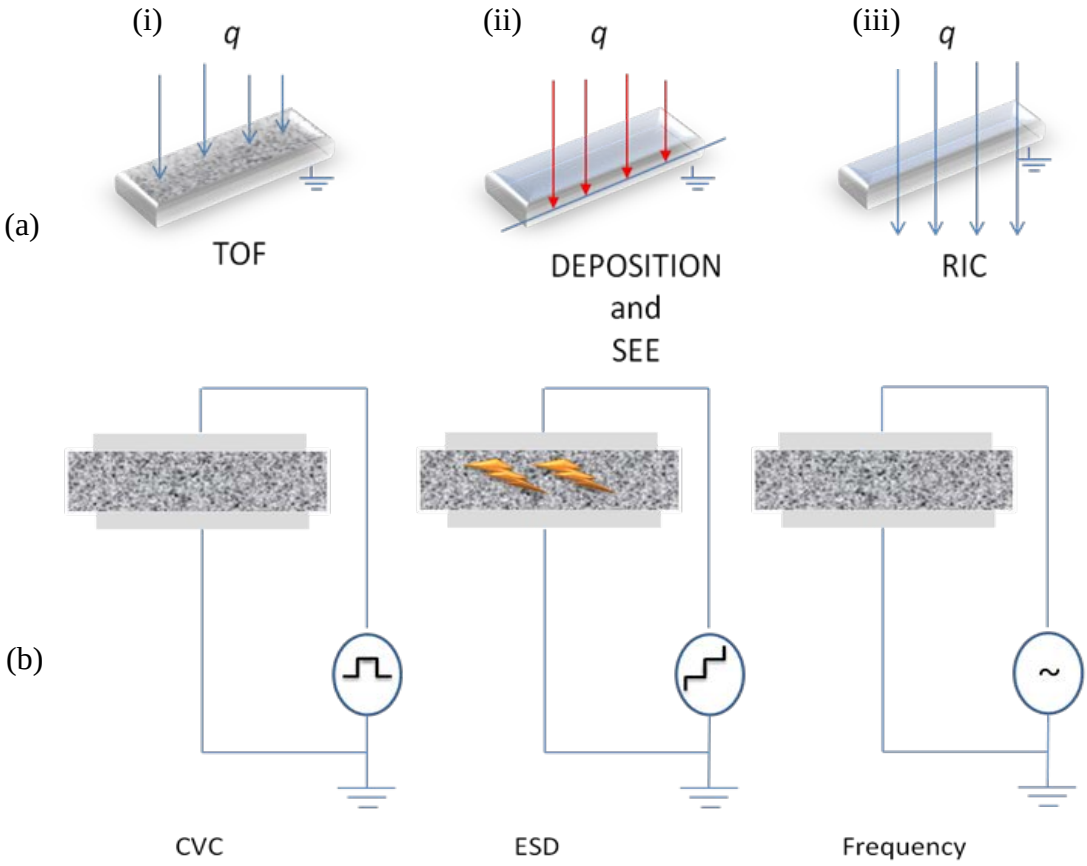

FIG 1.4. Simple characterization of experimental configurations. These diagrams provide a comprehensive classification of experimental configurations that describe all the ways in which charge is injected into or excited within a material by external influences. (a) Electron beam experiments: (i) Surface charge deposition for time of fight (TOF) experiments, (ii) bulk charge deposition and electron emission, and (iii) penetrating radiation for radiation induced conductivity (RIC). (b) Set of configurations corresponding to contact injection mechanisms: (i) Stepped or pulsed (constant) applied voltage measured in the Constant Voltage Conductivity (CVC) chamber, also called the Dark Current Conductivity (DCC) chamber, (ii) incrementally increased applied voltage measured in the Electrostatic Discharge (ESD) chamber, and (iii) periodic applied voltage measured with an inductance/ resistance/capacitance (LRC) meter to determine the frequency dependent polarization characteristics.

is a similar set up as the CVC chamber, but with protective electronics that permit observation of large breakdown events but not small charging currents. In the final experiment method shown in Fig. 1.4(b) (iii), the response of the material to a periodic narrow or wide step is studied. These measurements give information about the polarization, charging, and thermodynamic properties of the material near critical transitions. While this last measurement method has not yet been implemented at USU, it is shown in Chapter 4 that it is vital to understanding how the early charging in material occurs, in addition to

predicting information about the breakdown character of the material. All of the test methods depicted in Fig. 1.4 [with the exception of Fig. 1.4(b) (iii)] can be measured at USU over wide temperature ranges [~30 K to ~450 K for Figs. 1.4(a) and ~100 K to ~350 K for Figs. 1.4(b)].

Chapters 2 and 3 provide a complete theoretical description of electron transport covering a wide range of experimental application. These first three chapters set the stage for the development of new analytical and numerical models, which are applied in the context of two experimental systems used by the USU MPG to study spacecraft charging, a Constant Voltage Conductivity (CVC) chamber system, and a Surface Voltage Probe (SVP) system. The value of this approach comes from the fact that each of these experiments highlights different electron transport phenomena and charge injection mechanisms, but are shown to be the product of a single theoretical formalism. The specific data analyzed for the two methods discussed in Chapters 4 and 5 were acquired for a particular type of highly disordered materials, polymers, whose use is quite prevalent in spacecraft applications. Polymeric insulators can, and usually do, have particularly high disorder and require complex models to understand the resulting electrical behavior. They offer an excellent test bed for the theories put forth in this dissertation.

The USU Material Physics Group (MPG) has been developed to specifically address the spacecraft community's concerns for the charging of materials (Davies and Dennison, 1997; Kite *et al.*, 2000; Dennison *et al.*, 2004; Sim *et al.*, 2005; Abbott and Dennison, 2005). The USU MPG has built an extensive knowledge base of the behaviors observed in many spacecraft materials (Dennison *et al.*, 2009a). These databases have been implemented in engineering tools used in spacecraft design (Frederickson *et al.*, 1989; Dennison *et al.*, 2006a; Dennison *et al.*, 2009a) The accumulation of nearly two decades of work has provided the USU MPG with a unique platform from which to study the spacecraft charging problem.

The current USU MPG spacecraft charging engineering models for electron emission and transport are largely static in their predictions. Therefore, to make significant improvements in predicting time-dependent behaviors, new, more sophisticated time-dependent models largely developed for photoconductors based on the temperature, electric field, time, radiation dose and dose rate, and ESD event history must be applied in the context of the six fundamental systems depicted in Fig. 1.4. Consider a spacecraft near the critical conduction threshold depicted in Fig. 1.3, which undergoes a high-energy event, i.e., a sudden high flux of energetic particles. Depending on the charge deposition rate, induced dissipation

rate, and local electric field (or event induced field), the event may trigger an ESD and even cause a system failure. The resulting collection of charge and differential fields depends on the individual material's ability to respond in time to the environment. Not only is the time-dependent single event response important, but so is the history of the material (which is also dynamic). The need for a dynamic description of spacecraft charging for all temperatures, fields, doses, dose rates, polarizabilities, and time scales for charging or decay is clear.

1.3. Outline of Dissertation Structure

The organization of this work begins with an introduction to the spacecraft environment and current state of the USU MPG. This is followed by a description of the macroscopic physics of transport in HDIM (Chapter 2), and then an introduction to microscopic transport processes in HDIM (Chapter 3).

The task of unifying these models is addressed in this dissertation as follows. First, a comprehensive review of the literature has been completed and represents the basis for this work. Second, a common nomenclature (see the extensive and detailed Nomenclature section in the forward matter of this dissertation) and a unified description of the physical aspects—both from a macroscopic and a microscopic viewpoint—are developed and applied to each of the models. Finally, new information about physical connections and understanding are brought to light. The specific construction of this dissertation lends itself toward a decreasing level of theoretical and notational complexity, with a wide knowledge base to support and understand the assumptions and theories presented.

Chapter 2 focuses on transport mechanisms, which involve bulk extended states and (at most) a collection of trap states at a single (or mean) trap energy, to develop a comprehensive set of macroscopic transport equations, which can be used with many experimental platforms and with numerous types of materials with a specific focus on HDIM. We start with an introduction to simple Ohmic transport and the Maxwell equations to develop a basis upon which to understand simple Ohmic transport in ordered states but also the fundamental difference between it and charge transport in HDIM. These ideas are extended to more complex types of charge transport, such as drift and diffusion. This sets the stage to introduce the fundamental differences between charge transport in ordered materials and disordered materials. Then with an understanding of these differences and a set of simple physically motivated processes—built on our

understanding of disorder and a model of trapping and detrapping processes—the transport equations are derived. Chapter 2 closes with a discussion of dispersion highlighting the need for a detailed understanding of the charge dynamics in the disordered trapped states (i.e., we find that our simple one-dimensional mean energy models upon which the transport equations are built must be extended to more complex models of disorder).

Chapter 3 develops the complete theoretical basis upon which our understanding of microscopic charge transport is built. Chapter 3 contains the critical concepts to understand the nature of observed behaviors like dispersion. Chapter 3 is broken into three parts. First, in Section 3.1 an introduction to microscopic transport is developed for processes that involve transitions to—or between—an distribution in energy of the trap states. This section is crucial to understating the microscopic (or localized state) nature of the physics and how such microscopic theories relate to the macroscopic phenomena seen by the experimenter. As we see, it is not the single microscopic process that determines the material behavior, but rather the average microscopic processes (i.e., the average trapping and capture rate). Second, in Section 3.2 the models of average microscopic systems with connections to macroscopic behavior and applications to low-temperature and high field transport are covered. In this section, the first of the new models for low-temperature transport is presented. In particular, it is shown that the average microscopic models are consistent with current USU MPG models for low-temperature transport in both the low field and high field approximations. Having developed a solid microscopic theoretical framework upon which to connect and understand the resulting macroscopic behavior from Chapter 2, we develop the macroscopic phenomena, i.e., we recast the transport equations in terms of microscopic phenomena to understand the experimentally observed behavior.

In Chapters 4 and 5, the theoretical models based on Chapters 2 and 3 are extended and the resulting analytical expressions are applied to USU MPG data. Two of the major experimental systems in Fig. 1.1 are selected for study, the CVC and SVP. Thus, Chapters 4 and 5 bring together a large portion of the theoretical machinery to provide a deep understanding of the resulting behavior in each system, test our new formalism, and provide a set of new engineering tool, which can be used by spacecraft engineers in design. The resulting applications—cast in this new theoretical framework—provide a clear indication that all of the phenomena observed in the systems identified in Fig. 1.1 can be understood in terms of the

theoretical formalism presented. Further, we have found that by specifying how the charge is injected at the interface or into the bulk, strong ties can be made to additional phenomena, such as Schottky injection, Fowler-Nordheim injection, electron beam injection, and a number of other phenomena that have complicated information about the basic nature of HDIM.

1.4. Concluding Remarks

In conclusion, this dissertation is a largely theoretical treatment of the physics of charge accumulation, emission, transport, and depletion from both a microscopic and macroscopic perspective of materials science tailored to a specific set of applications and test methods related to spacecraft charging studies conducted at USU. This work brings together experimental and theoretical work from over 100 years of study in solid state physics, under a common nomenclature and a unified model of the physical mechanisms of conduction in HDIM and applies that knowledge to current USU MPG test systems. This work provides a new benchmark for the theoretical study and prediction of spacecraft charging. The expectations of this work include:

- Collection and development of theoretical work in a common nomenclature.
- Extension of current USU MPG mean field models to include a more complete description of material make up.
- Extension of current USU MPG static equilibrium models to include time dependence through use of rate equation models. Application of current theoretical models in charge transport to spacecraft applications.
- Application of resulting extended models to current USU MPG experimental systems
- Generation of new USU MPG engineering design tools.

As such, this work represents one of the most complete collections of ideas of the theory of spacecraft charging from a materials physics perspective; and yet, it is just a drop in the proverbial (leaky) bucket.

CHAPTER 2

OVERVIEW OF CHARGE TRANSPORT

2.1. Introduction

In the field of spacecraft charging, only modest attention from a modeling of perspective has been paid to the dynamics of charging in both the collection and dissipation of a space charge in a material. Many researchers (Frederickson *et al.*, 1989; Novikov and Rakov, 1995; Dennison *et al.*, 2009a) have been aware of this deficiency, yet the community is still working with a charging code (Davis *et al.*, 2007) that is largely static in its predictions. Further, over the last 30 years, since the core of the current NASCAP code was created, many advances in the understanding of charging dynamics have been made. It is a goal of the USU MPG to provide the integration of new models, experiments, and theory for the development and design of spacecraft systems. For nearly 20 years, the USU MPG has developed new experimental systems that serve as a benchmark for the spacecraft charging community (Dennison *et al.*, 2006a). Recently, it has become clear that a complete nonstatic description of charging is necessary to better avoid damage or even destruction of spacecraft (Dennison, 2010; Ferguson, 2012). The questions regarding how a material might behave in the space charging environment can be addressed by understanding a given material's response to particle flux, external and internal fields, and temperature as a function of time. In particular, one needs to be concerned with three major areas: nondestructive charging and decay, repairable charging, and completely destructive irreparable charging (breakdown). All of these areas are dynamic in nature and have a strong time, temperature, dose, and electric field dependence. Further, each of these areas is intimately tied to one another and they are related by similar behaviors, physical interpretations, and models.

The USU MPG models currently include field, dose and temperature dependence, but lack the time-dependent components necessary to predict true breakdown time and/or recovery time. Further, many of the USU MPG models are based on a single expression of the disorder in the material, henceforth referred to as the density of states (DOS), and in many cases do not reflect the true behavior of the material. The necessary theoretical work is presented here to provide time-dependent and low -temperature models, which are a function of more realistic expressions of the true material DOS. This outlines a wholly new way to understand the nature of HDIM. In all DOS types, the resulting theoretical models provide not only

a consistent way to understand behavior in any single experiment, but across all the USU MPG experimental systems and numerous other types of experimental systems (Sessler, 1987). Each of these models ties directly to the USU MPG experimental results (Hoffmann *et al.*, 2008; Dennison and Brunson, 2008; Dennison *et al.*, 2009a; Dennison *et al.*, 2009c; Sim and Dennison, 2010; Wilson and Dennison, 2010; Hodges, 2013). In order to highlight the differences between this dissertation's results and the previous work done by the USU MPG, a review of the USU MPG models pertaining to each application is given; Chapter 3 introduces applications to low-temperature transport, Chapter 4 discusses applications to parallel plate capacitor type configurations, and Chapter 5 presents applications to experimental systems in which charge has been embedded in the material by external sources (an electron beam, for example).

First, a review of fundamental concepts in conduction and the physics of HDIM are provided. As with any scientific investigation, the undertaking begins with a review of the current literature, models, experiments, and data. An extensive review was done prior to writing this document. As it turns out, the literature can be broken into two distinct bodies of information. The first is the macroscopic (classical) picture using, in one form or another, the Maxwell equations and a continuity equation. The second case describes the microscopic behavior of trapped and free carriers during transport through an HDIM. I have, therefore, arranged this dissertation along the same lines: macroscopic in Chapter 2 and microscopic Chapter 3. Chapters 2 and 3 develop the picture of charge transport that results from the literature review and resulting theoretical work. We begin with fundamental principles of physics as they pertain to transport theory in HDIM and build a new picture of electron transport in highly disordered insulating materials.

In the next section we begin with a simple overview of charge transport by evoking the Lorentz force law. This leads naturally to a discussion of the Drude equation and the simplest of ideas in transporting charge in materials, Ohm's law. This discussion is presented to provide the reader with a basic starting point from which the remaining concepts are built. In particular, once the classical Ohm's law is in place, a discussion of the differences between metals and semiconductors or insulators is made. By adding the Maxwell equations in the context of semiconductors, the stage is set to discuss the effects of disorder. It is in the difference between semiconducting or insulating crystals and the introduction of disorder that we find the final link to understand why disordered transport is so completely different from its more classical counterpart.

2.2. Fundamental Concepts of Charge Transport

2.2.1. Simple Conduction

How can we model charge transport and conductivity in disordered insulators as a function of material interactions with incident radiation, f, electric field, F, temperature, T, position, z, and time, t? In practice, the problem is very complex and requires a detailed understanding of the microscopic mechanism that characterizes the interactions of the injected charge with constituents of the material. The most general approach begins with the Lorentz force law, $\mathbb{F} = q_e F + v_e \times B$. Here q_e is the carrier charge, v_e is the velocity of the electron, and B is the magnetic field. In nearly all spacecraft studies, the magnetic field B is negligible. (Missions are planed that will send spacecraft into intense magnetic fields; the JUNO mission is an example.) For our purposes, we assume a zero magnetic field and the Lorentz law reduces to $\mathbb{F} = q_e F$; from this, an expression for the mean velocity of the electron is obtained by integrating over the time between collisions, τ, in a simple metallic medium. The result is $v_e = \frac{q_e \tau F}{m_e}$.

Using the Drude model, Ohm's law is written $J = -n_e q_e \, v_e$ and by substituting in the above expression for v_e, we have $J = -n_e {q_e}^2 \frac{\tau F}{m_e}$; J is the current density passing through a unit area and n_e is the number of electrons per unit volume (or number density) required to produce that current. Ohm's law, in its most common form, is written as $J = \sigma F$, where σ is the conductivity of the material. A comparison of these two expressions suggests that the conductivity should be written as $\sigma = n_e q_e \mu_e$, where the variable $\mu_e \equiv v_e / F$ is the mobility. The Drude formulation suggests that $\mu_e = \frac{q_e \tau}{m_e}$. What is learned from this investigation is that the mobility and the number density of available electrons n_e are the quantities that determine the observed electron transport behavior, i.e. the current. In this case, the mobility is proportional to the time between collisions and the number of electrons available to participate must be some function of the material or the way that the electrons are injected into the material.

In metals, there are no problems finding enough electrons to account for changes in current as the applied field is changed. However, as the temperature is increased, the number of collisions with phonons increases creating resistance to current flow. As the Drude formulation suggests, if the mean collision time is decreased by increasing the temperature, the electrons see more interactions and hence, a counter force or

resistance is observed as a function of the number of scattering events. This process is always true in a conduction band for a typical metal; thus, we expect the resistance to increase as a function of temperature.

In contrast, consider a semiconductor or perfect insulator (whose very name gives away the next step in our discussion). In a semiconductor, it is largely the excitation of carriers from the valence band (VB) across an energy gap to the conduction band (CB) that determines the conductivity. This process of excitation and the basic physics are presented in the solid state physics text by Ashcroft and Merman (1976) and reviewed in Section 2.4 and 2.5 of this dissertation. There is an energy required for charge carrier (electron) excitation across the gap, $\varepsilon_{gap} = (\varepsilon_{CB} - \varepsilon_{VB})$. The primary difference between a semiconductor and an insulator is the size of ε_{gap}; at room temperature there is a well-defined number of carriers in the CB resulting from thermal excitation, for an insulator there are nearly no carriers. The probability of an electron to make this jump is determined by the temperature of the material; thus, the higher the temperature the greater the number of carriers in the CB and the larger the conductivity, which results in a larger observed current. Since, in a metallic state, there are lots of electrons available, the effects of collisions can be easily seen. However, in a semiconductor (or worse yet, an insulator) there are very few electrons excited to participate in conduction. Thus, in a semiconductor or insulator, the conductivity is largely determined by the number of excited electrons and increases with temperature. Of course, temperature is not the only way to get electrons to jump the gap; one can also provide the requisite energy by irradiating the sample with either high energy electrons or photons. In fact, the conductivity is affected by many external stimuli in addition to the material composition.

For a single electron, the conductivity is defined as $\sigma = n_e q_e \mu_e$. A general form of Ohm's Law for any carrier type can be written as

$$\sigma_i = n_i q_i \mu_i, \tag{2.2.1}$$

where the subscript *i* now denotes a carrier type (say *e* for electron, *h* for hole, and so on). Then, the total conductivity of a given material is given by $\sigma_{tot} = \sum_i \sigma_i = \sum_i q_i n_i \mu_i$, where the summation is over all the conductivity mechanism active in a given material, each with a unique carrier type, density, and mobility with index *i*. The physics to describe a material is found in the dependence of n_i and μ_i on temperature, time, electric field, and incident radiation. The constraints for Eq. (2.2.1) are:

Charge carriers, q_i: The charge on an individual particle, e.g., electron, ion, hole or pseudo-particle, such as the exciton and polaron. Of these, only electrons are considered in this dissertation (see Section 2.2.2.1). Holes are assumed to be immobile and pseudo-particles do not contribute to the conduction processes in HDIM directly.

Mobility, $\mu_i(\dot{D}, F, T, t)$: This measures the tendency of an individual charge to move in response to the applied field, *F*. Mobility is defined as the ratio of carrier drift velocity, within the material to applied field, $\mu \equiv \frac{v_d}{F}$.

Carrier density, $n_i(\dot{D}, F, T, t)$: The density of a *collection of charges* per unit volume can depend on material properties, temporal response of charges, and external sources, such as the rate of deposited energy density (or dose rate), $\dot{D}$, the electric field, *F*, and temperature, *T*. In complex cases, material properties can be modified, through changes in microscopic structure, as a function of $\dot{D}$, *F*, *T*, and time.

Here we have ordered the parameters q_i, μ_i, and n_i as the charge on each type of carrier, the single carrier response, and the collective single carrier density. Given the simple description of macroscopic material response as a function of $\dot{D}, F, T,$ and t, we now ask what mechanisms within the material give rise to observed behaviors.

The answer to this question lies in the categorization of physical phenomena and an understanding of how they come about. There are a large number of observed mechanisms that can contribute to the measured current: polarization, spacecharge, diffusion, dispersion, carrier hopping, and secondary electron emission (SEE). Thus, we may write the total measured current as $J_{tot} = \sum_i J_i$. Some of the processes—such as polarization, diffusion, and dispersion, are fundamental physical processes that can be explained directly from first principles; others, like hopping and space charge limited current (SCLC) are composed of other more fundamental processes. An example is hopping, which involves thermal excitation of carriers and the local quantum potential, but can exhibit diffusive or dispersive behavior depending on material make up, temperature, and applied voltage. Each of these processes will be introduced in this dissertation in order of complexity. Thus, drift and diffusion are presented first, followed by a discussion of the more complex processes.

In order to extend this discussion on transport in HDIM, it is necessary to develop a set of equations that can describe all the known behaviors. These equations are called transport equations and form the backbone of this dissertation. First, an introduction to the types of carriers that are considered is needed. This is done to justify the use of a single carrier approximation, that carrier being the electron. The presentation of charge types is followed by the natural extension of our discussion to drift and diffusion, and finally, the derivation of the first four of the transport equations.

2.2.2. Charge Types

The specific focus of this dissertation on conduction in HDIM dictates the essential limitations on our consideration of the type of charge carriers, density of states, and the carrier mobility or conduction mechanisms. This dissertation will largely be limited to consideration of electrons as carriers. However, there are many cases, which are beyond the scope of this work, in which other carriers, such as holes, excitons, and polarons play a major role in the dark current conduction and photoemission processes (Böer, 2002; Kao, 2004; Baranovskii and Rubel, 2006; Chen, 2010). The action of holes does appear in this dissertation when we consider radiation induced conductivity, but is sparse and will, therefore, only be considered where specifically noted. What follows is a brief justification for our assumptions and a discussion of other types of carriers.

2.2.2.1. The Single Carrier Approximation

The idea that we can use a single carrier approximation to describe the behavior of charge transport in HDIM has its roots in semiconductor theory, which is based on semi-classical models of electron dynamics. As Ashcroft and Mermin note in their text “many of the concepts used in the theory of amorphous solids are borrowed, with little if any justification, from the theory of crystalline solids, even though they are only well understood in the context of periodic lattices” (Ashcroft and Mermin, 1976, footnote on page 62). Since the writing of this classic text, there have been numerous advances in understanding the differences between crystalline and amorphous systems. One particularly well known example where the line between ordered and disordered systems is well studied occurs in amorphous hydrogenated silicon, a-H-Si, whose amorphous semiconducting nature was studied extensively in the late 60’s and early 70’s and led to a number of insightful discoveries pertaining to a larger class of disordered

systems (Davies, 1969; Hertel and Bässler, 2008). Dennison and Ritter made significant gains in understanding the material structure and momentum density of amorphous carbon (Ritter *et al.*, 1984). The study of HDIM takes us a step further, as there is often no known ordered counterpart. In HDIM we have the added difficulty of very-low detectible currents rendering the Hall Effect insufficient to determine the majority carriers. To further complicate the problem, many researchers have shown the carrier concentration in HDIM is bipolar involving electrons, holes, and an interaction between the two (Baudoin, 2008; Cornet *et al.*, 2008; Chen, 2010).

While there are numerous techniques for determining the carrier majority, only two stand out as consistent, well-studied, and easily accessible ways to approach the problem of carrier majority determination in HDIM; these methods are thermally stimulated current emission (TSC) and pulsed electro-acoustic (PEA) measurements. Significant work by Sessler and Ieda using TSC have led to determination of the energetic distribution of states in the band gap caused by the disorder and, in many cases, the majority carrier concentration (Ieda *et al.*, 1972., 1980, 1984, 2003; Gross *et al.*, 1987; Ieda and Suzuoki, 1997). Originally suggested by Sessler and Gross, PEA methods study the deposition and transport of charge and its density within the material as a function of position and time for both contacting and noncontact electrode arrangements. This approach has provided what will likely be the final word in the study of charge transport in HDIM (Gross *et al.*, 1977, 1987; Sessler, 1987; Griseri *et al.*, 2004; Perrin, 2005).

All the above information is largely to say we do not know what the majority carrier is in most HDIM. So how can we justify the use of a single electron approximation? The simple answer is that models progress from simple to complex and, since the large majority of our understanding of HDIM is taken from semiconductors, we are prone to start in a similar place, i.e. assume a single electron and ask what happens in the material due to various interactions. The second reason was recognized in semiconductor work long ago (Rose, 1963); the equations for holes are the same as for electrons with differing numbers for relevant physical parameters, relaxation time, or effective mass as examples. In order to obtain a complete set of transport equations for a system that has both electrons and holes of comparable mobility, one simple doubles the number of equations and adds an interaction term that defines the rate at which electrons and holes can recombine. As it turns out, there is nearly always a majority

carrier (usually the electron). Finally, the use of a single carrier model is historically driven; most of the models in the literature (while admitting that they too fall short of a complete description) are single carrier models. Many authors have recognized this problem, but were able to use the single carrier approximation based on experimental designs that limited additional carrier contributions. For example, in a RIC experiment where the sample is in the open configuration (see Fig. 1.4), we are exciting electrons (not holes) across the energy gap creating a majority carrier. In such cases, blocking electrodes are used to ensure that bipolar recombination between injected carriers (holes, in this case) from contact surfaces and excited electrons does not occur (Sessler, 1987). In secondary electron emission (charge deposition) experiments—where electrons are trapped at some depth in the material—we clearly have an excess of electrons that will become carriers in the CB, again assuming that the rear electrode (ground plane) does not inject carriers of the opposite sign. Recently it has become clear that many effects in certain types of HDIM (LDPE, for example)—due to bipolar effects—cannot be neglected when internal fields, due to charge deposition, are high enough to induce charge injection from the ground electrode (Cornet *et al.*, 2008; Chen, 2010; Fitting, 2010).

Since the transport equations for electron carriers can be thought of as one side of a mirror set of equations, we need only develop the theoretical ideas for one set. This, finally, is the strongest reason for approaching this dissertation for a single carrier stand point. As we will see, developing a complete description for a single carrier system in the absence of recombination due to an additional carrier distribution is already sufficiently challenging and yields a complete model for transport in HDIM.

2.2.2.2. Holes

Consider an excited state of a molecule in which an electron has been removed from a filled orbital and occupies a previously empty orbital of higher energy (or leaves the influence of the original molecule altogether, creating the absence of electron ground state in the original orbital. i.e., an anion). One way to describe this modified excited molecular state is as the superposition of the original state for all the electrons in the ground state, a state for the excited (or removed) electron, and a state describing the now empty state previously occupied by the excited electron. In a more general way, we can think of electrons as being excited from the highest occupied molecular orbitals (HOMO), from neutral states in the

gap, or from the VB. William Shockley summed up the concept of a hole with the following quote: “The hole is really an abstraction which gives a convenient way of describing the behavior of the electrons. The behavior of the holes is essentially a shorthand way of describing the behavior of all the electrons” (Kao, 2004). In practice, a hole in this work is meant to describe (i) a positively charged entity that can accept an electron through the process of recombination, or (ii) the conduction of the absence of the electron (Ashcroft and Mermin, 1976).

2.2.2.3. Other Carriers

In the study of transport in disordered materials, there is a plethora of quasi-particle types that can contribute to conduction. The exciton and polaron are two examples of these quasi-particles. Most quasi-particles are confined to materials with much higher conductivities or much lower levels of disorder. The exciton and polaron are the only two that may play a role in HDIM transport (Kao, 2004). There are two types of exciton, Frenkle and Wannier (Ashcroft and Mermin, 1976). Of these, only the Frenkle exciton may play a part in HDIM conduction; however, its role is likely that of a simple trap and thus, will not be distinguished from simple Coulomb trapping in this work. Polarons may act as intermediaries in low-temperature transport, discussed in Chapter 3, providing energetic pathways for hopping electrons or acting as traps. The action of the polaron is not likely to be detectible at the macroscopic level and does not affect the average transport theories discussed in this dissertation.

This section has established the basis for the electron transport picture and given justification for the elimination of quasi-particles (including, holes, excitons, and polarons) as major contributors to the current. Using the electron picture a discussion of the transport equations can now be presented.

2.3. Macroscopic Transport

The transport in HDIM is known by many names: multiple trapping, trap controlled transport, dark current, etc. In this dissertation, the charge transport equations will be referred to as the transport equations. This approach provides a bird’s eye view of the physics and is the scaffolding upon which the effects of strong disorder found in HDIM can be understood, in addition to providing the necessary framework to extend any of the models presented in this dissertation. The transport equations are developed from the Maxwell equations and the charge continuity equation in macroscopic media using a given

expression for the observed current, J_c. Further, in many cases the continuity equation must include a source term, *S*, that describes additional changes in carrier flux. These fundamental equations are:

$$\nabla \cdot \boldsymbol{D} = \rho_c \quad \{\text{Gauss's Law}\}, \tag{2.3.1}$$

$$\nabla \cdot \boldsymbol{B} = 0 \quad \{\text{Unnamed}\}, \tag{2.3.2}$$

$$\nabla \times \boldsymbol{F} = -\frac{\partial \boldsymbol{B}}{\partial t} \quad \{\text{Faraday's Law}\}, \tag{2.3.3}$$

$$\nabla \times \mathbf{H} = \mathbf{J_c} + \frac{\partial \mathbf{D}}{\partial \mathrm{t}} \quad \{\text{Ampere's Law with Maxwell's displacement correction}\}, \tag{2.3.4}$$

and

$$\nabla \cdot \mathbf{J_c} + \mathrm{S}(\mathbf{r}, \mathbf{t}) = -\frac{\partial \rho_{tot}}{\partial \mathrm{t}} \quad \{\text{Charge continuity equation with source term}\}. \tag{2.3.5}$$

Here ρ_c is the free charge density, ρ_{tot} is the total charge density, ρ_b (shown below) is the bound charge density, $\boldsymbol{D}$ *i*s the electric displacement field, $\boldsymbol{B}$ is the magnetic field, $\boldsymbol{r}$ is the three-dimensional position vector, $S(\boldsymbol{r}, t)$ is the injected current that becomes either space charge or migrating trapped charge, and $\boldsymbol{H}$ is the magnetizing field. Only in rare cases is the effect of the magnetic field considered; thus, in general we concern ourselves only with Eq. (2.3.1) and Eq. (2.3.5). Note that inherent in these equations is the constitutive relation that relates the total charge density, displacement field and polarization charge given by:

$$\rho_{tot} = \rho_b + \rho_c. \tag{2.3.6}$$

$$\boldsymbol{D} = \epsilon_0 \boldsymbol{F} + \boldsymbol{P} \equiv \epsilon_0 \epsilon_\mathrm{r} \boldsymbol{F}. \tag{2.3.7}$$

$$\rho_b = -\nabla \cdot \boldsymbol{P}. \tag{2.3.8}$$

Here ρ_{tot} stands for the total charge, ρ_b is the bound charge due to polarization, and $\boldsymbol{P}$ for polarization. ϵ_0 and ϵ_r are the permittivity of free space and the relative permittivity, respectively. Since the current is the sum of effects produced by all species of carriers, molecular, and atomic sites, the charge density can be written as

$$\rho_i = q_i n_i. \tag{2.3.9}$$

Here *i* denotes the charge species, q_i is the electronic charge per carrier, and n_i is the charge carrier concentration. Note that we can refer here to charge in trapped states, bands, free charge, or even surface charge. For example, consider a system where we have injected a known amount of electron charge per unit volume, ρ_{tot}. Further assume that some of the charge resides in the CB and some in trapped states in

the band gap; then we can write the charge density as $\rho_{tot} = \rho_e + \rho_t$ or the number density as $n_{tot} = n_e + n_t$.

The difficulty in determining the flavor of macroscopic equations to use is a reflection of the complexity of the material and its environment, i.e., boundary conditions, experimental setup, DOS models, and population statistics. One simplification that is effective in reducing the complexity of working with these equations is to reduce the 3D expression to a 1D expression. Next, an approximation for the observed current is needed to describe how the charge concentrations change with distance and time. By doing this, expressions for the resulting field and time dependence can be obtained.

2.3.1. Drift

The drift current density can be written as a function of many variables (see Section 2.2.1). In particular, it has been suggested that the mobility, free carrier density, and applied field can all be complicated functions of dose rate, temperature, applied field, and time. For simplicity, assume that the density of carriers, n_e, and the applied field, F, are functions of both position and time, such that

$$J = q_e \mu_e n_e(z,t) F(z,t) \quad \{\text{1D Drift Current Density for electrons}\}. \quad (2.3.10)$$

Here, z is the one-dimensional spatial coordinate direction along which the drift occurs. This expression is true in many metals and semiconductors, and is the simplest possible nonzero expression for the current. In this case, the field and charge concentration both have been allowed to vary as a function of distance and time to make a stronger connection with the final form of the transport equations presented at the end of this chapter. Keep in mind that the entire right-hand side of Eq. (2.2.10) can be written as a function of applied field, temperature, dose rate, position, and time. The discussion of the 1D transport equations can now nearly be completely captured from this simple expression and manipulation of Gauss's Law (2.3.1) and the continuity equation (2.3.5) as

$$\frac{\partial}{\partial z}\hat{z} \cdot \boldsymbol{F} = \frac{\rho_{tot}(z,t)}{\epsilon_0 \epsilon_r} \quad \{\text{1D Gauss's Law}\}, \quad (2.3.11)$$

and

$$\frac{\partial}{\partial z} V = -F \quad \{\text{1D Scalar potential}\}, \quad (2.3.12)$$

which can be combined as

$$\frac{\partial^2}{\partial z^2}\mathrm{V} = -\frac{\rho_{tot}}{\epsilon_0\epsilon_r} \quad \{\text{1D Poisson's Equation or Laplace's Equation when } \rho = 0\}, \quad (2.3.13)$$

along with

$$\frac{\partial}{\partial z}\mathrm{J_c} + \frac{\partial \rho_{tot}}{\partial t} = q_e \mathrm{S(z,t)} \quad \{\text{1D One dimensional continuity equation}\}, \quad (2.3.14)$$

to yield the two fundamental 1D transport equations. The source term is $S(z,t)$; this term represents the injection of carriers into the material either by a contacting interface or by high energy impingement of carriers.

The macroscopic equations Eq. (2.3.11) through Eq. (2.3.14) form the backbone of nearly all the macroscopic derivations in this dissertation and will come into play frequently in Chapters 3 though 5. The derivation of the complete transport equations begins here with the manipulation of these macroscopic equations. First, we seek a solution for the number of electrons in a material as a function of some external source and electric field. Substituting the drift current from Eq. (2.3.10), $\rho_{tot} = q_e(n_e + n_t)$ and canceling the charge constant, an expression that relates charge density, charge carrier, electric field, and charge generation as a function of position and time can be found,

$$\frac{\partial n_{tot}(z,t)}{\partial t} + \mu_e \frac{\partial}{\partial z}[F(z,t)n_e(z,t)] = S(z,t). \quad (2.3.15)$$

There are many examples where *S(z,t)* is used to study material properties, most of which do not specifically identify the source term (Many and Rakavy, 1962; Weaver *et al.*, 1977; Schmidlin, 1977; Arkhipov and Rudenko, 1982c; Rudenko and Arkhipov, 1982b; Rudenko and Arkhipov, 1982c; Monroe, 1983; Arkhipov *et al.*, 1983; Sessler, 1987; Teyssedre and Laurent, 2005). As a note to the reader, the source term is only occasionally symbolically represented as *S(z,t)*. The inclusion of the source term allows a simple description of processes that create charge internal to the material. In general, we can think of light, electron beams, and contacting electrodes all as the sources. Equation (2.3.15) will be expanded later (see Chapters 4 and 5) to include the dependence of dose, dose rate, temperature, and applied field.

As an example of the application of Eq. (2.3.15), consider what happens when light of a frequency sufficient to excite electrons in a material across the band gap into the conduction band is applied to a sample, a semiconductor perhaps. For a description of the differences between metals, semiconductors and insulators, see Section 2.4.1. This type of excitation is commonly called photoconductivity or RIC. Electrons will be liberated from valence states into the conduction band, leaving holes (assumed

immobile $\mu_h \sim 0$) and creating an excess of electrons in the CB and therefore, an enhanced current. Let *G(z)* be defined as a generating term, which describes the interactions and related processes that determine the way in which carriers will be excited into the conduction band by the incident light. Let *R(z)* be defined as the recombination term, with its own set of interactions and processes. Since *S(z,t)* is a net source term, we can replace *S(z,t)* with *G(z,t)-R(z,t)*. While both of these terms are complex functions of the material, knowledge of their inner workings is not required to develop the transport equations further. Thus, for now *G(z)* and *R(z)* are taken at face value until a full description of their nature can be developed and the complete transport equations derived (see Section 2.6). Now Eq. (2.3.15) can now be written as,

$$\frac{\partial n_{tot}(z,t)}{\partial t} + \mu_e \frac{\partial}{\partial z}[F(z,t)n_e(z,t)] = G(z) - R(z). \tag{2.3.16}$$

In addition to Eq. (2.3.16), two more pieces are needed to properly describe the system. The relationship between the change in the number of holes or recombination centers must be considered. This expression also follows from the continuity equation and the assumption that the hole generation and recombination rates are equal to the electron counterparts (i.e., holes are created when electrons are excited to the CB and destroyed when electrons recombine with holes in the VB) and can be written as

$$\frac{dn_h(z.t)}{dt} = G(z) - \mathrm{R}(z). \tag{2.3.17}$$

Here the number of electron/hole pairs generated per unit time is controlled by *G(z)* and the number of electron/hole pairs that undergo recombination per unit time is *R(z)*. This process of excitation and recombination is analogous to pumping water into a fountain. Energy is supplied by the pump to send the water up to some potential and then the excited water returns to the reservoir with an equal amount of energy.

Thus far, only the continuity equation (2.3.15) and a simple expression for the drift current (2.3.10) have been used. Gauss's law, Eq. (2.3.11), is fundamental to understanding the connection between a charge distribution and the electric field or potential. Equation (2.3.16) and Eq. (2.3.17), along with Gauss's law or Poisson's equation, form three fundamental equations, which can be used to understand many phenomena in metals, pure semiconductors, and pure crystalline insulators. These three 1D equations in terms of charge concentration are repeated for clarity:

$$\frac{\partial}{\partial z}\hat{\mathrm{z}} \cdot \boldsymbol{F} = q_e n_{tot}/\epsilon_0\epsilon_r \qquad \{\text{Gauss's Law}\}, \tag{2.3.18}$$

$$\frac{\partial n_{tot}(z,t)}{\partial t} + \mu_e \frac{\partial}{\partial z}[F(z,t)n_e(z,t)] = G(z) - R(z)$$

{1D electron continuity equation with Ohm's law and source terms} (2.3.19)

and

$$\frac{dn_h(z.t)}{dt} = G(z) - \mathrm{R}(z)$$ {1D hole continuity equation with source terms}. (2.3.20)

The form of these equations changes depending on the sources, sinks, and types of behavior considered in the current density equation $J_{tot} = \sum_i J_i$. It will be shown that a global set of equations that describe all possible transport phenomena can be derived and adapted to predict transport phenomena for specific experimental applications. With this approach in mind, and the understanding these transport equations can be used to go from fields to currents or currents to fields, the discussion is extended to diffusion as the next step in developing a complete set of transport equations.

2.3.2. Diffusion

Diffusion is one of the fundamental assumptions in semiconductor physics (Ashcroft and Mermin, 1976; Fraser, 1983; McKelvey, 1993) and was used along with drift by Shockley (1950, 1951, 1976) to arrive at the famous semiconductor junction equations. How is diffusion included in this formulation? Diffusion is a simple process by which atoms or molecules move away from each other due to their mutual interaction toward some equilibrium value. Consider a particle moving in a group of similar particles with minimal interaction, but with some thermal energy. In this scenario a particle will execute a series of motions that are random in nature. The collection of all possible steps is called the Drunkard's walk (or Brownian motion). Einstein showed that after some large number of steps acting over an average length, a carrier will cross a distance using purely thermal energy. Collectively, we can think of a flux of particles that will result in a carrier density change,

$$f = -D\frac{dn_e}{dz},$$ (2.3.21)

where D is a constant and given by

$$D = \frac{\mu_e k_b T}{q_e} = \frac{k_b \tau_d T}{m^*}.$$ (2.3.22)

The coefficient D is defined as the Einstein diffusion coefficient D_e, and Eq. (2.3.21) is known as Fick's Law; it can be applied to any diffusive process. Note that μ_e is the mobility of the diffusing carrier,

T is the temperature, and τ_d is the extended carrier lifetime (in this case, the lifetime of our single electron). This leads to the definition of the diffusion current density,

$$J_D \equiv q_e D_e \frac{dn_e}{dz}. \tag{2.3.23}$$

The total electron current for a system with an applied field, *F*, and active diffusion is

$$J_{tot} = J_C + J_D = q_e n_e \mu_e F + q_e D_e \frac{dn_e}{dz}. \tag{2.3.24}$$

The sign of the resulting current is a competition between drift and diffusion. The astute reader may notice that we have a positive sign, and this would appear to be a problem; this is due to the fact that q_e is $-e$. Further, the field, *F*, is the negative of the gradient of the potential. For a detailed description of diffusion processes and a detailed discussion of Eq. (2.2.24) (see standard texts by Ashcroft and Mermin (1976) and McKelvey (1993).

As an example, consider the connection between diffusion and the generation and capture of electrons. This example highlights the connection between basic transport and generation-recombination models. Consider Fig. 2.1 with an Ohmic drift current passing through a semiconducting sample from $J(z)$ to $J(z+dz)$. For very small displacements, the current at $z+dz$ can be written as

$$J_{tot}(z+dz) \cong J_{tot}(z) + \frac{dJ_{tot}(z)}{dz}\, dz, \tag{2.3.25}$$

where the total flux due to the current is $J_{tot}(z) - J_{tot}(z+dz) \cong -\frac{dJ_{tot}(z)}{dz}\, dz$; notice if the gradient is zero, the current in is equal to the current out. Now consider the difference in flux due to generation-recombination of carriers, $G(z,t) - R(z,t)$. This must be exactly the change in the number of carriers per unit volume per unit time, so that

$$\frac{\partial n_{tot}(z,t)}{\partial t} = \frac{1}{q_e}\frac{dJ_{tot}(z,t)}{dz} + G(z,t) - R(z,t). \tag{2.3.26}$$

Our example does not include effects due to trapping, thus $n_{tot} = n_e$; however, we will use n_{tot} for completeness. Recall, from Eq. (2.3.24) that the total current in a system that has active diffusion is governed by

$$J_{tot}(z,t) = q_e n_e(z,t) \mu_e F(z,t) + q_e D \frac{dn_e(z,t)}{dz}. \tag{2.3.27}$$

We can now solve for the diffusion enhanced transport equation by combining Eqs. (2.3.26) and (2.3.27). This results in the following expression for the free carrier density:

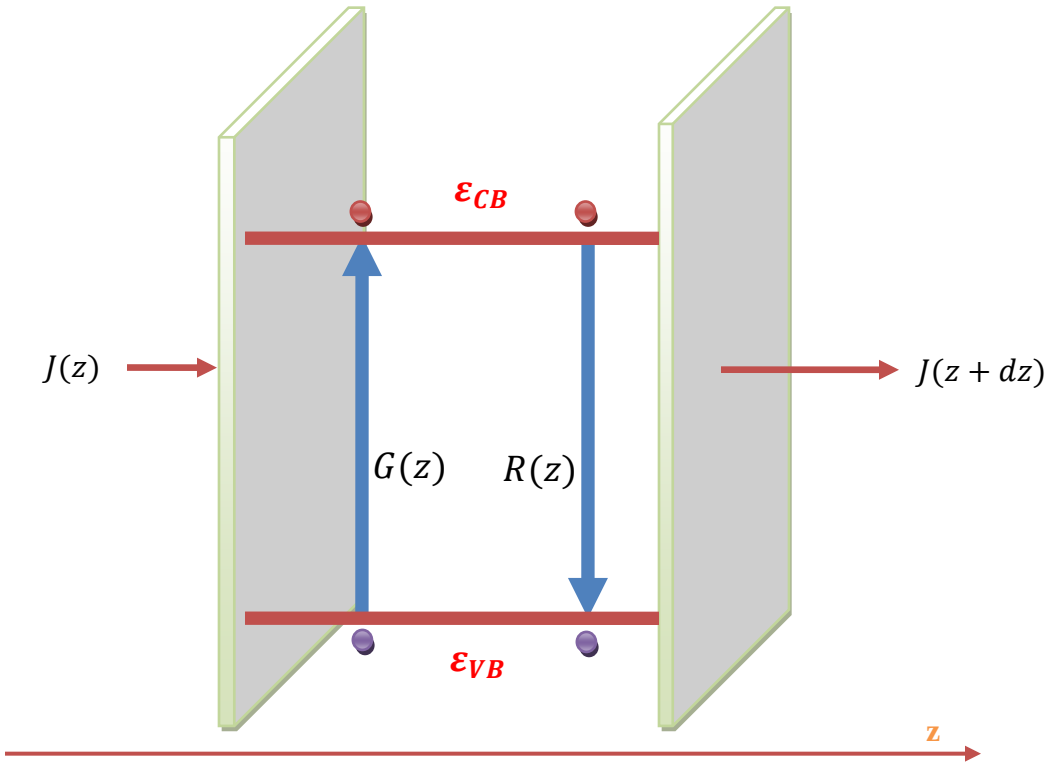

FIG 2.1. Effects of generation and recombination on the drift current flowing in the z direction. A sample bounded by two contacts is shown along with a simple reproduction of the conduction and valance band energies and with generation-recombination. The generation and recombination terms are charge source and sink terms, respectively.

$$\frac{\partial n_{tot}(z,t)}{\partial t} - \mu_e \frac{\partial}{\partial z}[n_e(z,t)F(z,t)] - q_e D \frac{\partial^2 n_e(z,t)}{\partial z^2} = G(z,t) - R(z,t). \quad (2.3.28)$$

This equation should look very familiar, as it is Eq. (2.3.16) with the addition of the diffusion term. In our example, the carrier generation is thermal and is not observable for wide band gap materials such as HDIM (thermal energy is insufficient to excite electrons across the gap in any measurable amount); only in systems with low flux and low fields does the diffusion term dominate the transport term. For further comments on the limitations of the diffusion model in the context of charging models see Sessler (1987) and Treadgold (1966).

When a radiation source is used to provide a larger excitation energy (much greater than the thermal energy), electrons can be populated across the gap (in the way suggested in our example) in larger numbers, drastically affecting the observed current. The reader should be alerted that in the radiation case, we may or may not have diffusion depending on the strength of the carrier density, applied field, and way

in which incident radiation is cast upon the sample, i.e., a uniform beam of electrons over a narrow region versus a beam that covers the sample to any number of other arrangements.

Having included the correction for diffusion, the one-dimensional transport equations can now be written as

$$J_{tot}(t) = q_e n_e \mu_e F(z,t) + q_e D \frac{dn_e(z,t)}{dz} \quad \{\text{Sum of currents } J_i\}, \tag{2.3.29}$$

$$\frac{\partial n_{tot}(z,t)}{\partial t} - \mu_e \frac{\partial}{\partial z}[n_e(z,t)F(z,t)] - q_e D \frac{\partial^2 n_e(z,t)}{\partial z^2} = G(z,t) - R(z,t)$$

$$\{\text{1D continuity with generation-recombination}\}, \tag{2.3.30}$$

$$\frac{\partial}{\partial z}(\boldsymbol{F} \cdot \hat{z}) = q_e \frac{n_{tot}(z,t)}{\epsilon_o \epsilon_r} \quad \{\text{1D Gauss's Law}\}, \tag{2.3.31}$$

and

$$\frac{dn_h(z.t)}{dt} = G(z) - \mathrm{R}(z) \quad \{\text{1D hole continuity with generation-recombination}\}. \tag{2.3.32}$$

These four equations describe the transport in terms of the electric field, temperature, position, and time. *G(z)* is driven by the dose rate of an external source. This can be any number of source types including heat, but is more generally used when the conductivity is enhanced by high-energy incident particles or light and largely refers to the internal generation of charge. The materials to which we can apply these equations are metals, semiconductors, and insulators. These ideas have been applied with great success to metals and semiconductors, but have seen limited application in the realm of HDIM.

What else need be considered? What happens when a material is not periodic or ordered, but disordered? Since the subject of this dissertation is transport in not only disordered but *highly* disordered materials, it is necessary to extend Eqs. (2.3.29) through (2.3.32) to include the effects of disorder. In the introduction to this chapter and Section 2.2, a series of processes were listed and briefly described. These processes are drift, diffusion, space charge limited current, and dispersion. The first two processes have been introduced and lead quite naturally to the transport equations. The last two require a detailed understanding of the nature and effects of disorder present in a material. We can view this as a transition from a perfect ordered world to one in which things are a bit more—and in some cases a lot more—messy. In principle, any number of processes can be evaluated by adding terms to the current density equation. As it turns out, approaching the problem from the sum of current densities becomes extremely cumbersome

beyond the inclusion of the drift and diffusion. The cumbersome nature will become clear in Section 2.6. Equations (2.3.29) through (2.3.32) are not yet complete and do not accurately describe the behavior of HDIM. The question is why?

Consider an electron beam normally incident on an insulating material. If the beam cannot penetrate the material, experimental observations by many researchers—including the USU MPG—have shown that a charge body will develop within the material resulting in a complex charge distribution. This distribution is dependent on the incident beam energy, beam fluence, temperature of the material, applied and internal electric field, and time; but most importantly, it depends of the nature of the disorder. The charge has become trapped by this disorder and the behavior of that trapped charge is entirely dependent on the material properties and any modification of those properties due to the environment. Therefore, a new description of the material beyond the simple band model is required. This is the subject of Sections 2.4 and 2.5.

2.4. Introduction to Disorder

How do the conductivity and mobility depend on the material properties when the crystalline order is significantly disturbed? The subject of this dissertation is the answer to this question for highly disordered insulating materials. These materials are generally wide band gap materials with considerable intrinsic and extrinsic disorder. The disorder results from a plethora of sources, including concentrations of impurity atoms, geometric irregularities, the geometry of polymer chains, and their impurities. Further, these materials are generally composed of polymer chains that do not lend themselves to the simplifications of a lattice construct and have a myriad of structural and internal degrees of freedom. Additionally, polar groups attached to the chains, crosslinking, and broken bonds have significant influence on carrier mobility (Wintle, 2003; Dennison *et al*., 2009e). This high level of disorder leads to a density of states (DOS) in the gap, with complex energetic and positional dependencies, which will drastically alter classical transport mechanisms.

In order to understand disorder in a physical way, develop a working picture of the interactions that affect transport, and provide a consistent theoretical framework upon which to extend current ideas, a simple, one-dimensional band model is presented by which we can study the effects of disorder. This

simple model starts from the crystalline point of view (upon which semiconductor theory is based) and is then extended to highly disordered systems. As it turns out, this simplified approach retains the basic notions of a more complete description of band structure and provides the necessary platform to describe in a compressive way why disorder affects the transport so dramatically. In particular, the introduction of localization of the atomic orbital wave functions, mobility edge, and a set of simple intraband disorder models provide a powerful basis to understand the answer to questions about transport in HDIM.

2.4.1. Crystalline to Disordered Insulators

Consider the situation depicted in Fig. 2.2 in which a collection of evenly spaced (1D) periodic identical atoms are brought close together. At zero temperature, and infinite separation, each isolated atom has highest occupied molecular orbitals (HOMO) and lowest unoccupied molecular orbitals (LUMO) with discrete, degenerate binding energies, respectively. As the atoms are brought together and the bonding and anti-bonding orbitals interact, they cause the discrete electron energy states of the individual atoms to form quasi-continuous bands separated by well defined "band gaps" (BG). The quasi-continuous symmetric bonding orbitals (HUMO) become a valence band and the anti-bonding orbitals (LUMO) become a conduction band. Fundamentally, the BG is an energy range in a solid where no allowed electron states exist. A simple calculation using the Kronig-Penny model will produce such a BG (Ashcroft and Mermin, 1976). Figure 2.2 depicts a simple representation of the DOS and band gap for a typical crystalline solid. This figure retains the basic notions of a density of extended states up to a band edge at the top of the valance band at energy ε_{VB} , a band gap $\varepsilon_{gap} = \varepsilon_{CB} - \varepsilon_{VB}$, and further extended states above the bottom of the conduction band at energy ε_{CB}. This simple model and extensions of it are used throughout this dissertation to explain the basic concepts of transport in disordered materials.

The distinction between conductors, semiconductors, and insulators follows from this purely quantum mechanical notion of a band gap in the DOS. The Pauli Exclusion Principle for fermions (electrons in this case) requires available states are filled at T=0 from lowest energies up to the Fermi energy, ε_F. If the threshold for filled states falls within a band, the material is a conductor with the first excited states an infinitesimal energy above ε_F. By contrast, for semiconductors or insulators, ε_F falls within a band gap and the first excited states is an energy ε_{gap} above the highest occupied ground state. The

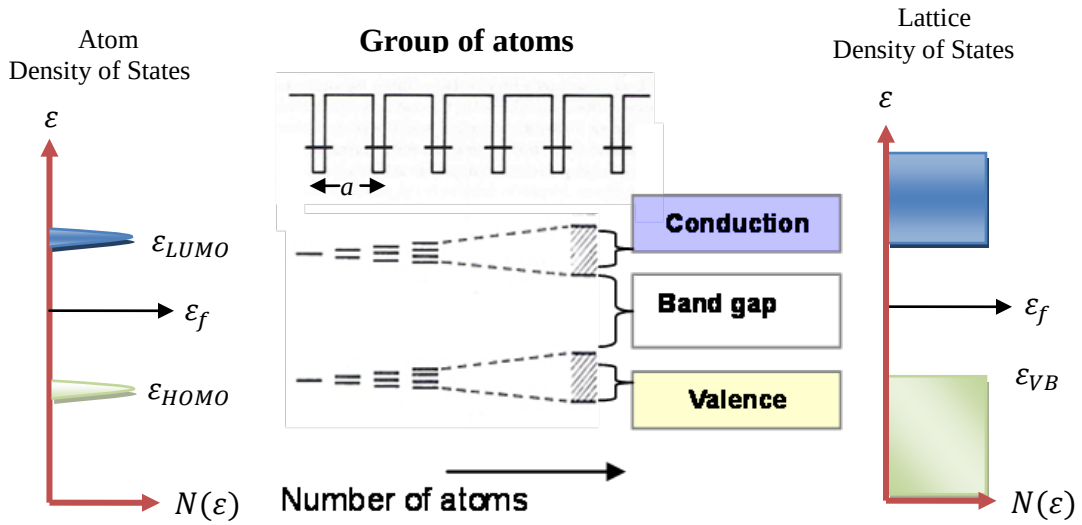

FIG 2.2. From single atoms to the density of states. Figure depicts the evolution of bands in a periodic arrangement of atoms (crystals) as atoms are brought together spatially. Here a is the atomic spacing, ε is the energy of a state, ε_{LUMO} is the lowest unoccupied molecular orbital, ε_{HOMO} is the highest occupied molecular orbital, ε_{CB} is the conduction band (energy upper-bound), ε_{VB} is the valence band (energy lower-bound), $N(\varepsilon)$ is the density of states and ε_f is the Fermi-level.

distinction between a semiconductor and an insulator is one of energy scale. If, at some finite temperature, there is a "reasonable" probability that electrons in the high energy tail of the Fermi distribution of the solid will have a thermal energy greater than ε_{gap}, the material is termed a "semiconductor"; otherwise, it is an "insulator." The occupation of the extended states determines the material's ability to transport charge. Thus, by definition, a "*highly insulating*" material is one in which there are very few, if any, conduction electrons in extended states.

Thus far, only crystalline materials have been discussed, along with their behaviors as a function of the band gap. A discussion of the deviations from simple ordered insulating materials is now prudent. Although there are many crystalline systems with band gaps sufficient to be called insulators, their behavior is consistent with an ordered system, in which a simple band gap structure is observed, (i.e., the band gap is empty). In simple insulating or semiconducting crystals, phonon scattering theory and intrinsic semiconductor theory predict the majority carrier mobility or conductivity quite well (Ashcroft and Mermin, 1976; Pope, 1982; Sah, 1991). Even for modest disturbances of the lattice, such as the introduction of dopants, the conductivity can be easily predicted. However, in many insulating materials

(polymers as the central example), the observed conductivity is not easily predicted due to extreme disorder (Fowler, 1956; Rose, 1961; Schmidlin, 1977; Blythe and Bloor, 2005).

There are many experimental results that directly highlight the difference between simple crystalline insulators and disordered systems (Anderson, 1958; Ashcroft and Mermin, 1976; Zallen and Scher, 1971; Pope, 1982; Sah, 1991; Blythe and Bloor, 2005), and many others from the extensive references cited in this dissertation. A clear example of this is found in measurements of the mobility of HDIM with respect to trap (impurity) concentration (Sah, 1991). Consider an impurity atom whose energy has been reduced from the CB edge either by intentional introduction of the impurity or by some disordered-induced mechanism acceptor that acts as a trap for free carriers. Since some time is required for the carrier to be released from the impurity trap, its progress is impeded. Thus, the higher concentration of trap states, the lower the mobility (Ashcroft and Mermin, 1976). This is in stark contrast to the introduction of a donor impurity that will be easily ionized in a standard semiconductor that results in increased electron mobility (Ashcroft and Mermin, 1976), and hence, an increase in conduction. The mobility of free carriers that results from disorder in HDIM is a defining factor in determining their behavior. In order to develop a working knowledge of why disordered systems behave in a fundamentally different way from metals and ordered semiconductors or insulators, it is necessary to present a detailed discussion of the origins of the disordered DOS in the band gap, the basic conduction mechanisms that involve the states in the gap, and their effects on mobility and subsequent conductivity.

2.4.2. Disorder

There are a number of ways in which a material may develop disorder, which is a deviation from a perfect periodic array of constituent atoms of infinite extent. These include disorder in atom type (or substitution disorder), positional disorder (e.g., vacancies, dislocations, or interstitials), finite size disorder (e.g., grain boundaries, surfaces and interfaces, and finite crystal size), and more exotic disorder (such as spin or magnetic disorder). Polymeric insulators can have particularly high disorder, and generally require very complex models of their structure and resulting DOS; the HDIM considered here are extreme examples of disorder in polymers. In HDIM, the polymer chains do not lend themselves to the simplifications of a lattice construct and have myriad structural internal degrees of freedom. Further polar

groups attached to the chains, crosslinking, and broken bonds have significant influence on carrier mobility (Wintle, 1991; Blythe and Bloor, 2005). These polar groups can also contribute to an overall material polarization, which influences the internal electric field felt by the carriers. Such disorder leads to deviations from the bonds of extended states and band gaps depicted in Fig. 2.2. The resulting localized states have energies within the band gap. In many cases, these localized states will move into the forbidden band gap and hence, form trap states for nearly free or injected electrons.

Before answers to questions about transport can be addressed, an explanation of the role of disorder in the localization of states leading to band tails, the mobility gap, and mobility edge must be discussed. The reader should be aware that there are disordered systems, such and polyacetylene, which are conducting under certain conditions. Disordered does not guarantee that the system will be insulating or localized (polyacetylene, for example, can be a disordered system and metallic.), but localized states do guarantee that the system will have a lower conductivity than the ordered counterpart. In this dissertation, the discussion of the effects of disorder will be limited to highly insulating materials whose transport characteristics are governed by disorder-induced localization.

2.4.3. Localization

To better understand the localized state, we first review the meaning of "localization" and discuss Anderson localization. There are many processes by which localization can occur. However, all such processes have a common concept. The idea is simple; through some process, the order of the system is disturbed altering the atomic orbital wave functions such that interactions with nearby states in the system are small as compared with the forces keeping the carrier localized. Figure 2.3 shows four diagrams for atomic wave functions that progress from extended states to strong localization. Consider the contrast between Fig. 2.3 (a)—which is an example of a periodic extended set of wave functions—in contrast to Fig. 2.3 (b). In Fig. 2.3 (b), an envelope has formed around a specific atomic site whose wave function has become localized. This is, in essence, what all localized states look like if viewed in terms of their wave functions. This picture is useful to visualize localization, but lacks the relevant detail to completely describe the problem. Now consider Fig. 2.4, which depicts the transition in DOS from a crystalline material to a disordered one, and is the next step in the evolution of our simple DOS model. In this figure,

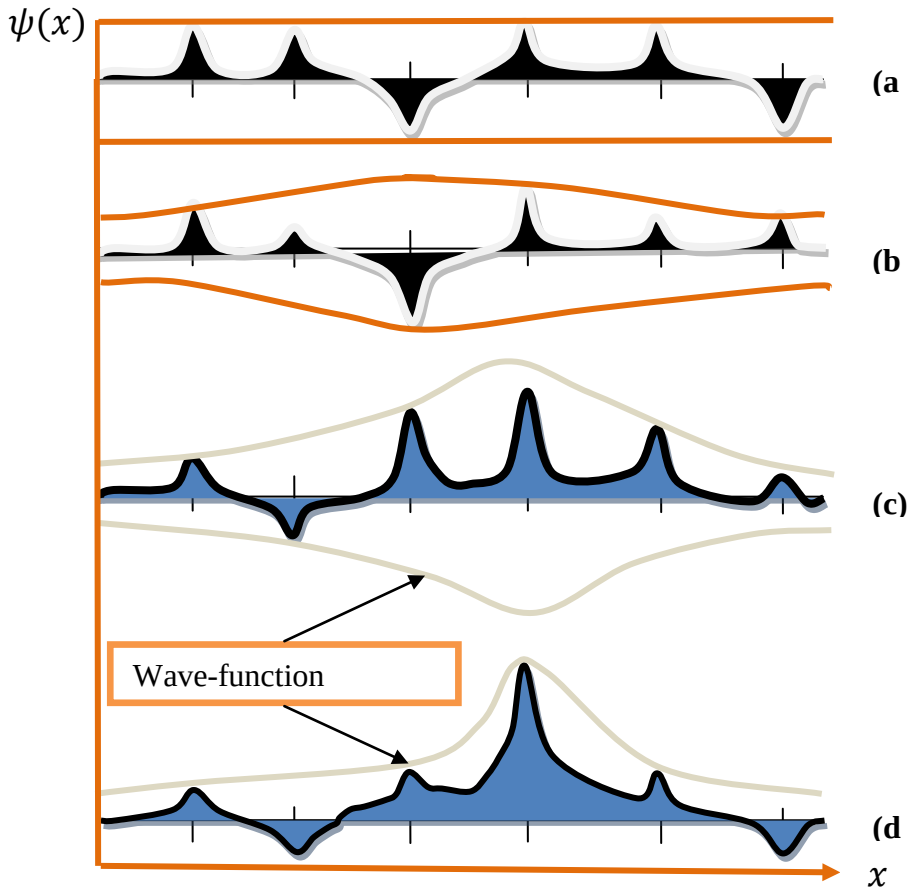

FIG 2.3. Schematic illustration of the form of the electron wave function in the Anderson localization model. (a) When the wavefunction extent is on the order of or greater than the lattice spacing. (b) When states are just nonlocalized, such that $\varepsilon \geq \varepsilon_c$. (c) When states are just localized, such that $\varepsilon \leq \varepsilon_c$. (d) Strong localization. After Mott and Davis (1979).

the disorder in the potentials is driving the dispersion of the DOS into the gap. Figure 2.3 showed the atomic view and Fig. 2.4 is the macroscopic one-dimensional average DOS view. How can we quantify this process and understand what the mobility edge means?

A seminal form of localization was proposed by Anderson (1958) and later adapted to explain conduction in semiconducting materials with doping (Mott, 1961, 1973, 1977, 1981, and 1984; Mott and Davis, 1979). Anderson asked how much energetic disorder is required to induce nearly free conduction in a system whose wave functions do not overlap significantly (Pope, 1982). Anderson worked from a localized disordered point of view toward a less disordered system in which extended conduction just begins to occur, often referred to as a percolation threshold (Zallen, 1983). Consider a system that is localized, with many random atomic energies due to disorder (see Fig. 2.4). The energy of a given site, ε_j,

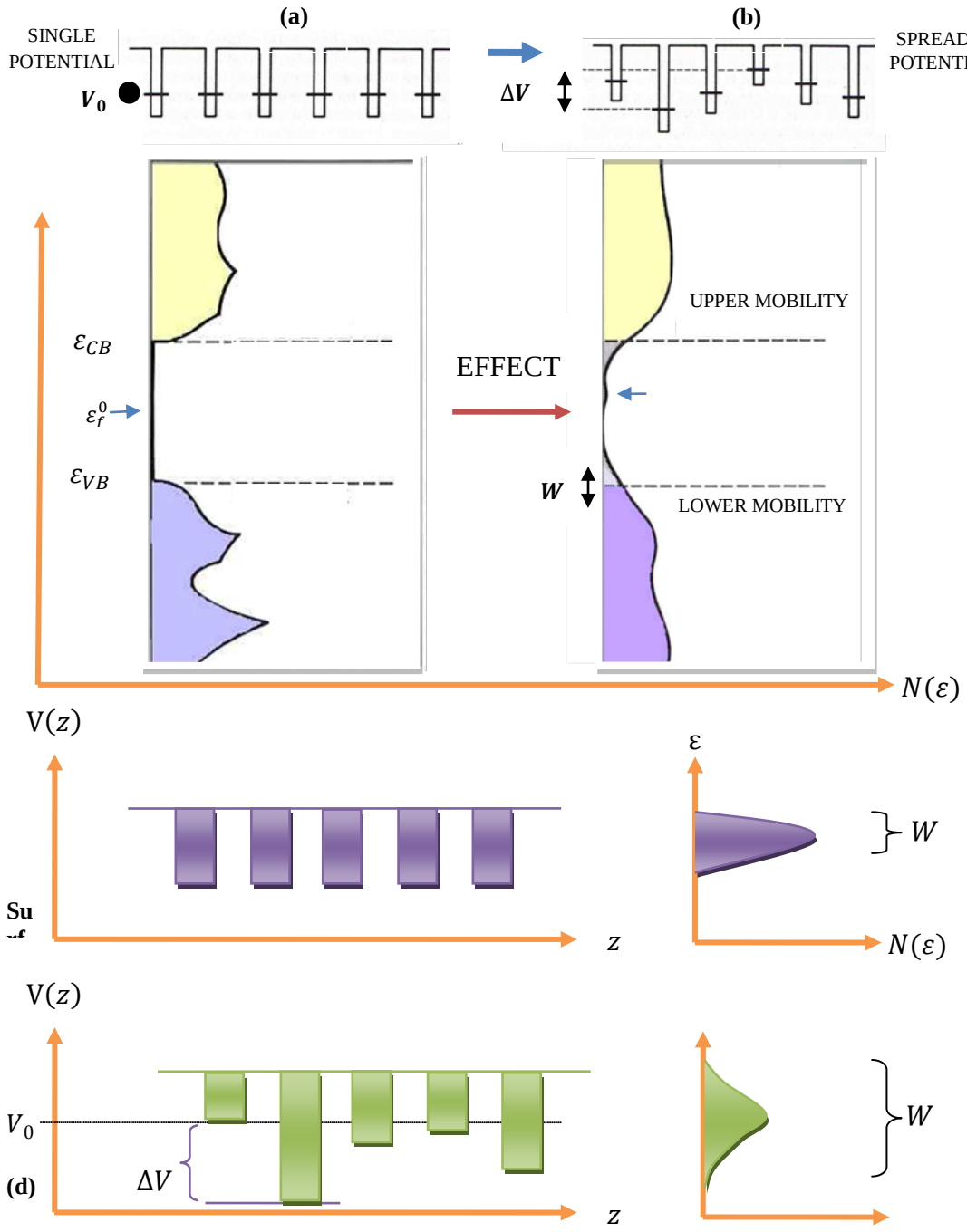

FIG 2.4. The effects of disorder on the crystalline DOS. (a) The DOS diagram for a simple crystal potential. When the potentials of the wave functions are disturbed, a spread of potentials is created of width, **W**. This leads of a spreading of the states at or near the CB edge into the gap, as shown in (b). When strong disorder is introduced, the concepts, of CB or VB edges are no longer valid. The CB and VB edges are replaced with the disordered counterpart, the mobility edges. (c) Periodic potential and resulting DOS distribution, with width, **W**. (d) Anderson model with random potential ΔV added to potential well depth and the resulting DOS distribution with wider width, **W.**

is a random variable, independent of time. The probability function describing the spread in values in ε_j for all the particles in the system is given by a width, *W*.

Anderson showed that when the interaction between sites *j* and *k*—given by some average potential, $<V_{jk}>$—is less than a critical value, V_c, no extended transport occurs. This critical value is suggested in Figs. 2.3 (b) and 2.3 (c) but not explicitly defined. As a first step in a quantitative description, we make a distinction between localized and delocalized states with the relations

$$\langle V_{jk} \rangle > V_c \tag{2.4.1}$$

for extended states, and

$$\langle V_{jk} \rangle < V_c \text{ and } \langle V_{jk} \rangle = \frac{W}{C_0} \tag{2.4.2}$$

for localized states. Here C_0 is a numerical constant, which will be defined shortly.

Alternatively, consider the behavior of a localized state system at *T*=0 (Zallen and Scher, 1971; Elliott, 1990; Legendijk *et al.*, 2009). From a practical point of view, if one observes an electron at site *j* with energy, ε_j, from some time, *t=0,* to a much later time and finds the electron stays in the region in which it started, the state is said to be localized and the electron is, in some sense, trapped. In this view, the electron has a finite probability of remaining within some radius of the initial state and therefore, has little or no chance of diffusing away. This suggests that the spread in energies *W* means localized states develop tails that extend well into the BG, hence their name *band tail states*. These band tails can be seen in Fig. 2.4 (b) extending into the once empty BG.

The description of the effects of localization has thus far only been described qualitatively. As it turns out, the complete mathematical description originally given by Anderson is quite complex. However, in order to gain a basic understanding of the interaction of wave functions shown in Fig. 2.3 and connect those ideas to the dispersion of energies, *W,* shown in Figs. 2.4 (b) and 2.4 (d), a simple model can be developed.

A simple, but compelling, discussion of the Anderson localization criteria that provides quantitative insight into how and why this physical process occurs is presented using a 3D Kronig-Penny potential model (Böer, 2002) with a potential energy well depth

$$W = 2\hat{m}I, \tag{2.4.3}$$

where the transfer integral is

$$I = \int \psi^*(r - R_j) H \psi(r - R_{j+1})\, dr. \tag{2.4.4}$$

The value, W, is the band width, R_j is the location of the j^{th} atom, $\widehat{m}$ is called the coordination number (the average number of adjacent accessible sites), and I is the transfer integral. Assuming hydrogen-like potentials (a good approximation for Coulomb centers), the transfer integral can be written as

$$I = I_0 exp\left[-\frac{r}{r_0}\right], \tag{2.4.5}$$

with

$$I_0 = \left\{\frac{3}{2}\left(1 + \frac{r}{r_0}\right) + \frac{1}{6}\left(\frac{r}{r_0}\right)^2\right\}\sqrt{\frac{2m_e e^2 \varepsilon_{\mathrm{gnd}}}{\hbar}}. \tag{2.4.6}$$

Here the value ε_{gnd} is the ground state energy of the wave function and the value $r_0 = \sqrt{\frac{\hbar^2}{2m\,\varepsilon_{gnd}}}$ is a characteristic fall off radius for the wave function (not quite a localization radius); for further detail, see Böer (2002). Given this simple model, the question can be asked what happens when we take a crystal potential centered about some average well depth, V_0 (see Fig. 2.4a) and perturb it by some change potential (well depth), $\pm\Delta V$. Clearly, this will produce a broader level energy distribution and create tails above and below the original CB edge (see Fig. 2.4b). Assuming a small $\Delta V << V_0$, (Mott and Twose, 1961) obtained the following approximation for the mean-free path of an electron,

$$\lambda = \frac{\hbar}{\pi}\left(\frac{2}{\Delta V}\right)^2 \frac{v_e}{a^3 N(\varepsilon)}. \tag{2.4.7}$$

Here a is the mean separation of defects to trap sites.

Using the well-known, nearly free electron approximation for the DOS near the band edge (Ashcroft and Mermin, 1976)

$$N(\varepsilon) = \frac{1}{2\pi^2}\left(\frac{2m_e^*}{\hbar^2}\right)^{3/2}\sqrt{\varepsilon}\, d\varepsilon, \tag{2.4.8}$$

Böer (2002) has shown that Eqs. (2.4.7) and (2.4.8), in the limit of small ΔV, become

$$\frac{\lambda}{a} = 32\pi\left(\frac{I}{\Delta V}\right)^2 = \frac{8\pi}{\widehat{m}^2}\left(\frac{W}{\Delta V}\right)^2. \tag{2.4.9}$$

Solving Eq. (2.4.9) for W and isolating the parameter, ΔV, the following expression for the spread of energies in terms of the change in potential is

$$W = \left(\frac{\lambda}{a}\frac{\hat{m}^2}{8\pi}\right)^{1/2} \Delta V. \tag{2.4.10}$$

This result makes quantitative contact with the phenomenological expression given in Eqs. (2.4.1) and (2.4.2). The constant in Eq. (2.4.1) is now shown to be $C_0 = \sqrt{\lambda\hat{m}^2/a8\pi}$. The condition for localization is $\frac{\lambda}{a} \lesssim 1$. An estimate of ΔV can now be made if we chose the coordination number, $\hat{m}$, to be ~ 4 typical for tetrahedrally bonded semiconductors; Eq. (3.1.14) suggests localization will occur for $\Delta V \gtrsim 0.35\, W$. For a complete review of these concepts and a detailed approach to estimating the change in potential required to cause disorder see Ramakrishna (1985) in Böer (2002). In the Anderson analysis, the problem of localization is treated in a much more rigorous way with attention paid to the subtle details. The expression obtained by Anderson, however, is essentially the same. For estimations of more accurate localization criterion and for definitions of more complex DOS, see Thouless (1974). For a detailed discussion of Anderson localization see Anderson (1958), Mott (1961), Mott and Davis (1979), Blythe and Bloor (2005), and Baranovskii and Rubel (2006),

This section developed a model for the process of localization, dispersion of states into the gap, and the understanding that our simple picture of transport from Section 2.3 is inadequate. The remaining questions regard the value of the DOS in the gap and the effect a specific distribution has on the mobility and subsequently, the conductivity.

2.4.4. The Mobility Edge

What is the effect of localization and the resulting DOS in the BG on the mobility of carriers? Figure 2.5 shows a hypothetical model DOS in which many of the major elements that comprise our discussion are presented. In particular, the effect of the DOS $N(\varepsilon)$ on the mobility (blue line) is depicted. When a system becomes localized, the energy-dependent mobility, $\mu(\varepsilon)$, is dramatically reduced due to the effects of the DOS in this gap. This is precisely why we see the blue line nearly vanish at the edge of the shallow and intermediate disordered states. Localized states within the band gap are now separated from extended states by a *mobility edge*—at an energy ε_{ME} —instead of a band edge; the region where there is negligible mobility is, therefore, called the *mobility gap*. The diagram also shows that varying degrees of localization and impurities can exist within the mobility gap and will alter the mobility. Since, on average,

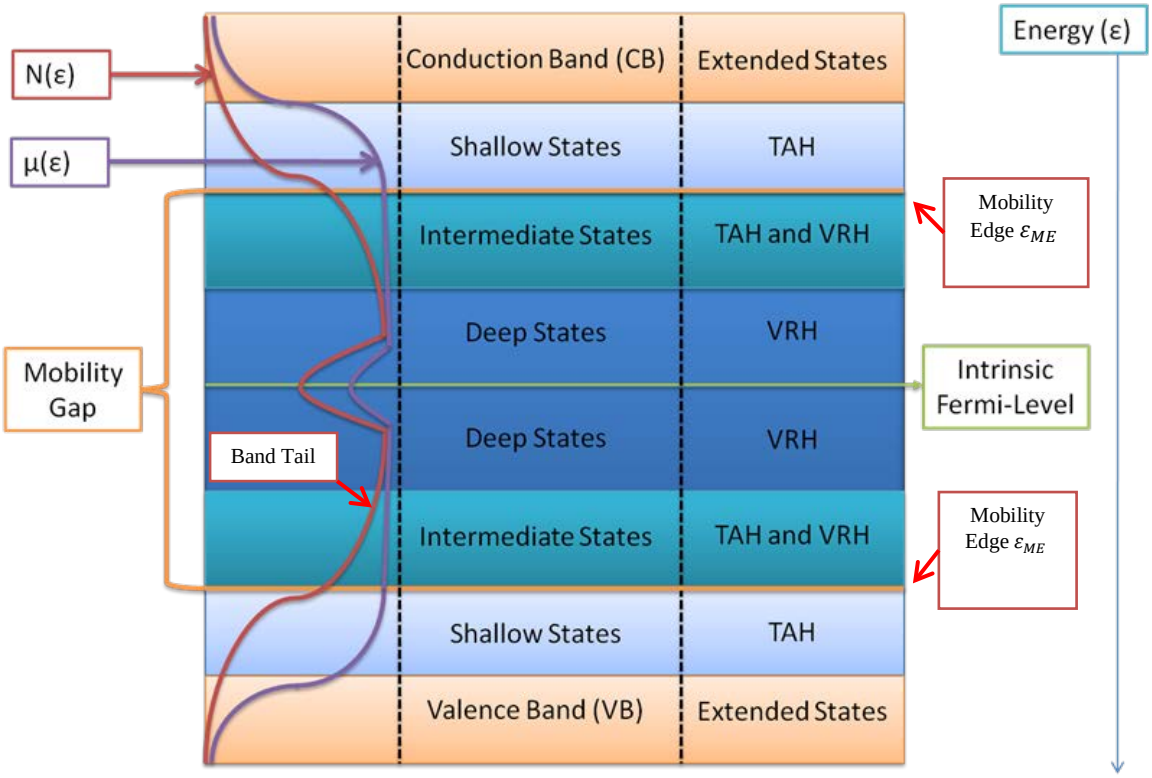

FIG 2.5. Composite density of states and mobility plot contrasted with conduction mechanisms. Figure identifies the regions within the DOS that participate in specific temperature-dependent phenomena; this is contrasted with the resulting mobility. Thermally activated hopping TAH controls the high-temperature behavior and variable range hopping (VRH) controls the low-temperature behavior. Typical band conduction begins at the mobility edge and increases with increasing energy; below the mobility edge (in the mobility gap) conduction proceeds by hopping.

the DOS often decreases away from the mobility edges towards the center of the gap, the energy regions of localized states in the vicinity of the mobility edges are called *band tails* (Baranovskii and Rubel, 2006). The dispersion or band tailing of states into the band gap is caused by Anderson localization. These tales are also referred to as Lifshitz or Urbach tails (Böer, 2002).

Halperin and Lax (1966) developed a quantum-mechanical theory for deeper tail states, based on the statistical fluctuation of the potential, ΔV, by lattice defects that incorporate a more realistic DOS than used in our description of localization, Eq. (2.4.8). The advantage of the Halperin approach is that it connects the Bohr radius, screening length, and correlation distance directly with an exponentially decaying DOS into the band gap (Böer, 2002).

Experimentally, band tails, and DOS distributions have been verified by several methods. Optical absorption is a popular experimental technique that yields information about the basic structure of the DOS in the gap. Shklovskii *et al.* (1971) have experimentally studied the optical absorption spectrum for amorphous materials. Their data suggest a strong dispersion of states into the BG. Unfortunately, the absorption spectrum only gives a rough sense of the nature of the DOS, as there may be many factors determining the overall structure. The effects of disorder, resulting DOS, and mobility can be experimentally tested in many way; these methods include optical absorption (Shklovskii *et al.*, 1971), thermally stimulated current emission (Ieda, 1984; Sessler, 1987; Arkhipov and Adriaenssens, 1995; Baranovskii and Rubel, 2006), electron spin resonance (ESR), and observation of the current (Monroe, 1985; Baranovskii and Rubel, 2006). Shklovskii (1984) and Böer (2002) give reviews of these ideas; Shklovskii provides the more detailed approach. Using the experimental techniques above and numerous theoretical endeavors, a set of DOS models has been determined, which allow for a physical understanding of the mobility edge, changes in the mobility, and transport phenomenal in general. This is the subject of the next section.

2.4.5. Density of States Models

We now return to a description of the energy distribution of the localized states found between the mobility edges, shown in Fig. 2.4 (b) and highlighted in Fig 2.5. Both of these figures suggest that there is more than one type of distribution necessary to describe the DOS in the mobility gap. One needs to consider at least two types of distributions, one that monotonically decreases from the band edge and one that shows a peak in the distribution within the BG. It is shown below that an exponential and a Gaussian DOS are appropriate models for these two general types for localized DOS. Many authors have used this fact in deriving expressions for the conductivity (Muller, 1963; Thouless, 1974; Davis, 1985). Often in the calculation of relevant integrals, the use of an exponential distribution is easier than even a constant. Thus, we can imagine a situation in which a calculation is done with an exponential DOS seeking a solution to a constant DOS; this method was used by (Muller, 1963) and has also been used by Monroe (1983, 1985, and 1986) and Davis (1985) to obtain expressions for the conductivity.

For the sake of completeness and to make ties to older literature, we consider six specific DOS modes as shown in Table 2.1 and Fig. 2.6. These are classified by three monotonically decreasing models [Linear, Fig. 2.6 (c); Power law, Fig. 2.6 (d) and Exponential, Fig. 2.6 (e)] and three peaked models [delta function, Fig. 2.6 (a); constant, Fig. 2.6 (b) and Gaussian, Fig. 2.6 (f)]. It should be noted that in this dissertation, all the DOS are functions of energy measured from CB edge toward the VB. This is often a source of confusion in the literature, as many authors will measure energy from the center of a distribution; the Gaussian DOS is a good example of this type of notation confusion (Baranovskii and Rubel, 2006). Note that the total DOS over a specific energy region in the BG, N_t, can be obtained by integrating the DOS distribution, $N(\varepsilon)$, over the effective energy region (not the entire BG, as this may include additional DOS or provide erroneous values when the distribution is integrated over regions where the DOS does not exist). Each DOS model is characterized by an energy scaling or width factor, ε_0^i (where i is the type of DOS), and ε_0^t (the first moment, based on the centroid of the distribution, given by $\frac{\int_0^\infty \varepsilon N(\varepsilon)d\varepsilon}{\int_0^\infty N(\varepsilon)d\varepsilon}$). For example, ε_0^p is the scaling energy for the power law DOS.

The interested reader may be concerned that the use of un-normalized DOS models will lead to erroneous values when performing calculations, which is correct, and unfortunately has occurred many times in the literature as many authors are concerned only with general behavior and not the magnitudes involved. The process of normalizing a given DOS is the same as for any such process; calculate the integral of the DOS distribution over the energetic interval that it spans, divide by the total DOS, and make sure you get one, i.e., $\int_{\varepsilon_{low}}^{\varepsilon_{high}} \left(\frac{N(\varepsilon)}{N_t}\right) d\varepsilon = 1$. This normalization is specific to the type of DOS and the region of energy that it spans; therefore, it should be calculated in each specific case! We, therefore, do not compute the normalization here, but only provide the DOS models in Table 2.1 along with a few representative centroid calculations; these are NOT complete centroid calculations and should be calculated for each DOS over each regions that a specific DOS spans in the BG. The reader is referred to Gillespie (2013) for calculations of normalization and moments of the distributions in Table 2.1. Unfortunately, in the literature, there are many cases where the DOS is used in an un-normalized form as only general characteristics were of interest to those authors. A considerable amount of work is required to re-derive each result (as we will see in Chapter 3), and that task is, therefore, left as future work. Further, there are a

TABLE 2.1. Density of states models.

Type of DOS Function	DOS Expression	Scale Factor (Width)	Centroid (Examples Only)
a) Delta	$N(\varepsilon) = N_t \delta(\varepsilon_0^t - \varepsilon)$	$\varepsilon_0^G \to 0$	ε_0^t *All intervals*
b) Constant	$N(\varepsilon) = (N_t / \varepsilon_0^c)$	ε_0^c	$\varepsilon_0^t \sim \frac{\varepsilon_0^c}{2}$ *Finite interval*
c) Linear	$N(\varepsilon) = \frac{N_t}{{\varepsilon_0^l}^2}\varepsilon$	ε_0^l	$\varepsilon_0^t \sim \left(\frac{2}{3}\right)\varepsilon_0^l$ *Finite interval*
d) Power	$N(\varepsilon) = \frac{N_t}{\varepsilon_0^p}(\varepsilon/\varepsilon_0^p)^P$	ε_0^p	$\varepsilon_0^t \sim \left(\frac{P+1}{P+2}\right)\varepsilon_0^p$ *Finite interval*
e) Exponential	$N(\varepsilon) = (N_t/\varepsilon_0^e) exp(-\varepsilon/\varepsilon_0^e)$ $\varepsilon_0^e \equiv k_b T_0^e$	ε_0^e *(1/e width)*	$\varepsilon_0^t \sim \varepsilon_0^e$ $infinite\ interval\ only$
f) Gaussian	$N(\varepsilon) = \frac{N_t}{\varepsilon_0^G\sqrt{2\pi}} exp\left(-(\varepsilon - \varepsilon_0^t)^2 / 2{\varepsilon_0^G}^2\right)$	ε_0^G *(Standard Deviation)*	ε_0^t infinite $interval\ only$

number of results in Chapter 3 that are discussed, but not derived. Thus, the form of the DOS models presented here are such that a connection to the normalization, and older literature from which the results are taken, and future work can be made. They will not be modified for this reason.

Taken together these six models represent nearly all the expressions used in the literature to describe transport. They are:

(a) *Delta function DOS*: Perhaps the oldest DOS model is the delta function, with a single well-defined trap energy, ε_0^t. It is useful in many applications, monotonically doped crystalline semiconductors as an example. In addition, in complex dynamic trapping models where analytical solutions are difficult, the use of this DOS allows for a first order expression of the model. It is shown below that this model is a limiting case of a Gaussian DOS, with a negligible width.

(b) *Constant DOS*: The constant DOS is perhaps the most well known model, as it was first used (in a slightly different form) to describe VRH (Mott, 1961). In the derivation of the VRH models by Apsley and Hughes (1975), this model takes center stage. Baranovskii and Rubel (2006) have shown that this model and VRH can be described in the context of the Gaussian DOS in the limit of infinite width,

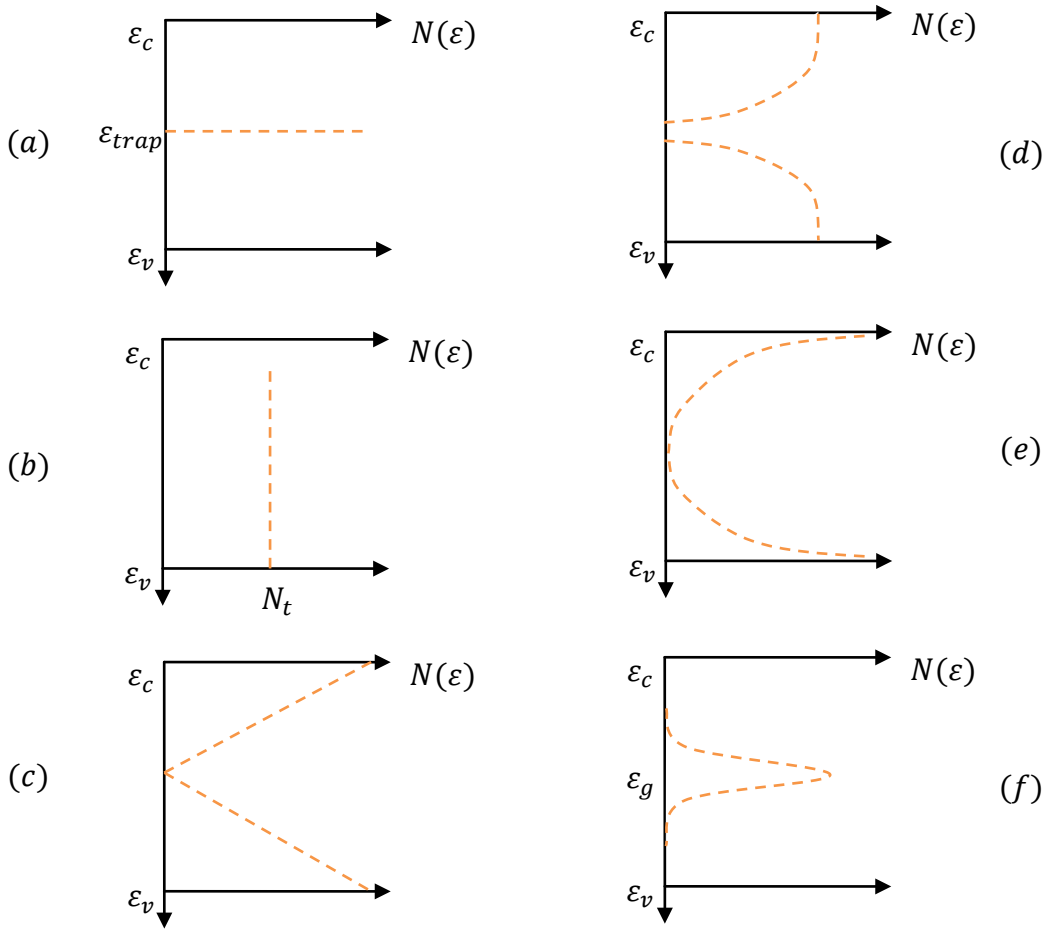

FIG 2.6. Profiles for the density of states models. This figure shows the energy profile of the density of states for six types of distributions. (a) Delta function DOS centered at energy, ε_{trap}. (b) Constant DOS. (c) Linear DOS. (d) Power law DOS. (e) Exponential DOS. (f) Gaussian DOS centered at energy, ε_g.

$\varepsilon_0^G \rightarrow 0$ on the interval $0 < \varepsilon < \varepsilon_0^t$. Further, Muller (1963) and Davis (1985) have shown that the constant DOS is the small energy limit of an exponential DOS (see below).

(c) *Linear DOS*: Used in the early analytical and computational descriptions of energy- dependent DOS models, it can be expressed in terms of an exponential; this can be seen by expanding the exponential DOS for small energies and keeping the first term. The linear model is, therefore, obsolete, except perhaps in special cases where a linear approximation can simplify the mathematics (This author is aware of no such cases). The linear model has a range on the interval $0 < \varepsilon < \varepsilon_0^l$.

(d) *Power Law DOS*: Used in the early descriptions of energy-dependent DOS models. This follows reasonably from the power law-like behavior of conduction band states in crystalline materials, such as Eq. (2.4.8) for which the power, p →1/2. In practice, this DOS has been replaced by the exponential and Gaussian models and is no longer being used. Baranovski suggests that this type of DOS does not describe any known behavior in HDIM (Baranovskii and Rubel, 2006). The power law model has a range limited to $0 < \varepsilon < \varepsilon_0^p$. The constant and linear DOS models are special cases of the power DOS model with p = 0 and p = 1, respectively.

(e) *Exponential DOS*: The exponential DOS is one of two prevalent models for HDIM. In fact, this DOS model is one of two that comprise the most powerful tools in understanding disordered transport (Scher and Montroll, 1975; Monroe, 1985; Zallen, 1983; Baranovskii and Rubel, 2006). The other model is the Gaussian DOS; it is discussed below. In Section 2.6, it is shown that the exponential DOS is responsible for a type of transport called dispersion, and in Chapter 3 it is shown that the exponential DOS leads naturally to a description of low-temperature transport, which cannot be predicted by systems without a DOS in the gap. Recall that in the introduction to this section, it was mentioned that the exponential and Gaussian DOS models were sufficient to predict behaviors resulting from the other four DOS model listed in Table 2.1. To make that point clear, a discussion of the scope of the exponential distribution is given in terms of other DOS.

The exponential DOS can be expanded as a power series in small energies, $\varepsilon \ll k_b T_0^e$—where T_0 is called a characteristic temperature that determines the strength and shape of the DOS—leading to constant, linear, or parabolic terms in the DOS and $\varepsilon_0^e \equiv k_b T_0^e$ so that

$$N(\varepsilon) = \frac{N_t}{k_b T_0^e} \exp\left(-\frac{\varepsilon}{k_b T_0^e}\right) = \frac{N_t}{k_b T_0^e}\left(1 - \frac{\varepsilon}{k_b T_0^e} + \frac{1}{2}\left(\frac{\varepsilon}{k_b T_0^e}\right)^2 + \cdots\right). \tag{2.4.11}$$

The relative strength of each term is determined by the magnitude of the energy, ε, with more terms needed for larger energies. For small energies or very large dispersion, we obtain a constant DOS; for large energies and modest dispersion, the full exponential distribution character is required. In the materials considered in this work, and HDIM in general, the exponential DOS and subsequent constant DOS are more than satisfactory for describing material behavior.

(f) *Gaussian DOS*: This DOS distribution is the second prevalent model used to describe HDIM. The prevalent use of amorphous materials in copier elements and display materials has brought about intense study of random organic solids [see Baranovskii and Rubel (2006) and references therein on p. 240]. Study of these materials has led to the use of a DOS that describes *pi*- or *sigma*-bonded main chain polymers, polyvinalcarbozal, as an example. The width of the energetic distribution is given by ε_G and the center of the distribution is ε_0^t.

The Gaussian DOS can be expanded as a power series in small energies, $(\varepsilon - \varepsilon_0^t) \ll \varepsilon_G$,

$$N(\varepsilon)\frac{N_t}{\varepsilon_0^G\sqrt{2\pi}}exp\left(-(\varepsilon-\varepsilon_0^t)^2/2{\varepsilon_0^G}^2\right) = \frac{N_t}{\varepsilon_G\sqrt{2\pi}}\left(1-2\left(\frac{(\varepsilon-\varepsilon_0^t)}{2\varepsilon_0^G}\right)^2+\frac{1}{2}\left(\frac{(\varepsilon-\varepsilon_0^t)}{2\varepsilon_0^G}\right)^4+\cdots\right). \quad (2.4.12)$$

For $(\varepsilon - \varepsilon_0^t)/\varepsilon_0^G$, it can be seen that if ε_0^G is large or the energy (as measured from the center, ε_0^t) is very small, this system should act like a constant (energy-independent DOS). Conversely, if the width of the distribution $\varepsilon_0^G \to 0$, then the Gaussian DOS will act like a delta function (Jackson, 1998). The former has been shown to produce VRH behavior (Mott and Twose, 1961; Baranovskii and Rubel, 2006). To this author's knowledge, using the Gaussian DOS as a delta function approximation in HDIM for the calculation of transport characteristics has never been considered. (It may be obvious.)

This section outlined six types of DOS distributions and reduced this set to two distributions, the exponential and Gaussian DOS models. A good description of the nature of the DOS is clearly important in understanding the nature of transport. However, the machinery to use this information has not been presented. One more set of ideas is needed before developing this needed mathematical machinery. How do the carriers interact with the DOS? This is the subject of the next section and it will be shown that the energy dependence of a given localized state is critical to understanding how long a carrier will remain trapped, thus determining the carrier lifetime and mobility.

2.5. Interacting with Disorder

At this point, it is clear that the picture of conduction in HDIM's is complex, requiring a deep understanding of the nature of the DOS and the way in which carriers in extended states interact with localized states in the gap. This subject is, in and of itself, very extensive, and is greatly simplified here to present only the basic notions required to understand the dynamic nature of transport in HDIM. The understanding of carrier capture and release, in addition to inter-band and intra-band interactions, is built on

the semiconductor and amorphous semiconductor fields (Rose, 1951, 1963; Mott and Twose, 1961; Ambegaokar *et al.*, 1971; Rudenko and Arkhipov, 1979, 1982a, 1982b, 1982c; Arkhipov and Rudenko, 1979; Arkhipov *et al.*, 1979, 1985a, 2006; Blythe and Bloor, 2005).

Fundamentally, the interactions of localized states with carriers, both within the mobility gap and between localized and extended regions, are based on thermal statistics. When a carrier is injected into an extended state above the mobility edge, that carrier will begin to lose energy through interactions with the material's local atomic structure. This process is generally called thermalization. Thermalization continues until that carrier no longer has enough energy to escape from some localized potential well. At this point, that carrier is considered captured or trapped. Once trapped, the release of the carrier is dependent on the phonon spectrum that imparts energy to the trapped carrier. Thus, the question becomes how long will the carrier remain trapped before receiving the necessary energy to escape. That is, what is the lifetime of the carrier in the trapped state? The answer depends on the material's temperature, and the energy needed for the carrier to be released (the well depth of the state in the gap).

The conductivity is a function of both the number of carriers in the extended states, the applied field, and the mobility of those carriers [see Fig. (2.2.1)]. The mobility is connected to the lifetime of a carrier both in a trapped state and in the CB:

$$\mu_{trap} = \frac{\tau_{CB}}{\tau_{CB}+\tau_{trap}}\mu_e. \tag{2.5.1}$$

Here μ_{trap} is the reduced trap mobility, τ_{trap} is the lifetime of a carrier in a trapped state, μ_e is the trap-free mobility (the mobility in the CB extended states), and τ_{CB} is the lifetime in the CB.

In order to give a clear description of the interaction of carriers with disorder, a simple band model is introduced. Figure 2.7 shows this model with a delta function DOS and a single trapping process. This model is the discreet counterpart of Fig. 2.4 (b), and is commonly used to describe extrinsic doped semiconductor behavior. The power of this model will become clear below and in Section 2.8, as will the ease with which we can include a full description of the effects of disorder.

How can we quantify the interaction of carriers in extended states using the picture in Fig. 2.7? It turns out that a simple rule used in many transition rate problems can be applied to develop our understanding of carrier interactions with disorder. The transition rate between two sites A and B, $\frac{dAB}{dt}$ is

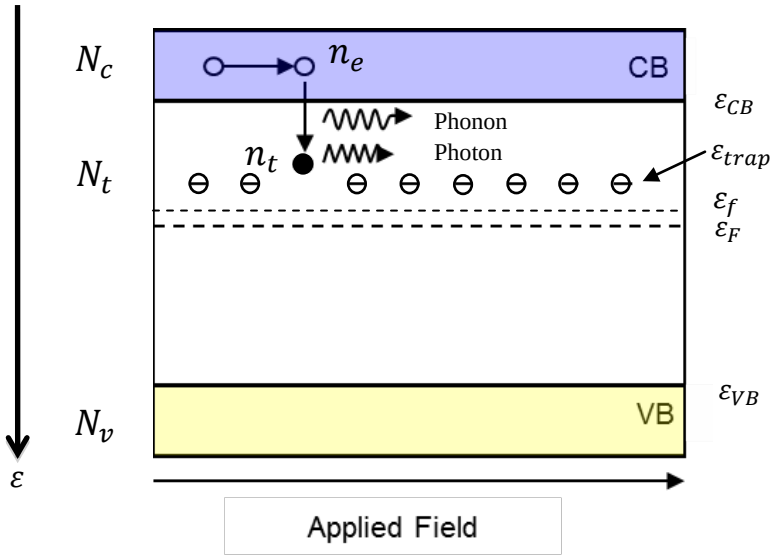

FIG 2.7. A simple DOS model. This figure shows a simple delta function DOS model centered at ε_{trap}, dark Fermi-energy, ε_F (heavy dashed line), Fermi-level, ε_f (light dashed line), number of carriers in the CB (extended states), n_e, density of traps, N_t, in BG, density of conduction states, N_c (blue region), and density of valence states, N_v (tan region). Here a single transition from the CB to a trapped state, n_t, is shown with the release of phonons or photons. Free electrons are denoted by an empty circle, empty traps by a dash, and filled traps by a black circle.

given by the product of an interaction coefficient, α_{AB}, some number of participating particles, N_A, at site A, some number of B sites, N_B, to which those particles can go, and the probability that the transition will occur, f_{AB}.

$$\frac{dAB}{dt} = \alpha_{AB}\, N_A N_B\, f_{AB}. \tag{2.5.2}$$

The transition rate $\frac{dAB}{dt}$ might be the rate at which electrons leave the conduction band and fill a trap state, then $\frac{dAB}{dt} \rightarrow \frac{dn_{et}}{dt}$; in that case $\alpha_{AB} \rightarrow \alpha_{et}$, $N_A \rightarrow n_e$, $N_B \rightarrow N_t$, and $f_{AB} \rightarrow f_{FD}$, where f_{FD} is defined as the Fermi-Dirac distribution function. This is exactly the process described in Fig. 2.7. An extended discussion of the application of Eq. (2.5.2) will be given in the following sections. Equation (2.5.2) essentially describes all the interactions with disorder that we will encounter in this dissertation. It provides the connection between microscopic and macroscopic physical processes in the HDIM. An example of how this concept is used is given below and expanded upon in Section 2.6 to define the trapping equations. First, a discussion of each of the terms in Eq. (2.5.2) is needed.

This discussion begins with the interaction coefficient and its constituent parts and concludes with a discussion of carrier release (ionization) and the distribution function f_{AB} (in this case, the Fermi-Dirac distribution function). Along the way, several of the ideas surrounding Eq. (2.5.2) will be considered including capture cross sections, carrier lifetimes, carrier release, and the Poole-Frenkle effect. This section will conclude with a discussion of Eq. (2.5.2) as an example to explain carrier capture into a trapped state from the conduction band.

The interaction coefficient describes the strength of the interaction between some group of participating particles (carriers or trapped electrons, in this case) and the place to which those particles will go (traps, the CB or recombination with holes in the VB). It is the product of a capture cross section for say, a trap, and the velocity of the transitioning particle (in this case, the thermal velocity), which gives

$$\alpha_{AB} = s_c v_A \tag{2.5.3}$$

with dimensions $\frac{L^3}{t}$. For electrons, v_A is generally the thermal velocity, $v_{T,}$ which is strongly dependent on the phonon spectrum and, therefore, the material temperature. For details on the electron thermal velocity, see Ashcroft and Mermin (1976b), Böer (2002), or Kao (2004). The capture cross section, s_c is an area that is representative of the atomic center (trap) closest to the particle. In fact, this process is exactly electron capture by an atomic center and is discussed below.

2.5.1. Capture Cross Sections

The simplest model of carrier capture follows from the Coulomb interaction between a positively charged center and a free electron. The Coulomb attractive center is a specific example that is well documented for semiconductors (Rose, 1963; Sessler, 1987). Commonly, the Columbic capture center is referred to as Langevin recombination (Tyutnev, 1996; Tyutnev *et al.*, 1996; Arkhipov, 1993b; Pivrikas, 2005). What is the radius, R_c , beyond which a passing carrier will not be captured? We can estimate R_c by asking what the minimum probability distribution of an electron is around a Coulomb center; i.e. where is the probability the lowest? The probability of finding an electron at some radius, r, must be proportional to the product of some spherical area (imagine a cross section of a funnel created by a potential well) and a Boltzmann factor that is scaled to reflect the Coulomb potential,

$$P(r) = 4\pi r^2 exp\left(-\frac{q_e V(r)}{kT}\right). \tag{2.5.4}$$

Setting the potential to $V(r) = -\frac{q_e}{\epsilon_r r^2}$ and minimizing the resulting function results in

$$R_c = \frac{{q_e}^2}{8\pi\epsilon_r\epsilon_0 k_b T}. \quad (2.5.5)$$

If we assume the cross section is related to the capture radius by the area formula, we obtain

$$s_c = \pi {R_c}^2 = \frac{{q_e}^4}{64\pi\,(\epsilon_r\epsilon_0 k_b T)^2}, \quad (2.5.6)$$

which has the dimension L^2.

For a material like LDPE, with a relative dielectric constant of ~ 2.4 at room temperature, we estimate a cross section of $\sim 4 * 10^{-12} cm^2$. Reassuringly, this is in good agreement with published values and capture cross sections obtained in the analysis of LDPE in this dissertation (see Chapters 4 and 5).

At first glance Eq. (2.5.6) has one immediately interesting result. Since the cross section scales as T^{-2}, at zero temperature the capture cross section should be infinite. At very low temperatures, there is no thermal energy to keep an electron (even one passing a very large distance away) from falling into a center or to excite it once captured. This temperature behavior and calculated magnitude is in good agreement with the literature. However, in Section 2.4 the DOS was found to have strong energy dependence. Since this energy dependence follows from deviations in the lattice potential, it is expected the capture cross section will also have some energetic dependence. In addition, there are a number of types of centers that can act as traps in addition to Coulomb centers; for example, regions of strong polarization and collective atomic behavior can lead to local potentials, which are not Columbic in character. In general, it is a good approximation to use the Columbic model, particularly in HDIM, as the centers do not generally interact and their potentials are, therefore, largely undisturbed. This is not true when high fields are present, and this question will be address when ionization is discussed below. For a more complete review of capture centers and cross sections see Rose (1951, 1955, 1963), Ashcroft and Mermin (1976), Sessler (1987), Sah (1991), and Böer (2002).

2.5.2. Lifetimes

A brief description of what a lifetime means and how it is used is presented here. In the simplest form, the rate of release or capture of a carrier determines its lifetime in a given state, for example, lifetime in the CB. From the discussion of the transition rate of carriers, an estimate of the lifetime τ of a carrier

can be found as $\tau = 1/[(\#\ of\ places\ to\ go)(velocity\ of\ carrier)(capture\ cross\ section)]$. This relation can be used to express the lifetime of a carrier in the conduction band in the presence of trapping, where the probability of trapping is much greater than that of recombination.

$$\tau_{et} = \frac{1}{n_t v_T s_c}. \tag{2.5.7}$$

This is usually the case when the fraction of filled traps is small, for example, in the limit of low trapped carrier density or higher temperatures.

However, if recombination or other processes are involved (which is almost always the case), then the lifetime equation must be modified. The derivation of extended, trapped, and recombination lifetimes requires the development of equations describing the energy, dose, field, and time-dependent number of carriers in both the extended and trapped states before complete carrier lifetime equations can be obtained. For excellent discussions regarding the derivation of carrier, trapped carrier, and recombination lifetimes with physical interpretations see Rose (1951) and Sessler and Yang (1999). I suggest that the reader begin with Rose and then follow with Sessler. Further discussions can be found in Fowler (1956), Elliott (1990), Sah (1991), Kao (2004), and Baranovskii and Rubel (2006).

2.5.3. Ionization

Thermally induced ionization occurs for both extrinsic and intrinsic disorder in nearly every transport mechanism considered in this dissertation. Thermal ionization is a statistical process, since it usually needs the presence of several phonons simultaneously (multi-phonon process) to deliver an energy significant enough to ionize an atom and contribute to conduction. In highly disordered and semiconducting materials, a typical starting point for describing the phonon spectrum is the Kubo-Greenwood treatment and its subsequent extension to DC conductivity (Mott and Davis, 1979). The simultaneous phonon excitations can be interpreted as a process involving a transient giant oscillation of a lattice atom (Sah, 1991). This results in the total energy of the ionized carrier exceeding that of the bottom of the CB. Further excitations of carriers from the trapped states occur by multi-phonon processes, as well as by exciting carriers from defects in the gap.

The simplest model of thermal ionization is a crystalline semiconductor, where the fraction of electrons excited across the band gap (without disorder) is given by the Fermi-Dirac (FD) distribution function (Ashcroft and Mermin, 1976),

$$f_{FD}(\varepsilon) = \frac{1}{1+exp\left[\frac{\varepsilon-\varepsilon_F}{k_bT}\right]} = \left(1 + exp\left[\frac{\varepsilon-\varepsilon_F}{k_bT}\right]\right)^{-1}, \tag{2.5.8}$$

where ε_F is the Fermi level. The probability of promotion to the CB of an electron from either a trapped state or a valence state is given by Eq. (2.5.8). However, the de-population or thermalization of carriers from the CB edge into trapped states or recombination centers is given by one minus the FD distribution,

$$1 - f_{FD}(\varepsilon)\ \frac{exp\left[\frac{\varepsilon-\varepsilon_F}{k_bT}\right]}{1+exp\left[\frac{\varepsilon-\varepsilon_F}{k_bT}\right]} = \left(1 + exp\left[\frac{-(\varepsilon-\varepsilon_F)}{k_bT}\right]\right)^{-1}. \tag{2.5.9}$$

Consider Fig. 2.7 and its distribution of carriers. In this case, the assumption is that $\varepsilon_{trap} \gg \varepsilon_F$. This assumption is valid as long the ratio of energy to temperature in the exponential term is large. This means that the temperature is not too high and the states are not too close to the Fermi level. For low temperatures, shallow states, and modest carrier concentrations, the Boltzmann approximation is adequate. Unless otherwise stated, the Boltzmann distribution function will be used for simplicity in this dissertation. Using this approximation yields:

$$\begin{aligned} f_{FD}(\varepsilon) \rightarrow \quad & f_{MB}(\varepsilon) = exp\left[\frac{-(\varepsilon-\varepsilon_F)}{k_bT}\right] \quad \{\text{Excitation}\} \quad . \\ 1 - f_{FD}(\varepsilon) \rightarrow \quad & f_{MB}(\varepsilon) = 1 \quad \{\text{Capture}\} \quad . \end{aligned} \tag{2.5.10}$$

Very often the probability of escape (or capture) from a site is written as a frequency or frequency factor v_{te}, where the subscript *te* refers to the transition from a trapped state to the CB. Thus, we can write a general escape (capture) probability as v_{AB}, where the transition occurs from state A to state B. It is, in fact, the product of the interaction coefficient, the number of available places the trapped carrier can transition to, and the probability that the transition will occur (where we now use the Boltzmann approximation).

$$v_{te}(\varepsilon) = v_{te}\exp\left[-\frac{\varepsilon_{trap}}{k_bT}\right], \tag{2.5.11}$$

and

$$v_{te} = \alpha_{te}N_e. \tag{2.5.12}$$

Equation (2.5.12) describes what is termed the frequency factor. Since $\alpha_{te}N_e$ is a function of the phonon spectrum the *attempt-to-escape frequency* is also the direct result of phonon processes (Mott and Davis, 1979). It should be noted, Schmidlin (1980) provides an excellent intuitive argument for the AC conductivity and a physical connection with the phonon frequency, ω_i ,

$$\nu_0 = \frac{\omega_i}{2\pi}. \tag{2.5.13}$$

It is useful to have information about the AC conductivity of a material, as it provides an alternative determination of the frequency factor.

As a simple example, consider the effects for Coulomb attractive centers that are close to the CB. The attempt-to-escape frequency can be estimated from the ionization radius, R_c, for a specific frequency and the *rms* (thermal) velocity of the electron (Ashcroft and Mermin, 1976; Böer, 2002),

$$\nu_0 = \frac{\nu_{rms}}{2\pi R_c}. \tag{2.5.14}$$

Using our relation for the capture cross section, Eq. (2.5.6) we can then write,

$$\nu_0 = \frac{\nu_{rms}}{2\pi\sqrt{\pi s_n}}. \tag{2.5.15}$$

We can estimate the value of ν_0 using this result and assuming a room temperature *rms* (thermal) velocity of ~ 10^7 cm/s and a capture cross section consistent with HDIM of ~ 10^{-12} cm^2. From this one obtains a value for the attempt to escape frequency of ~ 10^{12} attempts per second. In the literature, values for the attempt to escape frequency are consistently quoted in the range 10^{12} Hz to 10^{13}Hz for shallow centers (energetically close to the CB) (Blythe and Bloor, 2005). Boer notes here that this approximation is only useful for Coulomb attractive centers, which are common in many doped semiconductors and HDIMs. The literature suggests that ν_0 lowers considerably for deep states; for low temperatures in LDPE this number can decrease to 10^4 Hz (Teyssedre *et al.*, 2003, 2005, 2009). This is not surprising as the *rms* (thermal) velocity is a temperature-dependent function. Further with increasing disorder and decreasing number of interacting sites (wave function interaction), we expect both the cross section and thermal velocity to be affected.

The remaining ionization mechanisms are largely due to impact processes. In these systems, an electron either enters the system with or gains enough energy (between scattering events) to exceed the ionization energy (binding energy) of a center or state in the VB. This process excites or frees an additional carrier or carriers (usually a distribution of carriers). This process of impact ionization happens

in shallow states, across the band gap, and at band edges (Auger processes, as an example). These concepts are pertinent to radiation induced conductivity (Rose, 1951) and breakdown (Fothergill, 1998) and will, therefore, not be discussed in this dissertation. For a very comprehensive review of ionization processes and energy exchange mechanisms involved in semiconductors and HDIM see Sah (1991). All of the ionization processes can be enhanced by external fields, both electric and magnetic. In particular, for very-high electric fields one should consider the Poole-Frenkle effect. External and internal electric fields are well known for their strong effects on ionization processes; the simplest example of this is the acceleration of free charges by a strong electric field within a material whose subsequent energy can cause many types of ionization processes to occur. This phenomenon and its results have been discussed in (Poole, 1916, 1917; Sessler, 1987; Fothergill, 1998; Blythe and Bloor, 2005; Brunson, 2009; Sim *et al.*, 2012). A short discussion of the basic Poole-Frenkle field effect is given below, with attention paid specifically to its effect on the carrier excitation rate $v(\varepsilon)$.

2.5.4. Poole-Frenkle Field Effect

The Poole-Frenkle (PF) effect is a high field enhancement of the measured current that typically scales as $\sqrt{F}$ (Wintle, 1983; Fothergill, 1998; Kao, 2004; Brunson and Dennison, 2006, 2007; Dennison *et al.*, 2009a; Brunson, 2009). Since the PF effect is covered widely in the literature, we give only a very brief focused introduction. Such field-dependent behavior can be ascribed to many processes (Schottky injection, as an example). Here the physical explanation of the PF effect is used to provide an understanding of the effects of very high fields on HDIM.

Consider a Coulomb attractive center and an applied field of sufficient strength to tilt the band (i.e., to distort the local atomic potential). The thermal ionization energy is lowered, thus enhancing the release rate of carriers; see Böer (2002) following Frenkel (1938) and Poole (1916). Consider the action of an internal electric field over a distance, *z*, acting on a simple Columbic potential,

$$V(z) = \frac{q_e}{4\pi\epsilon_r\epsilon_0 z} - Fz. \tag{2.5.16}$$

Figure 2.8 shows the lowering (also called bending) of the electron binding energy by a factor $\delta\varepsilon_{PF}$ as a result of the applied field. The location where the barrier is lowered by $\delta\varepsilon_{PF}$ is $q_e V_{max}$, and can be found by setting $\frac{dV}{dz} = 0$ from Eq. (2.5.16); this yields an estimate for the change in binding energy,

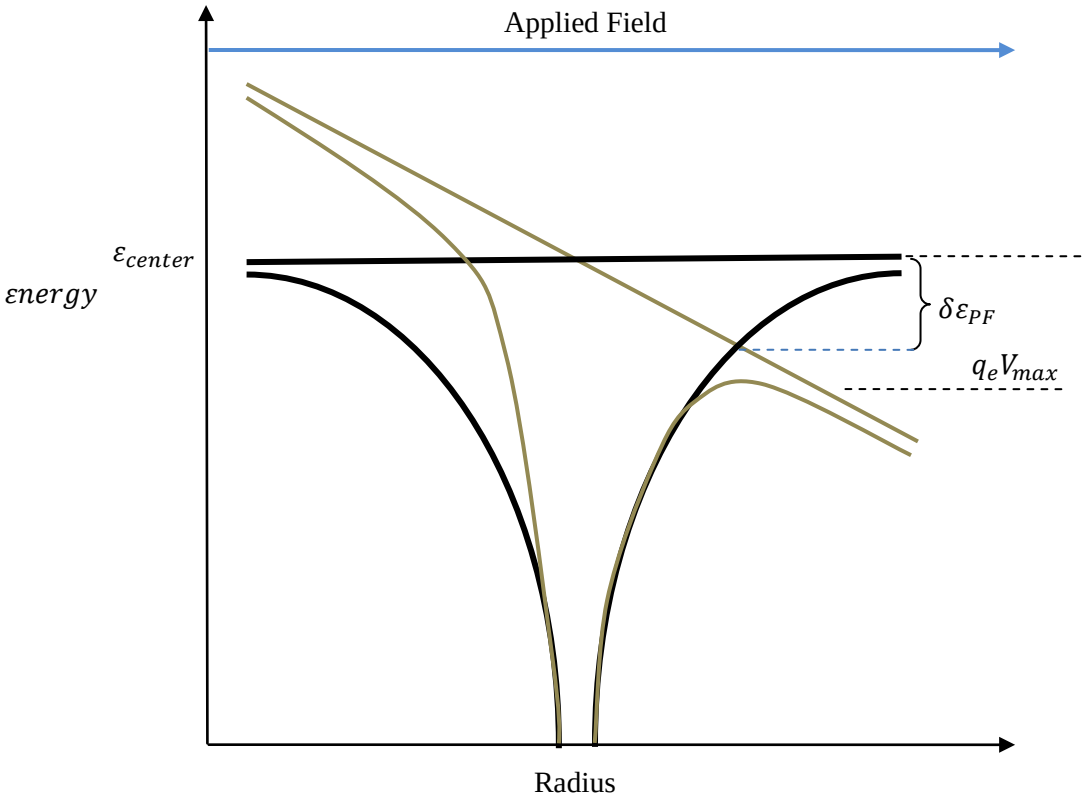

FIG 2.8. The Poole-Frenkel effect on a Coulombic center. Depicts the change in a Coulombic center due to an applied field, F, strong enough to deform the local potential. Dark lines show the unperturbed bound potential and free-state energy. Lighter lines show the corresponding energy levels for a charge in the presence of a strong field. $\delta\varepsilon_{PF}$ is the reduction in the potential barrier die to the field.

$$\delta\varepsilon_{PF} = q_e\sqrt{\frac{q_eF}{\pi\epsilon_r\epsilon_0}}\,. \tag{2.5.17}$$

Using our simple Boltzmann approximation, Eq. (2.5.10), for release of a carrier from a trap center, we have the frequency at this lowered energy barrier of

$$\nu_{PF} = \nu_0 exp\left[\frac{\varepsilon_{cb}-(\varepsilon_{center}-\delta\varepsilon_{PF})}{k_bT}\right], \tag{2.5.18}$$

where ε_{center} is the energy of the trap center in the BG. Since the phonon spectrum is responsible for release of a carrier from a potential well, one can estimate the field, F_{PF}, at which the Poole-Frenkle mechanism becomes important by setting the change in energy, $\delta\varepsilon_{PF}$, equal to the thermal energy, k_bT y:

$$F_{PF} = \frac{\pi\epsilon_r\epsilon_0}{{q_e}^3}(k_bT)^2. \tag{2.5.19}$$

It is common in the literature to define the Poole-Frenkle factor, $\beta_{PF} = \left(\frac{\pi\epsilon_r\epsilon_0}{{q_e}^3}\right)^{-1/2}$, which gives the familiar form, $\delta\varepsilon_{PF} = \beta_{PF}F^{1/2}$. Note, that this simple derivation does not account for atomic number; see Böer (2002) for an extension of this argument.

We can now use Eq. (2.5.18) with $\delta\varepsilon_{PF} = \beta_{PF}F^{1/2}$. This yields an estimate for the change in the carrier release rate due to the PF effect. The classical Poole-Frenkel model generally yields an ionization energy that is too high when compared with experiment. In addition, the threshold field, F_{PF}, is generally not observed. What is useful is that in experimental data, the onset of this ionization process is marked by the change in field dependence from *F* to $\sqrt{F}$. Very often this onset corresponds with the onset of space charge injection discussed in Section 2.6 (Montanari *et al.*, 1998, 2001, 2005; Teyssedre *et al.*, 2001, 2005, 2009; Montanari and Morshuis, 2005).

2.5.5. Interacting with Disorder

We now return to a discussion of the transition rate, expressed by Eq. (2.5.2), and the description of a carrier's (electron's) interaction with disorder. This is now feasible, as we have defined the interaction coefficient, α_{AB}, (see Eq. (2.5.3)), and the probability distribution function, f_{AB} (see Eqs. (2.5.8) and (2.5.9) or Eq. (2.5.10)), in addition to some of the ways in which these values might be modified. Recall that the transition rate between two states is given by (Eq. 2.5.2),

$$\frac{dAB}{dt} = \alpha_{AB}\, N_A N_B\, f_{AB}. \tag{2.5.20}$$

Again consider Fig. 2.7 and the interaction shown. In this case, the figure represents the decrease in the number of carriers in the conduction band, n_e, by trapping. (Assume some carrier distribution has been injected into the CB.) The number of candidates that can participate in the interaction is $N_A = n_e$, and the number of avalible places that a carrier can be trapped is the difference between the total number of traps and the number of electrons in the traps at a given time (i.e., the number of filled traps), $N_B = (N_t - n_t)$. Using the Boltzmann expression, Eq. (2.5.10) for the downward or trapping probability, $\downarrow f\left(\varepsilon_{trap}\right) \approx 1$, and replacing these quantities in Eq. (2.5.20) yields

$$\frac{dn_{et}}{dt} \approx \alpha_{et} n_e (N_t - n_t)1. \tag{2.5.21}$$

Equation (2.5.21) is the rate at which the number of electrons in the CB will decrease. Here the interaction coefficient subscript takes on the nomenclature used to describe a given process, α_{et}, as an example. It will be shown that n_{et} is, in fact, a function of time. Equation (2.5.21) with the time dependence describes (to first order) the short, time-dependent trap-filling process in HDIM. As we will see, it is used to describe electron beam deposition of charge into LDPE and Kapton™ discussed in Chapter 4.

We can extend this discussion to include several types of processes by considering the number of electrons available to participate in process, the number of places those electrons can go, and the probability that the transition will occur along with the respective interaction coefficient. Consider a complete cycle of processes in which electrons are first excited by some external source from the VB to the CB. Those electrons then become trapped and after some time are re-excited into the CB to finally recombine with holes in the VB. This is a common process found in HDIM when either light or high-energy electrons are incident on the material. Consider Fig. 2.9 in which these processes are represented, two excitation processes, (a) and (c), and two de-excitation processes, (b) and (d), (one trapping and one recombination). For the moment, we will ignore processes (e) and (f). Each of these processes is described by the probabilistic model given by Eq. (2.5.20), where the interaction coefficient α_{AB} is defined so that it denotes the process considered: α_{et} is CB to trapped state, α_{te} is trapped state to CB, and α_{er} is CB to recombination center (usually holes left by electron-hole pair generation). Process (a) demonstrates an excitation (generation) term, G_{ex}, which gives the rate at which electron-hole pairs are generated in the material—from the VB—and the rate at which electrons are excited to the CB. Figure 2.9 (a) has the form given by Eq. (2.5.20), but is written in a condensed notation where $\dot{D}$ is called the dose rate and ρ_m is the charge density. The dose rate term acts as an interaction coefficient, or probability term, and includes the number of available sites for excited electrons, while ρ provides the number of available participants. All terms in Fig. 2.9 have an excitation and de-excitation term, number of available carriers to participate (electrons), and number of places that the participants can go. For processes (b) and (d) the de-excitation term $1 - f_{FD}(\varepsilon) \cong 1$, where $f_{FD}(\varepsilon) \ll 1$. What should be clear is the need to understand which processes are important in the conduction of electrons and trapping of charge in a given HDIM. We now have all the basic building blocks to construct the transport equations for a simple delta function DOS. Section 2.6 uses

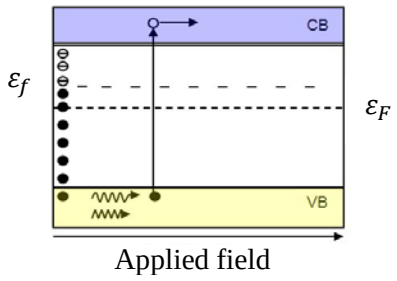

$$G_{ex} = \dot{D}\rho_m/\epsilon_0\epsilon_r$$

(a) Excitation by thermal or external sources

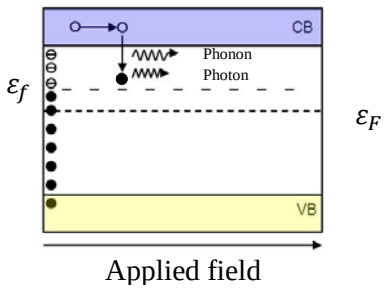

$$\alpha_{et}(\varepsilon)n_e(t)[N_t(\varepsilon) - n_t(\varepsilon,t)]$$

(b) Trapping

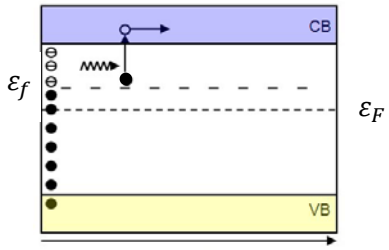

$$\int_{\varepsilon_F}^{\varepsilon_c} \alpha_{te}(\varepsilon)N_c n_t(\varepsilon,t)d\varepsilon\, f(\varepsilon)$$

(c) Detrapping due to thermal excitation

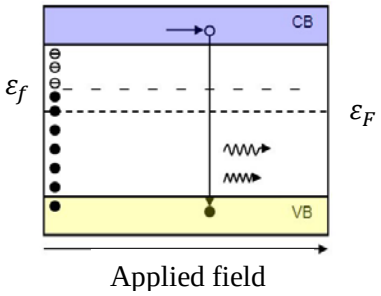

$$\alpha_{er}(\varepsilon)n_e(t)[n_e(t) + n_t(\varepsilon,t)]$$

(d) Recombination

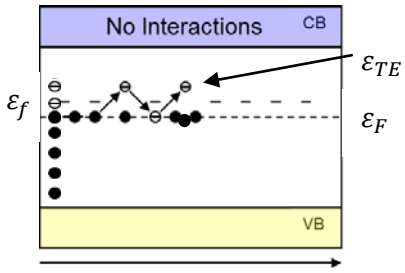

$$\alpha_{FTE}n_t(\varepsilon_F)N_{TE}(\varepsilon_{TE})P_{FTE}(\varepsilon_F)$$

(e) Low temperature hopping

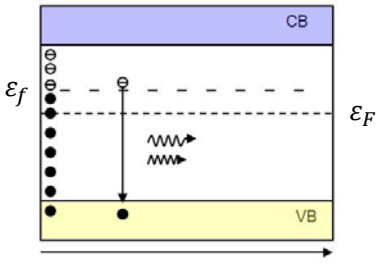

$$\alpha_{th}(\varepsilon)n_t(\varepsilon_t,t)n_h(t)P_{tr}(\varepsilon)$$

(f) Mid-band recombination

FIG 2.9. The six easy pieces of transport in HDIM. Free electrons are denoted by an empty circle, empty traps by a dash, and filled traps by a black circle. The vertical line of dark and open circles represent the distribution of filled and empty trap states. (a) Thermal processes or external irradiation that delivers energy sufficient to excite carriers across the band gap, creating holes in the valence band. (b) Carriers in the conduction band become trapped by localized states via thermalization (c) Carriers are re-excited into the conduction band from trapped states. (d) Carriers in the conduction band recombine with a hole in the valence band. (e) Low temperature transport; the CB is replaced by the effective transport energy (TE). (f) Low-temperature recombination that limits the flow of carriers in the transport band.

the methods described in this section to extend the delta function DOS model to include the complete energy dependence of more general DOS models and to develop the associated, more complete transport equations.

2.6. The Transport Equations with Trapping

The goal of this chapter is the development of a set of transport equations that can describe charge transport in HDIM, using a one-dimensional approach and the simple models for the DOS outlined in Section 2.4.5. Section 2.3 concluded with an explanation of the transport equations, which lacked any detailed description involving disordered states. In addition, no physical basis had been developed to describe how charge could interact with disorder beyond a delta function DOS. Sections 2.4 and 2.5 addressed the problems associated with the introduction of a simple energy-dependent disordered DOS for disordered systems with trap states and for interactions with that disorder. Using the tools developed in those sections, a complete set of transport equations is now developed, beginning with the trapping equation. Stated another way, we extend the four processes illustrated in Figure 2.9 by including two additional diagrams that depend on the energy distribution of the trap states.

Again consider Fig. 2.9, in which six transition processes are depicted, both as diagrams and mathematical models. The basic picture of the band model used in Section 2.5 and Fig 2.5 is retained in Fig. 2.9 with the exception that our delta function DOS—used in Fig 2.7—can now be any of the DOS models considered in Section 2.4.5 (see Fig. 2.6). The primary difference is the integration of the resulting trapping equations over the energy spectrum of the DOS used; thus, the mathematical models in Fig. 2.9 have been written as functions of energy. For convenience, it will be assumed that the spatial dependence of the trapped carriers is negligible (i.e., the trap distribution is homogeneous and isotropic); as the transport equations are developed, it will become clear how to include additional dependencies, such as charge position within the material. This is done to avoid confusion in the development of the trapping and transport equations. For examples of the application of these equations with spatial dependence see for penetrating radiation or RIC Fig. 1.4 (c) (Weaver *et al.*, 1977; Arkhipov and Rudenko, 1982c; Arkhipov, 1986, 1993a; Arkhipov *et al.*, 1987a, 1987b, 1997c; Arkhipov and Nikitenko, 1999); for nonpenetrating radiation (Sessler, 1987); for RIC and nonpenetrating radiation, see Figs. 1.4 (a) and (b) (Tyutnev *et al.*,

1982, 1983a, 1983b, 1984a, 1984b, 1984c, 1984d, 1985a, 1985b, 1985c, 1990; Dunaev *et al.*, 1992; Arkhipov *et al.*, 1997b, 1997c); and for parallel plate configurations [see Figs. 1.4 (c) and (d)] (Dissado and Fothergill, 1992; Dissado *et al.*, 2006).

The transition rate processes depicted in Fig. 2.9 are: (a) excitation by thermal or external sources across the band gap, (b) trapping of carriers in extended states, (c) excitation (detrapping) of trapped carriers, (d) recombination of carriers in extended states with immobile holes in the VB, (e) interstate transitions, and (f) recombination of carriers in deep trapped states with holes in the VB. In process (a), thermal excitation across the large band gap in HDIMs is negligible and therefore, only external sources (excitation) are considered here.

The generation of carriers—specifically electrons—in the material, $G_{ex}(z)$, due to an incident electron beam (or any external source), is a function of distance into the material. Beyond a penetration depth, z_p, in the material excited electrons, carriers are no longer generated; but, charge carriers are deposited from the beam. To distinguish these two processes, the number of electrons deposited per unit time is given by K(z_p); (see Fitting, 1975; Fitting *et al.*, 1979; Davies and Dennison, 1997; Thomson *et al.*, 2002; Clerc *et al.*, 2006; Dennison *et al.*, 2006b; Kite, 2007; Cornet *et al.*, 2008; Wilson and Dennison, 2010). We will return to a discussion of the deposition term at the end of this section and the generation term is discussed further in Chapters 4 and 5.

Thermal excitations (phonons) are considered only in process (c), whereas the release of phonons and photons are considered in processes (b), (d), and (f). A discussion of the process (f) and the probability of this transition occurrence, $P_{tr}(\varepsilon)$ (which is very small), and the mathematical description of (e) are left until Chapter 3, as they apply only to low-temperature conductivity and represent a wholly new type of transport process. The key piece of information to take away from processes (e) and (f) is that, whatever these processes may be, they are governed by transition rates to and from trapped states and some type of states in which transport can occur; thus, these processes must be governed by a set of transport equations that include trapping as a fundamental rate limiting process.

The processes in Fig. 2.9 represent all the interactions with disorder necessary for describing the transport of electrons in HDIM. Thus, the sum of processes (transition rates) involved in a given application will yield the appropriate transport equations. In addition to the changes in the relative

concentration of electrons in the extended and localized states, a set of conservation equations that connect the total number of electron carriers in the material at any time, *t*, is needed:

$$n_{tot}(t) = n_e(t) + n_t(t), \tag{2.6.1}$$

and the total number of electrons trapped in all the localized states at all possible trap depths and at some position, z_p, is given by

$$n_t(\mathrm{t};\ z_p) = \int_{\varepsilon_{low}}^{\varepsilon_{high}} n_t(\varepsilon, t;\ z_p)\, d\varepsilon. \tag{2.6.2}$$

ε_{low} and ε_{high} refer to the top and bottom of the DOS that contains the trapped electrons.

At this point we can look at a specific application to develop an expression for the transport equations. Assume that electrons are excited from the VB to the CB, leaving holes in their absence [as in Fig. 2.9 (a)], but that no deposition occurs. Such behavior can be expected for penetrating radiation, such as in Fig. 1.4 (a) (iii). Developing the trapping equations is now a simple matter of summing over the processes in Fig. 2.9 that relate the change in the number of electrons in extended and localized states (Weaver *et al.*, 1977). To obtain the time rate of change in the number of electrons in the CB due to interactions with disorder (trapping and release of electrons), we integrate the energy-dependent processes (b), (c), and (d), then sum (a) - (d) - (b) + (c) to obtain,

$$\frac{dn_e(t)}{dt} = G_{ex}(t, z_p) - \alpha_{er} n_e(t)[n_e(t) + n_t(t)] - \alpha_{et}\, n_e(t)[N_t - n_t(t)] + \int_{\varepsilon_f^0}^{\varepsilon_{CB}} \alpha_{te}(\varepsilon) f(\varepsilon) N_e n_t(\varepsilon, t) d\varepsilon \tag{2.6.3}$$

Here, for the first time, it has been explicitly suggested that the generating term $G_{ex}(t, z_p)$ depends on time. The distribution function, $f(\varepsilon)$, is left in a general form and is not yet assumed to have a certain type of statistical nature, such as Fermi-Dirac or Maxwell-Boltzmann. For the time rate of change in the number of trapped electrons, $n_t(t)$, we again perform integration over energy and do the sum over processes (b) - (c) to obtain

$$\frac{dn_t(t)}{dt} = \alpha_{et}\, n_e(t)[N_t - n_t(t)] - \int_{\varepsilon_f^0}^{\varepsilon_{CB}} \alpha_{te}(\varepsilon) f(\varepsilon) N_e n_t(\varepsilon, t) d\varepsilon. \tag{2.6.4}$$

Without the explicit integration of the energy-dependent terms, the equations cannot be reduced further. We have addressed the energy dependence of the interaction coefficient, which is the product of the electron thermal velocity with the trapped states capture cross section (see Section 2.5.1). The energy

dependence of the interaction coefficient is not well understood in HDIM and mention of it is sparse in the literature; it is, therefore, assumed that the interaction coefficient is a constant. The excitation from a trap state is governed by the distribution function, $f(\varepsilon)$, which, for the electron system, is most generally the Fermi-Dirac (FD) distribution. As in Section 2.5.3 the FD distribution will be approximated by the Boltzmann distribution (MB), i.e., $\alpha_{te}N_e f_{MB}(\varepsilon) = \nu_0 f_{MB}(\varepsilon) \approx \nu_0 exp\left[-\frac{\varepsilon}{kT}\right]$, where the relation between α_{te} and ν_{te} are given in Section 2.5.3.

Equations (2.6.3) and (2.6.4) can be greatly simplified by assuming that α_{er} is equal to α_{et}. These two terms deal with (i) recombination of electrons in the CB to the VB holes created during generation and (ii) the trapping of electrons in the DOS, respectively. There is no clear justification for this assumption other than its ability to simplify the transport equations. Many authors have used this assumption, but with little or no justification; see, for example, Weaver *et al.* (1977). It is possible, that since the electrons involved in these two processes always start in the CB, that the coefficients are determined predominantly by the properties of the CB, in which case the assumption is valid.

Additional assumptions are that the process (e) in Fig. 2.9 is only important at very low temperatures and that process (f) is negligible in the study of RIC. These assumptions are certainly not always true; however, many of the transport equations were developed for large fluence near room temperature and in semiconductor applications where (e) and (f) do not typically make large contributions to the observed macroscopic current. These assumptions have been noted here so that the reader will understand how the complete transport equations are related to the more common reduced set found in the literature. Keeping these assumptions in mind, we can write Eq. (2.6.3) and Eq. (2.6.4) as follows:

$$\frac{dn_e(t)}{dt} = G_{ex} - \alpha_{er}\, n_e(t)(\, n_e(t) + n_t(t)) + \int_{\varepsilon_f^0}^{\varepsilon_{CB}} \nu_0 exp[-\varepsilon/k_b T] n_t(\varepsilon, t) d\varepsilon, \tag{2.6.5}$$

and

$$\frac{dn_t(t)}{dt} = \alpha_{et}\, n_e(t)[N_t - n_t(t)] - \int_{\varepsilon_f^0}^{\varepsilon_{CB}} \nu_0 exp[-\varepsilon/k_b T] n_t(\varepsilon, t) d\varepsilon. \tag{2.6.6}$$

These two equations, together with the definition $n_{tot}(t) = n_e(t) + n_t(t)$ (see Section 2.3), are equivalent to the continuity equation, Eq. (2.3.30) introduced in Section 2.3, with an explicit dependence on trapping. Note that spatial and time dependence have been neglected in the generating term G_{ex}, and that the

recombination term is given by $R = \alpha_{er}\, n_e(t)\, n_{tot}(t)$. For clarity, we repeat Eq. (2.3.30) and highlight the recombination term:

$$\frac{\partial n_{tot}(z,t)}{\partial t} - \mu_e \frac{\partial}{\partial z}[n_e(z,t)F(z,t)] - q_e D \frac{\partial^2 n_e(z,t)}{\partial z^2} = G(z,t) - R(z,t),$$

where eliminating the spatial dependence and inserting the generation and recombination terms assumed in Section 2.3 gives

$$\frac{\partial n_{tot}(t)}{\partial t} = G(t) - R(t) = G_{ex}(t) - \alpha_{er}\, n_e(t)\, n_{tot}(t). \tag{2.6.6B}$$

We can illustrate the connection between Eqs. (2.6.5) and (2.6.6) and Eq. (2.3.30) by adding Eq. (2.6.5) and Eq. (2.6.6) together—and recalling that when a trap distribution is present, we have $n_{tot}(t) = n_e(t) + n_t(t)$—to obtain

$$\frac{dn_e(t)}{dt} + \frac{dn_t(t)}{dt} = \frac{dn_{tot}(t)}{dt} = G(t,z)_{ex} - \alpha_{er}\, n_e(t)[\, n_e(t) + n_t(t)] + \alpha_{et}\, n_e(t)[N_t - n_t(t)]. \tag{2.6.6C}$$

Note that the integrals in Eqs. (2.6.5) and (2.6.6) cancel upon addition. Looking closely at this result, the similarity between the last two equations is clear. There is an extra term in Eq. (2.6.21) that did not appear in the original continuity equation; the explanation for this is simple. When considering the generation term, *G(t,z)*, and recombination term *R(t,z)*, for Eq. (2.6.6B), we did not include the effects of the disordered DOS; i.e., initially we did not actually have continuity and the addition of the trapping equations have given us the missing term, the final term in Eq. (2.6.6C).

Equations (2.6.5) and (2.6.6) are the continuity equations with trapping, for the specific example introduced in Section 2.3. Thus, to describe the transport equations, we only need to add Eq. (2.6.6) to Eq. (2.3.29) through (2.3.32). The form of Eq. (2.6.6) is not the most general form. Assuming some functional dependence of the DOS (and, therefore, the trapped states) on the spatial position (of the material), one can write expressions for the filled trap state distributions $n_t(\mathrm{z},t) = \int_0^\infty n_t(z,\varepsilon,t)d\varepsilon$ and $N_t(z) = \int_0^\infty N_t(z,\varepsilon)d\varepsilon$, respectively. Taking the derivative of Eq. (2.6.6) with respect to energy, including spatial dependence, and using the definitions for interaction coefficients and attempt to escape frequency discussed in Section 2.4, Eq. (2.6.7) can be written as:

$$\frac{dn_t(\mathrm{z},\varepsilon,t)}{dt} = \alpha_{et} n_e(z,t)[N_t(\mathrm{z},\varepsilon) - n_t(\mathrm{z},\varepsilon,t)] - \alpha_{te} N_e exp\left[-\frac{\varepsilon}{kT}\right] n_t(\mathrm{z},\varepsilon,t). \tag{2.6.7}$$

Equation (2.6.7) is finally the complete, one-dimensional, energy- and time-dependent trapping equation. Many of the prolific authors in the field of charge transport have used some form of this equation to describe carrier interactions with the DOS in HDIM for radiation induced conductivity, charge dynamics in electron irradiated materials and electrets. Excellent representations of the application of Eq. (2.6.7) in one form or another is given by the following list: nonpenetrating radiation (Arkhipov, 1993a); RIC, nonpenetrating radiation and parallel plate configurations (Sessler, 1987); nonpenetrating radiation (Gross, 1964, 1978, 1980; Gross and Nablo, 1967; Gross and Nunes de Oliveira, 1974; Gross *et al.*, 1981a, 1981b, 2003a, 2003b; Giacometti *et al.*, 1985; Gross and de Oliveira, 2003) photo-excited RIC systems (Monroe, 1983); and multiple configurations (Baranovskii and Rubel, 2006).

We now return to the transport equations developed in Section 2.3 used to describe drift and diffusion in simple crystalline systems. Using Poisson's equation, $\nabla \cdot \boldsymbol{D} = \rho_c$, the continuity equation, $\nabla \cdot \left(\mathrm{J_C} + \mathrm{J_{inj}}\right) = -\frac{\partial \rho_{\mathrm{tot}}}{\partial \mathrm{t}}$, and a simple description of charge transport, a set of one-dimensional transport equations were developed in Section 2.3.1.2. We included the polarization and displacement currents explicitly, as they will be needed in Chapters 4 and 5. The generation and recombination terms defined above now take the place of their generic counterparts, *G(t,z)* and *R(t,z)*, used in Section 2.3.1.2. Collecting Eqs. (2.3.29), (2.3.30), (2.3.31), (2.3.32), and (2.6.7), we can write the complete transport equations in a compact form.

$$J_{tot}(z,t) = q_e n_e(z,t)\mu_e F(z,t) + q_e D\frac{dn_{tot}(z,t)}{dz} + \epsilon_0\epsilon_r\frac{\partial F(z,t)}{\partial t} + J_p(t)$$

{Sum of electron drift, diffusion displacement, and polarization current densities}, (2.6.8)

$$\frac{\partial}{\partial z}F(z,t) = q_e n_{tot}/\epsilon_0\epsilon_r \qquad \text{\{1D Gauss's Law\}}, \qquad (2.6.9)$$

$$\frac{\partial n_{tot}(z,t)}{\partial t} - \mu_e\frac{\partial}{\partial z}[n_e(z,t)F(z,t)] - q_e D\frac{\partial^2 n_e(z,t)}{\partial z^2} =$$

$$G(z,t)_{ex} - \alpha_{er}\, n_e(z,t)n_h(z,t) + \alpha_{et}\, n_e(z,t)[N_t(z) - n_t(z,t)]$$

{1D Continuity equation with drift, diffusion and source terms}, (2.6.10)

$$\frac{dn_h(z.t)}{dt} = G(z,t)_{ex} - \alpha_{er}\, n_e(z,t)n_h(z,t)$$

{1D hole continuity equation with generation and recombination terms}, (2.6.11)

and

$$and\ \frac{dn_t(z,\varepsilon,t)}{dt} = \alpha_{et} n_e(z,t)[N_t(z,\varepsilon) - n_t(z,\varepsilon,t)] - \alpha_{te} N_e exp\left[-\frac{\varepsilon}{kT}\right] n_t(z,\varepsilon,t)$$

{1D trapping continuity equation for electrons}. (2.6.12)

This set of equations covers a large class of carrier transport models in disordered materials whose application ranges from Xerox copier element design and radiation effects in materials to descriptions of electron transport in power cable design (Rose, 1951; Fowler, 1956; Mott, 1977; Tiedje *et al.*, 1980; Arkhipov *et al.*, 1984; Arkhipov, 1986; Sessler, 1987; Pai and Springett, 1993). The complexity of these equations, even in one dimension, is quickly becoming apparent. Manipulation of these equations for a specific application MUST be done with care. As an example of such modification, theories are explicitly developed in Chapters 4 and 5; subsets of these equations will be used to derive analytical models for all of the experimental configurations shown in Fig. 1.4, as used by the USU MPG. As we will find in each case, the complexity of the transport equations will decrease as a result of relevant assumptions based on each specific application.

There are two more phenomena, space charge limited current (SCLC) and dispersion, which can now be described using this new description of transport. These are critical to more fully understand transport phenomena in HDIM. These two phenomena, SCLC and dispersion, have been delayed in their introduction because both require the DOS interaction picture, transport equations as described above, and further mathematical detail to describe their behavior.

2.7. Space Charge Limited Current

In the early days of electronics technology, vacuum tubes were often used as components in electronic devices. The components are composed essentially of an anode and cathode placed in a sealed vacuum tube. The study of their operation, however, was often complicated by a simple phenomenon whose nomenclature has propagated in the literature to this day and greatly convolutes the definitions of "trapped charge" and "spacecharge." The phenomenon, called space charge limited current (SCLC) or electrode limited current, is often referred to as space charge (meaning trapped charge) however, these two ideas (spacecharge and spacecharge limited current) could not be more different (Sessler, 1987; Blythe and Bloor, 2005). Spacecharge limited current is caused by an excess of charge at the contact supplying charge carriers (a cloud of charge, which inhibits further charge injection). The charge cannot move away from

the contact fast enough (the material relaxation rate is slower than the injection rate), and the incoming charges experience the field from this “spacecharge” and their transport is retarded (Sessler, 1987). Child and Langmuir were the first to study this phenomenon in vacuum tubes and the resulting theory, called Child’s law, is the subject of this section (Rose, 1951).

In the literature relevant to this dissertation, the trapped charge due to disorder is often called “space charge,” but this is not what is generally meant by “spacecharge” in SCLC. With the advent of transistors and semiconductor doping, the application of SCLC theory found utility in determining current versus applied voltage (IV) curves. However, the use of doping in materials meant that charges were trapped or excited in ways that were not consistent with simple SCLC theory. As an example, when high potentials are applied to HDIM using metallic contacts, the trap barrier energies are lowered leading to a Poole-Frenkle-type behavior (Sessler, 1987) or modified Schottky emission (Fraser, 1983), depending on the type of material, contacting electrode, and distribution of trapped states near the interface (Sessler, 1987; Crine, 2004a, 2005a).

This nomenclature confused the study of current versus voltage in HDIM and made it difficult to differentiate between bulk and interface effects using purely an electrode contact method of study (Sessler, 1987). The use of electron beams as injecting sources allows for a nearly “pure” injection, free of interface effects. Thus, by comparison of the data between electrode studies and electron beam studies, the presence of electrode effects can be determined and quantified. Further, it will be shown in Chapter 4 the charging of an insulating material by an electron beam of modest energy is due largely to trapping effects in the bulk (thus, largely bypassing interface effects).

In order to address the effects of disorder at the interface or the bulk when SCLC is present, a set of modified SCLC equations is required. This allows for the characterization of the disorder in terms of one of four DOS types; delta function, constant, exponential, or Gaussian functions. A complete description for the use of the SCLC theory from the basic equation first derived by Child and Langmuir cannot be covered here. The complete derivation of the trap modified SCLC theory can be found in Kao (2004). Tables containing the trap modified expression for SCLC theory (written in the USU MPG nomenclature) can be found in the Appendix. In order to develop a working knowledge of the relevance of SCLC in the

study of HDIM, a short introduction is given to Child's law followed by a discussion of the effects of disorder.

At high voltages, currents in insulating and semiconducting materials are no longer Ohmic. In this case, we expect a change in the slope of the IV curves due to the buildup of an additional field. This process can be modeled using Poisson's equation (see Eq. 2.6.9),

$$\frac{dF(z,t)}{dz} = q_e \frac{n_{tot}(z,t)}{\epsilon_r \epsilon_0} = \frac{q_e}{\epsilon_r \epsilon_0}[n_e(z,t) + n_t(z,t)], \tag{2.7.1}$$

and an expression for the Ohmic current. In this context, we have written Poisson's equation with the separation of the free and trapped carrier concentrations as a function of distance into the sample and of time. In practical applications, we measure the SCLC in the equilibrium state, and thus, for now, we ignore the spatial and time dependence. Consider the current density [see Eq. (2.6.8)] written in the abbreviated form

$$J_{tot}(\mathrm{z}) = q_e \mu_e n_e F. \tag{2.7.2}$$

The first expression for the space charge current was given by Langmuir and Child (Mott and Gurney, 1964). Although it was Child and Langmuir (Rose, 1963) that first derived the limiting of charge flow due to a charge excess at the contacts, it was Mott and Gurney (1964) that applied these ideas to semiconductors and insulators. The process by which Mott and Gurney (1964) determined the SCLC is used in the derivation of all the SCLC equations presented in this dissertation (Batra and Seki, 1970). The basic Mott and Gurney (1964) equation was derived for a *trap free* semiconducting crystalline material. The definition of a trap-free material requires that the density of trapped carriers is zero and Eq. (2.7.1) reduces to

$$\frac{dF(z)}{dz} = q_e \frac{n_e(z)}{\epsilon_0 \epsilon_r}. \tag{2.7.3}$$

Using Eq. (2.7.2) and multiplying both sides of Eq. (2.7.3) by the field gives

$$F(z)\frac{dF(z)}{dz} = \frac{J_{sd} z}{\epsilon_0 \epsilon_r \mu_e}, \tag{2.7.4}$$

where J_{sd} is the steady state current, assumed to be constant in the material. Integration of Eq. (2.7.4) from the anode at $z=0$ to depth z gives $F(z)^2 = \frac{2J_{sd}z}{\epsilon_0 \epsilon_r \mu_e}$; integrating the square root of this result, again using

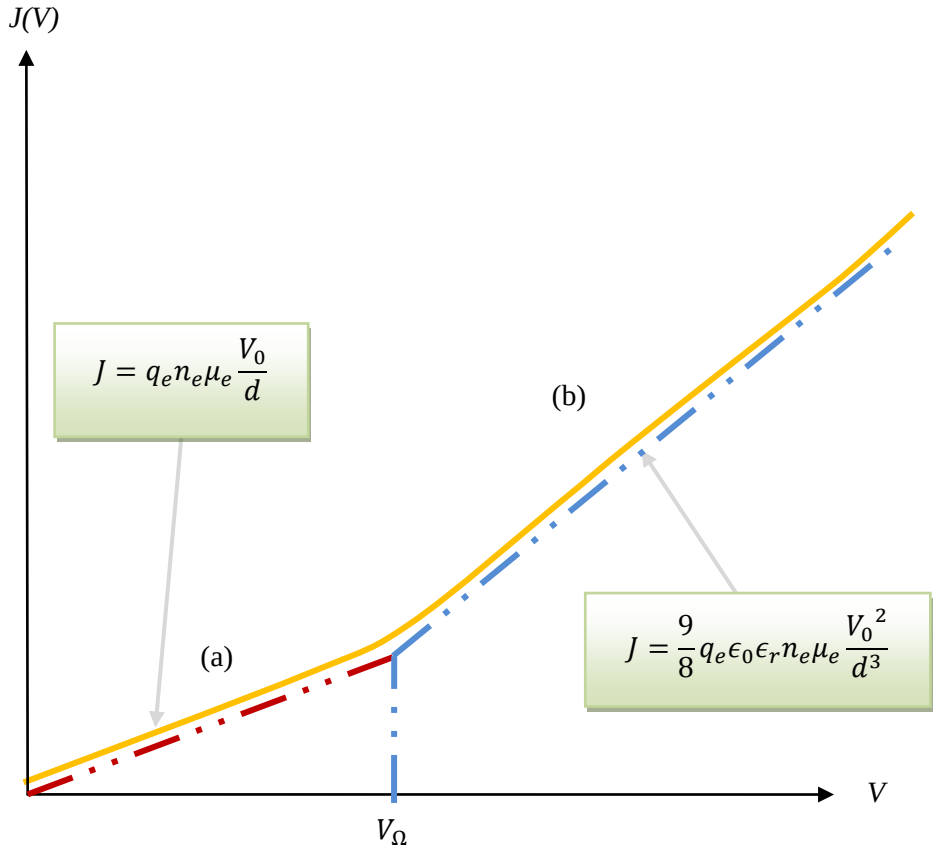

FIG 2.10. Space charge limited current. Depicts the character of current versus applied field behavior with a transition at the onset voltage, V_Ω: (a) Ohmic behavior (red curve), and (b) onset of SCLC due to electrode limited injection (blue curve).

$V_0 = \int_0^d F(z)dz$ (where V_0 is the applied potential), we obtain $V_0 = \frac{2}{3}\frac{\sqrt{2J_{sd}}z^{3/2}}{\sqrt{\epsilon_0\epsilon_r\mu_e}}$. Using the resulting equation and taking the square of both sides of this and solving for J_{sd} gives the result

$$J_{sd} = \frac{9}{8}\epsilon_0\epsilon_r\mu_e\frac{V_0^2}{d^3}, \tag{2.7.5}$$

found by Child and Langmuir and is referred to a Child's law (Rose and Lampert, 1959; Treadgold, 1966; Batra *et al*., 1970; Kao, 2004; Brunson, 2009).

The variation in measured current as a function of applied voltage is shown in Fig. 2.10. The voltage at which SCLC behavior based on Eq. (2.7.5) is first observed is called the onset voltage, V_Ω. An estimate of the onset voltage is obtained by setting Eq. (2.7.2) equal to Eq. (2.7.5); that is, by setting the Ohmic and SCLC contributions equal and solving for the transition voltage,

$$V_\Omega = \frac{8}{9}\frac{q_e n_e d^2}{\epsilon_0 \epsilon_r}. \quad (2.7.6)$$

Consider the electrode limited case in which the onset field of the SCLC regime is exactly determined by the ability of the charge to "relax" before more charge is injected. Simply stated, there is an amount of charge that can build up near the injecting electrode, resulting in a potential that fully inhibits the injection of additional charge, as long as the external experimental conditions remain unchanged. This is very different from a transit time, which is defined as the amount of time required for charge to traverse a region of the sample or the whole of the sample. Rearrangement of Eq. (2.7.6) allows us to identify the transit time and the relaxation time.

$$\frac{d^2}{\mu_e V_\Omega} = \frac{9}{8}\frac{\epsilon_0 \epsilon_r}{q n_e(z) \mu_e}. \quad (2.7.7)$$

Pope (1982) showed that the transit time is defined as $t_T = \frac{d^2}{\mu_e V_\Omega}$ and the relaxation time is $\tau_d = \frac{9}{8}\frac{\epsilon_0 \epsilon_r}{q n_e(z) \mu_e}$ (Blythe and Bloor, 2005). Thus, Eq. (2.7.7) says exactly what we surmised (in the beginning of this section) for electrode limited currents; the relaxation time is equal to the transit time, $t_T = \tau_d$, at the onset of SCLC.

Equation (2.7.5) and the resulting expressions for transit and relaxation time do not include any description of the DOS or their effects on the current versus voltage curve. It is not a simple matter to include the full character of a given DOS. This problem has been studied in detail by many authors; Kao has collected a set of expressions for each type of DOS discussed in Section 2.4.5, as given in Appendix A (Kao, 2004). The major difference between Kao's presentation and the one in this dissertation is nomenclature. The derivation of these equations is not given here; see Kao (2004) for a very complete development. In large part, we can characterize the extent of including an energetic description of the DOS with a simple modification to Eq. (2.7.5) by including a single factor, $\theta(\varepsilon)$, such that

$$J_{sd} = \frac{9}{8}\epsilon_0 \epsilon_r \mu_e \theta(\varepsilon)\frac{{V_0}^2}{d^3}. \quad (2.7.8)$$

This factor is a complicated function of the DOS, temperature, and (though not explicitly included) applied field. Further, $\theta(\varepsilon)$ ranges between zero and one, where $\theta(\varepsilon) \to 1$ for no DOS interaction (Mott type SCLC behavior) and $\theta(\varepsilon) \to 0$ for complete trapping. A value of zero –corresponding to T = 0 K— is not

physically realistic and is included only to illustrate that $\theta(\varepsilon)$ serves to reduce the slope of J versus V to zero.

Equation (2.7.8) describes an entirely new set of current regimes specific to a disordered material and subsequent trapping. It indicates that the slope of the SCLC region must be modified by the DOS and that we must consider the effects of completely filling up the trap distribution with carriers. Figure 2.11 shows the four distinct regions in the current versus voltage curve that result from disorder and trapping. In region (a) the current is Ohmic (i.e., proportional to the voltage). In region (b), the current versus voltage curve changes to a form consistent with Eq. (2.7.8). This change can be due either to a current-limited electrode (often called electrode limited) or to the build-up of deposited charge (often called space charge). In region (c), in the presence of traps, (if the carrier injection increases significantly such that the traps become filled or nearly filled) the current will jump radically due to the inability of the DOS to accept further charge. This process is unlikely to be observed as such a trapped charge density causes an internal electric field that is near the breakdown potential. In region (d), if the trapped charge does not lead to breakdown, the observed current should return to Eq. (2.7.5), offset by a finite current at a trap filled limit voltage, V_{TFL}. The behavior exhibited in Fig. 2.11 is quite similar to standard theories for extrinsic semiconductors, using a delta function DOS (Ashcroft and Mermin, 1976).

The effects of the DOS are not limited to the slope, but include modifications of the SCLC onset voltage and the effective sample depth. Measurements using pulsed electro-acoustic (PEA) techniques clearly show the position of injected charge (Sessler, 1987; Liu, 1993; Maeno, 2004; Griseri *et al.*, 2004, 2005, 2006; Perrin, 2005; Arnaout, 2010;). Such measurement indicates that for a capacitive-type experimental configuration [Fig. 1.4.b (i)], the charge stays near the contacting electrode (where it is injected), and leaks across the sample. Thus, the sample depth, *d*, is replaced by the effective depth, d_{eff}, which is that distance into the sample that the charge penetrates. The effective depth, V_{Ω}, V_{TFL}, and the relaxation times are all complicated functions of the DOS and injection properties of the material and its contacting electrode. Excellent reviews of the application and modification of these equations are given in Pope (1982), Abkowitz (1986), and Kao (2004). SCLC behavior has been experimentally verified in LDPE (Montanari *et al.*, 2001) and in Kapton™ (Many and Rakavy, 1962; Sessler, 1987; Alagiriswamy and Narayan, 2002; Gaur, 2008, 2010).

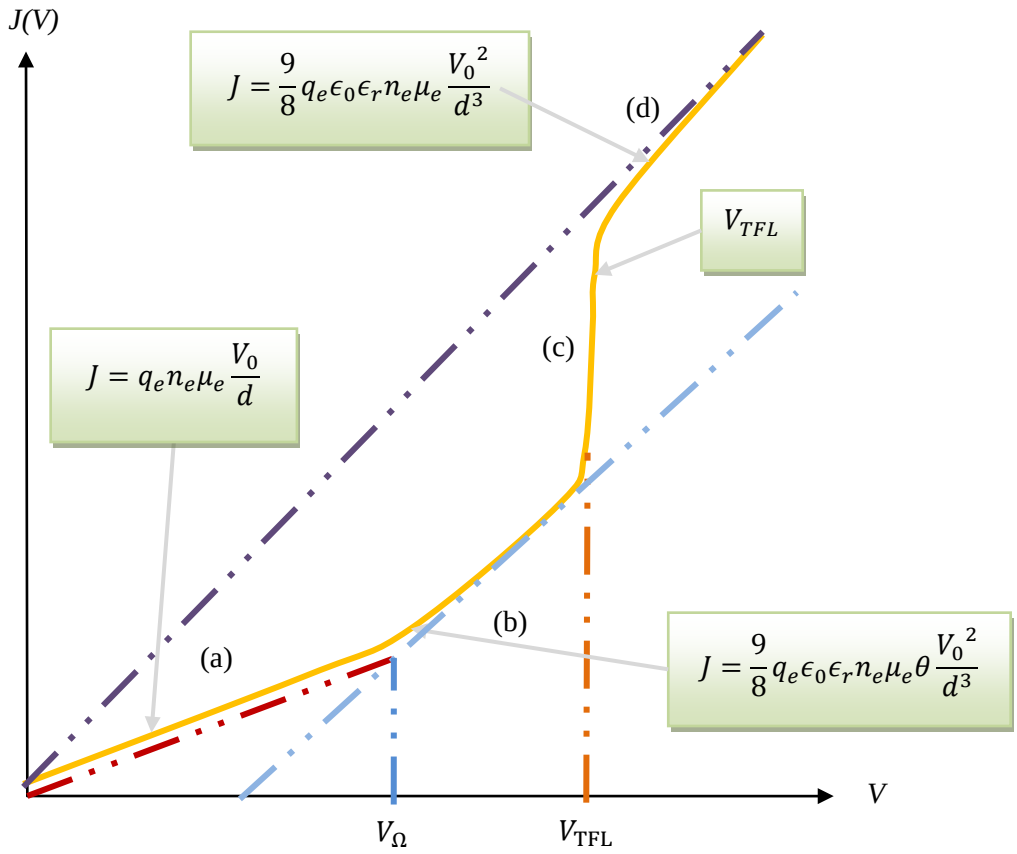

FIG 2.11. Space charge limited current density for disordered materials. Depicts the character of current versus applied field behavior in four distinct regions: (a) Ohmic behavior (red curve), (b) onset of SCLC due to electrode limitation or trapped charge build up with a transition at the onset voltage, V_Ω (blue curve), (c) trap filled limit voltage, V_{TFL}, at which the trap distribution is filled or nearly filled (orange curve), and (d) return to SCLC current flow (purple curve).

Measurement of the current versus applied voltage will provide a great deal of useful information about the material. In particular, from Eq. (2.7.8), the mobility can be estimated using

$$\mu_e = \frac{8\left(\frac{dJ_S}{dV_0^2}\right) d_{eff}^2}{9\epsilon_r \epsilon_0}. \tag{2.7.9}$$

The calculation of trap depth distribution (Montanari *et al.*, 2001) can be found by considering the behavior of the mobility using

$$\Delta 1 \varepsilon_{trap} = k_b T ln\left[\mu_e \frac{k_b T}{\nu_0 q_e a^2}\right]. \tag{2.7.10}$$

Here a is the mean distance between localization sites (see Sec. 2.4.3), which is essentially the same as $\bar{R}$ used elsewhere in this work (see Section 2.5.1 and Section 3). The trap depth used here, $\Delta 1\varepsilon_{trap}$, is then corrected for the high field Columbic interaction using

$$\Delta\varepsilon_{trap} = \Delta 1\varepsilon_{trap} - \frac{{q_e}^{3/2}F^{1/2}}{(4\pi\epsilon_r\epsilon_0)^{1/2}} = \Delta 1\varepsilon_{trap} - \tfrac{1}{2}\delta\varepsilon_{trap}. \tag{2.7.11}$$

The reader may notice that the second term in Eq. (2.7.11) is different from $\delta\varepsilon_{trap}$ found in Eq. (2.5.17), where the Poole-Frenkle effect was discussed. It is not clear to this author why this factor of ½ appears, but its presence is noted here and should be considered as future work.

SCLC theory is a powerful tool in the determination of the current versus applied voltage behavior. When used in conjunction with other experimental systems, which can characterize the DOS, mobility, and conductivity, SCLC theory can be used to gain further insight into, or confirmation of, material parameters.

2.8. Dispersion

In order to provide a lucid introduction to dispersive transport, we begin with a discussion of the difference between it and classical diffusive transport. Consider a photoconductivity experiment in which, at time zero, a sheet of charge is injected into the sample using an Ohmic photo-reactive contact, which provides an initial current density, J_0 (Orenstein *et al.*, 1982). This charge is allowed to traverse the material under the influence of a uniform applied electric field in a time, $\tau_{transit}$. In crystalline materials, this will lead to a current density versus time curve like that shown in Fig. 2.12 (a); this is classical diffusive transport. For noncrystalline materials—in which disorder is present—the current versus time curve (shown in log-log format) is like that shown in Fig. 2.12 (b); this is an example of dispersive transport.

The physical difference between the measured current density for a diffusive and dispersive system is described below by Eq. (2.8.1) and (2.8.2). In diffusion, the charge travels as a packet of fixed width, $z^{1/2}$, with a time dependence, $t^{1/2}$,

$$J_D(t) = J_0 \begin{cases} \sqrt{t/\tau_{transit}}\,; & t < \tau_{transit} \\ 0 \quad\quad\quad\quad\; ; & t > \tau_{transit} \end{cases}. \tag{2.8.1}$$

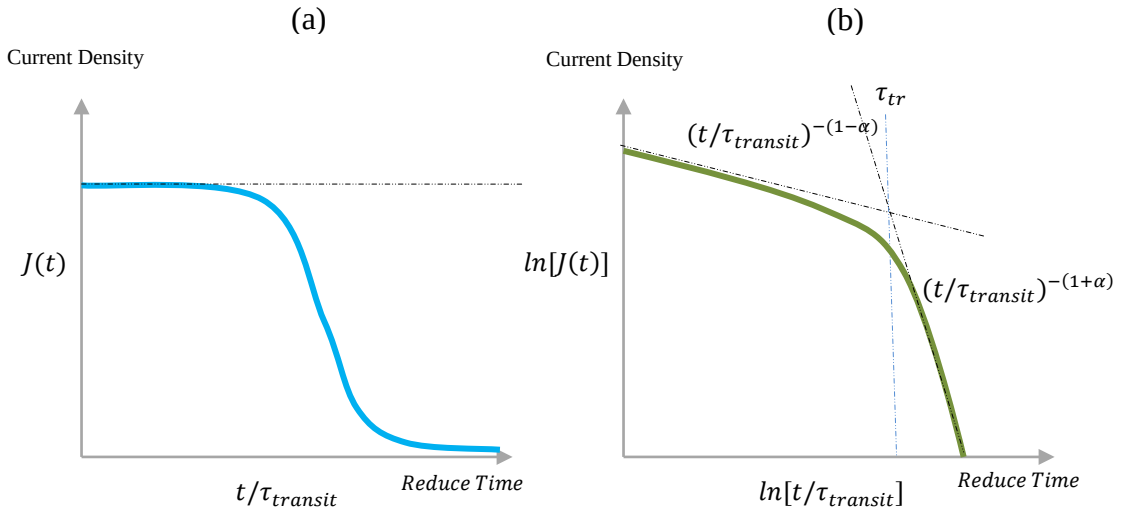

FIG 2.12. Diffusive versus dispersive transport. This diagram shows current versus time plots for two distinct types of transport. Specifically, it shows the basic difference between (a) classical diffusion transport, and (b) the dispersive transport mode. $\tau_{transit}$ is the transit time for the charge carriers to traverse the sample.

Well beyond the transit time, all charge has arrived at the rear electrode and $J_D(t)$ goes to zero. However, in dispersion, the peak of this charge packet is pinned at the interface or injection point and the charge centroid slowly disperses across the sample until the charge distribution makes electrical contact with the second electrode, at which time the rate of change in the observed current versus time plot changes. The expected current density profile for dispersion is represented by the phenomenological equation below (Scher and Lax, 1973a, 1973b; Scher and Montroll, 1975; Scher, 1977)

$$J_{disp}(t) = J_0 \begin{Bmatrix} (t/\tau_{transit})^{-(1-\alpha)} & t < \tau_{transit} \\ (t/\tau_{transit})^{-(1+\alpha)} & t > \tau_{transit} \end{Bmatrix}. \tag{2.8.2}$$

Here α is the dispersion parameter determined by the type of DOS. For a discussion regarding the connection of α to a specific type of DOS, see Chapter 4 or (Rose, 1951; Monroe, 1985; Baranovskii and Rubel, 2006).

To explain the radically different measured current density shown in Fig. 2.1, Scher and Montroll (1975) suggested in their seminal paper that the observed behavior was due to a random walk model with a broad distribution of random walker event times. To illustrate the difference between classical diffusive transport (also called Gaussian transport, not to be confused with the Gaussian DOS) and this new type of transport (dispersion), consider the two experiments shown in Fig. 2.13, but now recast in terms of the

motion of the deposited charge body. For experiment (a), we see a group of carriers that are injected into the sample at *t=0*. This group of carriers makes its way through the sample under the influence of some sufficiently low applied field (field effects are negligible) according to simple drift and diffusion described in Section 2.3. This produces the well-known current behavior depicted in Fig. 2.12 (a).

Now consider Fig. 2.13 (b), in which the main body of the carrier distribution is somehow held at the interface and only a few privileged carriers can traverse the sample. Here is where the Scher and Montroll interpretation gives us some insight as to the saintly nature of our speedy friends. The distribution of event times (random walkers) suggested means that there is a "dispersion" of walking times that make each successive step more difficult than the last (you may be reminded of a gambit in which you are asked to step half of the last distance to get to a point in space). For a modest number of carriers, the statistics of random walkers suggests that a few will get to the other side well ahead of the majority of carriers. This explains the time evolved distribution in Fig. 2.13 (b), as we step in time from $t_0 = 0$ to a time $t >> t_0$. The Scher and Montroll approach does explain the observed behavior, but lacks any real physical interpretation. Pollak (1972) showed that the "dispersive transport" follows directly from a broad distribution of localized state energies in the gap (the disordered DOS). Deeper traps retain charge carriers for longer times on average, so that as time goes on, more and more carriers are trapped in deeper states, thus slowing the progression of the charge front. Specifically, it was shown that dispersive transport can be derived from the transport equations and the exponential DOS! Dispersive behavior can arise in many situations due to energetic and spatial disorder of nearly any type. In studies of polarization, it has been found that if there are many polarization centers with different depolarization times, then we expect that the Fourier transform of the time data over a range of test frequencies will become broadened (Enis, 2002; Kao, 2004). The solution of the transport equations in the context of a dispersive system requires conceptual and mathematical tools not yet described in this dissertation. The original theoretical formulation for dispersive transport was for a system in which successive jumps between localized states governed the observed transport. This process, called *hopping*, is the dominant mode of transport at low temperatures. Our current set of transport equations does not explicitly include a description of low-temperature transport and requires the understanding and application of a distributed DOS. What happens when the temperature is so low that thermal excitation to the extended states (even from trapped states) no

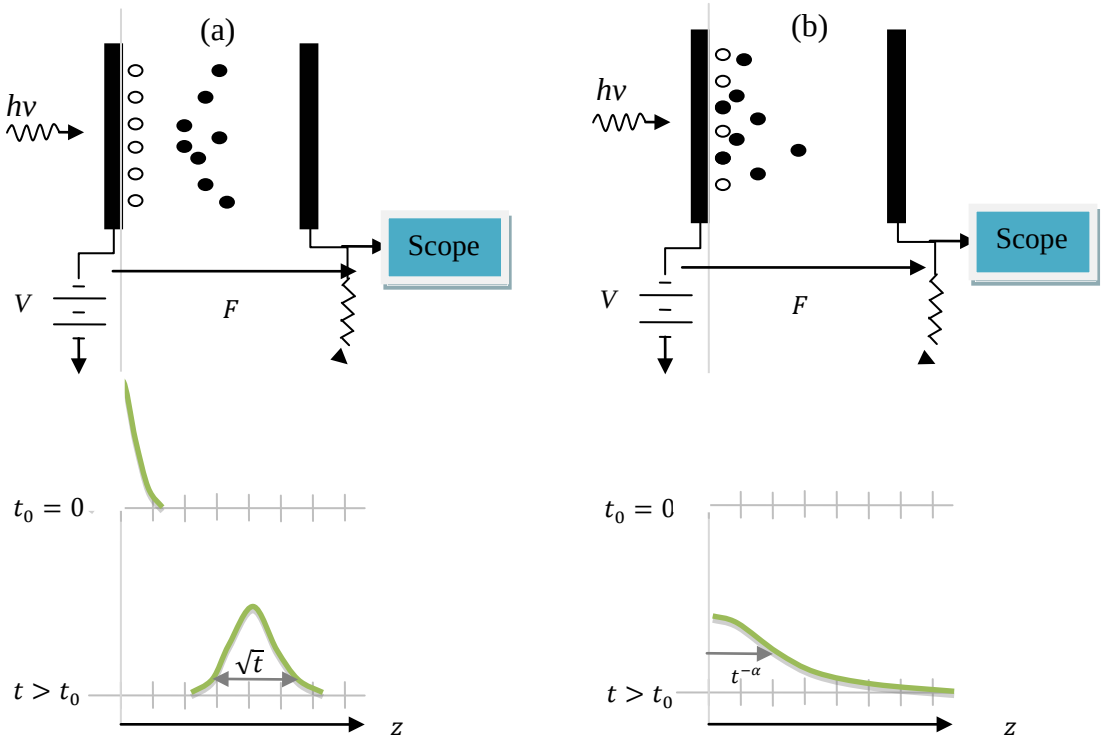

FIG 2.13. Dispersion versus drift and diffusion. The basic differences between (a) the classical model and (b) the random walk model. One side of the sample is exposed to a flash of light (shown as the jagged arrow) at time, $t = 0$. This creates a charge distribution at the interface given by the empty circles (note both (a) and (b) show the same initial charge distribution). At some time, $t > t_0$, the charge distribution has propagated into the sample (given by the dark circles). In (a) the positions of the moving charges (for $t > 0$) relative to each other are representative of the spreading of the carrier packet as it traverses the sample under the influence of the applied field. In (b) the positions are representative of a random walk in which the majority of carriers are pinned near the interface. In (a) the transit time is proportional to the thickness of the sample. In (b) the transit time is much more complex. After (Kao, 2004).

longer occurs? How is it that we can still observe a current and hence, transport? And what *is* hopping? These questions combine with at least two red flags in our development of transport theory that suggest important ideas have been overlooked. The first flag was the usefulness of the mobility edge and band tail states in our model (which has been largely ignored). Secondly, Fig. 2.9 and Fig 2.5 hint at deeper effects that result from the energetic description of the DOS, but no mention of where these ideas should lead has been discussed—at least not in detail. Further, Fig. 2.7 shows only a delta function DOS and does not in any way suggest that a distribution exits. Figure 2.9 shows only equilibrium processes. It is suggested that there is an extended DOS, but all of the carriers that actively participate in transport are at the Fermi level; and therefore, these processes also appear to act as if a delta function DOS was used. These diagrams are

misleading in the sense that they give very little information about the nature of the DOS. As it turns out, our understanding of dispersive transport and the nature of low-temperature transport are the red flags for both a new mode of transport (*hopping*), the extension of the transport equations to the low-temperature regime, and a more comprehensive description of the role of the DOS in transport at both low and high temperatures. This is the subject of Chapter 3.

CHAPTER 3

AVERAGE MICROSCOPIC PROCESSES

In Chapter 2, we developed the transport equations assuming that conduction occurred through extended states in the CB and that trapped carriers could be excited back into the CB by thermal activation (or through the effects of radiation). However, once the temperature is lowered sufficiently, trapped carriers can no longer gain enough energy through thermal excitation to be excited to the CB. At low temperatures, the ideas developed in Chapter 2 for electron transport appear to fail. However, measurements of semiconductors and HDIM clearly demonstrate charge transport at low temperatures (Zallen and Scher, 1971; Scher and Lax, 1973a, 1973b; Scher and Montroll, 1975; Böttger and Bryksin, 1985; Baranovskii and Rubel, 2006). In this chapter, a discussion of how low-temperature transport occurs, the machinery to understand the physical picture, and a complete set of low-temperature conductivity equations are developed.

How does low-temperature transport occur? This was the problem faced by the semiconductor industry in the mid-to-late 1950s and answered in 1961 by Mott and Twose, who published a seminal paper entitled, “The Theory of Impurity Conduction” (Mott and Twose, 1961). This paper presented the first complete description of low-temperature processes for doped semiconductors called *hopping*. Mott and Twose essentially used the ideas originally developed for ionic conductivity of atomic states in a crystal lattice and extended this to low-temperature conduction in semiconductors (Mott, 1973). Mott and Twose offer an excellent mathematical and conceptual development, often arriving at expressions for the wave function overlap and resulting conduction from first principles.

A simple explanation and a conceptual connection to our simple DOS models from Chapter 2 follow from Fig. 3.1 (a) and (b). Consider Fig. 3.1 (a), which shows an ideal donor delta function DOS, with an applied field and resulting motion of a single positive charge (a hole or electron vacancy). As time goes on, the hole is filled by a nearby donor electron and, therefore, the hole moves from one donor atom to the next. (It is assumed that they are sufficiently close together to conduct, but that the mobility is still reduced from extended state conduction (Mott and Twose, 1961). In this case, enough energy is available

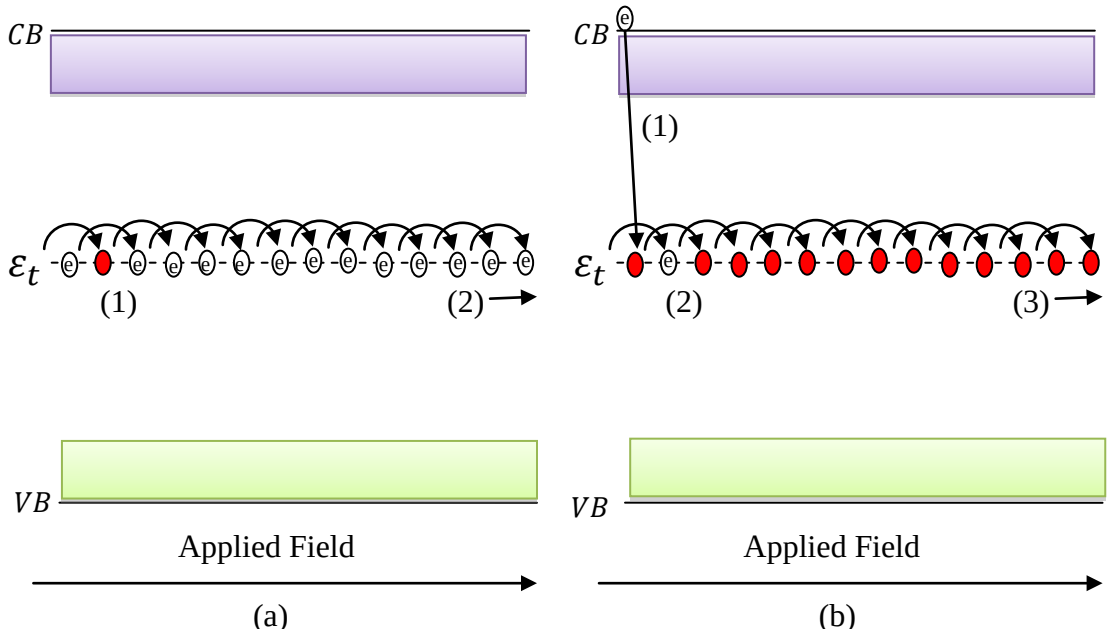

FIG 3.1. Low-temperature impurity hopping and thermally activated hopping. (a) The case where electrons hop between donor impurity states; an impurity electron moves from position (1) to position (2) under an applied electric field. (b) The case where an electron is injected into a delta function DOS from the CB (1) and hops from trap state to trap state (2) until the carrier reaches the rear contact or recombines with a hole emitted from the rear contact (3). In both (a) and (b), transport occurs via the defect DOS in the gap at energy, ε_t , which is a transport energy.

to drive the process of hopping for the hole (liberation of nearby electrons), but not enough that any of the electrons (not holes) can be excited from donor states into the CB.

Now consider Fig. 3.1 (b), which shows what can be thought of as a mirrored arrangement. In this case, the DOS is composed of acceptor states (traps) and a single electron is injected into the trap distribution from the conduction band; this is exactly our delta function DOS model from Chapter 2. Since the temperature is very low, the electron cannot be re-excited into the CB and, therefore, can only move by hopping from one trap state to the next in the same way as the hole in Fig. 3.1 (a). The two processes shown in Fig. 3.1 (a) and (b) are common themes in modern-day, low-temperature semiconductor design. These models, however, are only for a single level DOS and do not reflect the full character of the DOS in a disordered semiconducting or insulating material. How does a trap DOS with an energetic distribution (like those suggested in Table 2.1) affect the observed transport at low temperatures, and how can the transport equations be extended to model low-temperature conductivity?

The answer to the first question is the subject of this chapter, and a complete explanation requires additional ideas not yet covered. Consider Fig. 3.2 in which two different processes, (a) and (b), are depicted. The first process (a) —described in Chapter 2— is characterized by the transport equations [Eqs. (2.6.8) through (2.6.12)] and is often referred to as thermally activated hopping (TAH) or multiple trapping (MT). Note that only the latter of these two terms is truly accurate. A hop is necessarily a jump between two localized states, but in this scenario the electron may travel a great distance —much larger than the order of the spacing between localized states— before being recaptured. In actuality, the name TAH comes from ionic conductivity, which actually involves a hop between atomic sites; therefore, the name TAH is appropriate (Mott and Twose, 1961). Henceforth, TAH is used exclusively to refer to a thermally activated jump between localized states and MT refers to process (a). Multiple trapping is the process described by the transport equations derived in Chapter 2 and depicted in Fig. 3.2 (a). Note that the carrier that is hopping from one state to the next can arrive in the localized states by a number of means, the conduction band by losing energy, the valence band by gaining energy, and from impurities within the material. It is important to separate the ideas of Chapter 2, as they deal with MT and—at least at this point—not hopping. It will be shown how the macroscopic formalism of Chapter 2 can be extended to include hopping behavior.

The second process, shown in Fig. 3.2 (b), is the extension of the simple delta function DOS for low-temperature hopping, as described in Fig. 3.1 (b), to an energetically disordered DOS in an HDIM. There is clearly a drastic difference in this new depiction of low-temperature transport. In the Mott and Twose model, electrons come from the extended state region and are captured in a trapped state, where they undergo TAH conduction. In Fig. 3.2 (b), the electrons are excited from a deep distribution of trapped carriers. Further, jumps from the deep trapped carrier distribution are not excited in the same way. Rather, carriers can jump spatially and energetically; the mean spatial range, R, over which a carrier can jump varies with energy, W_j. Conduction occurs in a narrow energy range that is approximately a delta function (much like the Mott and Twose picture), but with the electrons coming to these states by an entirely different mechanism. This narrow band at which transport occurs is called the transport band (TB) and lies at the transport energy (TE), ε_t, below the mobility edge and above the charge distribution.

A key to understanding the TB is found in the study of percolation paths (Ambegaokar *et al.*, 1971; Zallen, 1983). The nature of a percolation path is simple. Consider a network of connections, whose numbers are slowly reduced by removing links, until only the minimum number of links (of the right type) required to form a single connecting path is left. This remaining path is called the percolation path, and the minimum number of links (this may be thought of as a density of connections as well) necessary to form it is called the percolation threshold. For a TB to form, localized states must have just enough wave function overlap to allow for conduction through a percolation network.

A special characteristic of the TB is the type of carrier transport (governed by TAH) from one localized state to the next. Since there is not enough thermal energy for a carrier to be excited any higher in the DOS, a hopping carrier has but two choices: (a) stay in the transport band and move to the next available site at approximately the same energy, or (b) lose energy and become trapped again in the deep distribution (the carrier reservoir). The carrier reservoir's upper energy bound is defined by the top of the trapped carrier distribution and is called the effective Fermi level, ε_f^0; all trapped carriers below ε_f are part of the reservoir. Deep states in the reservoir from which carriers are excited use quantum tunneling in combination with the thermal energy given to the carrier by the phonon spectrum to make a jump to the TB. (Note, this is not TAH.) It is understood that the ratio of trap separation energy, W_{ij}, to the the trap separation distance or range, R_{ij}, [more correctly, the field energy $(q_e R_{ij} F)$], determines to which site in the TB a carrier will jump. This type of hopping is called variable range hopping (VRH). VRH is often referred to as phonon-assisted-quantum-mechanical-tunneling and was largely put forward by Mott (Anderson, 1958; Mott, 1961; Dennison and Brunson, 2008; Brunson, 2009). Anderson put forward models with fixed range and a distribution for W_{ij} (see Sec. 2.3.4). Mott VRH is a specific case, where the trap DOS is constant in energy, but not in space. We will revisit this model in Section 3.2, where applications of the theory developed in this chapter are applied to USU MPG models and extended to include the exponential and Gaussian DOS distributions.

We now return to the connection between the transport equations and low-temperature transport. Consider Fig 3.2 (a), in which a single carrier descends toward the deeper states via thermalization. Because thermalization requires a discussion of how states move into deep states just after injection, we leave the discussion of thermalization until Section 3.1.8. For the moment, assume that a deep trap

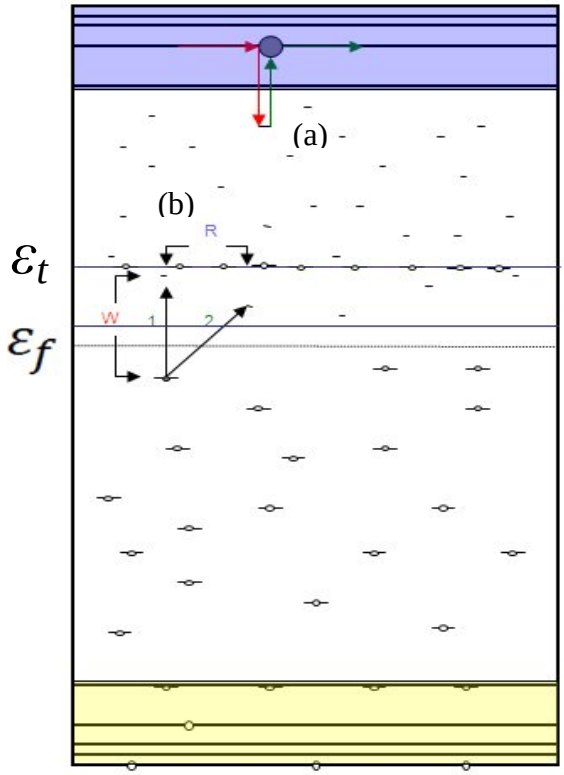

FIG 3.2. Hopping types in HDIM for an energetically depended trap DOS. (a) Simple trapping between extended CB and localized trap states, referred to as thermally activated hopping. (b) Variable range hopping where a combination between energy barrier and distance to the localized stated determines the hop between localized trap states. Here R is the separation and W_j is the change in energy between the two trap states. Note that the line to which the hop occurs is at the transport energy, ε_t.

distribution is formed and serves as a reservoir for VRH. Figure 3.3 (b) depicts the transport of carriers using VRH; this is an extension of the process depicted in Fig 3.1 (b) to highlight the dynamic nature of VRH. There are five steps required to describe VRH transport:

(1) the combination of quantum mechanical tunneling and thermal energy allow the deep trapped carrier to jump from below the ε_f to the TB;

(2) the carrier undergoes simple TAH between transport states at or near ε_t;

(3) the carrier losses energy to another intermediate level state, still considered part of the TB (This highlights that the TB has an energetic width.);

(4) the carrier makes a set of local, thermally-driven upward hops, which combine with TAH to allow for translation; and in the final step,

(5) the carrier loses its excess energy and is trapped in a new, spatially distant deep state.

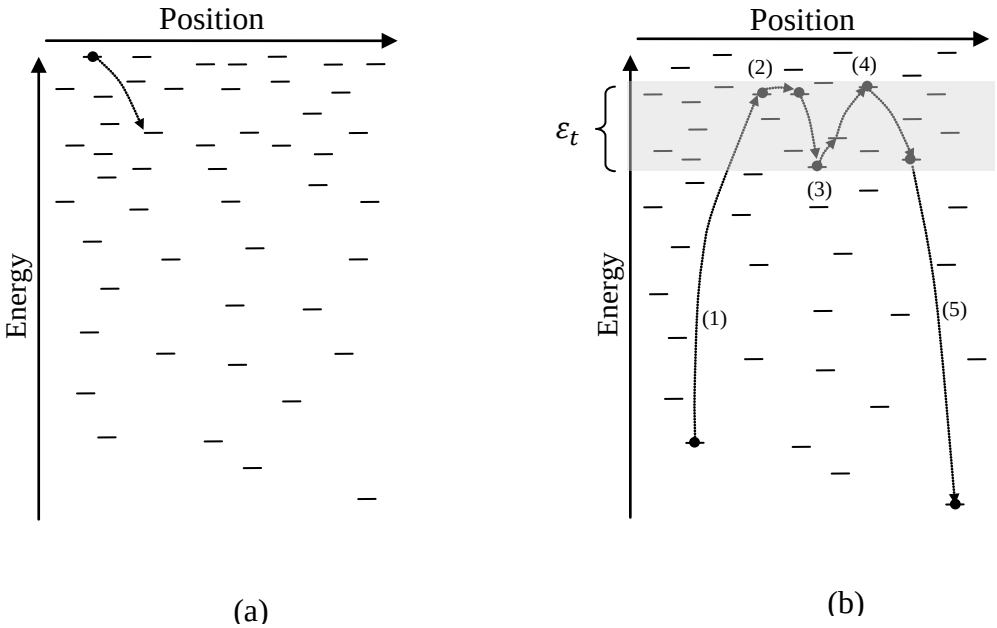

FIG 3.3. Thermalization and transport mechanisms for VRH. (a) Hopping directly to deep states without excitation. (b) The hopping transport process: (1) Excitation to shallow states (transport states at energy ε_t) due to thermal energy; (2) transport at ε_t; after (3) carriers can become trapped again in intermediate states (3) or proceed to step five; (4) Re-excitation from an intermediate state (3) to a state at the transport level (4); (5) Capture by a deep state (after Baranovskii and Rubel, 2006)

Like the extended states, the TB has some finite width in which carriers move. Unlike the extended state CB transport, in the TB the carrier, mobility is greatly reduced and transitions are TAH in nature.

Figure 3.3 (b) looks a great deal like MT transport, with the extended states replaced by the transport band and the trap distribution now deeper in the DOS. If fact, we used the same set of steps for MT transport in Section 2.6: excitation from a trapped state, transport in the extended states, and recapture, where here, equivalence is made between the extended states and the TB. The extension of the transport equations from the MT regime to low-temperature transport has been carried out by several authors (Schmidlin, 1977; Mott, 1984; Baranovskii and Rubel, 2006). One particularly lucid description of the connection between hopping transport and the transport equations was given by Schmidlin (1977). Schmidlin's paper clearly develops the relationship between a master hopping equation—called the Pauli master equation (PME)—and the transport equations. His work was a critical step in understanding the connections between continuous-time random walk (CTRW) models, general master hopping equations (GME) (Böttger and Bryksin, 1985), and a new expression of the transport equations. Schmidlin's insight

followed from attempts to explain dispersive transport in disordered materials and the need to classify localized states into transport and trapping centers (Schmidlin, 1977). In fact, the language to describe VRH and MT in fundamental terms did not exist until the classification of states was made; prior work treated all localized states on equal footing. Section 3.1 develops the resulting language, mathematical detail, and physical insight needed to describe low-temperature and dispersive transport in a consistent nomenclature. There are many applications of this new formalism connecting the transport equations and PME, with low- and high-temperature expressions for the conductivity (Sessler and West, 1976; Schmidlin, 1977; Arkhipov and Rudenko, 1979; Arkhipov *et al.*, 1979, 1983, 1984, 1985b, 1987c, 1996a, 1996b, 1997a, 2003b, 2005b; Tiedje and Rose, 1981; Monroe *et al.*, 1981; Tyutnev *et al.*, 1983a; Monroe, 1983, 1985, 1986; Sessler, 1987; Abramov *et al.*, 1987; Arkhipov and Nikitenko, 1993; Arkhipov and Bässler, 1994a, 1994b; Arkhipov and Adriaenssens, 1996; Sessler and Yang, 1999; Gross *et al.*, 2003b; Baranovskii and Rubel, 2006).

3.1. Average Microscopic Tools

3.1.1. Introduction

In the introduction to this chapter, a description of the anatomy of carrier transport in HDIM at low temperatures was presented and, subsequently, the connection between the PME and the transport equations was discussed. Included in our discussion of Fig 3.2 was the introduction of the effective transport energy, transport band, and the concept of thermalization as originally introduced in Chapter 2. Another concept not yet introduced is needed, called the Quasi-Fermi level (QFL). A detailed understanding of how carriers thermalize in the DOS is required before a complete understanding of the QFL can be given; this concept is, therefore, left until section 3.1.7. The purpose of Section 3.1 is to introduce the mathematical detail to describe thermalization, the transport band, the transport energy, Fermi level at the energy, ε_f, and the QFL; together, these concepts lead to a physical understanding of microscopic transport involving the strap states in HDIM.

The introduction of ideas begins with a modification of the simple probability picture for thermalization and re-excitation of carriers to transport (extended) states given in Chapter 2 and depicted in Figs. 2.7.1 (b) and (c). In this new picture, the quantum mechanical interaction between states must be

considered to adequately describe VRH and transport at the effective transport energy. This concept is referred to as the Miller and Abrahams hopping rate (MAR) (Miller and Abrahams, 1960). Next, we describe the energy (called the demarcation energy) used to separate the trap states into occupied or empty states using the MAR. The demarcation energy (DE) allows—for the first time—a description of the centroid of the trapped charge distribution as it moves to lower energies in the DOS during thermalization; in fact, the DE characterizes the thermalization, process. The DE is essential to understanding both how the carriers will redistribute in the DOS during thermalization and also their relative energy with respect to the TE. Having understood the thermalization process, we move to a development of the transport energy and define the time required for a thermalizing centroid of the distribution of trapped carriers to drop below the TE and begin hopping transport. The end of the thermalization process occurs when the DE coincides with the QFL. In many cases, the DE never reaches the QFL, and such systems will present a dispersive current versus time response. This section concludes with an investigation of the thermalization time. Having described all the mathematics and physical concepts, we present some applications (Section 3.2) and show a direct reformulation of the USU MPG VRH model in term of these new tools. This reformulation allows the USU VRH model to be written as a two parameter fit and includes temperature and field dependence.

3.1.2. Hopping Transition Rate

The rate at which hops are executed by carriers for states in different energetic and spatial regions governs the character of the distribution of carriers as they thermalize into the DOS, for transport at low temperatures in HDIM. The determination of the hopping rate for a disordered system is far from simple and, in general, requires a detailed knowledge of the phonon spectrum (Mott, 1961, 1973, 1977). In 1960, Miller and Abrahams published a theory that provided a simple approach to the complex system of disordered materials (Miller and Abrahams, 1960). It has been shown by many authors that this approximation will generally give a good first order estimation of the hopping rate (Ambegaokar *et al.*, 1971; Mott and Davis, 1971; Monroe, 1985). However, there are many exceptions to this formulation (Mott and Davis, 1971; Vukmirovic and Wang, 2010). An excellent review of the MAR approach and connection to percolation models is presented in Ambegaokar *et al.* (1971). In this dissertation, the MAR will be used exclusively to describe hopping transition behavior in HDIM. As it turns out, the MAR

contains all the essential physical information necessary to describe nearly any hopping system in which trapped electron-electron correlation (correlation between trapped carriers, not the traps themselves) is not a major influence on the transport; to this author's knowledge, this is always the case in HDIM, due largely to the significant spatial separation of localized states and the relative small number of carriers involved.

The simplest expression of hopping that allows for a concrete description of the MAR was derived by Ambrogekar using a percolation model and is given by the following equation (Ambegaokar *et al.*, 1971):

$$\nu_{ij} = \nu_0 exp\left[-\frac{2R_{ij}}{\eta}\right] \times \begin{cases} exp\left[-\frac{\varepsilon_{ij}}{k_b T}\right] & \varepsilon_{ij} > 0 \\ 1 & \varepsilon_{ij} < 0 \end{cases}. \tag{3.1.1}$$

Here, ν_{ij} is the hopping rate between occupied site, *i*, and unoccupied site, *j*, separated in energy by ε_{ij} and in distance by R_{ij} . The decay length or localization radius of the trap state wavefunctions associated with each trapped site is η and the attempt-to-escape frequency is ν_0 (see Section 2.4.3). The hopping rate is driven by two terms in Eq. (3.1.1); the first is range-dependent and the second results from the phonon spectrum. The mean transition rate given by Eq. (3.1.1) was shown in Section 2.4.2 to scale as the transfer integral between localized wavefunctions, as given by Eq. (2.4.4), evaluated at the mean separation distance between localized sites, $a = \bar{R} \equiv \langle R_{ij} \rangle$. There, for localized Coulombic centers, the transition rate transfer integral was shown to scale approximately as *exp(-2a/r_o)*, where r_0 is a characteristic fall off radius for the wavefunction (not quite a localization radius) [see Eqs. (2.4.5) and (2.4.7)]. For a more general localized wavefunction, the wavefunction falls off approximately exponentially at large distances from a trap site proportional to the decay length or localization radius of the trap state wavefunctions, η (see Fig. 2.3 and Section 2.4.3). Thus, the mean transition rate proportional to the square of the wavefunction is

$$\bar{\nu} \propto exp\left[-\frac{2\bar{R}}{\eta}\right] \approx exp\left[-\frac{2a}{r_0}\right] \; ; \quad \varepsilon_{ij} > 0. \tag{3.1.2}$$

$R, \eta,$ and a play an important role in understanding what kind of transport we observe. For large spatial disorder, little or no energetic disorder dependence is observed, which is often the case with simple ionic models like the TAH model (Dennison *et al.*, 2009b). In such a case, the average hopping distance is $a = \bar{R} \equiv \langle R_{ij} \rangle$, see Eq. (3.2.41) for an example. However, when significant disorder is present, both

spatially and energetically, the average hopping distance $\langle R_{ij} \rangle \neq a$ because it is a function of both spatial disorder and energy leading to hopping distances greater than the average distance between localized states, η is a function of energetic disorder (i.e., the exponential fall off of a wavefunction for tunneling through a barrier depends on the energetic height of the barrier), since on average localized states are much too far apart to interact. Thus, the type of disorder determines the relationship between the nearest neighbors, localization length, and hopping distance. Equation 3.1.2 allows any two these parameters to be expressed in terms of the other two.

The interdependence of the range and energy is not, at first glance, obvious. Consider the exponential DOS discussed in Section 2.4.5. In this model, the DOS decreases into the gap in an exponential way. Thus, for shallow traps close to the mobility edge, the overlap between states is greater than for deep traps. That is, η is larger and the hopping range is smaller near the TE than for deeper states. Recall the wave function envelope for localized states typically falls off exponentially at large distances from the trap site. It is the ratio (R_{ij}/η) that determines the strength of the VRH. For shallow traps $(R_{ij}/\eta) \ll 1,$ and the leading exponential term in Eq. (3.1.1) is approximately one. In the shallow trap case, Eq. (3.1.1) becomes the probability distribution discussed in Section 2.3 used to develop the transport equations. The DOS in most HDIM is a function of energy, and therefore the range is a function of energy, as well. (Here energy is measured as increasing from the mobility edge downward to the state of interest. The reader is cautioned not to confuse the usual convention for measurement of energy in the CB with respect to the VB, where energy is increasing as we move upward from the VB.) In our description of processes in the DOS, we speak of the energy as being deeper as we move downward away from the mobility edge (CB edge). This arrangement of the hopping range as a function of the decreasing DOS and with increasing energetic depth into the DOS is precisely why VRH occurs from deep states to shallower states, but not the other way around. It also explains why transport at the TB is governed almost entirely by TAH, as the TB is largely composed of much shallower states whose overlap is larger.

In order to classify trapped states during thermalization and transport, we need some new language. Consider the first few moments of thermalization. Carriers enter into the DOS and undergo nearly instantaneous capture by a shallow state; but, at energies close to the mobility edge, the carrier is

released almost as quickly as it is captured. However, at low temperatures, the carrier will not have enough energy to be excited upward; thus, its only choice is to find a state of nearly equal energy or to drop further into the DOS (loosing energy). We observe, as time goes on, that the centroid of the carrier distribution (or mean carrier energy) will decrease (or descend) on average into the DOS toward some equilibrium value. This process continues until the ratio (R_{ij}/η) is large enough that VRH begins to dominate the process, causing an upward hopping to counteract the thermalization and descent of the mean carrier energy. The energy centroid of the carrier distribution is time dependent, since each successive trapping and release event takes longer, the lower into the DOS the center of the distribution progresses. The energy that separates states that have released at least one carrier from those that have not is called the demarcation energy (DE) and is the subject of the next section. Further, it turns out to be advantageous to understand the thermalization process and DE when seeking solutions to the multiple trapping equations. The separation of states allows simplification of the solutions and interpretation of the resulting expressions for both low-temperature and high-temperature behavior. These ideas, in fact, lead to deep understanding of dispersive behavior (Rudenko and Arkhipov, 1978, 1979; Arkhipov *et al.*, 1979; Arkhipov and Rudenko, 1979, 1982a, 1982b; Tiedje and Rose, 1981; Monroe, 1986).

3.1.3. Demarcation Energies

Consider an electron relaxing from some excited state; say it was injected at or above the mobility edge. We know that progressive thermalization occurs with release and re-trapping of localized electrons. How can we write down a temperature- and time-dependent description of the central energy centroid? Consider again Eq. (3.1.1), but for the situation $(R_{ij}/\eta) \ll 1$ and some general energy ε<0; then

$$\nu(T) = \nu_0 \exp\left[\frac{-\varepsilon}{k_b T}\right]. \tag{3.1.3}$$

The time dependence is predominantly controlled only by the release events and, thus, the centroid of the thermalizing charge distribution must occur when the probability of release reaches unity. By definition, states above the DE have released their charges and those below have not. The DE is therefore defined as the energy where the probability of release from Eq. (3.1.2) is equal to one, such that $1 \cong \bar{\nu}(\varepsilon_d(t))t$, i.e., the rate of release multiplied by the retention time is the dwell probability. Measuring energy from the mobility edge downward, $\varepsilon = (\varepsilon_d(t) - \varepsilon_{ME})$, (Note, some authors measure energies from

the Fermi-energy upward and others from the CB edge downward, all of which can occur in energetically different places within the DOS), we can write the condition for the time evolution of the centroid demarcation energy as,

$$1 \cong \overline{\nu}(\varepsilon_d(t) - \varepsilon_{ME})t. \tag{3.1.4}$$

Using Eqs. (3.1.2) and (3.1.3), the expression for the downward demarcation energy during thermalization for the high temperature case is

$$\varepsilon_d \downarrow (t) = \varepsilon_{ME} - k_b T ln(\nu_0 t) \qquad \{\text{Downward Demarcation}\}. \tag{3.1.5}$$

The DE is usually presented with the TE energy set to zero, and we will follow this convention unless otherwise stated. This expression works for all the DOS of interest, as long as the ratio of hopping range to wavefunction overlap is small.

At some point, the decent of the DE will stop, as the downward hopping becomes balanced by the upward VRH mechanism. In the literature, one often encounters a discussion of two demarcation energies: one is due to simple thermal release from trapping states that is thermal in nature and a second DE that is driven by VRH. The separation of DE into two types is done only to highlight the different physical mechanism, but both follow from the MAR. Thus, the second DE is often called the *upward hopping demarcation energy*, $\varepsilon_d{}^{\uparrow}(t)$, driven only by VRH.

In the upward hopping regime, the hopping range dominates the MAR and the low T limit suggests $\nu_0 \exp\left[\frac{-\varepsilon}{k_b T}\right] \sim 1$. To find an expression for the upward DE, one sets the (mean) probability of an escape to one; i.e., $\nu_{\uparrow}\big(\varepsilon \uparrow_d (t)\big)t = 1$, just as before, but with the energy-dependent hopping range explicitly expressed as $R \rightarrow R(\varepsilon \uparrow_d (t) - \varepsilon_t)$ (Karkin *et al.*, 1979; Rudenko and Arkhipov, 1979; Orenstein *et al.*, 1980, 1982; Orenstein and Kastner, 1981; Monroe, 1985). This equation is solved for the value $\varepsilon \uparrow_d (t)$ in terms of the TE to which subsequent hops will occur. Using the expression for the upward hopping rate when VRH is active, Eq. 3.1.1, and replacing the energy by $\varepsilon \uparrow_d (t)$, we have

$$1 = t\nu_0 exp\left[\frac{-2R(\varepsilon\uparrow_d(t) - \varepsilon_t)}{\eta}\right]. \tag{3.1.6}$$

Expressed in terms of an energy-dependent mean hopping range, $\langle R(\varepsilon \uparrow_d (t) - \varepsilon_t)\rangle = \bar{R}(\varepsilon \uparrow_d (t) - \varepsilon_t) = a(\varepsilon \uparrow_d (t) - \varepsilon_t)$ and mean transition probability $<\nu\geq=\overline{\nu}=1$,

$$1 = \bar{\nu} = t\nu_0 exp\left[\frac{-2\bar{R}(\varepsilon\uparrow_d(t)-\varepsilon_t)}{\eta}\right]. \quad (3.1.7B)$$

Eq. (3.1.5B) allows the energy-dependent mean separation distance to be expressed in terms of the mean transition rate and the localized wavelength decay length.

We now assume that the mean hopping range for a 3D material can be found by using the DOS to estimate a sphere of radius $\bar{R}$ and volume per state of $\frac{4}{3}\pi\bar{R}^3$ around which hops may occur (Monroe, 1985). The density of states per unit volume is $\left[\frac{4}{3}\pi\bar{R}^3\right]^{-1} = n_t(t) = \int n_t(\varepsilon, t)\, d\varepsilon$. Here, the constant DOS is to be used (see Section 2.4.5), as it is mathematically simpler; however, the procedure to obtain the range is identical for all other DOS expressions. Using the constant DOS, $n_t(\varepsilon) = \left({N_t}/{\varepsilon_o^c}\right)$, and the fact that an upward hop will most likely occur from the DE to the TE, we can obtain an estimate for the mean range $\bar{R}$ of a hop

$$\bar{R}\left(\varepsilon\uparrow_d(t)\right) = \left[\frac{4\pi}{3}\frac{N_t}{\varepsilon_o^c}\left(\varepsilon_t - \varepsilon_d^{c\uparrow}(t)\right)\right]^{-1/3}. \quad (3.1.8)$$

This expression highlights the connection between the hopping range and the energy-dependence of the DOS. Using Eq. (3.1.5B) to express $\bar{R}$ in terms of the localization decay length and mean transition rate, and substituting Eq. (3.1.6) with the condition that $\nu_\uparrow\left(\varepsilon\uparrow_d(t)\right)t = 1$, we obtain an expression for $\varepsilon_d^{c\uparrow}(t)$ in a constant DOS

$$\varepsilon_d^{c\uparrow}(t) = \varepsilon_t - \left[\frac{6\varepsilon_o^c}{\pi N_t}\frac{1}{\eta^3}\right](ln[\nu_0 t])^{-3} \quad \{\text{Upward demarcation energy for a constant DOS}\}. \quad (3.1.9)$$

We can simplify this expression by defining an effective temperature equation,

$$T_0^c = \frac{24\varepsilon_o^c}{\eta^3\pi N_t k_b}. \quad (3.1.10)$$

Then Eq. (3.1.7) can be written as

$$\varepsilon_d^{c\uparrow}(t) = \varepsilon_t - \frac{k_b T_0^c}{4}(ln[\nu_0 t])^{-3}. \quad (3.1.11)$$

Many authors use a slightly different convention for the effective temperature in which the number 24 is replaced by 18 (Fritzsche, 1990); still others use a numerical constant, β, whose value ranges from 10.0 to 37.8 (Baranovskii and Rubel, 2006). This ambiguity results from different expressions of the MAR, application of the DOS, and spatial dimensionality of the system. See Baranovskii and Rubel (2006) for a

detailed treatment. Stated another way, the discrepancy in the constant results from different assumptions about the packing density of the density of states assumed in the MAR; for example in 3D for close packing of cubes, $[\bar{R}^3]^{-1} = 1$, for packing of spheres on a cubic lattice, $\left[\frac{4}{3}\pi\bar{R}^3\right]^{-1} = 1$ as used in Eq. (3.1.6), and for close packing of spheres on an HCP or FCC lattice, $[1.10\bar{R}^3]^{-1} \approx 1$. Another modification often found, is that the effective temperature is expressed as an energy by multiplying by the Boltzmann constant; such a convention yields a demarcation energy of the form

$$\varepsilon_d^{c\uparrow}(t) = \varepsilon_t - \frac{T_0^c}{4}(ln[\nu_0 t])^{-3}. \tag{3.1.12}$$

Quite often in the literature, the DE is presented without reference to the TE (Monroe, 1983, 1985, 1987); we leave a discussion of the TE until Section 3.1.5. These differences in notation, energy reference, and definition of the MAR cause confusion, but in the end, the energetic point at which the downward demarcation energy passes the transport energy is the point at which upward hopping (VRH) will begin to dominate. Generally, the time at which this occurs is referred to as the segregation time, τ_{seg}. A discussion of segregation time is also differed until Sections 3.1.5. Since the downward demarcation energy is assumed to be given Eq. (3.1.4) for all the DOS considered in this dissertation, we next summarize the upward demarcation energies for the exponential and Gaussian DOS.

To obtain expressions for the exponential and Gaussian DOS upward demarcation energies, the same procedure used to obtain Eq. (3.1.9) is followed. For the exponential DOS upward demarcation energy we obtain

$$\varepsilon_d^{e\uparrow}(t) = \varepsilon_{\mathrm{TE}} - k_b T_0^e ln\left(\frac{6}{k_b T_0^e \eta^3 \pi N_t}\right) - 3k_b T_0^e \ln\left[\ln(\nu_0 t)\right] \qquad \{\text{Exponential DOS}\}. \tag{3.1.13}$$

Here, $k_b T_0^e$ is the energy scale term for the exponential DOS (see Table 2.1), and T_0^e is the effective temperature. Fortunately, this form of the exponential DOS is very common in the literature and we, therefore, offer no alternative derivations (Orenstein *et al.*, 1982; Monroe, 1985, 1986; Shklovskii *et al.*, 1989; Arkhipov *et al.*, 2002b, 2005a, 2006; Baranovskii and Rubel, 2006; Fishchuk *et al.*, 2007). The derivation of the Gaussian equivalent leads to the following equation for the upward hopping rate:

$$ln(\nu_0 t)^3 \left(\frac{2}{\eta}\right)\left(\frac{3}{2\pi\varepsilon_G N_t}\right) + 1 = erf\left(\frac{\varepsilon_d^{G\uparrow}(t)}{\sqrt{2}\varepsilon_G}\right) \qquad \{\text{Gaussian DOS}\}. \tag{3.1.14}$$

A solution for the low-energy approximation can be obtained for early times in the thermalization process by using the small expansions for the *erf(x)* function (Abramowitz, 1965). For the cases of medium- to high-energy scales, there is no good approximation that allows for a simple determination of $\varepsilon_d^{G\uparrow}(t)$. The problem, of course, can be solved numerically.

Now that we have a reasonable description for the time evolution of the centroid of the carrier distribution, $\varepsilon_d{}^{\uparrow}(t)$, as it goes through the process of thermalization, a description of the complete charge body and thermalization process as a whole can be presented.

3.1.4. Thermalization

Consider a body of electrons injected into the extended conduction states of an HDIM at time, *t=0*. The electrons will make their way in time into the localized states via thermalization. In general, the carriers will be rapidly trapped in the localized states. If the capture cross section for all the states is the same (this is always assumed, but is likely not generally true for all temperatures), the electrons will populate the states uniformly beginning with the states highest in energy above or at the ME (Orenstein *et al.*, 1982). The carriers in shallow traps will be released much more quickly than those in the deeper traps. In the first moments of thermalization, not enough time has passed for excitation processes to have occurred, and therefore, only trap filling will take place. The mean time for an electron trapped in a particular state at a particular energy to be released is found when the product of the release rate and the elapsed time is unity:

$$\bar{\nu}(\varepsilon_d)t = 1. \tag{3.1.15}$$

Using the MAR, one observes that the deeper a carrier is into the DOS the longer it takes for release. It is clear then that the energy-dependence of the DOS and the carrier occupation distribution determine release time, and therefore, the observed current. Equation (3.1.13) only tells us how the centroid of the charge distribution will move downward in the DOS with time and temperature.

To understand the evolution of the trapped charge distribution during thermalization, we turn our attention to the *mean occupation number*, $f(\varepsilon, t)$, for trapped states (not to be confused with the Fermi-Dirac distribution function). In a classical Fermi-Dirac distribution, the point at which the occupation number goes from unity to zero is centered about the chemical potential. In such systems, there are no

states in the gap to trap carriers that would normally be in the CB and the system is in thermal equilibrium with the CB. In an HDIM, there is a distribution of trapped states in the gap (the DOS) and the chemical potential changes with time as the process of thermalization progresses. Thus, it is not surprising to find that the mean occupation number is a function of time and energy. For early times, electrons are trapped in the DOS across a wide range of energies (some of which are in thermal equilibrium with the CB, but most of which are not); deep states have a probability of release of approximately zero for early times. Clearly for trapping states within the BG, the mean occupation number cannot be unity for early times (it must be less than unity), since thermal equilibrium has not been achieved for the majority of trapped states. Schiff (1981) has shown that the mean occupation number goes as $f(\varepsilon,t) = F(t)\left\{1+\exp\left[\left(\varepsilon-\varepsilon_d^{\downarrow}(t)\right)/k_bT\right]\right\}^{-1}$, where *F(t)* describes the time-dependent evolution of carriers in the DOS. This difficulty highlights one of the complexities of carrier dynamics in HDIM. Excellent discussions of the mean occupation number and dispersion can be found in (Schmidlin, 1977; Noolandi, 1977a, 1977b, 1977d; Tiedje and Rose, 1981; Schiff, 1981) and (Orenstein *et al.*, 1982). Orenstein put forth a method for finding the mean occupation number in disordered systems (of any given DOS) by considering the product of the DOS, $N(\varepsilon)$, with the mean occupation number,

$$n_t(\varepsilon,t)d\varepsilon = f(\varepsilon,t)N(\varepsilon)d\varepsilon, \tag{3.1.16}$$

which must define the number of *trapped carriers*, and subsequently, describe the process of thermalization (Orenstein *et al.*, 1982).

Figure 3.3 shows the process of thermalization for an exponential DOS as a function of the time-dependent demarcation energy at successive times after excitation of carriers into the conduction band and subsequent re-trapping (Orenstein *et al.*, 1982). Figure 3.4 (a) shows the associated DOS, Fig. 3.4 (b) shows the mean occupation number, and Fig. 3.4 (c) shows Eq. (3.1.14), which is the continuum of trapped carriers and their evolving thermalization (Note, the area under the curve remains the same for all times). The process of capture and release causes the continuum of bound states to move deeper into the DOS toward the Fermi energy (equilibrium value of the QFL) as a function of time and temperature, until some equilibrium is established. This is the simplest picture that we can put forth, and does not include recombination or the effects of upward hopping. In fact, this model is strictly correct only for an

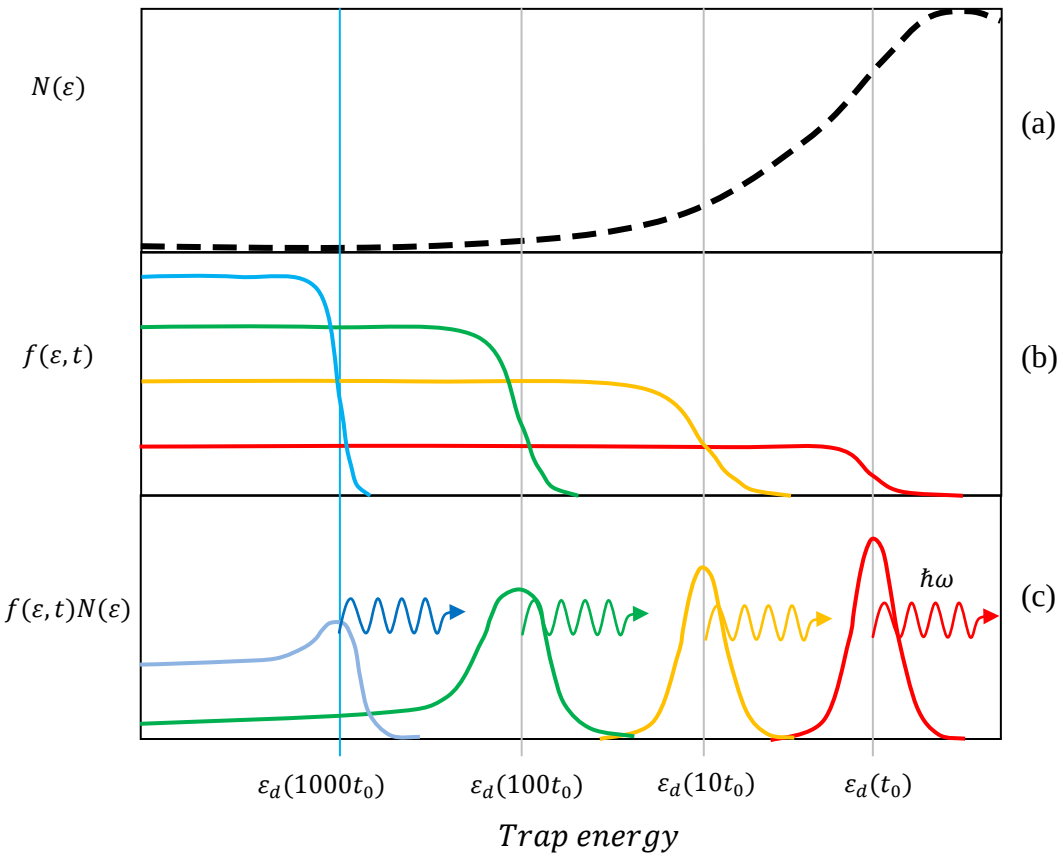

FIG 3.4. Thermalization of injected carriers and the change in trapped carrier distribution characterized by an energetic center, $\varepsilon_d(t)$. (a) The DOS, assumed here to be an exponential. (b) Mean occupation of states as a function of time and energy. (c) Product of the DOS and the mean occupation number, which leads to a description of the distribution of occupied trapped states near the demarcation energy. This process can involve luminescence through the emission of photons from shallow states in emitting low-energy (red) photons and shifting toward the high-energy (blue) photons as the charge body thermalizes into the DOS. (Orenstein *et al.*, 1982). Red, yellow, green, and blue curves are shown at successively later times t_o, $10t_o$, $100t_o$, and $1000t_o$, respectively.

energetically and spatially infinite slab with some externally excited electron distribution (i.e., no electron-hole pairs are created). For a detailed treatment of thermalization see (Orenstein *et al.*, 1982).

What other processes can we consider? In fact, we have already looked at one such process when deriving the upward demarcation energy. In this process at some energetically deep point in the DOS, say $\varepsilon^{\downarrow}{}_d(1000t_0) \sim \varepsilon^{\uparrow}{}_d(1000t_0)$, we can imagine that the evolving carrier distribution uncovers an additional, —but very small— distribution of trapped states whose special feature is that it can support VRH, perhaps through more closely spaced trap states. This new distribution will be the transport energy, ε_t.

As $\varepsilon^{\uparrow}{}_{d}$ continues its descent toward the equilibrium value, the population of the TE by electrons will grow larger as more carriers jump to the TE from energies at or below the DE located at ε_t.

We may also consider the effects of recombination, which will alter Figure 3.3 (c) in a fundamental way. Recall that above we have replaced the CB edge with the mobility edge or TE. We can now consider what disorder has done near the VB edge. The answer is that there is a valence mobility edge that is the mirror of the CB mobility edge. Thus, the process of carrier loss from the conducting [Fig. 2.9 (b)] or trapped [Fig. 2.9 (f)] states into the empty holes near the valence mobility edge (called recombination centers) will draw off carriers from the trap state distribution, thus decreasing its magnitude. This effect, called recombination limited transport, generally only occurs for low temperatures where the TE merges with the QFL (Fritzsche, 1990). For wide band gap materials, we generally only consider recombination with valence holes from the extended transport states (i.e., no intra-band recombination is considered). As the carrier distribution descends into the DOS, it losses energy to the local lattice via phonon or photon emission.

We now explicitly evoke the assumption used throughout this dissertation —that electrons are the primary carriers and the holes are immobile— and ask the question, how does the mean occupation evolve with time in the presence of recombination? We assume an Ohmic injection of photo-excited carriers that are uniform in space and energy, N_{inj}. This does not necessarily mean that the carriers are generated by a RIC-type process; in fact, the carriers can be injected by any means. The process of thermalization is independent of the injection mechanism, as long as there is no electric field large enough to distort the trap state distribution or initiate significant recombination from carriers that move directly from the trapped distribution to holes in the VB. We, therefore, use N_{inj} in place of a generating term, $G(z,t)$, to make this process distinct. This gives an instantaneous number of photo-excited free carriers, Δn_e, injected at time t_{inj}. We then can write down an expression for the change in the mean occupation number as a function of time, temperature, and energy as a differential equation (Orenstein *et al.*, 1982),

$$\frac{df(\varepsilon,t)}{dt} = \frac{\nu_0}{N_e}\left[n_e + \Delta n_e \theta(\mathrm{t} - \mathrm{t_{inj}})\right][1 - f(\varepsilon,t)] - \nu_0 f(\varepsilon,t). \tag{3.1.17}$$

Here the detrapping coefficient is given by $\alpha_{te} = \nu_0 / N_e$. We have also included an initial distribution of carriers, n_e, in the sample resulting from thermal excitation across the gap, from a set of donors, or other

injection mechanisms. However, for wide band gap materials, there is little such excitation and, therefore, this equation reduces to

$$\frac{df(\varepsilon,t)}{dt} = \frac{\nu_0}{N_e}\left[\Delta n_e \theta(\mathrm{t} - \mathrm{t_{inj}})\right][1 - f(\varepsilon,t)] - \nu_0 f(\varepsilon,t). \tag{3.1.18}$$

This is a rate equation for the mean occupation number as a function of trapping and release in the absence of recombination.

The calculation of the mean occupation number is involved and well described in Orenstein *et al.* (1982) and Schiff (1981); we will not reproduce the derivation(s) here. Orenstein has shown that the change in the observed unitless mean occupation number for an exponential DOS is

$$f(\varepsilon,t) = \frac{N_{\mathrm{inj}}}{N_t^e}\frac{\sin(T\pi/T_0^e)}{T\pi/T_0^e}\left(\frac{1}{\alpha_{te}N_e t}\right)^{1-T/T_0^e} exp\left(-\frac{\varepsilon}{k_b T}\right) \qquad \text{for} \qquad \varepsilon \gg \varepsilon_d, \tag{3.1.19}$$

and

$$f(\varepsilon,t) = \frac{N_{\mathrm{inj}}}{N_t^e}\frac{\sin(\pi T/T_0^e)}{\pi T/T_0^e}(\alpha_{te}N_e t)^{T/T_0^e} \qquad \text{for} \qquad \varepsilon \ll \varepsilon_d. \tag{3.1.20}$$

Equation (3.1.17) describes the evolution of the carrier distribution upward in energy for carriers in trapped states below the DE, and Eq. (3.1.18) describes the downward evolution of occupation for excitations above the TE. These two equations, taken together, suggest that as time goes on, carriers below the DE become more likely to be released and the occupation of states above the DE decreases. Both equations are distributions, and thus, together they suggest that the DE is the centroid of the occupied trap state distribution. Put another way, Eq. (3.1.17) is one side of the distribution and Eq. (3.1.18) is the other. Further, inclusion of the demarcation energy suggests a power law-type decay governed by the ratio of the system temperature *T* and T_0^e. This result is actually the hallmark for dispersive behavior (Orenstein *et al.*, 1982).

The product of the DOS and the mean occupation number evaluated at the DE, $N_t(\varepsilon_d(t))f(\varepsilon_d(t))$, provides a determination of the shape and centroid of the charge distribution as it moves deeper into the DOS, just as shown in Fig. 3.4. Now, however, the effects of additional interactions can be studied using the differential equation for the mean occupation number, given by Eq. (3.1.15) or Eq. (3.1.16). While a full investigation of the evolution of the charge body requires numerical calculations, the analytic expression allows some detail to be extracted. First, the equilibrium level, which is the effective

Fermi level, ε_f^0, is generally below the transport energy and above the dark Fermi energy ε_F. The demarcation energy will continue to move toward the dark Fermi energy until all of the trapped states have undergone at least one carrier release. In particular, for a system that displays dispersive behavior, this arrangement tells us that there is a dispersion of trapping energies below the transport edge; this means that the distribution spreads out as thermalization progresses, and we can study the evolution of that spreading. Further, we can study the movement of the charge distribution as it comes to equilibrium, and hence, the change from dispersive to diffusive behavior. Thermalization holds for both extended state and hopping conduction regimes, and can be explored via the multiple trapping formalism using the transport equations in conjunction with Eq. (3.1.16) and a description of the mean occupation number. Having discussed the way in which injected electrons thermalize into the DOS, we can now ask an important question: what is the energy, in a low-temperature system, at which transport of electrons occurs, i.e., what is the TE?

3.1.5. Transport Energies

The term transport energy (TE) was first coined by Monroe (Monroe, 1985, 1987), but was previously conceptually defined by Schmidlin (1977). The TE, $\varepsilon_t(T)$, is the optimal energy to which electrons in deep trapped states will hop in order to undergo transport. The TE is the energy at which equilibrium and nonequilibrium transport phenomena occur, for temperatures such that thermal excitation to CB extended states above the mobility edge is negligible; this assumes that there is no recombination from the trapped distribution to either holes or vacancies in the valance band (Fritzsche, 1990). Consider the path of a trapped electron at some energy, ε_i , deeper in the DOS than the mobility edge, such that it undergoes a quantum tunneling event (or VRH). Arkhipov *et al.* (2006), Schmidlin (1977), and Monroe (1985, 1987) have shown, based on the work of Miller and Abrahams (1960), that there should be a preferred energy for carriers to jump to. At this preferred TE, the mobility of the carriers is nonzero (but much lower than at the mobility edge), and thus, conduction may occur.

Arkhipov has shown that the typical expression for trap-controlled carrier transport is recovered with the band edge replaced by the transport energy in the MAR formalism (Arkhipov *et al.*, 2006):

$$\nu(\varepsilon, T) = \nu_0 exp\left(-\frac{\varepsilon_t(T)-\varepsilon_i}{k_b T}\right). \tag{3.1.21}$$

Here, ε_i is the energy from which a carrier jumps or is excited to in the TE. Since there is a distribution of trapped carriers with a distribution of energies, we represent a specific transitioning carrier with the sub-script *i*. This is a very important result, as it shows directly that the MT formalism can be applied in the context of hopping systems. In fact, it has been shown by many authors under numerous conditions that the use of the MT formalism in the hopping regime can correctly predict the measured current that results from charge transport (Schmidlin, 1977; Noolandi, 1977b, 1977c, 1977d, 1979; Tiedje and Rose, 1981; Arkhipov and Rudenko, 1982b, 1982c; Rudenko and Arkhipov, 1982b, 1982c; Raikh *et al.*, 1990; Arkhipov *et al.*, 2006). The temperature determines whether TAH- or VRH-type behavior will be dominant.

At low temperatures, the transport energy is deep in the band tail; the TE descends with temperature deeper into the gap (away from the ME) until it meets the Fermi level, at which temperature the transport will change its character completely. This has never been measured for HDIM, but is expected to be a constant conductivity independent of temperature (see Section 3.2.8). The behavior of such an intersection has been discussed at length (Fritzsche, 1990; Baranovskii and Rubel, 2006; Arkhipov *et al.*, 2006). The behavior of very low temperature transport (T<10K) is not the focus of this dissertation, and it is therefore left to the interested reader to investigate.

If we raise the temperature to some critical temperature, T_c , the transport energy will merge with the mobility edge and Eq. (3.1.19) recovers the typical expression for the thermally activated attempt-to-escape frequency, $\nu(\varepsilon)$, Eq. (2.5.11), found in the high-temperature expression for the transport models of Chapter 2. T_c is the temperature at which the hopping exchange of electrons between localized states becomes negligible and the dynamic behavior of carriers is accounted for by transport at or above the mobility edge. The addition of the TE to our transport models expands their application to all but very low temperatures.

The following development is an application of a general method to determine the TE, applied to the specific case of a constant DOS. The reader should note that the activation energy used here is the difference between the initial site energy, ε_i, and the TE, $(\varepsilon_t - \varepsilon_i)$. We can find the TE by minimizing the attempt-to-escape frequency about some energy, ς ; this is true because the process of upward hopping to

the TE is an energy minimization that balances the quantum tunneling potential with thermal energy. Then, Eq. (3.1.1) becomes

$$\nu_{\uparrow}(\varepsilon(t),\delta) = \nu_0 exp\left(-\frac{2R(\varepsilon_i-\varsigma)}{\eta}-\frac{\varsigma}{k_bT}\right), \tag{3.1.22}$$

where

$$\bar{R}(\varepsilon) = \left[\frac{4\pi}{3}\int_{\varepsilon}^{0} N(\varepsilon)d\varepsilon\right]^{-1/3}. \tag{3.1.23}$$

The limits of integration are chosen based on the DOS; in this case we integrate from some general energy, ε, to the ME (usually assigned as the zero energy point). For a constant DOS [see Table 2.1 (c)], a specific expression for the mean hopping range (see Eq. 3.1.6) is

$$R(\varepsilon) = \left[\frac{4\pi}{3}\frac{N_t^c}{\varepsilon_o^c}\varepsilon\right]^{-1/3}. \tag{3.1.24}$$

Given Eq. (3.1.20) for the frequency of upward transition and this specific expression for the mean hopping range, Eq. (3.1.22), we can ask: what is the optimal hopping rate for some energy, ς, i.e., what is the maximum hopping rate,

$$\frac{d\nu_{\uparrow}(\varepsilon_i,\varsigma)}{d\varsigma} = 0 \ . \tag{3.1.25}$$

In Mott's evaluation of VRH, he used a constant DOS in which the value of the initial site energy is the QFL, thus $\varepsilon_i \rightarrow \varepsilon_f^c$ (Baranovskii and Rubel, 2006); this assumes that thermalization is complete and that the system is in equilibrium with the TE. Inserting Eq. (3.1.22) into Eq. (3.1.20) and applying Eq. (3.1.23), we obtain the following equation for the value, ς,

$$\varsigma(T) = \varepsilon_f^c(\mathrm{T}) - \left(\frac{k_bT}{3}\left[\frac{3\varepsilon_o^c}{\pi N_t^c\eta^3}\right]^{1/3}\right)^{\frac{3}{4}}. \tag{3.1.26}$$

This equation represents the difference between the initial site energy—where $\varepsilon_i \rightarrow \varepsilon_f^c$ is the equilibrium condition—and the final site energy to which the carrier will hop, (i.e., the change in energy). The transport energy as measured from the mobility edge is,

$$\varepsilon_f^c(T) = \left(\frac{k_bT}{3}\left[\frac{3\varepsilon_o^c}{\pi N_t^c\eta^3}\right]^{1/3}\right)^{\frac{3}{4}} \qquad \{\text{TE constant DOS}\}. \tag{3.1.27}$$

Equation (3.1.25) can be written in terms of the effective temperature Eq. (3.1.8) as,

$$\varepsilon_f^c(T) = (4/3)^{3/4}\ \frac{k_bT_0^c}{4}(T/T_0^c)^{3/4} \qquad \{\text{TE for constant DOS}\}. \tag{3.1.28}$$

Here, we have used a superscript on the characteristic dispersion temperature, T_o, to denote the type of DOS used. Note that in the zero temperature limit, Eq. (3.1.26) goes to zero, but that the change in energy—Eq. (3.1.24)—goes to the Fermi energy, $\varepsilon_f^c(T=0) \rightarrow \varepsilon_{\mathrm{F}}^{\mathrm{c}}$. Equation (3.1.24) bears a strong resemblance to the standard expression for the Fermi level (chemical potential) as a function of temperature for extrinsic semiconductors (Ashcroft and Mermin, 1976), and we should not be surprised to find that excitation of carriers from deep states to the TE changes the QFL. These two results are exactly what you would expect. In Section 3.1.7, we will use Eq. (3.1.26) to define the QFL for the constant DOS.

The same procedure can be carried out for the exponential and Gaussian DOS to obtain equivalent expressions for the TE relative to the mobility edge. For the exponential DOS, we find

$$\varepsilon_{\mathrm{t}}^{\mathrm{e}}(T) = 3k_bT_0^e ln\left[\frac{3\eta T_0^e}{2T}\left(\frac{4\pi}{3}N_{\mathrm{t}}^e\right)^{1/3}\right] = \frac{3k_bT}{\alpha} ln\left[\frac{3\eta}{2\alpha}\left(\frac{4\pi}{3}N_{\mathrm{t}}^e\right)^{1/3}\right] \quad \{\text{TE for exponential DOS}\}. \tag{3.1.29}$$

Here, $\alpha = T/T_0^e$ is the dispersion parameter (see Table 2.1) and $k_bT_0^e$ defines the width of the exponential distribution and is, in a sense, an effective temperature (see Chapter 2).

For the Gaussian DOS, the situation is more complex due to the mathematics required to obtain the expression for the transport energy. The derivation of the Gaussian TE follows an identical development to that of the constant and exponential DOS, but yields a complicated function,

$$\varepsilon_{\mathrm{t}}^{\mathrm{G}}(T) = \varepsilon_{\mathrm{o}}^{\mathrm{G}} * \Upsilon\left[N_t^G\eta^3, \frac{k_bT}{\varepsilon_{\mathrm{o}}^{\mathrm{G}}}\right] \quad \{\text{TE for Gaussian DOS}\}, \tag{3.1.30}$$

where $\Upsilon\left[N_t^G\eta^3, \frac{k_bT}{\varepsilon_{\mathrm{o}}^{\mathrm{G}}}\right]$ is the unitless function defined through the transcendental equation

$$exp\left(\frac{\Upsilon^2}{2}\right)\left[\int_{-\infty}^{\Upsilon/\sqrt{2}} exp(-x^2)dx\right]^{-1/3} = \left[9N_t^G\eta^3(2\pi)^{1/2}\right]\frac{k_bT}{\varepsilon_{\mathrm{o}}^{\mathrm{G}}}. \tag{3.1.31}$$

Here, x is a dummy integration variable, the function, Υ, is a function of the reduced dimensionless quantities $N_t^G\eta^3$ and $\frac{k_bT}{\varepsilon_{\mathrm{o}}^{\mathrm{G}}}$, and the solution for Υ is a complicated expression that can only be solved numerically. For the Gaussian DOS, the TE only makes sense for $k_bT << \varepsilon_{\mathrm{o}}^{\mathrm{G}}$ [$\varepsilon_{\mathrm{o}}^{\mathrm{G}}$ is the energy width (standard deviation) of the Gaussian distribution], where the VRH regime is dominant (Baranovskii and Rubel, 2006). A complete discussion of the Gaussian TE is given by Baranovskii and Rubel (2006), Vissenberg (1998), and Arkhipov *et al.* (2006). For very low temperatures, Baranovskii provides a new theoretical framework whose complexity necessitates that it be left as future work. However, the

calculation of the low-temperature mobility and conductivity follow from the same assumptions as were made to obtain the TE for the other DOS, as discussed in Section 3.2.7 (Arkhipov *et al.*, 1987c; Arkhipov *et al.*, 2003c; Baranovskii and Rubel, 2006).

3.1.6. Segregation Time

While understanding the physical roots of the TE is important to understanding the energy at which transport occurs, the energy difference between the initial site and TE is the quantity more often used in calculations and extracted from experimental results. A qualitative understanding of the TE is very useful in determining when the downward hopping and upward hopping dominate. If fact, we should expect that beyond some characteristic time, the upward hopping or VRH regime begins to dictate the nature of the observed current. The time at which this happens is called the segregation time.

The time dependence of upward and downward hopping regimes makes it clear that at some time, the hopping probabilities will become equal. This is the termination of the filling or downward hopping regime, and is the time where the upward hopping to the TE becomes the dominant process in the conductivity. Recall that for low-temperature systems, the TE lies below the electron mobility edge. Thus, it takes a time called the segregation time (ST), τ_{seg}, for the centroid of the carrier distribution to descend to the TE. In order to determine the ST, we set the derivatives of the upward and downward demarcation energies equal (That is, we minimize the difference between the upward demarcation energy and downward demarcation energy, given by Eq. (3.1.4) and (3.1.9), respectively.) and evaluate them at τ_{seg}. For a constant DOS, we obtain

$$\tau_{seg}^{c} = \frac{1}{\nu_0^c} exp\left(\frac{-3T_0^c}{4T}\right)^{1/4} \qquad \{\text{Segregation time for constant DOS}\}. \tag{3.1.32}$$

Recall from Eq. (3.1.8) that we have defined the value, T_0^c, as an effective temperature for a constant DOS, so that

$$T_0^c = \frac{24\varepsilon_o^c}{k_b \eta^3 \pi N_t^c}. \tag{3.1.33}$$

First, we note that the application of Eq. (3.1.31) for the constant DOS gives the correct $T^{1/4}$ temperature dependence expected for the VRH conductivity (in accordance with Mott's law of variable range hopping (Mott and Davis, 1971), as derived by Apsley and Hughes (1974, 1975). In the USU MPG theory,

(Dennison *et al.*, 2009a), the segregation time is embedded in the expression for the conductivity, and we will revisit this result in Section 3.2.1. The segregation time is the time required for the energetic centroid of the charge body to drop below the TE and the time after which application of our theories are valid. The segregation time is not the time required for the carriers to come to thermal equilibrium, which is rather called the thermalization time. Further, τ_{seg} is not the time required for the maximum conductivity to occur. In general, the segregation time is a very short time ~ 10^{-9} s or faster; we must keep in mind this estimated value is for semiconductors and is very likely to be much longer in HDIM due to the large energetic distribution of trapped states.

We now present the results of similar calculations for the remaining DOS models (Monroe, 1985; Fritzsche, 1990; Baranovskii and Rubel, 2006). For an exponential DOS, by minimizing the difference between the upward and downward demarcation energies using Equations (3.1.12) and (3.1.4), respectively, we find

$$\tau_{seg}^{e} = \frac{1}{\nu_0^e} exp\left(\frac{3T_0^e}{T}\right)^{1/4} \qquad \{\text{Segregation time for exponential DOS}\}. \qquad (3.1.34)$$

In a Gaussian DOS, no analytical expression for the segregation time is found; this is obvious since the upward demarcation energy is a numerical quantity and it follows that any approximation of the Gaussian segregation time will also be numerical. This difficulty is explored in Section 3.1.8.

3.1.7. Fermi Levels

Often, in the literature, one encounters the use of terms like “effective Fermi level,” “quasi Fermi level,” or even “new Fermi level,” as distinguished from the Fermi energy or Fermi level. The use of these terms originated from semiconductor physics to describe the situation where the population of each type of charge carrier (electrons or holes) is displaced from thermal equilibrium. In an extrinsic semiconductor, the Fermi level (chemical potential), ε_f , is the temperature-dependent energy at which occupation, $f(\varepsilon,T)$=½, characterizing the equilibrium distribution of carriers in the material at some temperature, T (Ashcroft and Mermin, 1976). In wide band gap materials, such as HDIM, there is little or no thermal generation of carriers—at room temperature or even at the glass transition, melting, or decomposition temperatures—and the temperature-dependent Fermi level, ε_f, does not deviate appreciably from the Fermi energy ε_F. Deviations from this chemical potential that depend on other variables lead to monikers of “effective“ or

"quasi" Fermi level (QFL). In HDIM, the deviations can be caused by external injection of carriers (dependent on deposited charge or charge deposition rate), RIC (dependent on deposited energy or power), or similar processes that add to or modify the carrier distribution of the material.

The equilibrium Fermi level of HDIM is changed by the injection of a charge carrier into the material (through N_{inj}) and $\varepsilon_f(T) \rightarrow \varepsilon_f^o(T, Q, \dot{Q})$. That is to say, in HDIM the equilibrium Fermi level or chemical potential is a function of the amount of space charge, which acts to fill additional trap states and raise the energy at which the occupation of trap states is equal to ½. If the material has a DOS in the gap (as do HDIM), the type of carrier distribution will determine the direction the equilibrium Fermi level will move (toward the CB for electrons and toward the VB for holes). If the injection of carriers (electrons in this case) is constant and the flux is small, then a small fraction of the DOS will fill—to a new equilibrium value—as the process of thermalization completes; it will fill up to the equilibrium Fermi level, $\varepsilon_f^o(T, Q)$, for constant charge injection. (The value of the equilibrium Fermi level depends on the experimental details and the material DOS.) The equilibrium Fermi level of HDIM is also changed by the injection of energy, which can create conduction electrons (G_{ex} through RIC) or generate new trap states ($\dot{N}_T(\varepsilon) \equiv dN_T(\varepsilon)/dt$) in the material; then, $\varepsilon_f(T) \rightarrow \varepsilon_f^o(T, D, \dot{D})$. For RIC, this is the effective Fermi level used to describe the steady-state irradiation of the material.

To understand the quasi-Fermi level, consider the nonequilibrium case, which occurs before thermalization completes; the centroid of the distribution thermalizing in the DOS really is the QFL, $\varepsilon_f^{QFL}(t, T, D, \dot{D}, Q, \dot{Q})$—by definition—as it is displaced from the equilibrium Fermi level. In Section 3.1.4, it was shown that during thermalization, the centroid of the charge distribution is given by the DE; we have called the DE the Fermi level in Sections 3.1.3 and 3.1.4 to avoid confusion. This was done for two reasons: first, the QFL becomes the equilibrium Fermi level after the completion of thermalization; and second, an introduction of the TE, thermalization, and the DE is required to make the difference between the Fermi level and QFL clear. An excellent description of the QFL, the DE, and the derivation of the occupancy is given by Schiff (1981) and Rose (1951, 1963) gives an equally excellent description of the steady-state Fermi level and QFL in photo-excited semiconductors.

Consider a simple representative example, based on the Mott and Twose model, for the calculation of the QFL. This example is useful in developing a basic notion of the QFL, when thermally activated and RIC excited electron distributions are present. This is followed by a very short discussion of estimated QFL values in hopping systems for the constant, exponential, and Gaussian DOS models. The depth of theoretical detail is kept to a minimum, as descriptions of the QFL under all of the conditions we might encounter in the study of HDIM cannot be presented here.

In a semiconductor, the population of states in a band (CB or VB here) due to thermal processes is given by the Fermi-Dirac distribution function (or Maxwell-Boltzmann distribution, if the temperature is high enough) (Ashcroft and Mermin, 1976). Using the Law of mass action, the Fermi level (chemical potential) of an intrinsic semiconductor is determined from the ratio of the number of accessible valence states, N_v, to the number of accessible conducting states, N_c, and their relative energy difference, as (Ashcroft and Mermin, 1976)

$$\frac{N_v}{N_c} = exp\left(\frac{\varepsilon_f - \frac{1}{2}(\varepsilon_{VB}+\varepsilon_{CB})}{\frac{1}{2}k_bT}\right). \tag{3.1.35}$$

This yields the well-known expression for the temperature dependence of the Fermi level for the intrinsic semi-conductor

$$\varepsilon_f(T) = \frac{1}{2}(\varepsilon_{VB} + \varepsilon_{CB}) + \frac{k_bT}{2} ln\left(\frac{N_v}{N_c}\right). \tag{3.1.36}$$

At low temperature, $\varepsilon_f(T{\sim}0)$ approaches $\frac{1}{2}(\varepsilon_{VB} + \varepsilon_{CB})$, which is the Fermi energy, ε_F, midway between the conduction and valence band edges. Note that the Fermi energy is at the center of the band gap for $T = 0$ for intrinsic semiconductors, even though there are no states in the gap. Equation (3.1.34) is only useful in modeling HDIM for radiation induced or thermally excited carrier distributions or extrinsic semiconductors where there are no localized states in the gap.

However, this simple model can be extended to include a delta function DOS of localized states in the gap by considering doping in extrinsic semiconductors. The standard model has N_D dopant states in a delta function distribution at a single energy, ε_d, below the conduction band edge at ε_{CB}. The calculation of the extrinsic Fermi level again follows from the law of mass action, with the replacement of the number

of accessible valence states, N_V, at energy, ε_{VB}, by the number of available dopant states, N_D , in the delta function DOS at ε_D

$$\varepsilon_f(T) = \frac{1}{2}(\varepsilon_D + \varepsilon_{CB}) + \frac{k_b T}{2} ln\left(\frac{N_D}{N_c}\right). \tag{3.1.37}$$

A connection with the delta function DOS model (see Section 2.4.5) can be made with these standard results for the equilibrium Fermi level for the case of delta function DOS for impurity dopants in extrinsic semiconductors. We assume that there are no acceptor states in the BG. By simple analogy, with N_t trap states in a delta function DOS centered at ε_0^t, we find

$$\frac{n_e}{N_t} = exp\left[\frac{-2\left(\varepsilon_f^0(\mathrm{T}) - \varepsilon_0^t\right)}{k_b T}\right], \tag{3.1.35A}$$

and

$$\varepsilon_f^0(\mathrm{T}) = \varepsilon_0^t - \frac{k_b T}{2} ln\left(\frac{n_e}{N_t}\right). \tag{3.1.38}$$

Here, n_e is the number of excited carrier electrons from the trap states, ε_f^0 is the equilibrium Fermi level, and $\varepsilon_0^t = \varepsilon_{trap}$ is the position of the trap state delta DOS in the gap. This is a first-order approximation to the equilibrium Fermi level in a simple material with a delta function DOS and without carriers excited from the VB or other distributions.

We can correct Eq. (3.1.36) for thermal excitation or RIC by including a term for holes in the valence band in a way similar to Eq. (3.1.34). An important application is found when we consider the time dependence of releasing electrons from the trap states; the number of excited carriers, $n_e(t)$, is a function of time before equilibrium is established. Recall from Section (3.1.3) that there is a time required for the release of trapped electrons associated with thermal excitation given by Eq. (3.1.2). This means that the QFL (nonequilibrium Fermi level) will be above its steady-state value (equilibrium Fermi level) until the release of carriers is compete, the material reaches equilibrium, and the QFL drops to the equilibrium Fermi level. This is the process of thermalization and the energy level associated with the QFL is the time-dependent demarcation energy discussed in Section (3.1.3); there is nothing else it can be. By considering the nonequilibrium position of the Fermi level, we arrive at an approximation for the QFL, in a single DOS model in which RIC is the driving excitation mechanism of the free carriers.

Determination of the Fermi level for each of our models for the energy-dependent DOS (see Section 2.4.5) is necessary to determine at what temperature we should expect to see changes in the observed conduction behavior. In the end, each experimental configuration and DOS must be considered on an individual basis to obtain a reasonable estimate for the QFL and resulting equilibrium Fermi level. (Here we only provide examples for specific methods!) A full understanding of the QFL must be obtained through a study of the thermalization process (i.e., the demarcation energies) under specific experimental conditions.

The condition by which the QFL is found in a complex DOS has two forms. The first form has already been used with the derivation of the demarcation energies (see Section 3.1.3). We can consider the derivation of the Fermi level by evaluating the demarcation energies for upward and downward hopping, at the thermalization time, τ_T. Since the demarcation energies (QFL) are representative of the centroid of the charge distribution, we evaluate it at the thermalization time.

$$\varepsilon_f^{QFL}\left(t, T, D, \dot{D}\right) = \varepsilon_a^{\uparrow}(\tau_T). \tag{3.1.39}$$

This expression will give us an estimate of the equilibrium Fermi level after the system has just come to equilibrium (or thermalization has just terminated). The application of (3.1.37) does not yield a useful expression for the equilibrium Fermi level, since we have no estimate for the thermalization time.

The second form is to consider the number of elections released from trapped states, by use of Eq. (3.1.38) given below. One must be very careful with this integration and the limits. In an exponential or Gaussian system, the integration can be done over the entire DOS including carriers in Eq. (3.1.37) in the TB. This works for two reasons: (i) the number of carriers in the TB is negligible in comparison to the trapped distribution, and (ii) the DOS goes to zero in the limit of infinite energies. The second condition does not hold for a constant DOS, where the integration must be carried out over a finite range of energies from the equilibrium Fermi energy to the TB (usually the TB or CB energies are assigned the zero energy reference) for a system in which we consider only electrons (no holes or hole trapping). This can be taken into account by the use of a Heaviside step function in the definitions of the appropriate DOS models [for an example of the use of the Heaviside step function in the DOS, see Kao (2004)]. However, in the literature, the DOS models are not generally written in this way; thus to keep contact with the literature, the

common form will be used for the DOS models shown in Table 2.1. Thus, the generalized form of Eq. (3.1.35A) for an arbitrary energy-dependent trap state DOS is

$$n_e(t,T) = \int_{\varepsilon_A}^{\varepsilon_B} N(\varepsilon)\left\{1 + exp\left[\frac{\varepsilon - \varepsilon_f^0(t)}{k_b T}\right]\right\}^{-1} d\varepsilon. \tag{3.1.40}$$

Here the DOS, *N(ε)*, can be any of the models listed in Table 2.1. The integration effectively is performed over the extent of the DOS distribution (a finite region for the constant, linear, and power law DOS, -∞ < ε < TE, for the exponential DOS, and all energies for the Gaussian DOS). Equation (3.1.38) can be solved to obtain an expression for $\varepsilon_f^0(t,T)$.

Since we can experimentally determine the effective transport energy, a semi-empirical Fermi level can be determined for the constant DOS by rearranging Eq. (3.1.27) to obtain

$$\varepsilon_f^c(T) = \varsigma(T) + \left(\frac{4}{3}\right)^{3/4} \frac{k_b T_0^c}{4}\left(\frac{T}{T_0^c}\right)^{3/4} \qquad \{\text{Equilibrium Fermi level for constant DOS}\}. \tag{3.1.41}$$

In Eq. (3.1.40), $\varsigma(T)$ is the measured value and the RHS of the expression is the TE.

An expression for the exponential DOS has been evaluated by several authors (Fritzsche, 1990; Anta, 2002). Anta used Eq. (3.1.38) to obtain an approximation to the equilibrium Fermi level and QFL (Anta, 2002),

$$\varepsilon_f^e(t,T) = -k_b T_0^e ln\left[n_e(t) \Big/ N_t\left(1 + \frac{\left(\frac{\pi T}{T_0^e}\right)^2}{6} + \frac{7\left(\frac{\pi T}{T_0^e}\right)^4}{360}\right)\right]$$

{Equilibrium Fermi level for exponential DOS}. (3.1.42)

This expression is only good for low carrier concentrations. Baranovskii showed that as the temperature goes to zero, Eq. (3.1.41) becomes a constant (Baranovski and Rubel, 2006); in fact, Baranovski showed that there is a critical temperature, T_c^e, below which the Fermi level becomes temperature-independent. The details of the Fermi level, QFL and transport energies—for the constant and exponential DOS—can be more complex expressions than those presented in this dissertation; other expressions for the Fermi level and the QFL, for more complex experimental arrangements, can be found in (Fritzsche, 1990).

For the Gaussian DOS, the estimation of the Fermi level and QFL are complicated by the numerical nature of the demarcation energy. However, in the infinite time limit, the demarcation energy relaxes to an equilibrium energy, $\langle \varepsilon_\infty \rangle$, given by the energetic average of the DOS, which is the equilibrium Fermi level for the Gaussian DOS (Baranovskii and Rubel, 2006),

$$\langle \varepsilon_\infty \rangle = \frac{\int_{-\infty}^{\infty} \varepsilon N(\varepsilon) d\varepsilon}{\int_{-\infty}^{\infty} N(\varepsilon) d\varepsilon} = \lim_{t\to\infty} \varepsilon_d^{G\uparrow}(t) = \frac{-{\varepsilon_G^o}^2}{k_b T} \sim \varepsilon_f^G \text{ \{Equilibrium Fermi level for Gaussian DOS\}.} \quad (3.1.43)$$

Notice that the Fermi level is measured from the center of the Gaussians DOS distribution, ε_o^t.

The equilibrium Fermi level, $\varepsilon_f^0\left(T, D, \dot{D}, Q, \dot{Q}\right)$, and QFL, $\varepsilon_f^{QFL}\left(t, T, D, \dot{D}, Q, \dot{Q}\right)$, are key factors in determining the transport characteristics of an HDIM. It is the energetic position of the QFL relative to other energies (e.g., the electron and hole mobility edges, the Fermi energy, and variable energy levels, such as the TE) that determines whether high or low temperature, dispersive, or diffusive transport is observed. For example, if thermalization is not complete and the carriers are spread out energetically in the DOS with a large distribution of wait times, dispersive transport will be observed; this can occur in high- and low-temperature applications. For low-temperature transport, the QFL or equilibrium Fermi level must be below the TE, but close enough to it, for VRH to occur. If the system is in equilibrium and Fermi level is well below the TE, recombination with holes can occur directly from the Fermi level; transport will still occur primarily at the TE, but is deemed recombination limited (Fritzsche, 1990; Baranovskii and Rubel, 2006). If the QFL is above the TE, transport is by extended state conduction at or above the electron mobility edge.

The specific equilibrium Fermi level and QFL are determined by the type of DOS and particular application we are interested in. However, there are some basic rules of thumb that we can understand, based on the type of DOS considered. For the constant, delta function, and Gaussian DOS (recall from Section 2.4.5 that the constant and delta function DOS are limiting cases of the Gaussian DOS), thermalization generally occurs very quickly in contrast to the exponential DOS, which typically presents with a large range of trapping energies; i.e. in the constant DOS, the demarcation energy (QFL) descends to the equilibrium Fermi level very quickly. This explains why dispersion is not generally observed in materials with constant DOS like LDPE. Dispersion is very commonly found in materials with exponential

DOS. In materials with the Gaussian DOS, a spectrum of transport behaviors is observed suggesting that it may be the most general model (Baranovskii and Rubel, 2006).

The question, "How fast will thermalization be completed in a given DOS?" determines what behavior will be observed for a given application. We have not yet determined the time required for the QFL to come to equilibrium at the Fermi level. This time is the thermalization time and is the subject of the final part of Section 3.1.

3.1.8. Thermalization Time

The calculation of the thermalization time is fundamentally based on the energy of the Fermi level. It is a measure of how fast the centroid of the charge body comes to thermal equilibrium (i.e., a measure of how fast the demarcation energies or QFL reach the equilibrium Fermi level). Since dispersive phenomena are caused by a range of event times, dispersive behavior occurs before thermalization can compete. After thermalization, the carrier transport will be diffusive in nature, assuming deep state recombination is not a factor. Estimation of the thermalization time must be done differently for each type of DOS and is, in general, a complicated calculation. In Section 3.1.7 we presented a basic notion that allows for the definition of the thermalization time, τ_T. However, the determination of τ_T depends on where the Fermi level lies with respect to the TE (or CB for extended state transport). If the Fermi level is situated above the TE, then only the downward demarcation energy (QFL) determines the thermalization time. If the Fermi level is situated below the TE, then the upward demarcation energy (QFL) determines τ_T. Thus, we can write down the following two rules as a guide for determining the thermalization time:

(i) If the equilibrium Fermi level is above the TE, then downward hopping terminates at the Fermi level; thus, $\varepsilon \downarrow_d (\tau_T) = \varepsilon_f^0$ gives the thermalization time and (ii) if the equilibrium Fermi level is below the TE, then downward hopping terminates at the Fermi level; thus, $\varepsilon \uparrow_d (\tau_T) = \varepsilon_f^0$ gives the thermalization time.

We present expressions for three types of DOS (constant, exponential, and Gaussian) for completeness. These expressions were not obtained using the rules stated above, and each requires significant calculation; thus, the details of the derivations must be found in their original references. Zvyagin has calculated the QFL for a constant DOS and obtained the following estimate (Fritzsche, 1990):

$$\tau_T^c(\mathrm{T}) = \frac{1}{\nu_0} exp\left[\frac{4}{3}\left(\frac{\mathrm{T}_0^c}{T}\right)^{\frac{1}{4}}\right] = \frac{1}{\nu_0} exp\left\{\frac{4}{3}[\alpha_C(\mathrm{T})]^{-1/4}\right\} \quad \{\text{Thermalization time for a constant DOS}\}. \quad (3.1.44)$$

Zvyagin claims without proof, that the equilibrium value of the QFL was used to obtain this approximation; I was unable to confirm this. However, Eq. (3.1.42) has the feature expected from VRH in a constant DOS, that is that τ_T^c goes as $T^{-1/4}$.

For the exponential DOS, the theory is well developed by Monroe and the thermalization time for high-temperature transport (Kastner and Monroe, 1982) was found to be

$$\tau_T^e(\mathrm{T}) \approx \frac{1}{\nu_0^e}\left\{\frac{N_t}{N_e}\frac{\frac{T}{T_0^e}\sin\left(\frac{T\pi}{T_0^e}\right)}{1-\frac{T}{T_0^e}}\right\}^{\frac{1}{1-\frac{T}{T_0^e}}} = \frac{1}{\nu_0^e}\left\{\frac{N_t}{N_e}\frac{\alpha_e(\mathrm{T})\sin[\alpha_e(T)\pi]}{1-\alpha_e(\mathrm{T})}\right\}^{1/1-\alpha_e(\mathrm{T})}$$

$$\{\text{Thermalization time for a exponential DOS at high T}\}. \quad (3.1.45)$$

An expression for the low-temperature thermalization time requires extensive calculation and will not be presented here; the interested reader should see Tiedje *et al.* (1981) and Fritzsche (1990).

For the Gaussian DOS, the derivation of τ_T^G is nontrivial, again due to the numerical nature of the problem. However, the basic process by which we can derive the thermalization time is considerably easier to set up, as we have a value for the Fermi level, ε_T^G, from Eq. (3.1.42). Despite the difficulty in understanding how equilibration of the thermalization charge distribution occurs, we have already developed the machinery to define the thermalization time. Using our definition for the hopping rate, Eq. (3.1.5), the TE from Eq. (3.1.28), and Eq. (3.1.42), we can write down an expression for the time required for the charge distribution to relax to the Fermi level,

$$\tau_T^G = {\nu_0}^{-1} exp\left[\frac{2R(\varepsilon_0^{\mathrm{t}})}{\eta} + \frac{\varepsilon_0^{\mathrm{t}} - \langle\varepsilon_\infty\rangle}{k_b T}\right] \quad \{\text{Thermalization time for a Gaussian DOS}\}. \quad (3.1.46)$$

Equation (3.1.44) cannot be solved in closed form because the transport energy is numerical in nature. However, once a value for the TE is obtained, Eq. (3.1.44) is very simple to calculate. We can also use Eq. (3.1.12)—the transcendental expression for the upward demarcation energy—to obtain an estimate of the thermalization time by setting $\varepsilon_d{}^{G\uparrow} = \varepsilon_f^G = \langle\varepsilon_\infty\rangle$ and solving the resulting transcendental equation for $t = \tau_T^G$. In either case, these calculations, the verification of their accuracy, and further investigation must be left for future work.

In Section 3.1 a great deal has been said about study of charge distributions in materials with a highly disordered DOS. From the MAR, we have shown that a charge body entering a disordered DOS in the gap undergoes a thermalization process and carrier transport that is defined by the demarcation energies, transport energy, and segregation time. In addition, a summary discussion of the QFL and thermalization time was given for each of the DOS. We now understand that these theoretical tools describe not only low-temperature hopping transport, but can be used to understand the high-temperature MT behavior, as well (see, for example, Schmidlin, 1977, 1980; Monroe, 1983, 1985, 1986; Baranovskii and Rubel, 2006). While the majority of this theory is widely used in disordered semiconductor physics, *it has not been extensively tested for HDIM*. In Section 3.2 an investigation of the USU MPG VRH models is presented and connected to the ideas of this section. The resulting equations clearly show the power of the tools developed in Section 3.1 and gives new insight into the nature of the USU MPG multiple trapping models. The theoretical ideas presented here are a summary of a considerably more detailed theory for low-temperature transport; the interested reader is encouraged to see Mott and Twose (1961), Baranovskii and Rubel (2006), Arkhipov *et al.* (2006), Fritzsche (1990), and Vissenberg (1998).

3.2. Applications

This section discusses the application of the average microscopic tools presented in Section 3.1 to low-temperature, steady-state conductivity as a function of applied field and temperature. Further, we present expressions for equilibrium VRH in materials with a constant, exponential, and Gaussian DOS (see Table 2.1). As a specific example—and a concrete application—we extend the USU MPG VRH model in the context of the theoretical tools developed in Section 3.1. This section begins with a review of the USU MPG multiple trapping VRH model; this model is then rewritten in the context of the segregation time. We then extend the segregation time to include field dependence and again reformulate the USU MPG VRH. The USU MPG model (written in terms of a field-dependent segregation time) highlights a phenomenological form of the segregation time commonly found in the literature, which is then used to make a clear connection to a new field- and temperature-dependent description for equilibrium VRH in a material with a constant DOS that follows directly from the theory developed in Section 3.1. This new expression allows for a simple and intuitive description of VRH for a constant DOS, connects the tools

developed in Section 3.1, and links the results of recent theoretical work in low-temperature physics (Baranovskii and Rubel, 2006) with the concrete and experimentally verified USU MPG model (Dennison and Brunson, 2008). The USU MPG model was originally developed by Apsley and Hughes (1974, 1975) and used a three-dimensional averaging technique, which is based on a complex three-dimensional averaging of the hopping behavior; the Apsley model did not include the concepts introduced in Section 3.1 (transport energy, segregation times, etc.) as these ideas had not yet been developed. In recent semiconductor and HDIM work, the use of a general segregation time has been shown to describe a wide class of temperature-and field-dependent phenomena, but this model is not theoretically grounded. We show that this form of the segregation time appears in the USU MPG model, and therefore, is theoretically grounded through the fundamental work of Apsley and Hughes (1974, 1975) and Mott (1961, 1973, 1977).

The discussion of the USU MPH model is followed by a presentation of VRH expressions for the exponential and Gaussian DOS to provide a complete set of low-temperature conductivity equations for the three major DOS models (constant, exponential, and Gaussian). A full discussion of the VRH conductivity models—for the exponential and Gaussian DOS—cannot be given here, as each application requires a great deal of additional development. However, we show that the TAH model used by the USU MPG —which is derived from the transport equations in the high-temperature, high-field limit—results from the Gaussian VRH model. This chapter concludes with comments on the connections between the transport equations and VRH behavior, in addition to very low temperature behavior, where the VRH expressions presented in this section are no longer valid.

The USU MPG has developed a set of engineering tools for the estimation and mitigation of spacecraft charging (Brunson and Dennison, 2008; Dennison *et al.*, 2009a). Dennison *et al.* (2009b) summarizes the theoretical understanding of the USU MPG prior to this dissertation and includes a discussion of thermally activated hopping, radiation induced conductivity, variable range hopping, and electrostatic breakdown. In Sections 3.2.1 to 3.2.5, we focus only on the VRH model discussed in Dennison and Brunson (2008) and the applications of the new tools to that work. Note that the application of Section 3.1 to the USU VRH models and new models described in Sections 3.2.6 through 3.2.8 are all new additions to the USU MPG theoretical knowledge base. The USU MPG VRH model can be written as

$$\sigma_{VRH}^{c}(\mathrm{T,F}) = \left(\frac{N_t q_e{}^2 \nu_0^c \eta^2}{2\,\varepsilon_0^c}\right)\left(\frac{24\varepsilon_0^c}{k_b T \pi N_t \eta^3}\right)^{1/4} \mathrm{Z}_{V1}(\beta_V) exp\left[-\left(\frac{24\varepsilon_0^c}{k_b T \pi N_t \eta^3}\right)^{\frac{1}{4}} \mathrm{Z}_{\mathrm{V2}}(\beta_V)\right]. \quad (3.2.1)$$

Here $\mathrm{Z}_{\mathrm{V1}}(\beta_V)$ and $\mathrm{Z}_{\mathrm{V2}}(\beta_V)$ are complicated functions of the parameter $\beta_V \equiv 4FT_V/3F_V T$, which is itself dependent on the ratio of electric field energy to thermal energy (Dennison *et al.*, 2009a). A discussion of the derivation of Eq. (3.2.1) and the complex functions $\mathrm{Z}_{\mathrm{V2}}(\beta_V)$ and $\mathrm{Z}_{\mathrm{V2}}(\beta_V)$ can be found in Apsley and Hughes (1974, 1975) and Dennison *et al.* (2009a). The parameter, $T_V \equiv 24\varepsilon_0^c/N_t\eta^3 k_b \pi$; Dennison uses the parameter α as the inverse localization radius and, in this dissertation, $\alpha \equiv 1/\eta$. Further, $\int_0^{\varepsilon_F} N(\varepsilon)d\varepsilon \equiv N_t/\varepsilon_0^c = N_{E_F}$ is the total number of states in the DOS near the Fermi level. The field parameter is $F_V = 64\varepsilon_0^c/q_e N_t \eta^4 k_b \pi$. The expansions of Eq. (3.2.1) for low and high electric fields are easily obtained by expanding the complex functions $\mathrm{Z}_{\mathrm{V2}}(\beta_V)$ and $\mathrm{Z}_{\mathrm{V2}}(\beta_V)$ for small and large beta (Dennison *et al.*, 2009a) (see the USU MPG group archives for the Mathcad™ sheet, Hopping Resistivity Plots, developed by Dennison, for the details of the low and high T, as well as low- and high-field expansions of the model). Since Eq. (3.2.1) is very cumbersome, we will work with the low- and high-field approximations, which will greatly simplify the connections with Section 3.1. First the low-field expression is discussed, followed by the high-field expression.

3.2.1. Low-Field Behavior

We start our analysis of Eq. (3.2.1) in the low-field limit to build up the idea of an effective temperature and its contribution to the segregation time. Consider the low-field USU MPG VRH model, as given by Dennison *et al.* (2009a),

$$\sigma_{VRH}^{c}(\mathrm{T,F}) \approx \left(\frac{N_t \eta^2 q_e{}^2 \nu_0^c}{2\varepsilon_0^c}\right)\left(\frac{24\varepsilon_0^c}{k_b T \pi N_t \eta^3}\right)^{1/4} exp\left[-\left(\frac{24\varepsilon_0^c}{k_b T \pi N_t \eta^3}\right)^{1/4}\left[1 - \frac{\beta_V(T,F)^2}{4}\right]\right]. \quad (3.2.2)$$

The function, $\beta_V(T,F)$, is defined in terms of fundamental quantities as the unitless ratio of electric field energy, $q_e F\eta$, to thermal energy, $k_b T$,

$$\beta_V(T,F) \equiv \frac{q_e F \eta}{2k_b T}. \quad (3.2.3)$$

Recall from Section 3.1.6 and Eq. (3.1.30) that the segregation time for a constant DOS can be written as a ratio of effective temperature to measured temperature as

$$\tau_{seq}^{c}(\mathrm{T}) = \frac{1}{\nu_0^c} exp\left(\frac{-18\varepsilon_0^c}{k_b T \eta^3 N_t \pi}\right)^{1/4} = \frac{1}{\nu_0} exp\left(\frac{-3T_0^c}{4T}\right)^{1/4}. \quad (3.2.4)$$

Now, comparing Eq. (3.1.31) with the definition of T_V found in Dennison *et al.* (2009a) we can set $T_0^c = T_V$, and in the very-low-field limit, we can rewrite Eq. (3.2.2) in a suggestive way

$$\sigma_{VRH}^{c}(\mathrm{T,F}) \approx \sigma_0^C \left(\frac{T_0^c}{T}\right)^{1/4} exp\left[-\left(\frac{T_0^c}{T}\right)^{1/4}\left[1 - \frac{\beta_V(T,F)^2}{4}\right]\right]. \quad (3.2.5)$$

For very low fields, we assume the $\beta_V(T,F)$ term is negligible and define the leading term as the maximum conductivity $\sigma_0^C \equiv N_t \eta^2 {q_e}^2 \nu_0^c / 2\varepsilon_c$. We can then write Eq. (3.2.5) as

$$\sigma_{VRH}^{c}(\mathrm{T,F}) \approx \sigma_0^C \left(\frac{T_0^c}{T}\right)^{1/4} exp\left[-\left(\frac{T_0^c}{T}\right)^{1/4}\right] = \sigma_0^C [\alpha_c(\mathrm{T})]^{-1/4} exp\{-[\alpha_c(\mathrm{T})]^{-1/4}\}. \quad (3.2.6)$$

This is the expression derived by Mott and Davis in their seminal work on VRH (Mott and Davis, 1971). We now write Eq. (3.2.6) in terms of the segregation time Eq. (3.2.4) or Eq. (3.1.32) to make contact with Section 3.1 and the charge distribution thermalization process

$$\sigma_{VRH}^{c}(\mathrm{T,F}) \approx \sigma_0^C \ln\{[\nu_0^c \tau_{seq}^c(\mathrm{T})]^{-\mathrm{p}}\} [\nu_0^c \tau_{seq}^c(\mathrm{T})]^{\mathrm{p}}. \quad (3.2.7)$$

Here we have solved Eq. (3.2.4) for $-\left(\frac{T_0^c}{T}\right)^{1/4}$ and inserted this into Eq. (3.2.6). The power $p = (4/3)^{1/4} \sim 1.075$. Therefore, if the values of σ_0^c and ν_0^c are known (measured), the conductivity can easily be predicted from the segregation time (or time to come to equilibrium); and conversely, if the conductivity of the equilibrium state is known, so is the segregation time. This is a simple form of the VRH law that connects the time required for the carrier distribution to come into equilibrium to the transport band with the observed conductivity. It is well known that the application of a high electric field will distort the DOS and change the release rate of trapped carriers (Pollak, 1972). The work of Pollack and Eq. (3.2.7) suggests that, by exploring the segregation time as a function of field, a prediction for the effects of high fields on the VRH rate should follow; i.e., we can use the simple tools of Section 3.1 to estimate and understand the VRH conductivity as a function of temperature and field.

3.2.2. Field-Dependent Demarcation Energies

How can we modify the segregation time to reflect the effects of high fields? There are two ways we can modify the treatment from Section 3.2.1 to include field dependence. The first is a simple modification of the MAR with an effective field term. This modification is due to the lowering of the

energy barrier for the escape of trapped carriers. (This is exactly like raising the energetic position of the trapped states or using a higher temperature (Wintle, 1983).) Following the work of Fritzsche (1990) and Cleve *et al.* (1995), we add a term to Eq. (3.1.1) for the energy difference between hopping sites. The additional term is a field modification term equal to the ratio of the mean carrier energy, $\frac{1}{2}(\varepsilon_d - \varepsilon_0^t)$, to the energy acquired by a carrier moving between adjacent trap sites in a field, *F*, $\eta q_e F = k_b T_F$. We thus find an estimate of the change in our hopping rate due to the applied field,

$$\Delta\nu_{\downarrow}(\varepsilon_d, \varepsilon_0^t) = \nu_0 exp\left(-\frac{(\varepsilon_d - \varepsilon_0^t)}{k_b T_F} - \frac{\varepsilon_i}{k_b T}\right). \tag{3.2.8}$$

Notice that for very high fields, Eq. (3.2.8) suggests that the hopping behavior will be dominated by the temperature, as expected. (We assume that terms for the low-field behavior have been dropped and ignore the low-field limit.)

The second effect of a high applied field is on the DOS. How does applying a torque—or some other modification—due to the applied field affect the DOS available for trapping? Several authors have suggested a first order approximation of the DOS equation to estimate the effects of high applied fields:

$$N(\varepsilon, F) = N(\varepsilon)\left[1 + \frac{\eta q_e F}{k_b T_{bend}}\right], \tag{3.2.9}$$

which is the first order approximation of

$$N(\varepsilon, F = 0) = N(\varepsilon)\exp(k_b T_F / k_b T_{bend}). \tag{3.2.9a}$$

Here, T_{bend} characterizes the difficulty with which changes (or bending of the band structure) in the DOS can be made by the applied field, *F*. For example, if we chose an exponential DOS, T_{bend} represents the difficulty with which the band tail—that determines the shape of the DOS—can be distorted (Baranovskii and Rubel, 2006). For a constant DOS—in which VRH occurs deep in the gap— T_{bend} is likely to be very large; the energy required to change the energetic configuration of deep states is much higher than for shallow states near the mobility edge. Alternately, $k_b T_{bend}$ can be thought of as the energy to create an HDIM defect state (such as a kink in a polymer chain) through the application of a field-induced stress. Then, the exponential term in Eq. (3.2.9a) is a Boltzmann factor with a ratio of field-induced energy to defect energy that governs the equilibrium number of field-induced defects created.

Given the modifications by Eq. (3.2.8) and Eq. (3.2.9), we can derive a new segregation time by repeating the process used in Section 3.1.6—resulting in Eq. (3.1.30)—and find the expected change in the segregation time due to a very high field.

The segregation time is defined by the equality of the time derivative of the upward to downward demarcation energies. Thus, we first develop expressions for the upward and downward demarcation energies and then find the new segregation time. First, we derive the upward demarcation energy, for a constant DOS; this follows from $\nu^{\uparrow}(\Delta\varepsilon_d(t,F))t = 1$ and yields the expression

$$(\nu_0 t) = \ exp\left[\frac{2R(\Delta\varepsilon_d,F)}{\eta}\right]. \tag{3.2.10}$$

The hopping range, $R(\varepsilon_d, F)$, is calculated using the modified DOS, Eq. (3.2.9), as

$$R(\varepsilon_d,F) = \left[\left(\frac{4\pi}{3}\right)\frac{N_t}{\varepsilon_0^c}(\varepsilon_d - \varepsilon_{\mathrm{f}}^{\mathrm{o}})\left(1+\frac{T_F}{T_{bend}}\right)\right]^{-1/3}, \tag{3.2.11}$$

where again, $T_F \equiv \frac{q_e F\eta}{k_B}$. Using Eqs. (3.2.10) and (3.2.11), the upward demarcation energy is

$$\Delta\varepsilon^{\uparrow}{}_d(t,F) = \frac{6\varepsilon_0^c}{\pi\left(1+\frac{T_F}{T_{bend}}\right)N_t\eta^3} ln^{-3}(\nu_0^c t) + \varepsilon_{\mathrm{f}}^{\mathrm{o}}. \tag{3.2.12}$$

Notice that this expression goes to the effective Fermi level in the limit of very long times or very high fields. This result is consistent with the depopulation of trapped electrons for very long times and the effect of reducing the escape potential for the trapped electrons due to very high fields.

For the downward hopping demarcation energy, we require $\nu\downarrow\left(\varepsilon^{\downarrow}{}_d, \varepsilon_t\right)t = 1$, which leads to

$$ln(\nu_0 t) = \frac{\varepsilon_0^t}{k_b T} + \frac{(\Delta\varepsilon^{\downarrow}{}_d - \varepsilon_0^t)}{k_b T_F}. \tag{3.2.13}$$

Solving for the downward hopping demarcation energy, we find

$$\Delta\varepsilon^{\downarrow}{}_d(t,F) = \ -k_b T_F ln[\nu_0^c t] + \varepsilon_0^t\left(1+\frac{T_F}{T}\right); \tag{3.2.14}$$

note that this new demarcation energy goes to ε_0^t for $T_F \to 0$. The demarcation energy for the downward hopping regime, Eq. (3.2.14), has two terms. The right-hand side is the time-dependent term, which is accelerated by the increasing the field. The second term changes the transport energy as a function of the field and temperature. The change in demarcation energy at the segregation time (i.e., to get the total segregation time) is as expected; one must add the low-field term, $k_b T ln[\nu_0^c t]$.

As before, the segregation time is found by setting the derivatives of ${\varepsilon^{\uparrow}}_d(t,F)$ and ${\varepsilon^{\downarrow}}_d(t,F)$ equal and evaluating the resulting expression at τ_{seg}. Here the notation $\tau_{seg}^{c,F}$ denotes that this is the segregation time for a constant DOS with field enhancement. Setting Eqs. (3.2.12) and (3.2.14) equal gives

$$\frac{6\varepsilon_0^c}{\pi\left(1+\frac{T_F}{T_{bend}}\right)N_t\eta^3} ln^{-4}\left(\nu_0^c\,\tau_{seg}^{c,F}\right) = k_b T_F. \tag{3.2.15}$$

Solving Eq. (3.2.15) for $\tau_{seg}^{c,F}$,

$$\tau_{seg}^{c,F}(\mathrm{T},\mathrm{F}) = \frac{1}{\nu_0^c}\, exp\left[\left(\frac{k_b\pi T_F\left(1+\frac{T_F}{T_{bend}}\right)N_t\eta^3}{6\varepsilon_0^c}\right)^{-1/4}\right] = \frac{1}{\nu_0^c}\exp\left(\left[\frac{4T_F}{T_0^c}\left(1+\frac{T_F}{T_{bend}}\right)\right]^{-\frac{1}{4}}\right). \tag{3.2.16}$$

We can make contact with the field-dependent terms in the Apsley and Hughes model (Dennison *et al.*, 2009a) in the high-field limit. Inserting, $T_F \equiv \frac{q_e F\eta}{k_b}$ into Eq. (3.2.16) and assuming that for a zero temperature system, $T_{bend} \to \infty$ (it is assumed that the polymer chains are frozen in place), with a high field that is not large enough to distort the material, we can find an expression for the zero temperature high-field segregation time

$$\tau_{seg}^{c,F}(\mathrm{T},\mathrm{F}) \quad = \frac{1}{\nu_0^c}\, exp\left[-\left(\frac{1}{4}\right)^{1/4}\left(\frac{64\varepsilon_0^c}{\pi(\eta q_e F)N_t\eta^3}\right)^{1/4}\right]. \tag{3.2.17}$$

The high-field expansion of the USU MPG VRH model is

$$\sigma_{VRH}^c(\mathrm{T},\mathrm{F}) = \left(\frac{N_t {q_e}^2\eta^2\nu_0^c}{4\varepsilon_0^c}\right)\left(\frac{64\varepsilon_0^c}{\pi(\eta q_e F)N_t\eta^3}\right)^{1/4} exp\left[-\left(\frac{64\varepsilon_0^c}{\pi(\eta q_e F)N_t\eta^3}\right)^{1/4}\right]. \tag{3.2.18}$$

Comparing Eq. (3.2.17) and Eq. (3.2.18), it is clear that we have arrived at the correct segregation time for the high-field limit with the slight exception of the numerical factor $(1/4)^{1/4}$; this factor turns out to be very suggestive and is discussed below. First, we can improve the comparison by defining an effective temperature, $T_0^{high} \equiv (64\varepsilon_0^c/\eta^3 N_t k_b\pi)$ [similar to the effective temperature used in Eq. (3.2.14)], and conductivity, $\sigma_0^{C-high} \equiv (N_t {q_e}^2\eta^2\nu_0^c/4\varepsilon_0^c)$, so that Eq. (3.2.18) becomes

$$\sigma_{VRH}^{C-high}(\mathrm{T},\mathrm{F}) = \sigma_0^{C-high}\left(T_0^{high}/\mathrm{T_F}\right)^{1/4} exp\left[-\left(T_0^{high}/\mathrm{T_F}\right)^{1/4}\right]. \tag{3.2.19}$$

This is a very suggestive form that is clearly related to the high-field segregation time and has a familiar ratio of effective temperature to field energy. Using Eq. (3.1.8) and again, solving for T_0^c/T_F and inserting this into Eq. (3.2.17), Eq. (3.1.18) can be written as a function of the segregation time

$$\sigma_{VRH}^{C-high}(\mathrm{T},\mathrm{F}) = \sigma_0^{C-high}\ln[\left(\nu_0^c\tau_{seg}^{c,F}\right)^{-p}]\left(\nu_0^c\tau_{seg}^{c,F}\right)^{p}. \quad (3.2.20)$$

This high-field result has exactly the same form as the low-field result Eq. (3.2.7). Here $p = (1/4)^{1/4} \sim \frac{\sqrt{2}}{2} = 0.707$, which is a different constant than we found for the low-field case (~1.075), suggesting that the power is field- and temperature-dependent; this is an important point and we will revisit this idea in the next section. It is clear that the effective temperature is strongly field-dependent; it affects the hopping rates and energy distribution of the DOS. How can we develop a more complete description of the low- and high-field behavior? The answer lies in the nature of the effective temperature. Recall that we modified the hopping rates in Eq. (3.2.12) and the DOS in Eq. (3.2.14) to estimate the effects of the applied field. All of these modifications lead to the definition of an effective temperature, but in the low-field case, the effective temperature is not the same as in the high-field case. The answer to our question is also complicated by the effects of material degradation at high fields. For example, in the derivation of Eq. (3.2.17) we assumed a zero temperature limit; this is not a realistic assumption for most polymer systems and, in fact, in a nonzero temperature system, Eq. (3.2.16) can be expressed as

$$\tau_{seg}^{c,F}(\mathrm{T},\mathrm{F}) = \frac{1}{\nu_0^c}\exp\left(\left[\frac{T_{bend}\,T_0^c}{4\,T_F^2}\right]^{\frac{1}{4}}\right). \quad (3.2.17a)$$

Equation (3.2.17a) suggests that it is unlikely that one would see a constant conductivity at very high fields; this is due to the increase in the number of new localized states resulting from degradation processes, which is far less likely at very low temperature. In fact, it can be shown that the exponent in Eq. (3.2.20) will be a function of T_{bend}/T_F. Further, due to electric field-induced stress, the energy gained by carriers in between scattering events could heat the local lattice causing the conductivity to rise further than predicted with increasing field. The point at which high-field processes become destructive is not well understood and is certainly an upper limit for our discussion of VRH. For a discussion of breakdown processes and high-field phenomena, refer to Kao (2004), Montanari *et al.* (2001, 2005), Teyssedre *et al.* (2005), and Fothergill (1998). For this reason, it is prudent to focus on the low-field expansion and its extension to a more complete effective temperature.

3.2.3. Generalized Effective Temperature

So far, we have described the field dependence in the very low and very high regimes, but not at any intermediate scales. Further, our simple models using the segregation time do not provide a complete description of both the field and temperature behavior for all temperature and field ranges of interest. How can we describe transport in the presence of both temperature and field? In the literature there are a number of theories that predict the field dependence (Gill, 1972; Pollak, 1972) for VRH conductivities in several DOS types, and a few that predict both the electric field- and temperature-dependence in the low-temperature regime (Fritzsche, 1990; Cleve *et al.*, 1995; Vissenberg, 1998). Several studies have looked at the effects of temperature and field on the steady state energy distribution of electrons (distribution after thermalization) using numerical simulations (Marianer, 1992; Cleve *et al.*, 1995; Baranovskii and Rubel, 2006). Many of these authors sought an analytical expression to describe temperature- and electric field-dependence using a single effective temperature and the theoretical methods described in Sections 3.2.1 and 3.2.2 (with considerable more detail). These analytical expressions are compared with the more complete numerical results to attempt to develop a phenomenological based effective temperature expression. While the numerical simulations have met with some success in describing the measured behavior, analytical methods have met with only marginal success. However, a phenomenological expression for the effective temperature has been developed (Cleve *et al.*, 1995; Baranovskii and Rubel, 2006):

$$T_{eff}(F,T) = \left[T^p + \left(C\frac{q_e F \eta}{2k_b}\right)^p\right]^{1/p} = [T^p + (C_1 T_F)^p]^{1/p}. \tag{3.2.21}$$

Here C, C_1, and p are unitless numerical constants determined by simulation. The additional formulation in Eq. (3.2.21) has been added to highlight the role of the effective field temperature. The value of p is typically two and C ranges from 0.05 to 0.09 (Baranovskii and Rubel, 2006). In all the literature this author reviewed, only the exponential and Gaussian DOS are explored with respect to Eq. (3.2.21). *There is no context this author found that discusses this equation and a constant DOS!* Although it was shown that the exponential DOS gives the constant DOS in the limit as the energy scale goes to infinity, few calculations have been done in this limit (Grant and Davis, 1974). To this author's knowledge and that of Baranovski, no currently complete analytical theory exists that can predict an effective temperature of this type.

However, we have shown in Sections 3.2.1 and 3.2.2 that there appears to be some function that describes the effective temperature behavior. It was, in fact, the process of deriving expressions for the VRH conductivity in terms of the segregation time that this author noticed the connections mentioned. In Section 3.2.4, we show that Eq. (3.2.21) can be included in a very natural way into the USU MPH VRH model.

3.2.4. VRH for a Constant DOS

Consider the effective temperature portion of Eq. (3.2.14) for the field-dependent segregation time that resulted from both modification of the DOS and the hopping rate,

$$T_{eff} \approx T_F \left(1 + \frac{T_F}{T_{\text{bend}}}\right). \tag{3.2.22}$$

This equation is, itself, an effective temperature and bears a strong resemblance to the phenomenological equation developed in Eq. (3.2.21). Also, we have in several instances shown that the inclusion of the segregation time in our expressions for the VRH conductivity requires the use of a power, *p*, which changes with field. This suggests two things: (*i*) that we should try to incorporate Eq. (3.2.22) into our expression for the low-temperature conductivity, and (*ii*) that this phenomenological approach can almost certainly be linked to changes in the MAR, demarcation energies, effective transport level, and resulting segregation times. We do not have time to explore how Eq. (3.2.22) might have come about analytically [we suggest expanding Eq. (3.2.9) as a starting point]; however, inclusion of the Eq. (3.2.21) into the Apsley and Hughes model is quite simple. Consider Eq. (3.2.21) written as the inverse fourth root of the effective temperature

$$\frac{1}{T_{eff(F,T)^{1/4}}} = \left[T^p + \left(C\frac{q_e F\eta}{2k_b}\right)^p\right]^{-1/4p} = [T^p + (C_1 T_F)^p]^{-1/4p}. \tag{3.2.23}$$

Separating out the temperature dependence, we obtain a function, which contains the ratio of field to thermal energy.

$$\frac{1}{T_{eff(F,T)^{1/4}}} = T^{-1/4}\left[1 + \left(C\frac{q_e F\eta}{2Tk_b}\right)^p\right]^{-1/4} = T^{-1/4}\left[1 + C_2\left(\frac{\mathrm{T_F}}{\mathrm{T}}\right)^p\right]^{-1/4}. \tag{3.2.24}$$

Using the USU MPG VRH model, Eq. (3.2.2), as a guide (specifically, we look at the power of β_ν and the leading constant for the argument of the exponential term), we guess that p = 2, C =1 or $C_2 = (C_1)^p$. Applying these values to Eq. (3.2.24) gives

$$\frac{1}{T_{eff(F,T)^{1/4}}} = T^{-1/4}\left[1+\left(\frac{q_eF\eta}{2Tk_b}\right)^2\right]^{-1/8}. \quad (3.2.25)$$

If we now define $\beta_v\,(F,T) \equiv \frac{q_eF\eta}{Tk_b}$ and expand Eq. (3.2.25) for small β_v, keeping only the first two terms while multiplying both sides by the fourth root of the sample temperature, we arrive at a very familiar expression,

$$\left(\frac{T}{T_{eff(F,T)}}\right)^{1/4} = \left[1-\frac{\beta(F,T)^2}{4}\right]. \quad (3.2.26)$$

This is exactly the term found in the USU MPG VRH model for low fields, which we present here for ease of comparison,

$$\sigma^c_{VRH}(\mathrm{T,F}) = \left(\frac{N_t{q_e}^2\eta^2\nu_0^c}{2\varepsilon_0^c}\right)\left(\frac{24\varepsilon_0^c}{(k_bT)\eta^3\pi N_t}\right)^{1/4} exp\left[-\left(\frac{24\varepsilon_0^c}{(k_bT)\eta^3\pi N_t}\right)^{1/4}\left[1-\frac{\beta(\varepsilon,T,\eta)^2}{4}\right]\right]. \quad (3.2.27)$$

Using the definitions $\sigma_0^{C-low} \equiv (N_t\eta^2{q_e}^2\nu_0^c/2\varepsilon_c)$ and $T_0^c \equiv (24\varepsilon_c/k_b\pi\eta^3N_t)$, comparing Eq. (3.2.5) with (3.2.7) and incorporating Eq. (3.2.26), we can write the following version of the USU MPG VRH equation for low fields as

$$\sigma^c_{VRH}(\mathrm{T,F}) \approx \sigma_0^{C-low}\left(\frac{T_0}{T}\right)^{1/4} exp\left[-\left(\frac{T_0}{T_{eff(F,T)}}\right)^{1/4}\right]. \quad (3.2.28)$$

The phenomenological equation for the effective temperature: (*i*) reduces the model parameter dependence to three values with no additional numerical factors; (*ii*) connects our expressions for the segregation time in the low-field limit to the conductivity; (*iii*) shows that the phenomenological expression can be derived from an analytical model (that of Apsley and Hughes); and (*iv*) describes both the temperature and field dependence! Further, by making a comparison with the form of the segregation equation given by Eq. (3.2.15), we can make an educated guess as to the true form of the segregation time:

$$\tau^{c,F}_{seg}(\mathrm{T,F}) = \frac{1}{\nu_0^c} exp\left[-\left(\frac{T_0}{T_{eff(F,T)}}\right)^{1/4}\right]. \quad (3.2.29)$$

Here there are two so-called effective temperature expressions; one is the zero field limit given by T_0^c, and the other is a field driven effective temperature. In hind sight, it seems better to have called T_0^c the temperature scaling constant as it is a non-field-dependent material, parameter-based term. This convention for T_0 has been used so that the reader can easily connect with the literature and allows one to see the difference between the real effective temperature and this scaling term. The effective

temperature will likely describe higher order field dependence and hopping charge transport; this, however, must be left for future work. One might criticize the order in which we have arrived at these results; it would be far more satisfying to have started from first principles and derived Eq. (3.2.22). However, those connections are clearly possible; the machinery developed in Section 3.1 gives us both a deep understanding of the processes occurring in HDIM as carriers undergo transport, but also provides tools with which we can estimate the results of much more complex approaches. That is the fundamental point of this chapter.

One connection that has not been discussed is the application of the transport equations given in Chapter 2 to the low-temperature regime. In part, this resulted from the fact that one needs the tools of Section 3.1 to understand how to manipulate the transport equations in the low temperature and/or high-field limit. For an excellent explanation of the connection between the transport equations and hopping conductivity, see Schmidlin (1977). In addition, the work of Esipov shows how to modify the MT equations to incorporate high-field effects (Esipov, 1991). In fact, Esipov shows that inclusion of the field-dependent effective temperature, Eq. (3.2.8), and field-dependent DOS, Eq. (3.2.9), leads to an expression for the VRH conductivity that bears a strong resemblance to the expressions found by Apsley and Hughes (1974, 1975). Simply put, all of the low-temperature conductivity expressions are essentially limiting cases of the transport equations in the equilibrium state. It should be possible to developed a complete numerical code based on the transport equations using the theory of Section 3.1

Hopping is a vast subject, covering nearly all aspects of solid state and quantum physics. As such, there are many methods by which to calculate the hopping conductivity under both AC and DC fields. A successful, physically simple, and intuitive approach has been developed by many authors and is commonly used to understand dark current hopping conductivity in amorphous semiconductors (Schmidlin, 1977; Monroe, 1983; Monroe *et al.*, 1993; Arkhipov and Bässler, 1994a; Vissenberg, 1998; Baranovskii and Rubel, 2006). This method uses the low-temperature transport theory described in this chapter and percolation theory (Zallen and Scher, 1971) to provide expressions that can be used to understand the conductivity of HDIMs. The theory developed in this chapter has also been extensively employed to understand hopping conductivity resulting from exponential and Gaussian DOS models.

In the following two sections, we review the VRH results for the exponential and Gaussian DOS models. I will not present a detailed discussion of these models, as they require considerable additional development of ideas in percolation theory and mean field theory. However, in each instance, there is a rich literature to guide the interested reader. Thus, what follows is a short summary of the results of such investigations and relevant parameters.

3.2.5. VRH in an Exponential DOS

A similar expression to Eq. (3.2.27) for a material with an exponential DOS was developed by Vissenberg (1998) for the VRH conductivity using the theory developed in Section 3.1 and percolation theory:

$$\sigma_{VRH}^{e}(N_t,T) = \sigma_0\left(\frac{\pi\eta^3 N_t (T_0^e/T)^3}{8B_c\Gamma\left(1-\frac{T}{T_0^e}\right)\Gamma\left(1+\frac{T}{T_0^e}\right)}\right)^{T_0^e/T}. \tag{3.2.30}$$

Here, B_c is the percolation parameter approximately 2.6 to 2.8 for most materials (Vissenberg, 1998; Li, 2007; Arkhipov *et al.*, 2006), Γ(x) is the gamma function, and N_t is the total number of trapped carriers per unit volume. Note, the value of N_t is the equilibrium steady state concentration of trapped carriers and is not time dependent. The temperature-dependent density of trapped carriers is given by

$$N_t(\varepsilon_f^o,T) = N_t\, exp\left(\frac{\varepsilon_f^o}{k_b T_0^e}\right)\Gamma\left(1-\frac{T}{T_0^e}\right)\Gamma\left(1+\frac{T}{T_0^e}\right), \tag{3.2.31}$$

where ε_f^o is the equilibrium Fermi level. The percolation parameter, B_c, is defined as the density of active current transmitting bonds (those that allow hops at the TE) divided by the density of transport sites in the percolating system. The percolation parameter is the critical number of bonds for conductivity to begin and is given by N_{bond}; the number of sites to which those bonds connects is N_{site}, thus $B_c = N_{bond}/N_{site}$. The calculation of a random resistor network using percolation theory is covered in detail in (Pollak, 1972; Bässler, 1984, 1993; Böttger and Bryksin, 1985; Hertel *et al.*, 1999; Arkhipov *et al.*, 2006); an excellent general review of percolation theory can be found in Zallen and Scher (1971).

Equations (3.2.30) with Eq. (3.2.31) can be written in a suggestive form using the relation between the gamma function and the *sin(x)* function (Abramowitz, 1965):

$$N_t(\varepsilon_f^o, T) = N_t \, exp\left(\frac{\varepsilon_f^o}{k_b T_0}\right)\left[\frac{\pi\left(\frac{T}{T_0^e}\right)}{\sin\left(\pi\frac{T}{T_0^e}\right)}\right]. \quad (3.2.32)$$

This expression for the number of trapped carriers appears often when evaluating MT models using an exponential DOS (Arkhipov *et al.*, 2006; Orenstein and Kastner, 1979, 1982; Orenstein *et al.*, 1980; Monroe *et al.*, 1981; Monroe, 1985, 1986). Equation (3.2.32) can also be solved for the equilibrium Fermi level; if the number of trapped carriers is known, this is a useful approach. Equation (3.2.32) and the VRH equation, Eq. (3.2.30), then yield a simple form for the conductivity

$$\sigma_{VRH}^e(N_t(\varepsilon_f^o, T), T) = \sigma_0\left(\frac{\eta^3 N_t\left(\varepsilon_f^o, T\right) exp\left(\frac{\varepsilon_f^o}{k_b T_0^e}\right)}{\left(\frac{T}{T_0^e}\right)^3 8B_c}\right)^{1/\left(\frac{T}{T_0^e}\right)}. \quad (3.2.33)$$

Equation (3.2.33) bears a strong resemblance to the time- and temperature-dependent equations when evaluating the transport equations with an exponential DOS; the interested reader can compare Eq. (3.2.33) with results in Rose and Lampert (1959). Further, a comparison with other work for RIC and TOF systems involving dispersive transport and exponential DOS (Schmidlin, 1977; Orenstein *et al.*, 1980; Tiedje *et al.*, 1981; Tyutnev, 1996; Tyutnev *et al.*, 2002a, 2003, 2006a, 2007) yields similar expressions, suggesting a very close connection. The Eq. (3.2.30) does not explicitly show the segregation time or transport energy; good discussions of these parameters can be found in (Esipov, 1991; Cleve *et al.*, 1995; Li, 2007). There are a number of ways that Eq. (3.2.33) can be manipulated to reflect different physical properties, such as trapped carrier density, total carrier density, and number of carriers in the transport band all as a function of time, temperature, and field. For an introduction to how such calculation are made see Vissenberg (1998), Baranovskii and Rubel (2006), and Fritzsche (1990).

Equation (3.2.33) does not include field dependence. Li (2007) expanded the work of Vissenberg and Matters to include electric field dependence and derived the following expression for the temperature- and field-dependent conductivity in an exponential DOS,

$$\sigma_{VRH}^e(F, T) = \sigma_0\left[\frac{\pi\left[N_t(\varepsilon_f^o, T)\eta^3\right](k_b T)}{2B_c(q_e F\eta)}\left(\frac{1}{\alpha}\right)^3 exp\left[\frac{\pi\alpha}{\sin(\pi\alpha)}\right]\left((2-\eta q_e F/k_b T)^{-2} - (2+\eta q_e F/k_b T)^{-2}\right)\right]^{1/\alpha}, \quad (3.2.34)$$

where we have defined $\alpha(T) \equiv T/T_0^c$. The calculation to obtain Eq. (3.2.34) is essentially the same as that used to obtain Eq. (3.2.30), with the exception that the MAR hopping rate was modified with a field

term, $q_e F cos(\theta) R_{ij}$, as was done in the derivation for the USU MPG VRH model (Apsley and Hughes, 1974, 1975; Dennison *et al.*, 2009a). This approach is used in many field-dependent approximations. The authors have made the following assumptions, which are included for completeness: (*i*) the site positions are random, (*ii*) the energy barrier for the critical hop is large, and (*iii*) the charge carrier concentration is very low.

For high fields $>10^7$ V/m (approximately 274 volts for a 27.4um sample), the Li equation, Eq. (3.2.34), predicts an activated behavior (Li, 2007). This result should be tested against Kapton™ whose threshold for breakdown is thought to be high enough to withstand such a field, and also is expected to have an exponential DOS. The work of Li (2007) has only been tested against Monte-Carlo simulation, whereas the work of Vissenberg (1998) has been shown to provide good fits to real data from polythienylene and pentacene (Vissenberg, 1998; Baranovskii and Rubel, 2006). To this authors knowledge, neither of these formalisms have been tested for HDIMs.

3.2.6. VRH for a Gaussian DOS

In order to discuss the VRH equilibrium conductivity in a Gaussian DOS, we must first address the mobility. In the literature, the description of transport in a Gaussian DOS is nearly always characterized by the mobility. This is likely because inorganic materials, which typically display a Gaussian DOS (Hertel, 2008), are studied by time of flight methods, which lend themselves to the characterization of the mobility. The mobility and resulting conductivity is generally experimentally characterized by Bässler (1993),

$$\mu = exp\left[-\left(\frac{\varepsilon_0^G}{k_b T}\right)^2\right]. \tag{3.2.35}$$

Note that the mobility goes as T^{-2}. This temperature dependence is a well-known signature for a Gaussian DOS.

While detailed percolation and random resistor network models have accounted for the behavior given by Eq. (3.2.35), simple analytical formulas have been elusive. In the literature (Arkhipov and Bässler, 1994a; Arkhipov *et al.*, 2002c, 2005a; Baranovskii and Rubel, 2006; Fishchuk *et al.*, 2007; Hertel and Bässler, 2008), there is a disparity in the approach to the calculation of the transport properties resulting from the Gaussian DOS. In the 1980's, Arkhipov (Arkhipov and Rudenko, 1982c; Rudenko and

Arkhipov, 1982b, 1982c; Arkhipov *et al.*, 1983) and Bässler (1993) addressed the very complex nature of hopping in a spatially and energetically disordered DOS. In particular, they tried to find a more transparent approach to the complex models of the time (Böttger and Bryksin, 1985), leading to the intuitive physical interpretations developed in Section 3.1 (Baranovskii and Rubel, 2006). The work of Arkhipov *et al.* (2006), Bässler (1993), and Baranovskii and Rubel (2006) are all based on averaging procedures, similar to those found in other theoretical calculations (Apsley and Hughes, 1974, 1975). For example, Arkhipov (Arkhipov, 1999; Arkhipov *et al.*, 2001a, 2001b, 2002c, 2003a, 2005a, 2005b; Reynaert *et al.*, 2005) obtained the following expression for the mobility in VRH regime with a Gaussian DOS:

$$\mu = \frac{q_e \nu_0^G \sqrt{\pi} N_t \eta^5}{2\varepsilon_0^G} exp\left[-\frac{1}{4}\left(\frac{\varepsilon_0^G}{k_b T}\right)^2\right]. \tag{3.2.36}$$

This expression does not characterize the electron mobility properly when compared with experimental results (Baranovskii and Rubel, 2006). Percolation theory showed that one must consider all hops (not just the average) to the transport energy and it was found that the averaging procedure used by Arkhipov and others to obtain Eq. (3.2.36) will predict a trapped carrier concentration and thermal dependence that is slightly lower than the measured values (Baranovskii and Rubel, 2006). Since there are disparities between the different authors, we largely follow (Baranovskii and Rubel, 2006).

This presentation has the merit of being simple and allows for first order characterization material parameters for low fields. Baranovskii and Rubel (2006) and references therein have shown that the averaging procedure does, in fact, deviate from Monte-Carlo calculations (which seem to be more accurate) and further, they have presented a slightly more complex framework that requires some modest numerical calculation in the form of transcendental equations. In Section 3.1, we encountered these numerical expressions when describing the TE, DE, and thermalization time in the context of the Gaussian DOS. The calculations can be done in Mathcad™—or a similar mathematical calculation package—with reasonable ease. In order to calculate the mobility using the methods prescribed by Baranovski, the following set of equations must be solved numerically.

$$\ln\left[\left(\frac{q_e \nu_0^G R(\varepsilon)^2}{k_b T}\right)^{-1} \mu\right] = -2\left[\frac{4\sqrt{\pi}}{3B_c} N_t \eta^3 \int_{-\infty}^{\Upsilon/\sqrt{\pi}} \exp[-t^2]\, dt\right]^{-\frac{1}{3}} - \Upsilon\left(\frac{\varepsilon_0^G}{k_b T}\right) - \frac{1}{2}\left(\frac{\varepsilon_0^G}{k_b T}\right)^2, \tag{3.2.37}$$

where $\Upsilon\left[N_t \eta^3, \frac{k_b T}{\varepsilon_G}\right]$ is the function defined Eq. (3.1.29) as satisfying the transcendental equation

$$exp\left(\frac{\Upsilon^2}{2}\right)\left[\int_{-\infty}^{\Upsilon/\sqrt{2}} exp(-x^2)dx\right]^{-1/3} = \left[9N_t\eta^3(2\pi)^{1/2}\right]\frac{k_bT}{\varepsilon_0^G}. \quad (3.2.38)$$

In order to obtain the conductivity, we must estimate the number of carriers in the TB. The calculation of the number of carriers in the transport band follows from the product of the DOS and the Fermi-Dirac distribution function evaluated from the transport energy to the QFL, ε_f^{QFL}:

$$n_e = \int_{\varepsilon_t}^{\varepsilon_f^{QFL}} \frac{N_e(\varepsilon)}{1+exp\left[\frac{\left(\varepsilon-\varepsilon_f^{\mathrm{G}}\right)}{k_bT}\right]}\,\mathrm{d}\varepsilon. \quad (3.2.39)$$

Since the value of the TE is estimated numerically, the conductivity given by Eq. (3.2.40) must be evaluated for each TE as the temperature and field change. The motion of carriers in the transport band at the TE is essentially a reduced-drift mobility; thus, we can model the transport using an Ohmic approximation,

$$\sigma_{VRH}^G = q_e\mu n_e. \quad (3.2.40)$$

Here, it is assumed that the injected carrier concentration is known and that the concentration is largely near the FL; that is, $\langle\varepsilon_\infty\rangle \sim \varepsilon_f^{\mathrm{G}}$. Expressions for the QFL are developed in Section 3.1.7 and will not be repeated here. Equations (3.2.37) though (3.2.39) constitute the theoretical construction needed to describe the mobility and resulting conductivity accurately in a Gaussian DOS, without the presence of a strong applied field.

The Gaussian DOS produces both dispersion and drift behavior (Bässler, 1993; Baranovskii and Rubel, 2006). Time of flight data have shown that the dispersive behavior occurs when the energy scale of the DOS is comparable to or larger than the thermal energy, $\frac{\varepsilon_o^{\mathrm{t}}}{k_bT} \gtrsim 1$. In such a case, the observation experimental time is less than the thermalization time (Bässler, 1993). This means that the carrier charge distribution does not have sufficient time to reach the equilibrium level before the carriers recombine or reach the rear electrode; therefore, we see a range of release times causing dispersion. For thermalization times faster than the experimental time (i.e., $\frac{\varepsilon_o^{\mathrm{t}}}{k_bT} \ll 1$), one will measure either a short dispersive period followed by diffusive transport or purely diffusive transport. The Gaussian DOS behavior is unlike that of the exponential DOS in its dispersive response. In an exponential DOS, the charge distribution will dive deeper into the tail for very long times; in HDIM it can be months. Kapton™ is believed to have an

exponential-type DOS and our measurements (Hodges *et al*., 2013) have observed decay times greater than 20 days (see Chapter 6). An exponential DOS is nearly always dispersive at low temperatures and only shows nondispersive behavior at temperatures or concentrations high enough to initiate activated CB transport or to saturate the DOS. In the Gaussian system, the time to equilibrium (end of thermalization) is strongly controlled by $\frac{\varepsilon_o^t}{kT}$, and small changes in this value cause large changes in the thermalization time; hence, the termination of the dispersive regime occurs on a much shorter time scale (fractions of seconds to longer time scales).

Bässler (1993) and later Mozer (2005) have applied expressions for the VRH mobility in a Gaussian DOS (both spatial and energetically Gaussian distributions) with temperature- and field-dependence. The most common expression for the mobility as a function of both temperature and applied field was developed by Bässler (1993),

$$\mu(T,F) = \mu_0 exp\left[-\frac{2}{3}\left(\frac{\varepsilon_o^t}{k_b T}\right)^2\right] exp\left[C\left(\left(\frac{\varepsilon_o^t}{k_b T}\right)^2 - \Sigma^2\right) {F_{eff}}^{1/2}\right]. \quad (3.2.41)$$

Here, Σ is a unitless, spatial disorder parameter whose value is zero for no disorder, and one for high disorder; *C* is a constant defined in Bässler's original paper as a parameter that takes into account the concentration dependence of the material (Bässler, 1993). The effective field term, $F_{eff} = \frac{q_e F \Delta x_{ij}}{2k_b T}$, connects the spatial hopping distance, Δx_{ij}, to the ratio of the applied field energy, $q_e F \eta$, to thermal energy, $k_b T$.

To obtain an expression for the effective field, one must sum all of the possible hops (sum over all *i* and *j*); this process again requires knowledge of percolation theory and will, therefore, not be discussed here [see Bässler (1993)]. This effective field term and its application play an important role in understanding what kind of transport we observe. We can investigate a simple model that will allow us to understand how application of Eq. (3.2.41) proceeds. Imagine that the spatial disorder parameter, $\Sigma = 1$ (that is, we have large spatial disorder), and the energetic disorder parameter, $\varepsilon_0^G = 0$ (little or no energetic disorder), which is often the case with simple ionic models like the TAH model (Dennison *et al.*, 2009b). Consider the case where a carrier is allowed to jump forward and back a distance $+a$ and $-a$ (let a be the

lattice spacing), respectively, and consider the mobility between two sites at $+a$ and $-a$. Under these circumstances, Eq. (3.2.41) becomes

$$\mu(T,F) = \mu_0 \left(exp\left[C \left(\frac{q_e F a}{2 k_b T} \right)^{1/2} \right] - exp\left[C \left(\frac{-q_e F a}{2 k_b T} \right)^{1/2} \right] \right). \tag{3.2.42}$$

This is the MAR of the thermally activated hopping model that we expect for ionic conductivity, a TAH model. In fact, Bässler (1993) states that in simulations—which consider the zero energetic disorder limit—the Arrhenius behavior (common to TAH) is expected from a Gaussian DOS. If we now imagine including a material in which there are many different site separations (not just *a*), then the sum must be done for each *i* and *j*. The complexity of the model can be extended to include complete energetic and spatial disorder [see Bässler (1993) for details].

While the calculation of the Gaussian model may seem cumbersome, its numerical implementation is simple (often employing a Monte-Carlo algorithm). For an excellent discussion of this model, its applications, connections to the theory in Section 3.1, and additional details on the derivation of relevant parameters, see Baranovskii and Rubel (2006), Hertel (2008), and Arkhipov *et al.* (2006).

3.2.7. Very Low Temperature

There exists a temperature below which even the VRH process fails to describe the electron transport. This temperature, T_{low}, marks the lower bound for our theoretical description. Below T_{low} the transport energy is equal to the QFL or below it deep in the tail of the charge distribution. This situation leads to a mixture of nondegenerate and degenerate trapped electron population (Fritzsche, 1990). In this temperature regime, our picture of transport with excitations from the charge distribution to the transport energy and subsequent hopping is invalid. In order to describe the transport picture, we must resort to an energy loss model in which recombination with holes directly from the QFL is the dominant process and the conductivity is expected to become temperature independent, as it is dependent only on the capture cross section between the trapped carrier and a hole. For an exponential DOS, the effective temperature can be estimated as (Fritzsche, 1990; Baranovskii and Rubel, 2006; Arkhipov *et al.*, 2006).

$$T_{low} = T_0^e \left(\frac{9\pi}{2} n_t \eta^3 \right)^{1/3} \qquad \{\text{Exponential DOS only}\}. \tag{3.2.43}$$

In amorphous semiconducting materials like a-Si:H, this temperature is ~ 50 K or less (Fritzsche, 1990). If we assume that Eq. (3.2.43) reflects the character of T_{low} for most materials, use the fact that the DOS in HDIM—like LDPE and Kapton™—are large, and assume the number of trapped electrons, n_t, is small when compared with the DOS (true for most applications), then it is clear that the temperature at which we would expect this phenomenon to become relevant is very low indeed. If we estimate these parameters for highly insulating materials; $T_0^c = 1000\ K$, $\eta = (1.05 \cdot 10^{-7})\ cm$ and the number of trapped carriers is ~ 10^{18} cm^{-3} (this is a gross overestimation) under constant irradiation (specifically, photo-excitation), we obtain a value of $T_{low} \sim 11\ K$. This is, in fact, an extreme upper limit, where an unusually high number of carriers is assumed; this is not likely in most of the materials considered in this work. Thus, in HDIM, we generally do not expect to encounter this low-temperature limit at practical temperatures.

If a low-temperature regime is observed, it is expected to be a diffusive type transport at practical temperatures, in the absence of recombination. In a diffusive system for higher temperatures, the relationship between mobility and the diffusion coefficient is given by the Einstein relation (Fritzsche, 1990). However, for temperatures at or below T_{low} in inorganic noncrystalline materials, the conductivity does not depend on temperature (Fritzsche, 1990; Baranovskii and Rubel, 2006). In this temperature region, the diffusion coefficient changes form. For an exponential DOS, the relationship between the diffusion coefficient and the mobility can be written as

$$\mu_{low} \approx \frac{q_e}{k_b T_0} D. \tag{3.2.44}$$

There are no expressions this author is aware of for the other DOS models in this limit. Low-temperature transport is a large area of study and is mentioned largely for completeness; see for example Böttger and Bryksin (1985) or Baranovskii and Rubel (2006). However, since spacecraft often operate at temperatures below ~50 K, where this effect is possible in semiconducting materials with spatial and energetic disorder, it is an important set of ideas to mention.

3.3. Summary

In Chapter 3, a dynamic description of the way in which charge moves within the DOS has been developed. In short, the process of thermalization dominates the dynamic description of charge motion in

the DOS; this process is characterized by the demarcation energies, transport energy, Fermi level, thermalization time, and segregation time. These ideas—coupled with knowledge of hopping transport for a large span of temperatures and fields— provide a nearly complete intuitive description of charge transport in HDIM. The application of the theory developed in Section 3.1 covers a huge class of transport phenomena. In Section 3.2, we applied the average microscopic tools to VRH transport for HDIM with a constant DOS and showed that it is fully consistent the USU VRH multiple trapping models used previous to the writing of this dissertation.

We now return to a discussion from the introduction of the possible experimental configurations and how the results of Chapters 2 and 3 enhance our understanding of those methods. Recall that a set of experimental configurations were identified in Chapter 1. Three of these configurations modeled incident radiation charging and the other three contact injection charging (see Fig. 1.4). The key to understanding what behavior will be measured in any one of these arrangements is the material response. In Chapter 2, a complete discussion of the transport equations (at high temperatures) was given that provides a starting point to describe any one of these experimental arrangements. What was missing was a description of the internal dynamics of the injected electron charge distribution and its subsequent transport (i.e., hopping transport, demarcation energies, thermalization, transport energies, and the segregation time); these ideas were the subject of Chapter 3. By combining the theory developed in Chapter 3 with the transport equations from Chapter 2, nearly all transport phenomena [RIC, drift, dispersion, SCLC, TAH, VRH, and secondary electron emission (SEE)] in both semiconducting and HDIM can be understood as the interaction of electrons with energetically and spatially disordered trap states and transport states.

An excellent example of the application of the transport equations and thermalization is given by Monroe in the high temperature transport regime (Tiedje, 1980; Monroe, 1983, 1986). Monroe considers two types of DOS profiles in a single doped amorphous material. The dopant is modeled by a delta function DOS (exactly like our simple model in Chapter 2) and the amorphous part is modeled by an exponential DOS. Monroe then employs the demarcation energy to derive expressions during different times of the thermalization process to understand the observed photoconductivity. The resulting equations predict dispersive behavior for intermediate times (during which there is a high photoconductivity) and then—after thermalization completes—a diffusive behavior that results from the doping states is observed

at a lower TAH conductivity. In fact, Monroe is able to describe the times at which trapping and release events between the respective DOS profiles change dominance in the observed current. One critical final point must be made, this is simply that the transport equations (as described in Chapter 2) can now be used to describe macroscopic transport at low temperatures by including the microscopic description described in this chapter. Specifically, the CB will be replaced by the TE (which now acts as a conduction band within the BG with a much lower mobility than its high-temperature counterpart) and the trapped states—at or below the Fermi level—will serve as the trapped distribution that drives transport through a dispersion of trapped carrier release times. This is a very useful result that allows a description of low-temperature transport (above the critical temperature) using the macroscopic transport equations. Note, in such an application of the transport equations, great care should be taken to include the microscopic description of transport to physically interpret parameters and the DOS in the transport equations. Specifically, it is expected that the trapping rates, detrapping rates, measured mobility of charge at the TE, and effective DOS will appear differently at low temperature than at high temperature. For a very detailed discussion regarding the connection between the transport equations, hopping (or stochastic) transport, and macroscopic phenomena like dispersion see Schmidlin (1977).

There are many such examples at various temperatures, applied fields, and experimental configurations for the application of what is often called stochastic transport. One should not come away from Chapters 2 and 3 with the idea that stochastic transport is limited to low temperatures. On the contrary, dispersion (which is driven by exponential or Gaussian disorder in the DOS) can occur at low or high temperature and be described in both cases by the macroscopic transport equations. However, a detailed physical description of dispersion must be made at the microscopic level and thus requires the theory presented in this chapter. In the literature, the term stochastic transport has been used to describe both macroscopic and microscopic phenomena [see, for example, Scher and Montroll (1975) and Bässler (1993), respectively]. Here are a few very useful papers and books that highlight the use of the tools developed in this chapter: (Grant and Pollak, 1972; Davis, 1974; Schmidlin, 1977; Orenstein and Kastner, 1982; Orenstein *et al.*, 1982; Kastner and Monroe, 1982; Monroe, 1983, 1986; Berlepsch, 1985a, 1985b; Sessler, 1987; Fritzsche, 1990; Arkhipov, 1999; Arkhipov *et al.*, 2000, 2001a, 2001b, 2001c, 2002a, 2002b, 2003a, 2003c, 2006; 2004, 2005a, 2005b; Nikolaenkov *et al.*, 2003; Molinie, 2005; Tyutnev *et al.*,

2005, 2006a, 2006b, 2006c, 2007, 2008a, 2008b, 2008d; Baranovskii and Rubel, 2006; Fishchuk *et al.*, 2007).

It cannot be stressed enough that there is need for careful evaluation of the experimental configuration and nature of the resulting data when applying these theories. In order to get a truly complete understanding the HDIM, these materials must be studied under multiple experiential configurations and the measurements compared with both analytical and numerical expressions. It is clear that the problem of studying charge transport in HDIM requires numerical modeling of a more complex set of equations than have been presented in this dissertation. However, one of the advantages of multiple experimental platforms (available at the USU MPG) is the ability to clearly define specific charge injection profiles, make good approximations in applying the theory, which can be tested, and then check the results for consistency between each of the methods. To that end, the next two chapters investigate simple application of the ideas from Chapter 2 and 3 to two of the experimental systems described in Fig. 1.4.

CHAPTER 4

CONSTANT VOLTAGE CONDUCTIVITY CHAMBER ANALYSIS

4.1. Introduction

This chapter discusses the application of the theory developed in Chapter 2 and Chapter 3 to constant voltage conductivity (CVC) chamber measurements of HDIM. Specifically, we study the charging and discharging of the HDIM LDPE under the application of a step voltage, and the resulting current density as a function of temperature, electric field, and time. The CVC chamber is a parallel plate capacitor system in which a large range of voltages and temperatures can be applied to a sample. Experimental details of the CVC chamber and results to date will not be reviewed here but are well documented in (Dennison and Brunson, 2008; Brunson, 2009; Dennison *et al.*, 2009a; Dekany *et al.*, 2013). The CVC chamber is a metal-insulator-metal sandwich in which there are two metal-insulator interfaces (electrodes). We will assume—for simplicity—that electrons are injected at one of the electrodes and that the remaining electrode –usually the ground plane–does not inject electrons or holes. This is not the only type of CVC experimental system. Sessler has proposed a noncontact method that removes problems associated with the metal-insulator interface and solves the resulting transport equations (Sessler, 1987). This method explores transport of free and displaced charges in addition to polarization of the bulk material.

One may ask why these types of experiments are interesting. In spacecraft applications, materials are isolated objects; they are connected to other materials and are affected by potentials from the spacecraft, as a whole, or nearby materials whose electric field is significant. These fields operate from very short to extremely long time scales, over a wide range of temperatures, and simultaneously interact with the spacecraft environment. We, therefore need information about the response of an HDIM under as large an experimental range as possible, i.e., dependence on how the charge is injected or created within the sample due to stimuli such as temperature, applied field, pressure, and sample history. In this chapter, we focus on capacitive-type measurements that can quantify the effects of metal-insulator interfaces, bulk-insulator electron transport, and resulting electric fields.

The USU MPG CVC chamber allows materials to be tested over very long times (seconds to months), very low to very high temperatures (~100 K to 400 K), and across a wide range of applied fields

(up to electrostatic breakdown fields $> 5 \times 10^7\ Vm^{-1}$), while accurately measuring the extremely low current densities that result, down to the order of 10^{-16} A. The low-current, long-duration measurement capability is critical to characterizing electron transport in HDIM. Together these capabilities allow tests of conductivities $< 20^{-22}(\Omega\ cm)^{-1}$ with decay time constants of years (Dekany *et al.*, 2012). Long-term testing provides information on dark current conductivity and true equilibrium transport properties of the HDIM when charge is injected through a metal-insulator interface.

The CVC system allows for several important areas of study to be addressed, in addition to time-dependent behavior; variable range hopping (VRH), thermally activated hopping (TAH), space charge limited current (SCLC), thermally stimulated current emission (TSCE), electrostatic discharge (ESD), and, with some minor modifications, the study of photo-induced effects. Three of these fields of study are covered in this dissertation: TAH, VRH, and SCLC. TAH is a natural consequence of the transport equations and will not be discussed here. Low temperature VRH behavior is discussed in Chapter 3. Low temperature measurements can be used to understand hopping transport dynamics in dark or deep space conditions where very low temperatures are likely to make CB transport impossible, which lead to much longer charge dissipation times and a higher likelihood of material breakdown. For information on the application of the USU MPG VRH model to CVC data (on LDPE, which has a constant DOS), see Dennison *et al.* (2009a) and Dekany *et al.* (2012). In addition, the CVC system allows for the study of current density versus voltage dynamics (SCLC) discussed in Section 2.7.1. This can elucidate both the charge injection from contacts, and the nature of the DOS for both the bulk material and surface states. The physical models for current density versus voltage (SCLC) studies were discussed in Section 2.7.1. There is insufficient space or time to discuss the application of VRH theory or SCLC theory in this dissertation; they are, therefore, left as future work. The TAH, VRH, and SCLC models together represent an extremely powerful set of tools for the study of HDIM. Each of these bodies of theory overlaps the other, providing information about the type of DOS, temperature dependence, applied field dependence, capture cross section, charge injection (penetration) depth , and electron capture and release rates.

The remainder of Chapter 4 develops and applies theoretical expressions, which describe the current density measured at the rear contact electrode as a function of time, applied field, temperature, and material parameters. This model is not meant to be the final word in HDIM charging under CVC type

conditions. What it does is show that simple approximations to the transport equations can yield a physically insightful and accurate determination of the bulk material parameters and resulting decay of the observed current density. These results can then be checked against literature values and other USU MPG experimental results.

The structure of this chapter is broken into nine sections: (1) introduction, (2) discussion of the physical picture, (3) introduction to and reduction of the transport equations, (4) a discussion of the problems associated with charge injection and the solution, (5) polarization effects, (6) development of the USU CVC charging model, (7) application of the new model to USU MPG data, (8) introduction to decays models, and (9) concluding comments. The discussion of the physical picture will outline the necessary physical intuition to understand what happens in an HDIM under the conditions of a CVC-type experiment. This then sets the stage to discuss the transport equations and why certain assumptions are made to reduce them to a simpler form. This physical picture highlights the difficulties in determining the rate at which charge is injected into the sample due to interface and bulk processes. We present a model that decouples the injection problem from the bulk transport and allows for a simple charging expression to be developed, which can accurately describe the observed current density as a function of time.

The charging of an HDIM is only half the picture. Once the applied voltage is removed, the charges must decay to ground (at the rear electrode). The final theoretical discussion in Section 4.7 is, therefore, focused on decay models in CVC type systems. We do not develop a complete model for the decay of trapped charge after the cessation of the applied field; instead an outline and modification of a current theory is given. We close the chapter with some comments on the weaknesses and strengths of the approaches used, important observations, and comments.

4.2. Physical Picture

Charge motion in any material can be understood as three processes acting together to move charge from a higher potential to a lower one. First, in order for there to be free charge in HDIM it must either be injected into the material or be excited within the material (RIC is an example of excitation). The excitation of charges due to RIC does not occur in a CVC system (see Chapter 5). Second, charge must move through the material via the CB (or TB for very low temperatures). In HDIM, the process of

transport is interrupted by the trapping and release of electrons as they traverse the sample under an applied field or a self-induced field due to the interaction between the charge itself and a ground plane. Finally, the excess charge is absorbed or neutralized at a ground plane or oppositely charged electrode.

In this dissertation, it is the second process (bulk transport) that we are most interested in and not the nature of the injection profile or absorption of electrons (at the rear or grounded electrode) after they traverse the sample. Bulk processes are characterized by specific material parameters, such as the trapping rate, v_{et}, detrapping rate, v_{te}, mobility, μ_e, DOS, N_t, and resulting conductivity, σ. As it turns out, each of the experimental systems discussed in Chapter 1 have very different ways of injecting the charge, which are more difficult to understand than bulk processes; their effects are specific to the experiment and not to the material under test. Bulk processes are largely the same regardless of the injection methods, assuming the applied field is not too high and the makeup of the material is not altered by water content or changes in manufacturing process. By studying the decay of current under many experimental conditions, we can understand the common action of bulk transport processes. Electrostatic discharge (ESD) is an exception to this, as it represents dramatic changes in the internal structure and defect density of the material and will not be discussed here. For more information on ESD refer to Crine *et al.* (1989a), Crine (2007), Kao (2004), and Sessler (1987).

Since the observed current is strongly affected by the injection processes, there are some difficult issues to overcome in determining the bulk material parameters in a CVC experiment. The charge injection and absorption processes are extremely important and cannot be ignored, as they strongly affect the observed current. How, then, can we describe the observed current and separate out the injection from the bulk processes? In order to approach this problem, we must consider how electrons come to equilibrium after a step voltage is applied.

Consider Fig. 4.1, in which the process of injection is depicted in three stages: uncharged, initial injection at time, $t \gtrsim 0$, and injection long after injection, $t \gg 0$. Figure 4.1 represents a simple parallel plate capacitor, in which the HDIM is sandwiched between two conducting electrodes. The depth of the sample, *d*, is measured in the *z* direction; this is also the direction of the applied electric field, *F*. In Fig 4.1(a), there is no injected charge or applied field and the sample is uncharged (often called the virgin state); the traps in the material are unfilled and are represented by straight lines. Figure 4.1(b) depicts the

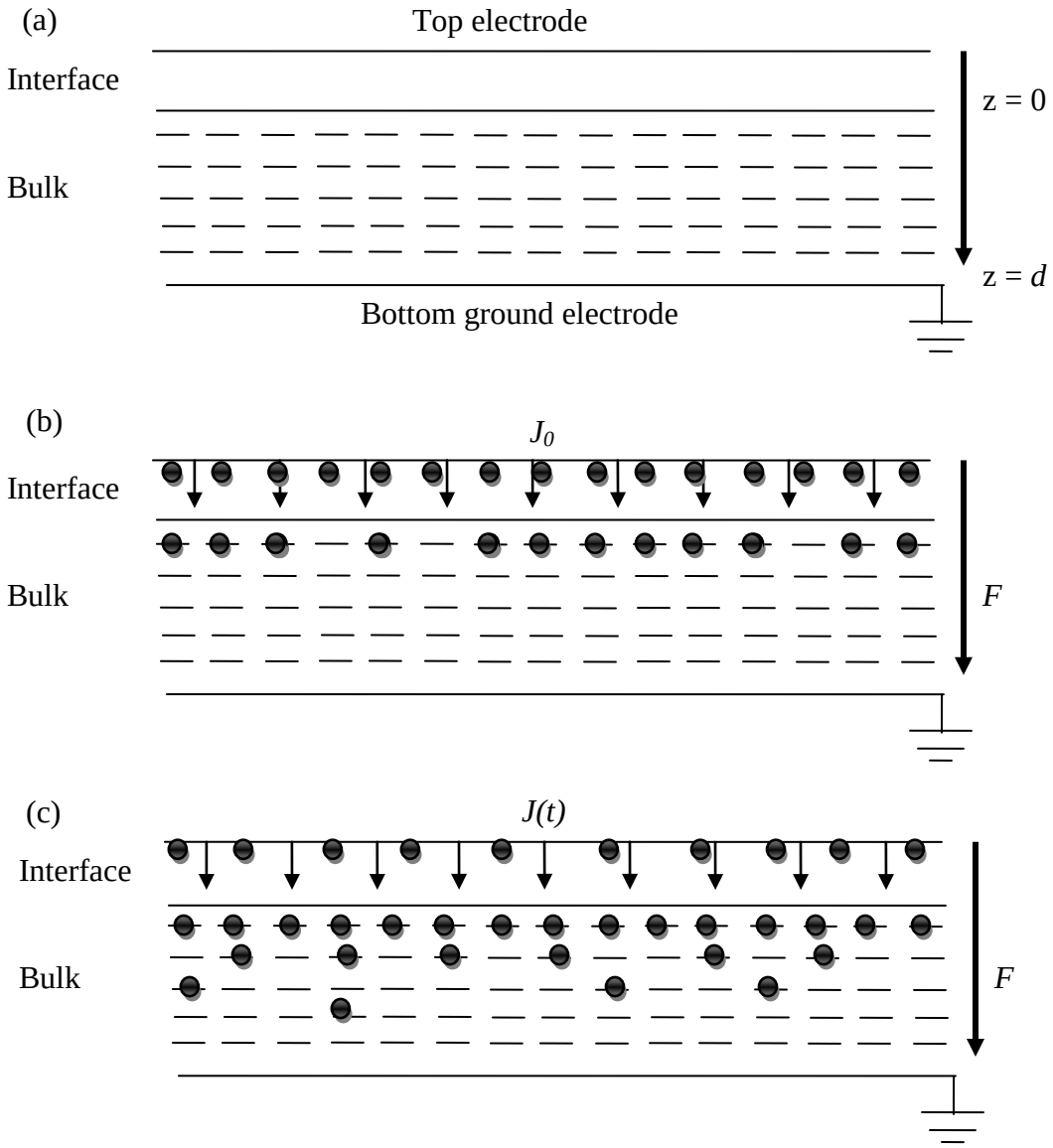

FIG 4.1. Physical picture for the CVC apparatus. (a) The initial uncharged configuration before the application of an electric field. Traps are depicted as empty lines. (b) After the application of a voltage, charges enter the material and become immediately trapped in surface or bulk states. (c) After some time, the number of electrons trapped in the material reaches semi-equilibrium, resulting in an electric field, which acts to counter the applied field and slow the injection of further electrons.

injection of electrons due to an initial current, J_0, at nearly the instant the field is applied and the injection process that occurs; electrons in filled trap states are shown as solid circles. The injection of electrons is at its highest rate at very early times and all the injected electrons are either trapped at the interface by surface traps or go into the CB resulting in a high observed current. Surface traps are generally of a different

nature than bulk traps and are further modified by the electronic interaction at the metal-insulator interface and the applied field (Walden, 1971; Wilcox, 1971; Wintle, 1974a; Toomer and Lewis, 1980).

A number of physical phenomena can affect the injection of charge at the interface: (i) polarization (dipolar, hopping, and space charge), (ii) ionic drift, (iii) Poole-Frenkle behavior, (iv) Fowler-Nordheim behavior, and other physical processes, such as barrier tunneling (Walden, 1971). Clearly, the interface region is very difficult to characterize (Tahira, 1985). To avoid this problem, many investigators use low applied fields and Ohmic contacts to limit interface affects; however, the injection rate is still affected by the trap filling process and is not constant. Consider the difference between Fig. 4.1(b) and Fig. 4.1(c). In Fig. 4.1(b) the injection current density is J_0; but as time progresses, a field due to the trapped charge distribution builds up. This space charge builds up and produces an internal field, thus decreases the injection of electrons from J_0 to some value determined by a function $J_s(t)$, which represent the current density at the surface that enters the sample. Thus, even if the action at the interface region on the injection current density were ignored, the injection current density must be a function of the time-dependent trapped charge distribution; this problem cannot be avoided (Walden, 1971; Wilcox, 1971; Wintle, 1974a, 2003; Toomer and Lewis, 1980; Tahira, 1985; Iwamoto, 1995; Ferreira and de Almeida, 1997; Liufu, 1998). In Section 4.4, we discuss the charge injection model used in this dissertation to account for the metal-insulator interface and charge trapping effects.

In order to see how the charge injection model can be included in the transport equations (to obtain an estimate for the measured current density and bulk material parameters), we must first develop a set of reduced transport equations specific to the experimental system that describes the bulk transport process. A discussion of the transport equations, bulk material parameters, physical processes that describe the thermalization of electrons, and connection to the DOS has already been given in Chapter 2 and Chapter 3, and will not be covered here.

4.3. Transport Equations

We begin with the full transport equations developed in Chapter 2 [Eqs. (2.6.8) through (2.6.12)] and use the fact that there is no external excitation due to RIC (RIC will be addressed in Chapter 5). This means that no electron-hole pairs are created; thus, terms involving α_{er} can be eliminated and N_{ex}

represents only the injection of electrons at the interface. This assumption eliminates Eq. (2.6.11) and modifies Eq. (2.6.10). Further, displacement and polarization currents are added, so that we start with the following set of transport equations;

$$J_{tot}(z,t) = q_e n_e(z,t)\mu_e F(z,t) + q_e D\frac{dn_{tot}(z,t)}{dz} + \epsilon_0\epsilon_r\frac{\partial F(z,t)}{\partial t} + J_p(t)$$

{Sum of electron drift, diffusion, displacement, and polarization current densities}, (4.3.1)

$$\frac{\partial}{\partial z}F(z,t) = q_e n_{tot}(z)/\epsilon_0\epsilon_r \qquad \{\text{1D Gauss's Law}\}, \qquad (4.3.2)$$

$$\frac{\partial n_{tot}(z,t)}{\partial t} - \mu_e\frac{\partial}{\partial z}[n_e(z,t)F(z,t)] - q_e D\frac{\partial^2 n_e(z,t)}{\partial z^2} = G(z,t)_{ex} + \alpha_{et}n_e(z,t)[N_t - n_t(z,t)]$$

{1D Continuity equation with drift, and diffusion}, (4.3.3)

and

$$\frac{dn_t(z,\varepsilon,t)}{dt} = \alpha_{et}n_e(z,t)[N_t(z,\varepsilon) - n_t(z,\varepsilon,t)] - \alpha_{te}N_e exp\left[-\frac{\varepsilon}{k_bT}\right]n_t(z,\varepsilon,t)$$

{1D trapping continuity equation for electrons}. (4.3.4)

This set of equations describes the trapping and transport of charge throughout the bulk of the sample. Using the physical picture developed in Section 4.2, we can make a few assumptions that will allow us to quickly develop a simple model. First, assume that the majority of injected charge stays near the interface due to trapping, and second that the charge moves very slowly into the material with time. These two assumptions are shown to be reasonable by analyzing PEA measurements of HDIM under constant poling fields (Auge *et al.*, 2000; Montanari *et al.*, 2001; Tzimas *et al*., 2010). The essential effect of these assumptions is to remove the spatial dependence. This is not true; the charge does move and will spread through the sample given enough time. The approximations of the problem work because the spreading of trapped charge through the material is considerably slower than the decay of the current density to a semi-equilibrium value (Note, both the injection current density at the surface of the material and at the rear collecting electrode decay in a similar way.). This model assumes that there is no diffusion, because the majority of the carriers are in trapped states. The trapped charges are spatially fixed near the interfaces until their release, due to thermal processes; the trapped charge distribution represents the majority of the charge in the material. The observed current density is largely due to the free charge in the CB; there is no specific displacement current considered. This free charge must come from either direct

injection (from the contacting electrode) or is excited into the CB from the trapped charge distribution by thermal processes described by Eq. (4.3.3). Having made these assumptions, the transport equations are reduced to the following form,

$$J_{tot}(t) = q_e n_e(t) \mu_e F(t) + \epsilon_0 \epsilon_r \frac{\partial F(t)}{\partial t} + J_p(t)$$

{Sum of electron drift, displacement, and polarization current densities}, (4.3.5)

$$\frac{\partial n_{tot}(t)}{\partial t} = \alpha_{et}\, n_e(t)[N_t - n_t(t)] + G(t)_{ex}$$

{1D Continuity equation with drift, diffusion and source terms}, (4.3.6)

and

$$\frac{dn_t(\varepsilon,t)}{dt} = \alpha_{et} n_e(t)[N_t(\varepsilon) - n_t(\varepsilon,t)] - \alpha_{te} N_e exp\left[-\frac{\varepsilon}{k_b T}\right] n_t(\varepsilon,t)$$

{1D trapping continuity equation for electrons}. (4.3.7)

Equations (4.3.5) through (4.37) form the basis for the CVC charging model. Only one of the three equations includes an injection term, Eq. (4.3.6). Our goal is to show that this is the injection function considered by Walden and to arrange Eqs. (4.3.5) through (4.3.7) to give an expression for the measured current density.

By recalling that $n_{tot} = n_e + n_t$, integrating Eq. (4.3.7) over all possible energies where a distribution of trapped electrons, $n_t(\varepsilon, t)$, is assumed, and using the result to rearrange Eq. (4.3.6), we obtain

$$\frac{\partial n_e(t)}{\partial t} - \alpha_{te} N_e \int exp\left[-\frac{\varepsilon}{kT}\right] n_t(\varepsilon,t) d\varepsilon = G(t)_{ex}. \quad (4.3.8)$$

Equation (4.3.8) has been written in a suggestive form. It implies that the change in the number of electrons in the CB, $\dot{n}_e(t)$ (which is responsible for the resulting current density) is a function of the injected electrons governed by G_{ex} and thermal excitation of carriers from trapped states (first term on RHS). The dimensions of G_{ex} are number of electrons per unit volume per unit time. It is very important to realize that N_{ex} is not a constant, but must be a function of the electric field, temperature, and time, resulting from the buildup of trapped charge as described in our physical picture, given by $G_{ex}[F_s(t), T, t]$ (see Section 4.2); the temperature dependence is implied by the form of Eq. (4.3.8). Further, these electrons are injected from an external source and are *not* due to RIC. This injection function must contain all the information

about the change in the field due to the building trapped electron distribution and active metal-insulator interface effects, such as Fowler-Nordheim behavior, which is exactly what we would expect for an HDIM. For early times, electrons are injected into the material with relative ease, and the second term on the LHS of Eq. (4.3.8) is nearly zero. As the number of trapped electrons builds up, $G_{ex}[F_s(t)]$ is reduced due to the electric field resulting from the trapped electrons, $n_t(\varepsilon, t)$. Once thermal equilibrium is established (thermalization is completed and the trapped electrons distribution is in thermal equilibrium with the CB; see Section 3.1.8), the total number of injected carriers reaches an equilibrium value or saturation current density.

The electric field, due to trapped charges, is never large enough to completely stop the injection of new electrons, but it will settle at a steady state value. If all the charge was perfectly trapped, the equilibrium electric field, due to the trapped charge, would equal the applied field causing injection. In such a case, one would have a condition where charges could only be injected after some were released from trapped states and Eq. (4.3.8) would be

$$\alpha_{te} N_e \int exp\left[-\frac{\varepsilon}{k_b T}\right] n_t(\varepsilon, t) d\varepsilon = -G_{ex}(t). \tag{4.3.9}$$

While Eq. (4.3.9) is unphysical (since the field created by the trapped charge distribution cannot stop carrier injection into the CB band), it does makes it clear that the injection current must depend on the trapped charge distribution; it cannot be a constant in an HDIM.

We can derive an expression for the number of electrons in the CB by integrating Eq. (4.3.8) to determine the number of electrons excited per unit volume as a function of time,

$$n_e(t) = \alpha_{te} N_e \int exp\left[-\frac{\varepsilon}{kT}\right] \left(\int_0^t n_t(\varepsilon, t) dt\right) d\varepsilon + N_{ex}(t), \tag{4.3.10}$$

The dimensions of $n_e(t)$ are number of carriers per unit volume, where we use the definition

$$N_{ex}(t) \equiv \int_0^t G_{ex}(\acute{t}) d\acute{t}. \tag{4.3.11}$$

Equation (4.3.10) makes a clear connection between the trapped electron distribution, $n_t(\varepsilon, t)$, and injection of electrons, $N_{ex}(t)$.

The use of Eq. (4.3.10) is problematic, due to its dependence on the trapped electron distribution, i.e., the trapped charge distribution depends on the injection rate and the injection rate depends on the trapped charge distribution. Thus, another approximation must be made that will allow us to see how to—at

least in part—separate this relationship. During early times in the charging of the HDIM, the number of trapped electrons is on the order of or smaller than the number of injected electrons. It follows that the number of excited electrons from the trapped distribution to the CB is smaller than the number of conduction electrons. For early times before thermalization completes (see Section 3.1.8), the excitation of carriers from the trapped states is nearly zero. Even for long times—where the charge distribution is near equilibrium—the additional carriers due to thermal excitation from the trapped distribution must be much less than the CB density; we therefore drop the first term on the RHS of Eq. (4.3.10) to obtain

$$n_e(t) \cong N_{ex}(t). \tag{4.3.12}$$

Equation (4.3.12) is physically justified and highlights the relationship—in a rather obvious way—between the electron injection density and the CB electron density. Remember that the injection term is a function of the trapped charge distribution, from Eq. (4.3.9).

In an HDIM, it is the effects of trap filling that have the largest impact on the observed current density decay. Thus, an expression for the number of trapped electrons per unit volume per unit time is needed; Eq. (4.3.7) describes this process. Integrating Eq. (4.3.7) over energy, an expression for the total number of trapped electrons per unit volume per unit time is

$$\frac{dn_t(t)}{dt} = \alpha_{et} n_e(t)[N_t - n_t(t)] - \alpha_{te} N_e \int exp\left[-\frac{\varepsilon}{k_b T}\right] n_t(\varepsilon, t) d\varepsilon. \tag{4.3.13}$$

Note, that $\alpha_{et} n_e(t)$ is, by definition, the ability of the material to capture the available electrons entering the CB; i.e., $\alpha_{et} n_e(t)$ is proportional to the charging current density at the metal-insulator interface, $J_s(t)$. From Section 2.5 we know that the dimensions of $\alpha_{et} = s_c v_T$ are volume per unit time and the dimensions of $n_e(t)$ are number of electrons per unit volume so that the product of the interaction coefficient and the number of electrons in the CB has dimensions of inverse time; this is the number of electrons captured per unit time or simply the trapping frequency, v_{et}. Note that this trapping frequency appears to be a function of time, but that this only occurs because the number of injected electrons is a function of time; i.e., the relationship between the bulk trapping frequency and the time dependence of the number of electrons in the CB has been coupled. If thermal excitation of carriers from the trapped states is neglected, we can use Eq. (4.3.12) to see the equivalence, $\alpha_{et} n_e(t) \cong \alpha_{et} \acute{N}_{ex}(t)$, and $\alpha_{et} n_e(t)$ is easily shown to be $s_c J_s(t)/q_e$. The solution to the coupling problem is now evident; we need an expression for $J_s(t)$, from which the bulk

trapping frequency, v_{et}, can be obtained. Applying the condition that the release rate of trapped charges given by the last term on the RHS of Eq. (4.3.13) is negligible, Eq. (4.3.13) becomes

$$\frac{dn_t(t)}{dt} = \frac{s_c J_s(t)}{q_e}(N_t - n_t(t)). \tag{4.3.14}$$

Equation (4.3.14) is a fundamental result of this chapter and has been used by many authors to describe material charging due to injection of charge carriers. Equation (4.3.14), when solved, describes the time-dependent trapped charge distribution using a variety of charge injection schemes including: multiple applications (Sessler, 1987), contact injection (Kao, 2004), contact injection and breakdown (Liufu *et al.*, 1998), secondary electron emission (Cornet *et al.*, 2008), and corona charging and material breakdown (Nissan-Cohen, 1986; Fitting, 2010). We will use Eq. (4.3.14) in Chapter 5 to describe secondary electron emission charging and the resulting surface potential created by trapped charge.

The solution of the differential equation Eq. (4.3.14) is common and can be found in nearly any text on differential equations (Spiegel, 1971). We solve Eq. (4.3.14) for the time-dependent number of trapped electrons using the form $y(x) + py(x) - q(x)y^n(x) = 0$ with $n = 0$,

$$n_t(t) = N_t exp\left[\frac{-s_c\int_0^t J_s(\acute{t})d\acute{t}}{q_e}\right]\int_0^t exp\left[\frac{-s_c\int_0^{\acute{t}} J_s(\bar{t})d\acute{t}}{q_e}\right]\frac{s_c}{q_e}J_s(\acute{t})d\acute{t}. \tag{4.3.15}$$

The current density in Eq. (4.3.15) has dimensions of charge per unit area per unit time, the ratio of the capture cross section, s_c, to charge, q_e, has dimensions of area per unit charge, their product has dimensions of inverse time, and the integral has dimensions of inverse volume. Equation (4.3.15) can be used to calculate the number of trapped electrons for any injection function, $J_s(t)$, such that the incoming electrons are strongly trapped. If—as in a semiconductor—the electrons are only weakly trapped, then the last term on the RHS of Eq. (4.3.13) must be included; inclusion of this term results in a differential equation that cannot be solved in closed form. Equation (4.3.15) can also be used to numerically calculate the number of trapped electrons when the surface injection current density is known; i.e., we can use experimental data to determine the value of $n_t(t)$. Since the injection term clearly drives the number of electrons in trapped states, it affects the measured current density at the rear electrode. Thus, a model for the injection current density, $J_s(t)$, in Eq. (4.3.15) and its physical basis is required. This is the subject of Section 4.4.

4.4. Charge Injection

The injection problem discussed in Section 4.2 has been addressed by many investigators (Wilcox, 1971; Walden, 1971; Wintle, 1974a; Kao, 1976, 2004; Toomer and Lewis, 1980; Liufu *et al.*, 1998). The work of Wilcox (1971) and Walden (1971) provide excellent descriptions of the problems involved. A very comprehensive, physically insightful, and easily applied theory was developed by Walden (1971) and later modified by Wintle (1974b). This semi-phenomenological theory characterizes the injection current density, $J_s(t)$, at the metal-insulator interface as a function of time. Walden shows that the behavior of $J_s(t)$ depends on the type of injection mechanism at work [e.g., Fowler-Nordheim, Schottky injection, space charge limited injection (Fothergill, 1998), various tunneling mechanisms (Wintle, 1974a), and electron beam injection (Hodges, 2013)], in addition to the trapped charge distribution. The model we use in this dissertation is based on Walden's model as modified by Wintle, (1974b) who provided a simple (nearly universal) form of the injection current density. In what follows, we give a brief outline of the derivation for the injection current density function.

Consider the electric field, $F_s(t)$, at the surface of the HDIM must change as the trapped charge distribution builds up. Remember we are assuming that only electrons are injected into the material through the metal-insulator interface to a uniform depth, R; this is quite different from a simple capacitor model where we assume positive charges are at one side where the potential is high (from which the electric field extends) and negative charges at the other side (where the field lines terminate) where the potential is low. While this simple capacitor model is still useful, we now have an injected electron distribution at or near the interface of the material. Consider Fig. 4.2 in which the applied field, F_0, the surface field, $F_s(t)$, the field due to trapped charge, and the superposition of internal fields, $F(t)$, are shown. Note, that $F(t)$ is different from the surface field, but the spatial dependence has been omitted for simplicity. At time, $t = 0$, $F_s(t)$ must be equal to the applied field, F_0, but as time goes on $F_s(t)$ must be reduced by the electric field due to the trapped charge distribution, $F_t(t)$. In a general way, we can write the following equation for the electric field at the surface

$$F_s(t) = F_0 - F_t(t). \tag{4.4.1}$$

Since, in practice, we know the applied field, only $F_t(t)$ is required to estimate this relation. From Gauss's law, Eq. (4.3.2), we can write

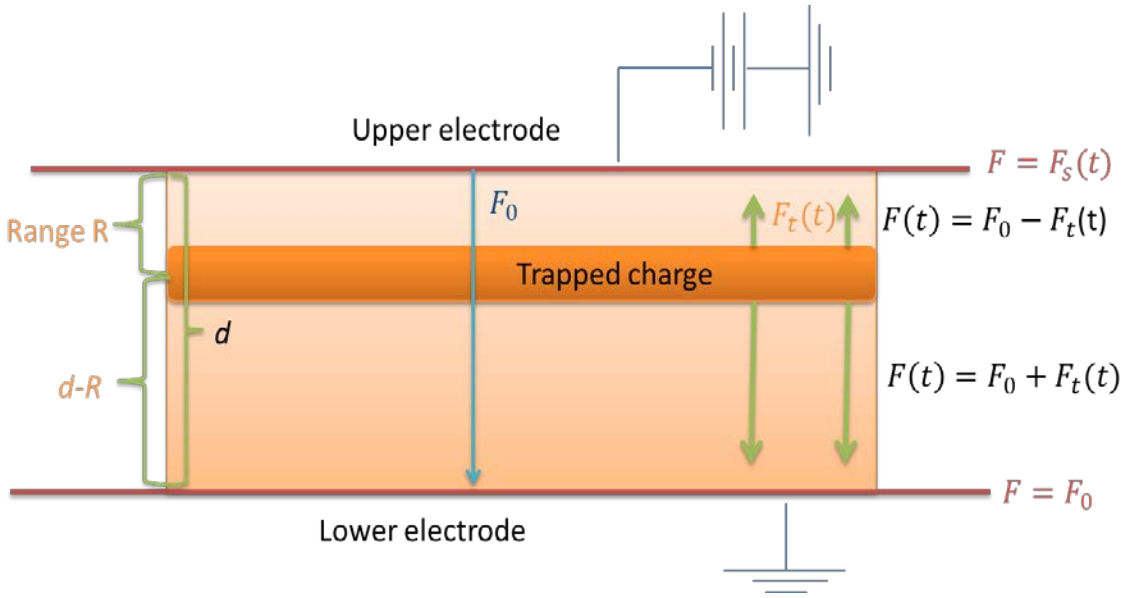

FIG 4.2. Basic electronic and field configuration of the CVC measurement system. All of the electric fields in the system are shown, except the polarization field: applied field, F_0, field due the trapped charge distribution, $F_t(t)$; surface field, $F_s(t) = F_0 - F_t(t)$, field at the ground plane, F_0; and the superposition of fields at intermediate points, $F(t)$. The battery and ground are shown for reference. The range, R, that the electrons penetrate into the sample, the distance between the trapped charge distribution and the rear, electrode, $d - R$, and the sample depth, d, are also shown.

$$\frac{\partial}{\partial z}F_t(z,t) = q_e n_t(z,t)/\epsilon_0\epsilon_r. \tag{4.4.2}$$

If we assume that the uniform areal charge distribution at depth R is the product of a time-dependent function and a time-independent 1D spatial function, which is uniform from $z = 0$ (the collecting electrode at ground) to $z = (d - R)$, then the spatial dependence of the trapped charge distribution can be approximated by a step function, $n_t(z,t) = n_t(t)\theta\big(z - (d - R)\big)$. Note, that PEA measurements reveal that the spatial dependence in the z direction of the charge distribution is Gaussian or exponential; extension of our uniform charge distribution approximation is left for future work. Under these conditions, we can integrate Eq. (4.4.2) with respect to z from $z = 0$ to $z = d - R$ to obtain an expression for the field due to the trapped charge distribution

$$F_t(t) = q_e n_t(t)(d - R)/\epsilon_0\epsilon_r. \tag{4.4.3}$$

Using Eqs. (4.4.1) and (4.4.3), a new equation for the electric field at the surface of the sample can be obtained

$$F_s(t) = F_0 - q_e n_t(t)(d - R)/\epsilon_0\epsilon_r. \tag{4.4.4}$$

Equation (4.4.4) gives us both the electric field at the surface of the sample and the potential at the surface of the sample, since $F(t) = -\nabla \cdot V(t)$. Eq. (4.4.4) suggests that if all the charge were exactly on the surface of the sample (e.g., *R = 0)* then there would be a trapped charge field. This result is consistent with a DOS at (or near) the surface of the material acting to trap charge and create a counter field, $F_t(t)$; it is also consistent with the requirement that all the trapping occurs at or near the surface of the material (a result consistent with PEA measurements). Note also, that when $R \geq d$ for penetrating radiation, the field goes to F_0, suggesting that the charge distribution is outside of the material; this is the expected result. The field between the trapped charge distribution and the rear electrode is the applied field plus the field due to the trapped charge distribution and is the field that drives the current measured at the rear electrode.

Equation (4.4.4) gives a first-order approximation for the electric field at the surface of the material, which must be directly tied to the currents flowing in the sample. For the CVC model, we seek an expression for the current density measured at the rear electrode. Walden addresses the problem of finding an expression for the surface potential based on the injection behavior of charge at the surface and subsequent trapping of that charge. We will use the theory of Walden and Wintle to develop an expression for the injection current density using Eq. (4.4.4). We outline the derivation of Walden below.

Essentially, we need a relationship between the injection profile caused by the application of an electric field and the effects caused by the electronic nature of the metal-insulator interface combined with the electric field generated by the trapped charge given by Eq. (4.4.4). First, consider how the electric field changes at the surface of the material,

$$\frac{dF_S(t)}{dt} = -\frac{q_e(d-R)}{\epsilon_0 \epsilon_r}\left(\frac{d}{dt} n_t(t)\right). \tag{4.4.5}$$

The total charge that will pass through the surface to the rear electrode must be $q_e dn(t)/dt$, where $n(t)$ is the total number of electrons that passes through the surface as a function of time. Recall that $n(t)$ is the volume density of electrons and that the current density is defined as charge per unit area per unit time; with this in mind, we can write the current density that passes through the surface of the insulator as $J_s(t) = -q_e d \frac{dn(t)}{dt}$; d is the depth of the sample as the current passing through the surface must be the current that will eventually traverse the sample. Equation (4.4.5) does not explicitly contain the total current, but it is quite clear that some fraction of the total current must be trapped in the insulator.

Consider the action of the chain rule on Eq. (4.4.5) i.e., $\frac{dn(t)}{dt} \rightarrow \left\{\frac{dn(t)\cdot dn_t(t)}{dn_t(t)\cdot dt}\right\}$; using Eq. (4.4.5) and the relation for the current density at the interface, the change in the trapped charge distribution, Eq. (4.4.5) becomes

$$\frac{dF_s(t)}{dt} = -\frac{q_e d_1}{d\epsilon_0\epsilon_r} J_s(t) \frac{dn_t(t)}{dn(t)}. \tag{4.4.6}$$

An expression for the change in the trapped charge distribution to the total charge, $\frac{dn_t(t)}{dn(t)}$, is needed. This is a very useful relation in and of itself. For example, in their secondary electron emission chamber, the USU MPG can measure the total charge, surface injection current density, and the resulting surface potential to determine the behavior of the injection current and ratio of trapped to total charge; an extended discussion of the relationship between Eq. (4.4.6), surface potential, and secondary electron emission will be given in Chapter 5.

Walden makes an experimentally based phenomenological assumption to extend Eq. (4.4.6); the form of the ratio of total electrons to trapped electrons is assumed to be a power law of the injection current density, $J_s(t)$, to the initial current density, J_0, of the uncharged sample. Using this assumption, one gets

$$\frac{dn_t(t)}{dn(t)} = \left(\frac{J_s(t)}{J_0}\right)^{n-1}. \tag{4.4.7}$$

Equation (4.4.7) is a simple power law relationship in which total trapping is given when $n = 1$ and partial trapping for $n > 1$; increasing *n* implies stronger trapping. A detailed analysis of the physical roots of Eq. (4.4.7) and its validity have been given in Wintle (1974b). Using Eqs. (4.4.5) and (4.4.7) an expression that describes the relationship between the trapped-electron, distribution-dependent electric field, the injection current at the surface, and time is found to be

$$t = -\frac{\epsilon_0\epsilon_r d}{(d-R)J_0}\int_{F_s(0)}^{F_s(t)} \left(\frac{J_s(\acute{F}_s)}{J_0}\right)^{-n} d\acute{F}_s. \tag{4.4.8}$$

Equation (4.4.8) is Walden's central result; it allows the time dependence of any surface field-dependent function to be found. Walden explores four major types of injection: (*i*) Pooler-Frenkle, (*ii*)Fowler-Nordheim, (*iii*) pure exponential, and (*iv*) power law. Wintle (1974a) has explored these injection types and found essentially that all yield a similar form for $J_s(t)$. As an example, the simplest derivation for the current density at the surface is found by using the power law form of $J_s(\acute{F}_s)/J_0 = (F_s(t)/F_0)^p$ with *p* as

constant greater than one. Using this power law form and Eq. (4.4.8), the following form for the injection current density is easily found to be

$$J_s(t) = J_0(1 + t/\tau_{onset})^{-\frac{p}{np-1}}. \quad (4.4.9)$$

Remember that this is the surface current density, not the measured current density at the rear electrode. The product of $np \geq 1$ is always greater than or equal to one since—by definition—both are independently greater than or equal to one. The variable, τ_{onset}, is a characteristic onset time for the injection current density, not to be confused with a decay time or $\tau_{transit}$. In practice, the onset time describes the time at which the current density at the metal-HDIM interface will begin to diminish due to trapping processes and field effects. A note to the reader: Eq. (4.4.8) does follow directly from Walden's work, though Eq. (4.4.8) has a different form in Walden's paper. However, Wintle (1974b) makes this relationship very clear, and the interested reader should explore both papers to understand how Eq. (4.4.8) came about and how it should be used; i.e., use Eq. (4.4.8) with caution.

Wintle (1974a) generalizes the resulting injection current density at the interface, providing a simple model, which can be used to overcome the coupling between bulk trapping and the resulting injection current density without a detailed consideration of the metal insulator interface effects. It turns out, for most injection phenomena—when moderate to strong trapping is considered—the injection current density can be well characterized by

$$J_s(t) = J_0(1 + t/\tau_{onset})^{-m} + J_{sat}. \quad (4.4.10)$$

Here, J_0 is the initial injection current density at time $t = 0$, J_{sat} is the equilibrium injection current density as some time, $t >> \tau_{onset}$, and m is a generalized power that is dependent on the strength of the trapping of injected electrons [see Eq. (4.4.7)] and the strength of the field-dependent injection rate [see Eq. (4.4.8)]; for HDIM, J_{sat} will not be observed until the equilibrium current is measured. Since the saturation current, J_{sat}, is so small in HDIM, it is omitted from Eq. (4.4.5) and included again in the total current density equation (see Section 4.6). Equation (4.4.5) is a fundamental result and is used in the derivation of the USU MPG CVC and SVP charging models as the primary electron injection term (see Chapter 5).

The interested reader should consult Wintle (1974b), Wilcox (1971), and Walden (1971) for a complete development of all the ideas discussed in this section; there is a great deal to be learned from

these papers. In this dissertation, we will use the form given by Eq. (4.4.10) as the surface current density injection term. CAUTION: *This result must be worked out in more detail for each type of metal-insulator interface, applied field, temperature dependence, and type of injection mechanism*. It is critical that a study of Eq. (4.4.7) be undertaken, in addition to application of the theory presented in Chapter 2 on SCLC, to develop a complete picture of the injection current density dependence on the applied field, electric field due to the trapped charge distribution, and time. With that said, Eq. (4.4.10) has been applied successfully in a number of experimental trials (Walden, 1971; Wilcox, 1971; Wintle, 1974b; Liufu *et al.*, 1998; Kao, 2004); note, however, that Kao uses a physically unjustified form of the equation. Using Eq. (4.4.10), a model for the number of trapped charges as a function of time will be derived in Section 4.6. All that remains is the development of the finial charging model—based on Eq. (4.3.15)—which describes the long-term time dependence of the charge transport in HIDM for CVC type experiments. Before approaching the solution for the observed current density at the collecting electron, the short-term time dependence due to polarization at the interface will be discussed in order that a complete picture of the charging in the CVC system can be presented in Section 4.6.

4.5. Polarization

In spacecraft systems sudden changes in the local potential can occur, leading to significant changes in the charge stored within or on the surface of an HDIM. Such a short timescale change in the charge configuration or local electric field can lead to breakdown as the time to relax the excess field or change in charge concentration is greater than the breakdown time of the material. In order to determine how spacecraft materials will respond to such short timescale behavior, the subject of polarization must be discussed. The nature of polarization in HDIMs yields information about critical breakdown phenomena, energies of dissociation for molecular segments, and short timescale material response (Crine, 2007). It is prudent to include a short-term polarization component in the CVC charging model. Polarization, as a subject, has been covered in great detail in the literature, and we will not present an extensive discussion of the subject here. For an excellent review of different types of polarization in HDIM: for multiple types see Sessler (1987), Kao (1976, 2004), for simple types see Blyth and Bloor (2005), and for ESD types see Crine *et al.* (1989a), Crine (2004a, 2004b, 2005b), and Dang *et al.* (1996).

Polarization in HDIM occurs often, and the effects of such behavior operate on very short time scales or are so weak as to be washed out by more dominant charge transport process (e.g., charge trapping or injection effects). It has been suggested that LDPE does not have a polarization component (Brunson, 2009). This is simply not true; indeed the relaxation map of LDPE has been developed in great detail by Frubing *et al*. (2001) and Crine (2007) and references therein. In many applications (where the HDIM is in contact with a metal or even a semiconductor), particulates will diffuse into the material (Crine, 2007) leading to an enhanced polarization component in the observed current density.

There are a number of types of polarization that can occur (Kao, 2004). However, in HDIM only three types are generally attributed to observed effects: dipolar, space charge, and hopping polarization (Kao, 2004). While the hopping dynamics are important to an understanding of transport, in general the effect is quite small and we, therefore, focus on space charge and dipolar polarization. The space charge we refer to here is interfacial and occurs at the metal-insulator interface (Zhang *et al.*, 2002). A buildup of interfacial space charge can occur for many reasons, but is most often attributed to surface trapping or SCLC. This body of charge can polarize and has a characteristic decay time associated with that polarization. The dipolar response of an HDIM is typically quite small, as HDIM are usually nonpolar materials (Kao, 2004); if charged ions or molecular segments from the contact diffuse into the HDIM the dipolar response will be enhanced (Frubing *et al.*, 2001; Crine, 2004b). In addition, if the temperature of the sample is near the glass transition, a type of molecular polarization can occur, which may be significant (Crine, 2007). The study of the relaxation peak near the glass transition (Crine, 2007) yields information needed to understand the change in energy required to reorganize the material and understand the polarization characteristics. Since both the dipolar and hopping polarization terms typically do not make a significant contribution to the polarization current, we consider only excess charge due to SCLC at the interface as a source. A detailed description of the connection between HDIM and space charge polarization can be found in Kao (2004) and Sessler (1987). In this dissertation, a very simple model for the polarization response is presented, but a more detailed analysis is left for future work.

In this dissertation, we assume a form for the polarization conductivity decay originally developed for the USU MPG (Dennison and Brunson, 2008),

$$J_p(t) = \left(\frac{(\epsilon_r^{\infty}-\epsilon_r^{0})\epsilon_0}{\tau_p} exp\left[-t/\tau_p\right]\right) F_s, \tag{4.5.1}$$

where ϵ_r^{∞} is the asymptotic dielectric constant after extended application of the electric field (generally the atomic or electronic contributions), ϵ_r^{0} is the initial dielectric constant just as the field is applied, F_s is the electric field at the surface, τ_p is the polarization decay time, and $\left((\epsilon_r^{\infty} - \epsilon_r^{0})\epsilon_0/\tau_p\right)\ exp\left[-t/\tau_p\right]$ is change in the time-dependent polarizibility (Dennison and Brunson, 2008a; Hodges, 2013). This is a common expression for the decay of a signal due to polarization. In the original work by Dennison, the expression is derived for free and bound charges at the interface. By combining the work of Kao (2004) with that of Dennison (2008c) and experimentally measuring the relaxation map [A relaxation map is created by experimentally testing HDIM materials' response time as a function of applied field onset time] or—for AC systems—frequency [see Frubing *et al*. (2001)] of the HDIM of interest, a very accurate picture of the short timescale response of the HDIM can be made; this, however, must too, be left to future work. Eq. (4.5.1) is a simple approach that offers a good approximation to short timescale behavior, but additional physical insight is needed to extract useful material parameters beyond the decay time.

In order to create a complete model of the injection current for all timescales, we must include the polarization term in the current density. In this construction, we ignore the time dependence of the electric field at the surface, F_s, as the time scales are so short, i.e., $F_s \rightarrow F_0$. The polarization current density is

$$J_p(t) = F_0\epsilon_0 \left(\frac{\epsilon_r^{\infty}-\epsilon_r^{0}}{\tau_p}\right) exp\left[-t/\tau_p\right]. \tag{4.5.2}$$

Equation (4.5.2) can be written in a simple form as

$$J_p{}^{\downarrow}(t) = J_{p0} exp\left[-t/\tau_p\right]. \tag{4.5.3}$$

Here, the down arrow implies that we are talking about the decay of a polarized sample. For charge up, a similar expression can be written as

$$J_p{}^{\uparrow}(t) = J_{p0}\left(1 - exp\left[-t/\tau_p\right]\right). \tag{4.5.4}$$

In most cases, it is expected that the sample will charge up under the application of a step voltage from zero current density to a maximum value, J_{p0}, (Dennison and Brunson, 2008). In the case of a space charge polarization, the charge must relax after the application of the step voltage.

Thus, we propose that the total polarization observed should be the product of some charge up and subsequent decay. The following phenomenological expression is used without proof [refer to Hodges (2013) for a discussion of this] to describe the expected polarization current,

$$J_p(t) = J_{p0}\left(1 - exp\left[-t/\tau_p\right]\right) exp\left[-t/\tau_p\right]. \quad (4.5.5)$$

At time, $t = 0$, Eq. (4.5.5) will be zero and for very long times, it will again be zero; the maximum is given by $J_{.p0}\tau_p ln(1/2)$. This vanishing behavior is a useful property, since the long-term decay of the measured current density must be controlled by the trapping dynamics in the HDIM, not the polarization, which is a very short term effect. USU MPG data taken on LDPE in the CVC system for polarization suggests that the polarization decay time is on the order of 0.5 s or less and that nearly all polarization current density is gone after a few seconds; this is consistent with space charge polarization decay times (and, unfortunately, the experimental response time) (Brunson and Dennison, 2008). The application of Eq. (4.5.5) must be done carefully, as it would be quite easy to end up characterizing the response time of the equipment and not the material. For this reason, it is strongly recommended that polarization studies be done in addition to the CVC type experiment to obtain good measurements on the real polarization response of the material. For additional formulations of this expression and others, connection to the capacitance, and resistivity, and an expression for the decay time see Brunson and Dennison (2005, 2008), Kao (2004), and Sessler (1987). Note, Kao (2004) gives a more accurate estimation for the decay time due to interfacial polarization (space charge).

The sum of current densities gives a total observed current density at the rear electrode, which can be written as

$$J(t) = J_p\,(t) + J_{Leak}(t). \quad (4.5.6)$$

The leakage current, $J_{Leak}(t)$, is the current due to charge transport in the HDIM. Thus, in order to finish out model of the observed current density in HDIM, we must complete our derivation of the charging model.

4.6. Charging Model

In order to derive an expression for the charge transport in an HDIM, we must first derive an expression for the time-dependent trap filling (in terms of the charge injection model of Section 4.4),

extend that model to the observed current density, and then include the result in Eq. (4.5.2), which gives the sum of currents. We begin with Eq. (4.3.15), which gives the number of trapped electrons as a function of time and the charge injection function, $J_s(t)$. Equation (4.3.15) was left in a general form in Section 4.3, so that we could develop an expression for the charge injection function; it is represented here for reference

$$n_t(t) = N_t exp\left[\frac{-s_c\int_0^t J_s(\acute{t})d\acute{t}}{q_e}\right]\int_0^t exp\left[\frac{-s_c\int_0^{\acute{t}} J_s(\tilde{t})d\tilde{t}}{q_e}\right]\frac{s_c}{q_e}J_s(\acute{t})d\acute{t}. \tag{4.6.1}$$

By inserting Eq. (4.4.5) in Eq. (4.6.1) and completing the integration, an expression for the time-dependent density of trapped electrons is found

$$n_t(t) = N_t\left(1 - exp\left[\frac{s_c J_0 \tau_{onset}}{q_e(1-m)}\left(1 - \left[1 + \frac{t}{\tau_{onset}}\right]^{1-m}\right)\right]\right). \tag{4.6.2}$$

Equation (4.6.2) has the expected behavior for the density of trapped electrons as a function of time, $\tau_{m=0} = (s_c J_0/q_e)^{-1}$. At t = 0, Eq. (4.6.2) is zero and at $t \sim \infty$, it approaches N_t. The power is constrained such that $0 \leq m \leq 1$. A simple exponential is obtained when $m = 0$, consistent with case where the trap filling and release are on the same order; thus, the equilibrium injection rate is reached in a short time. For the case where $m \sim 1$, the time to decay to equilibrium is nearly infinite; this is consistent with a long thermalization time of the charge distribution common in most HDIM (see Chapter 3). Once the trapped charge distribution—given by Eq. (4.6.2)—is known, a number of calculations can be completed: time-dependent surface potential, time-dependent electric field in all parts of the sample, and conduction electron density. In Chapter 5, the dependence of the surface potential due to the trapped charge distribution will be explored. We are interested in the observed current at the rear electrode, which will require further use of the transport equations.

Given Eq. (4.6.2) and the transport equations from Section 4.3, a simple model that describes the bulk transport of the injected electron distribution can be developed. Consider the simplified version of Eq. (4.3.5),

$$J_{tot}(t) = J_d(t) + J_p(t) + J_c(t), \tag{4.6.3}$$

which is the sum of current densities introduced in the beginning of this chapter. Here the total current is the sum of the displacement, polarization, and conduction currents (or just drift current). The conduction current density is negligible (when compared to the effects of the change in the trapped charge distribution)

until equilibrium is established. Once the trapped states reach an equilibrium value and the current becomes nearly constant, one is observing the conduction current density; this is equivalent to saying that the DOS is saturated and is therefore called the saturation current, J_{sat}. The polarization current (discussed in Section 4.5) is negligible after a few hundred seconds (or less) for most HDIM. The majority of the time dependence in the observed current is due to the buildup of the trapped charge distribution. The change in the trapped charge distribution is directly related to the change in the electric field due to the trapped charge distribution; it is, therefore, a displacement current. Using Eq. (4.3.5), the displacement current is found to be

$$J_d(t) = -\epsilon_0 \epsilon_r \frac{\partial F_s(t)}{\partial t}. \tag{4.6.4}$$

Using Eqs. (4.4.3) and (4.6.4), an expression for the displacement current can be found

$$J_d(t) = -q_e \frac{\partial n_t(t)}{\partial t}(d - R). \tag{4.6.5}$$

Here it has been assumed that the applied field has no time dependence once turned on. Using Eq. (4.6.2), an expression for the change in the trapped charge distribution can be found as

$$\frac{\partial n_t(t)}{\partial t} = -\frac{s_c J_0 N_t}{q_e}(1 + t/\tau_{onset})^{-m} exp\left[\frac{s_c J_0 \tau}{q_e(1-m)}\left(1 - \left(1 + \frac{t}{\tau_{onset}}\right)^{1-m}\right)\right]. \tag{4.6.6}$$

Equation (4.6.6) has the correct dimensions of inverse volume. Equations (4.6.6) and (4.6.5) give an expression for the displacement current due to the trapped charge distribution

$$J_d(t) = J_0 N_t s_c (d - R)(1 + t/\tau_{onset})^{-m} exp\left[\frac{s_c J_0 \tau_{onset}}{q_e(1-m)}\left(1 - \left(1 + \frac{t}{\tau_{onset}}\right)^{1-m}\right)\right]. \tag{4.6.7}$$

Here the product of the total DOS, capture cross section, and charge depth, $s_c(d - R)N_t$, is unitless so that the dimensions of Eq. (4.6.7) are just current per unit area. Equation (4.6.7) describes only the displacement current due to the changing trapped charge distribution. Using Eq. (4.5.5) for the polarization from Section 4.5 and Eq. (4.6.3)—for the sum of current densities—we can write down our result for the USU MPG charging model

$$J_{tot}(t) = J_0 s_c N_t d\left(1 - \frac{R}{d}\right)\left(1 + \frac{t}{\tau}\right)^{-m} exp\left[\frac{s_c J_0 \tau}{q_e(1-m)}\left(1 - \left(1 + \frac{t}{\tau}\right)^{1-m}\right)\right]$$
$$+ J_{p0}\left(1 - exp\left[-t/\tau_p\right]\right) exp\left[-t/\tau_p\right] + J_{sat} \quad \{\text{USU MPG CVC Charging Model}\}. \tag{4.6.8}$$

Equation (4.6.8) is the central result of Chapter 4. While this result may seem complex, it will be shown in Section 4.8 that this model fits data taken using the USU CVC system on LDPE very well. There are a couple of important points to make about Eq. (4.6.8). First, the LDPE data analyzed here do not contain any notable polarization component. Second, the current decay due to trapping processes is distinctly different in character and timescale from the polarization component. This model can usually be reduced to the following form without loss of generality by neglecting the time-dependent polarization:

$$J_{tot}(t) = J_0 s_c N_t d(1 - R/d)\left(1 + \frac{t}{\tau}\right)^{-m} exp\left[\frac{s_c J_0 \tau}{q_e(1-m)}\left(1 - \left(1 + \frac{t}{\tau}\right)^{1-m}\right)\right] + J_{sat}$$

{Reduced USU MPG CVC Charging Model}. (4.6.9)

Equation (4.6.9) has only five free parameters, as the initial injection current density and the saturation current density are generally measurable. The DOS is well known for some HDIM, can be studied by a multitude of methods, and is, therefore, bounded. The charge depth *R* has been established in PEA measurements and is, therefore, also bounded. Wilson and Dennison have presented a simple, single parameter expression for R over a wide energy range and types of materials (Wilson and Dennison, 2010). The onset time, τ_{onset}, is estimated in (Walden, 1971) for each of the injection mechanism mentioned in Section 4.4; it is a function of the initial electric field at the surface, F_0, trapping power, *m* [see Eq. (4.4.7)], dielectric constant, $\epsilon_0\epsilon_r$, and initial injection current, J_0. For the power law injection term Walden, 1971) estimates that the onset time is

$$\tau_{onset} = \frac{\epsilon_0 \epsilon_r F_0}{m J_0}. \quad (4.6.10)$$

The onset time is then only a function of two unknown parameters *m* and J_0. Using Walden's expression for the onset time will further reduce the number of parameters down to four. However, this reduction is at the cost of a complicated form of Eq. (4.6.9); Eq (4.6.9) is left in its current form as the inclusion of the onset time will complicate the form of the equation.

We can explore Eq. (4.6.8) to see if its behavior is consistent with predictions by Walden (1971). In particular, Walden derives both exponential and power law expressions, using a single power law-type injection term by changing the value of the *np* product, which controls the power, *m*. Notice that if $m = 0$, Eq. (4.6.8) becomes a pure exponential [refer to Eq. (4.6.11)] and if $m \sim 1$, Eq. (4.6.8) becomes a pure power law [refer to Eq. (4.6.12)]:

$$J_{tot}(t) = J_0 s_c N_t d(1 - R/d) exp\left[\frac{-s_c J_0 t}{q_e(1-m)}\right] + J_{sat}. \quad (4.6.11)$$

$$J_{tot}(t) = J_0 s_c N_t d(1 - R/d)\left(1 + \frac{t}{\tau}\right)^{-m} + J_{sat}. \quad (4.6.12)$$

The interested reader may be curious if there is a connection between the power, *m*, and other variables used in this dissertation such as $\alpha(T) = T/T_0$, found in equations that describe dispersive transport. The answer is yes, *m* is a complex function of the injection profile and the DOS [see (Wintle, 1974b)]; this information will not be covered in this dissertation and left to future work. Equation (4.6.11) is exactly the form of the measured current found by both Walden (1971) and Wintle (1974b), but Eq. (4.6.12) is new. The exponential behavior is a solution of the differential trapping equation, Eq. (4.3.14), when the surface injection current density is a constant, J_0. In CVC-type measurements—coupled with PEA testing —the range of electrons, *R*, is always found to be much less than the sample depth; this means the ratio of *R/d* is << 1 and can be ignored, further reducing the number of free parameters.

By using Walden's injection function and the trapping equations, it has been shown that all the expected behavior can be accounted for by using a physical description of the behavior of the injected charge in an HDIM. Further, the prediction of the measured current density is written in terms of fundamental material parameters and measurable values that can be cross checked with other experimental systems. In Section 4.8, Eq. (4.6.12) will be applied to data from the CVC chamber. We will revisit the charge injection function and the solution to the trapping equations in Chapter 5 and show that consistent results for the physical material parameters can be obtained.

4.7. Decay Model

Consider Fig. 4.1 (c) in which the trapped charge distribution is in equilibrium; this means *J(t)* has been on for a very long time. If *J(t)* is suddenly removed—i.e., the applied voltage is turned off—then the only electric field present will be due to the trapped charge. This trapped charge distribution and the resulting field can be measured at the surface of the HDIM (Liufu *et al.*, 1998; Hodges, 2013), but it also creates a field between the grounded rear electrode (at which we measure current) and the trapped charge distribution that creates a discharge force, (i.e., the charge will tend to move toward the grounded rear electrode (Sessler, 1987). Charge is released by thermal excitation from trapped states to the CB and the trapped charge released is, therefore, dependent on the temperature of the HDIM. Further, very high

internal fields tend to be present for even modest trapped charge distributions, leading to a lowering of the energy barrier heights of trapped states; i.e., it is easier for electrons to escape when higher internal fields are present (see Section 3.2). Initially, the internal field is high, but will decrease (as a function of the trapped charge magnitude) with time slowing the release of electrons from trapped states. Once an electron is released, it must still traverse the sample under the action of the internal electric field between the charge distribution and the rear electrode. The path the electron takes is through the uncharged HDIM to the ground plane. Remember most of the charge is near the metal-insulator interface; this means that there is a very high probability that an electron will be re-trapped and released many times at different spatial points along its journey through the sample. This creates a very difficult situation when we are attempting to estimate the measured current. However, the majority of the decay—in the measured current density—occurs because the trapped charge distribution is dispersing (i.e., we are largely going to measure a displacement current at the grounded rear electrode).

In this section, we deal with intermediate times much longer than the polarization decay time, but much less than the transit time. We assume that the observed current density is due entirely to decay of the trapped charge distribution; this assumption is supported by PEA measurements, which show that the trapped charge distribution remains almost entirely at one spatial location (with a narrow distribution) (Griseri *et al.*, 2005; Montanari *et al.*, 2005; Dissado *et al.*, 2006). Since we are assuming the conduction of the electron density is small across the sample, we can also neglect the re-trapping processes. This is likely not a realistic approximation, but will provide an estimate of the measured current density; as it turns out, this approximation allows a great deal of information to be obtained from real data (Dissado *et al.*, 2006).

Many authors have provided solutions to the transport equations under similar conditions (Treadgold, 1966; Arkhipov, 1993a; Liufu, 1998; Alagiriswamy and Narayan, 2002; Kao, 2004; Sessler *et al.*, 2004; Dissado *et al.*, 2006). In this section, we seek a simple solution to the transport equations that allows for a reasonable estimate of the measured current density, physical insight into the nature of the problem, and a solid theoretical basis upon which better models can be built. Dissado *et al.* provide the basis for a simple, but effective, model for the discharge of HDIM under CVC conditions (Dissado *et al.*, 2006). Dissado's model is the basis for the USU MPG CVC discharge model. We outline the derivation

as follows; the transport equations are used to develop a simple, but general, expression for the decay of the trapped charge distribution. The model for the trapped charge distribution is then used to estimate the electric field and the displacement current.

Consider the time, energy, and temperature-dependent number of trapped electrons given by Eq. (4.3.4). Since we are neglecting the re-trapping of electrons Eq. (4.3.4) becomes

$$\frac{dn_t(\varepsilon,t)}{dt} = -\alpha_{te} N_e exp\left[-\frac{\varepsilon}{k_b T}\right] n_t(\varepsilon,t). \tag{4.7.1}$$

Note that at time, $t = 0$, all the electrons in the HDIM are in trapped states and there is no external source of excitation. This means that the change in the CB electron concentration must be equal to the negative change in the trapped charge distribution

$$\frac{dn_{tot}(\varepsilon,t)}{dt} = \frac{\mathrm{d}n_e(\varepsilon,t)}{\mathrm{d}t} + \frac{\mathrm{d}n_t(\varepsilon,t)}{\mathrm{d}t} = 0 \qquad \{\text{Charge Conservation}\}, \tag{4.7.2}$$

or

$$\frac{-dn_t(\varepsilon,t)}{dt} = \frac{dn_e(\varepsilon,t)}{dt}. \tag{4.7.3}$$

Here the density of conduction electrons has been written as a function of energy only because it depends on the trapped charge distribution. Equation (4.7.1) can be solved for $n_t(t)$ using the same solution methods used to obtain our charging model (see Section 4.6); i.e., Eq. (4.7.1) is of the form $y(x) + py(x) - q(x)y^n(x) = 0$ with $n = 0$ and $q(x) = 0$. We obtain the following solution for Eq. (4.7.1):

$$n_t(\varepsilon,t) = \mathrm{N}_t(\varepsilon)\, exp\left[-\int_0^t \nu_{te} exp\left[-\frac{\varepsilon}{k_b T}\right] dt\right], \tag{4.7.4}$$

where $N_t(\varepsilon)$ is the energy-dependent DOS and we have used Eq. (2.5.12) to convert the constant $\nu_{te} = \alpha_{te} N_e$ (see Section 2.4.5). In general, the energy dependence of the thermal release of electrons from trapped states is a function of time, $\varepsilon = \varepsilon(t)$; i.e., the time release of charges from trapped states is a time-dependent process (see Section 3.1.3). Since Eq. (4.7.4) is written as a function of energy, it can be evaluated at any single energy assuming that the trapped electrons at different energy levels are not affected by each other. This is not true in general (see Section 3.1.8), but since many trapped charge distributions act as if they were at a single energy level or a very narrow range of energies, we can perform the time integration without taking into account the time dependence of the release rate. This yields

$$n_t(\varepsilon, t) = \mathrm{N}_t(\varepsilon)\, exp\left(-tv_{te} exp\left[-\frac{\varepsilon}{k_b T}\right]\right). \tag{4.7.5}$$

Equation (4.7.5) can be integrated over a range of energies (we can view them as a set of discreet energy levels that do not interact with one another) to obtain an expression for the time evolution of the trapped charge distribution

$$n_t(t) = \int_{\varepsilon_{min}}^{\varepsilon_{max}} \mathrm{N}_t(\varepsilon)\, exp\left(-tv_{te} exp\left[-\frac{\varepsilon}{k_b T}\right]\right) d\varepsilon\,. \tag{4.7.6}$$

In principle, Eq. (4.7.6) can be solved for any energy range and DOS function. The DOS types are given in Section (2.4.5). In this section, only a constant DOS will be used to obtain a solution; for solution of Eq. (4.7.6) using an exponential or delta function DOS see Monroe (1985); there is no closed form solution (that this author is aware of) for the Gaussian DOS. We bound range over which the constant DOS is allowed to have trapped electrons to a narrow region between the limits of integration given in Eq. (4.7.6). The exact solution of Eq. (4.7.6) is then

$$n_t(t) = -\frac{N_t k_b T}{\varepsilon_c}\left\{E_i\left(e^{-\frac{\varepsilon_{max}}{k_b T}} v_{te} t\right) - E_i\left(e^{-\frac{\varepsilon_{min}}{k_b T}} v_{te} t\right)\right\}. \tag{4.7.7}$$

In Eq. (4.7.7), $E_i(x)$ is the exponential integral (Spiegel, 1971).

Equation (4.7.7) describes the time-dependent decay of electrons from trapped states as a function of temperature. This expression is most useful when the minimum and maximum energies are not too far apart; said another way, this is when the number of trapped charges in the DOS is not so large as to incur corrections to Eq. (4.7.7) due to high internal electric fields. For the case where the internal electric field modifies the trap depth energies, a correction for the field must be added. In this chapter we do not discuss the solution of Eq. (4.7.7) with inclusion of the time-dependent electric field, as it requires additional theoretical development beyond the scope of this dissertation, namely a sophisticated numerical model. We do, however, show how to include the electric field dependence.

It is simple to develop the expression from which a numerical model for the temperature-, time-, and field-dependent density of trapped electrons can be built. From Section 2.5.4, we know that the energy barrier of a trapped state is modified by the electric field in the following way:

$$v_{te}[\varepsilon - (d - R)q_e F(t)] = v_{te} exp\{-(\varepsilon - (d - R)q_e F(t))/k_b T\}. \tag{4.7.8}$$

The electric field, *F(t)*, is between the charge distribution and the rear electrode and *d-R* is the distance between the center of the trapped electron distribution; for most cases, the trapped charge distribution is so close to the injecting electrode that *d-R~d*. Using Eqs. (4.7.7) and (4.7.8) with a constant DOS, we obtain an expression for the field-dependent number of trapped electrons

$$n_t(t) = -\int_{\varepsilon_{min}}^{\varepsilon_{max}} \frac{N_t}{\varepsilon_0^c} exp\left[-tv_{te}exp\left[-\left(\varepsilon - dq_eF(t)\right)/k_bT\right]\right] d\varepsilon. \tag{4.7.9}$$

Using Eq. (4.4.3) for the electric field and Eq. (4.7.9), an expression involving the electric field between the trapped charge distribution and the grounded rear electrode is obtained:

$$F(t) = -\frac{N_t dq_e}{\epsilon_0 \epsilon_r \varepsilon_0^c} \int_{\varepsilon_{min}}^{\varepsilon_{max}} exp\left[-tv_{te}exp\left[-\left(\varepsilon - dq_eF(t)\right)/k_bT\right]\right] d\varepsilon. \tag{4.7.10}$$

Equation (4.7.10) can be solved for the electric field numerically, but there is no closed form solution that can be obtained without strong approximations. Dissado *et al.* do provide an analytical solution to Eq. (4.7.10) for the decay of trapped charges in epoxy resin under CVC conditions (Dissado *et al.*, 2006).

How do we estimate the current density at the rear electrode? First, we can suppose that the observed current at the rear electrode is due to a displacement current, given by Eq. (4.6.4). Second, we can assume that the rear electrode ground connection is injecting counter charges to cancel the displacement current, thus keeping the rear electrode at ground. Both the trapped charge distribution and the induced charge at the grounded collecting electrode determine the time dependence and magnitude of the electric field. This is the basic physical model used in Dissado *et al.* (2006) to estimate the measured current density.

It is very instructive to review Dissado's paper and measurements using PEA methods therein, to obtain a complete picture of the charge density behavior discussed here. (For that matter, any PEA measurements on HDIM in a CVC-type experiment will provide the necessary picture.) In particular, special attention should be paid to the position, type, and magnitude of charge distributions at both the front (assumed to float after the cessation of voltage) and rear (grounded measurement electrode) electrodes. Dissado suggests that the charge neutralization process at the rear electrode is due to Schottky injection (this is one of the injection models suggested in Section 4.4) is

$$\frac{dQ_{inj}}{dt} = J_{inj} = J_0 \exp(-\varphi/k_bT) \exp\left\{\left[\frac{{q_e}^3}{4\pi\epsilon_0\epsilon_r}\right]^{1/2} \frac{[F(t)]^{3/2}}{k_bT}\right\}. \tag{4.7.11}$$

Here, Q_{inj} is the injected charge per unit area (which must be equal to the displacement charge), φ is the energy barrier at the metal-insulator interface, *F(t)* is the electric field generated between the trapped charge distribution and the grounded rear electrode found by solving Eq. (4.7.10), and $J_0 \exp(-\varphi/k_bT)$ is the initial current density. Using an expression similar to Eq. (4.7.11), Dissado derives and expression for the current density as a function of the electric field (the Walden model). Since the injection current must be equal to the displacement current, Eq. (4.7.11) can be written entirely in terms of the electric field using Eq. (4.6.5) as

$$\epsilon_0\epsilon_r \frac{\partial F(t)}{\partial t} = J_0 \exp(-\varphi/k_bT) \exp\left\{\left[\frac{{q_e}^3}{4\pi\epsilon_0\epsilon_r}\right]^{1/2} \frac{[F(t)]^{3/2}}{k_bT}\right\}. \tag{4.7.12}$$

Equation (4.7.12) is the charge neutrality condition at the grounded rear electrode resulting from the electric field. Equation (4.7.12) can be rearranged to give an expression for the current density

$$\epsilon_0\epsilon_r \frac{\partial F(t)}{\partial t} \exp\left\{-\left[\frac{{q_e}^3}{4\pi\epsilon_0\epsilon_r}\right]^{1/2} \frac{[F(t)]^{3/2}}{k_bT}\right\} = J_0 \exp(-\varphi/k_bT). \tag{4.7.13}$$

Dissado claims that the expression on the RHS of Eq. (4.7.13) is the measured current density at the rear electrode, $J_{meas}(t)$; he develops a very complex expression. It seems true the energy barrier must be a function of time, and Dissado suggests Eq. (4.7.13) can be written as

$$J_{meas}(t) = \epsilon_0\epsilon_r \frac{\partial F(t)}{\partial t} \exp\left\{-\left[\frac{{q_e}^3}{4\pi\epsilon_0\epsilon_r}\right]^{1/2} \frac{[F(t)]^{3/2}}{k_bT}\right\}. \tag{4.7.14}$$

A more realistic approach would seem to be gained by solving Eq. (4.7.12) for the resulting electric field and then using Eq. (4.7.11) to obtain the true injection current; however, this is not the approach Dissado takes and will be left for future work. Equation (4.7.14) is complicated and only solvable by numerical methods unless—as Dissado did—many approximations are made. The inclusion of the Schottky injection function does highlight the need for extended studies on the nature of the metal-insulator interface; this was addressed in Section 4.4.

Thus, we are left with the task of deriving a simple equation to estimate the current density at the rear electrode, which can yield estimates for the material parameters. As is turn out, we have already developed all the necessary components to such build a model. Using Eq. (4.6.5) for the displacement current—with *d*-*R* replaced by *d*, the sample depth—and Eq. (4.7.7); we write the following expression for the measured current density at the rear electrode

$$J_{meas}(t) = -q_e \frac{dN_t k_b T}{\varepsilon_0^c} \frac{d}{dt}\left\{E_i\left(e^{-\frac{\varepsilon_{max}}{k_b T}} \nu_{te} t\right) - E_i\left(e^{-\frac{\varepsilon_{min}}{k_b T}} \nu_{te} t\right)\right\}. \quad (4.7.15)$$

Equation (4.7.15) does not include changes in barrier energy due to field dependence, effects due to metal-insulator injection at the rear contact, or spatial dependencies; it is a simple approximation. However, for modest electric fields, temperatures near 300 K, and low energy barrier differences at the rear contact Eq. (4.7.15) should describe the observed behavior reasonably well. Equation (4.7.15) is the primary result of this section and is the USU CVC discharge model. While this expression could have been presented much earlier in the discussion, the lack of completeness would not have been apparent. A number of detailed discussions of models similar to the one developed in this section, Dissado's work, and previous work by the USU MPG (Dennison *et al.*, 2009a) can be found in the literature (Many and Rakavy, 1962; Mizutani *et al.*, 1977; Berlepsch, 1985a; Sessler, 1987; Fromhold, 1990; Alagiriswamy and Narayan, 2002).

The USU MPG has not taken data on the decay of charged samples after the cessation of voltage. Therefore, only a limited analysis will be presented in the next section. However, there is ample data on many types of insulators in the literature—Dissado *et al.* (2006) is an excellent place to start—that may be used to test the USU MPG model. Such an analysis will not be presented in this dissertation and is left for future researchers.

4.8. Analysis

In this section, the charging (Section 4.6) and discharging (Section 4.7) models are explored. First, we apply the simplified USU MPG CVC charging model, Eq. (4.6.9), to data taken on LDPE. The results are briefly discussed and some observations about the nature of the observed behavior are made. Second the results of the USU MPG CVC discharge model Eq. (4.7.14) using the parameters obtained from the investigation of the charging model is presented. The discharge model is not compared with data; it is presented only to explore its use, behavior, and how it should be a better predictor of the intrinsic material conductivity than the charging model. Keep in mind that this chapter is meant only to show that the theories presented in Chapters 2 and 3 can be used—even in a simple form—to understand and predict measured current densities, surface potentials, and resulting electric fields. This chapter is not the final word on charge and discharge models under CVC conditions.

Details of the CVC experimental apparatus and sample preparation procedures are given in Brunson (2009) and Dekany *et al.* (2008, 2012) and will not be repeated here. The specific LDPE sample tested has a depth (thickness) of 27.4 μm and the effective sample area is 1.0×10^{-4} cm^2. The applied voltage is 100 V resulting in a 3.65 MV/m applied field. The sample was tested at room temperature under a vacuum of $\sim 1.0 \times 10^{-4}$ Torr. This particular test was done using a battery system to supply the applied voltage with a significantly reduced background noise (Dekany and Dennison, 2009). The battery system has the advantage of a very low noise background and well-known current versus voltage characteristics. The test procedure applies a constant voltage for the duration of the experiment and monitors the resulting current at the grounded rear electrode. Figure 4.3 shows the resulting data plotted on a log-log scale and fit with Eq. (4.6.9). The black points are the data and the thin yellow line is the fit, shown in the lower plot. The data extend over nearly three orders in magnitude in current density and nearly five orders in magnitude in time; with the exception of the first 100 s—where there are no data—the fit is excellent. The upper plot shows the residual between the fit and the data. The scale of the residual is 1.0×10^{-15} A/m^2, two to three orders of magnitude lower than the scale of the current density measured in the lower plot. The fit agrees with the data to within <1% throughout. The increase in the spread of the data points is due to limitations in the instrumentation of ~ 200 aA (Dekany and Dennison, 2009); note, aA is *atto amps*, stated here because it is a very unusual unit to encounter. In fact, it seems likely that the region where the current density appears to reach equilibrium is really an instrumentation measurement limit; this conjecture will be ignored.

Figure 4.4 again shows the data (black) and fit (green), but adds another fitting function, which is the solution of Eq. (4.3.14) with no injection function. This solution, a simple exponential function, is a poor fit; this clearly highlights the need for the injection function described in Section 4.4. The USU MPG CVC model is a combination of an exponential and a power law function [see Section 4.6 or Eq. (4.6.9)]. For LDPE, the power law-type behavior clearly dominates, suggesting very strong trapping of the incoming charge.

The USU MPG CVC model is a good fit to the data; but, does it accurately predict the material parameters? The fit of Eq. (4.6.9) was done using IGOR 6.1 data analysis software and yields the parameter values shown in Table 4.1. Here s_c is the capture cross section and N_t is the DOS. These two

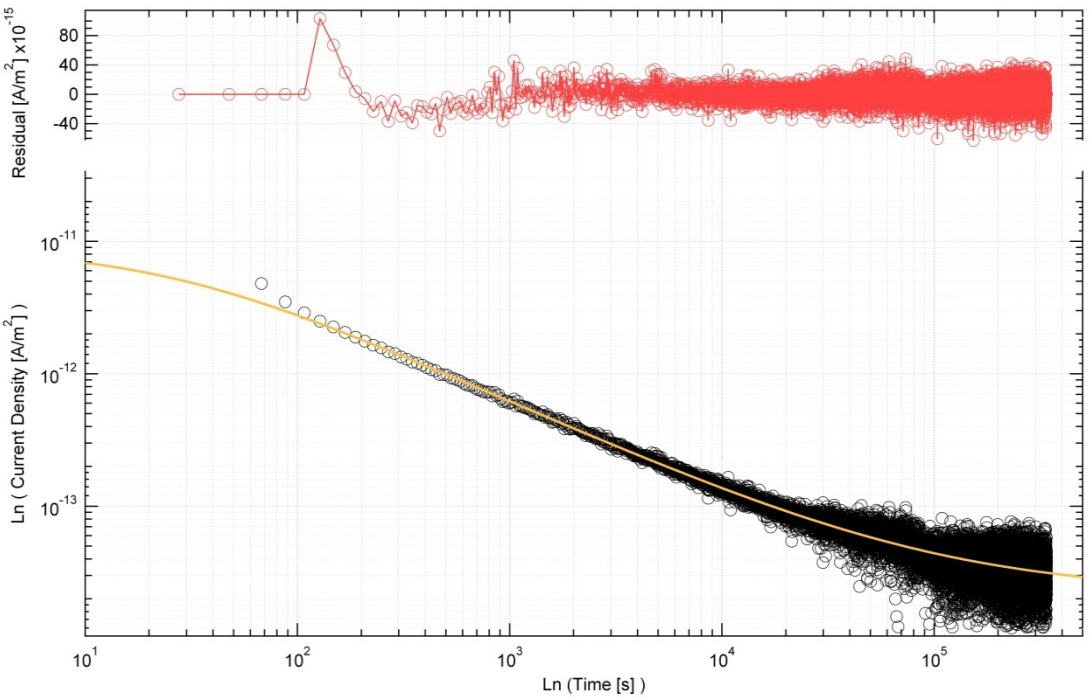

FIG 4.3. Fit to LDPE data using the USU MPG model. Data for LDPE with an applied field of 3.65 MV/m at room temperature (black data points). The USU CVC charging model, Eq. (4.6.9), is applied (green line). This plot is on a log-log scale to highlight the power law-like behavior. The residual (top red curve) suggests an excellent fit, limited by instrument resolution.

values are consistent with the literature (Rose, 1963; Sessler, 1987) and additional measurement made by the USU MPG discussed in Chapters 5. J_0 is the initial injection current density, J_{sat} the saturation current density (likely an instrumentation limit), m is a power, τ_{onset} is the onset time, and d is the sample thickness. The parameter values in Eq. (4.6.9) are grouped in products (with the exception of m and τ_{onset}); this allows for some ambiguity in their determination. For example, s_c and J_0 form a product pair in the argument of the exponential and the magnitude of the function; in addition, N_t and d form a product pair in the magnitude. The upper and lower bounds of each of these parameters must be established by comparison with other experiments within the USU MPG and literature results. In this dissertation some cross comparison is done, but a great deal of work is needed to build confidence. However, as we will see, the values obtained for all parameters are in the expected ranges.

The least useful parameters are the two extrinsic parameters (the initial current, J_0, and the saturation current, J_{sat}) as they depend more on the limits of the apparatus than on the intrinsic material

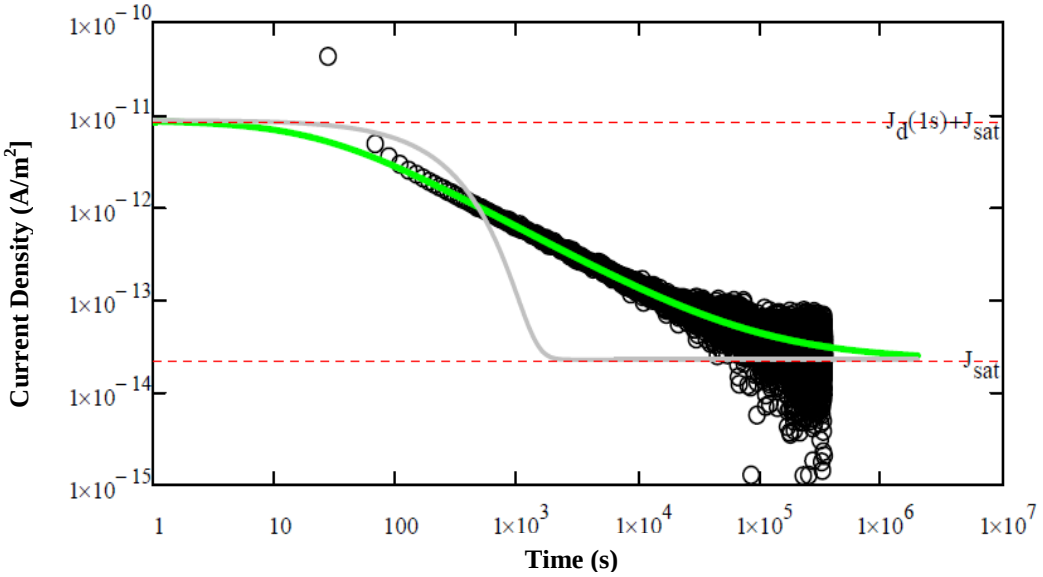

FIG 4.4. Fit with USU MPG CVC model and pure exponential. The data are shown in black, the USU MPG model of Eq. (4.6.9) in green, and the exponential solution of Eq. (4.6.9) for when no interface charging is considered (i.e., when *m =1*). It is clear that the exponential solution is a poor estimation of the measured current density. The maximum current density and minimum current density are shown as dotted lines for reference.

properties. However, the initial and saturation current density can be used to estimate the maximum and minimum bounds, in addition to the change in conductivity. The internal field due to trapped charges is usually much less than the applied field; we can, therefore, get a first order estimate of the upper and lower bounds on conductivity during the charging process by looking at the ratio of the initial and final current densities to the applied field. Thus, we can establish the upper bound for the conductivity as $J_0/F_0 = \sigma_{up} =$ 9.15·10^{-17} [Ω-cm]$^{-1}$ and the lower bound as $J_{sat}/F_0 = \sigma_{lower} =$ 9.15·10^{-21} [Ω-cm]$^{-1}$; these are only estimates and should not be confused with other conductivities. The upper value is consistent with measured conductivities typical of LDPE ~ 10^{-17} to 10^{-20} [Ω cm]$^{-1}$ (Montanari *et al.*, 2001, 2005; Dennison and Brunson, 2008; Brunson, 2009).

The lower bound is not a reasonable estimate of the conductivity, since the flow of electrons is impeded by the charge distribution; this behavior is consistent with an increasing trapped charge distribution and resulting electric field. Why should we expect that the measured saturation current density is not a good predictor of material conductivity (assuming that it is a physical limit and not an instrumentation limit)? Figure 4.5 shows the trapped electron density as a function of time. The green

section is the portion of the function used to produce the observed charging of LDPE; i.e., the green curve is all we need to predict the observed behavior. The value of the DOS N_t obtained in the fit is consistent with previous work (Nath and Perlman, 1989; Wysocki, 1995; Tzimas *et al.*, 2010), but it is clear from Fig. 4.5 that only a small fraction of the DOS, only 0.05 ppm, is actually filled; this effect can lead to a significant underestimation of the DOS. This partial filling of the DOS is expected. If the DOS were to fill to a large fraction of its capacity—say 100 times the observed value—the internal electric field would exceed the electrostatic breakdown field strength and would cause material breakdown. In fact, long before the break down, the DOS would begin to degrade as field stress produced additional defects (Liufu, 1998).

We should expect that the way in which charge is injected into the material has a lot to do with how the DOS will fill and to what level it will fill. Consider a body of charge at a distance, R, from the surface of the sample, whose field is opposite to the applied field but equal in magnitude (as in Fig. 4.2). Using Eq. (4.4.3) to estimate the density of trapped states—creating the charge body opposite to the applied field F_0—we find the density of this charge body can be no larger than 3.8×10^{15} cm^{-3}, much smaller than the total DOS; i.e., in a perfect world, the applied electric field, F_0—used in this LDPE test—still could not fill up the DOS. In the real world Columbic shielding, polarization, and other internal effects reduce the field due to the trapped charge distribution; thus, slightly more charge is needed to produce a counter field equal to F_0. We also know from Section 4.6 that the more charge that is trapped, the higher the internal electric field and the lower the activation energy required to release the charge (electrons) from their trapped states; i.e., the way the trap distribution fills up changes with electric field, creating a situation in which electrons are released with greater frequency as the internal field is increased. This effect is often expressed as a field-dependent conductivity.

There is one very good reason that the internal field cannot ever be equal to the applied field. Consider what will happen if the electric field, F_0, is increased to a value, F_{fill}, that ideally, will inject enough charge to fill the DOS. In a perfect world, the field that is required to fill up the DOS, N_t, is ~100 MV/m, which is a factor of 10 greater than the estimated long-endurance time breakdown field strength for LDPE of between 1 and 10 MV/m (Montanari *et al.*, 2001; Crine, 2007). The crossover between electrostatic breakdown and a nondestructive density of charge is explored in Liufu *et al.* (1998) and Kao

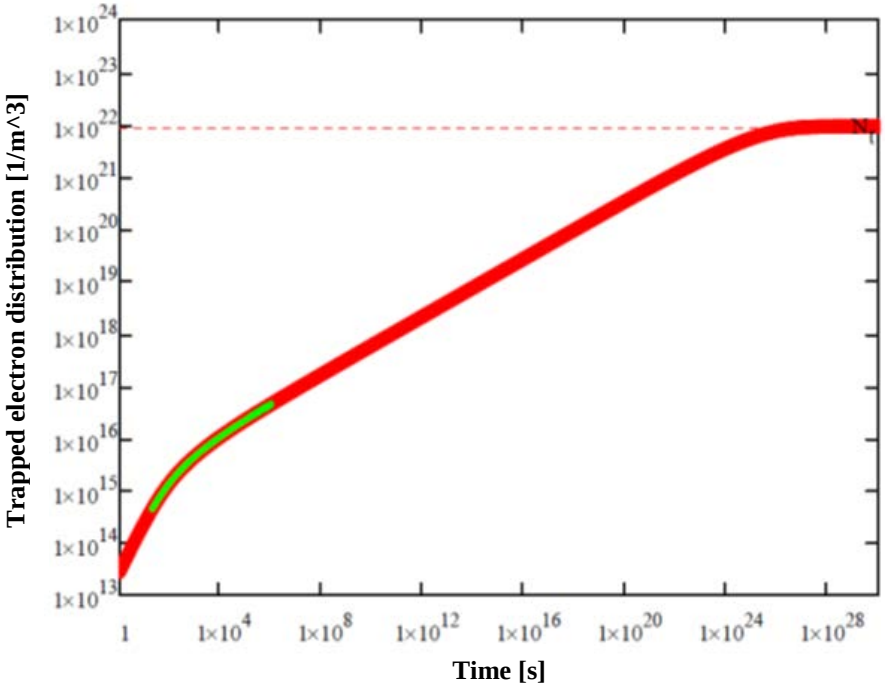

FIG 4.5. Trapped electron density time evolution. Electric field-dependent trapped electron density of the DOS by injected electrons at the metal-insulator interface. The green line represents the region of the curve (or total DOS) needed to characterize the filling of trapped states in LDPE. It is expected that the DOS is not completely filled during the charging of HDIM by contact injection at low fields; in this case, the applied field is $\sim 100\ MV/m$.

TABLE 4.1. Fitting parameters for USU MPG CVC model.

Parameter	J_0	S_c	N_t	d	τ_{onset}	m	J_{sat}
Value	2.34×10^{-12}	1.47×10^{-14}	$9.14 \times 10^{+16}$	27.4	25.1	0.724	2.25×10^{-18}
Units	A/cm^2	cm^2	1/cm^3	µm	sec	NA	A/cm^2

(2004). The USU MPG CVC model can be extended to include the effects of high field degradation and material breakdown using the approach of Liufu.

Our discussion of the USU MPG analysis has not yet included the effects of polarization. Some polarization data for LDPE have been taken using the USU MPG CVC system (Dennison and Brunson, 2008). Adequate data are not available to discuss the polarization effects of LDPE; therefore, a short discussion of the expected effects of the complete USU MPG CVC charging model given by Eq. (4.6.8) is presented. Using the parameter values obtained by fitting the simple USU MPG CVC model, a fit to the LDPE data set using Eq. (4.6.8) shown in Fig. (4.6) is obtained. The use of the polarization terms— shown

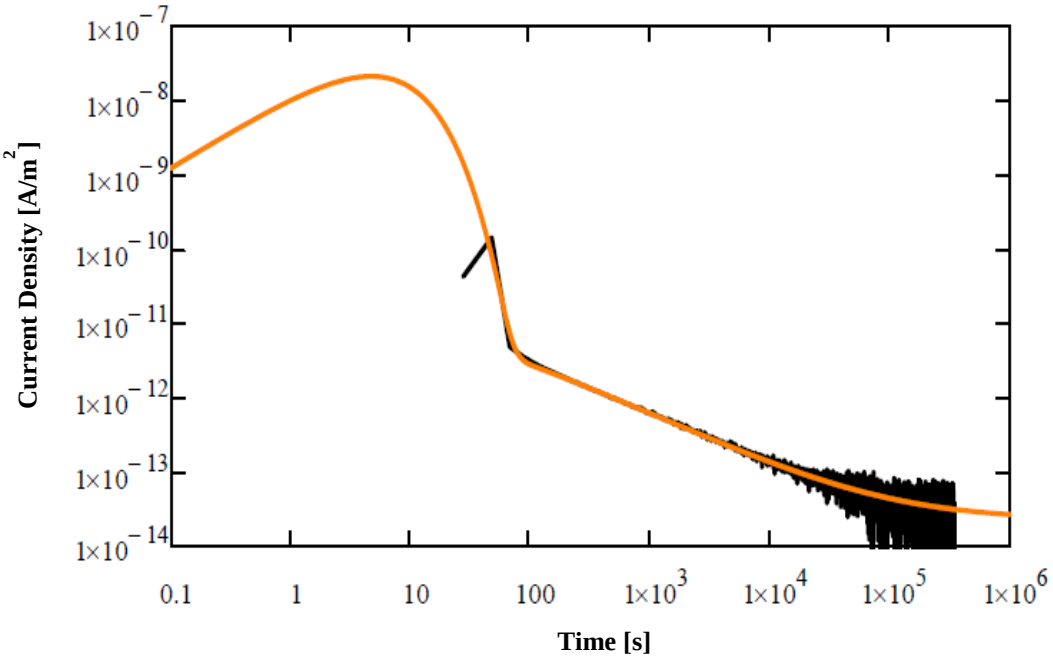

FIG 4.6. USU MPG CVC charging current density model. The current density (black dots) is derived from USU MPG CVC data taken on LDPE at 1.0 MV/m using Eq. (4.6.8). The fit (orange line) is the sum of the polarization and displacement current densities.

separately in Fig. 4.7—eliminates the small error for times less than 100 s seen in Fig 4.3; the polarization decay constant is 1.2 s, while the charging time constant is τ_{onset} ~ 25 s. This disparity in the polarization time and charging time constant seems to suggest that they are very different mechanism, as one would expect. While this short timescale behavior may not be polarization, but rather an instrument response time, the model presented in Eq. (4.6.8) is clearly capable of describing polarization (or short timescale) behavior. There are good arguments to suggest that LDPE does have a polarization component. However, after 10 s, it is expected that any anomalous signal due to the instrument should have subsided. Thus, while more study is needed, the inclusion of the polarization terms seems necessary to describe the short timescale response of the HDIM (LDPE in this case).

The ratio of the measured current density to effective electric field changes with time as $J(t)/F(t) = \sigma(t)$. The conductivity is not a one-to-one ratio as is found for Ohmic behavior, but decreases as the current tends toward a constant saturation current. Thus, the conductivity tends asymptotically toward the dark current conductivity at long t, leading to an unphysical result. This result suggests that, for an ungrounded sample in the presence of an electric field, it is possible to trap the charges in the material for

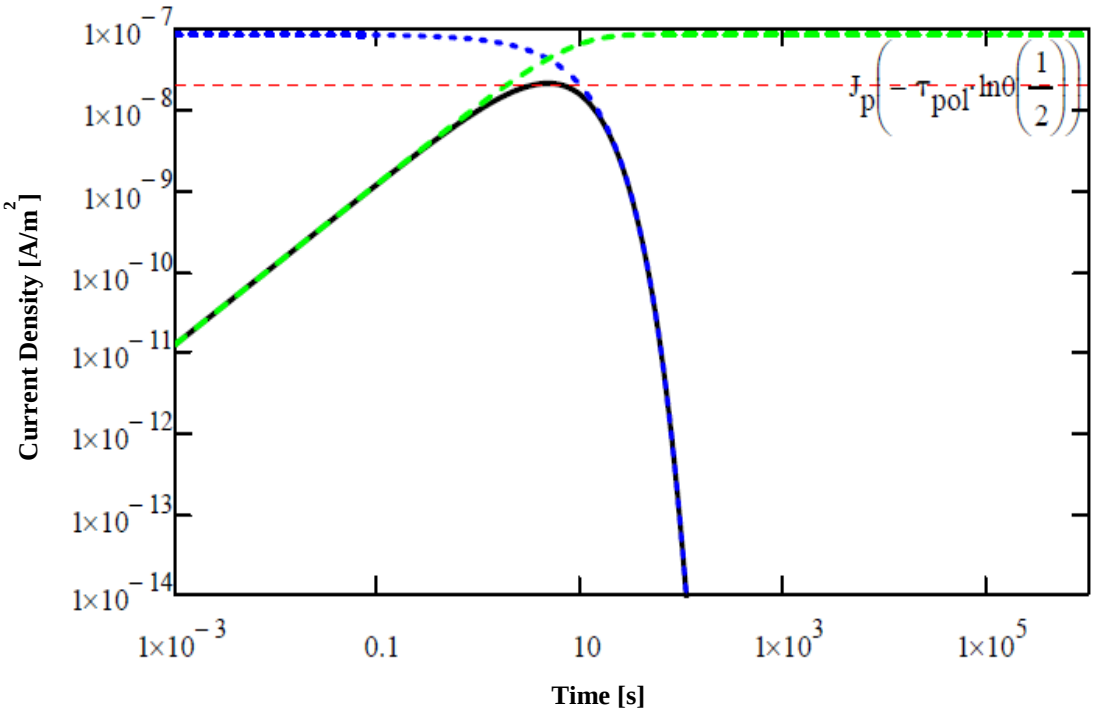

FIG 4.7. Composite polarization current density response. The total polarization current density (solid blue curve) and the initial polarization (dashed yellow line), and the relaxation of the polarized charge (dashed blue curve) are shown. Note the use of $ln\theta$ function for the dashed black line representing the turning point; this is a special type of natural log function used in Mathcad™ for data that goes through zero on the x axis.

times longer than expected when only the material conductivity is considered, i.e., spacecraft materials may be able to store charge for extremely long times (months) leading to a near breakdown situation or a situation where a much smaller change in local electric fields, incident charge, or material temperature can trigger a breakdown event. These results suggest that the true material conductivity can only be obtained by study of the decay of charge distribution after the cessation of voltage.

The USU MPG has not analyzed data acquired for the current density decay after the cessation of voltage, as of the writing of this dissertation. However, the theory developed in Section 4.7 can be explored using the material parameters found for the charging of LDPE (see Table 4.1). In order to keep the analysis as simple as possible, Eq. (4.7.15) has been used to calculate the estimate for the measured current density; Eq. (4.7.15) does not include the effects of the internal electric field on the detrapping dynamics or metal-insulator interface effects (see Section 4.7). Equation (4.7.15) must be calculated numerically as the exponential integral does not have a closed-form solution. The result of the numerical

integration for the expected decay of the measured current density is shown in Fig. 4.8. Figure 4.8 (b) shows the actual result of Eq. (4.7.15) and Fig. 4.8 (a) shows the absolute value of Eq. (4.7.15). Mathcad™ was used to perform the numerical calculations, and appears to perform better when the absolute value is used. In addition to the current density, the time-dependent internal electric field is calculated. Given the time-dependent internal electric field and current density, the time-dependent conductivity can be calculated as $J(t)/F(t) = \sigma(t)$; Fig. 4.9 shows the result (red curve). Why does the conductivity appear to change so dramatically as a function of time?

The explanation to our question is best understood in terms of the thermalization and excitation processes described in Chapter 3; the argument goes as follows. Assume that the quasi-Fermi level is very high in the DOS due to partial filling of the DOS. For early times—when the Fermi level is near the CB edge—charge is quickly released from energetically shallow states (near ε_{min}) to the CB leading to an enhanced conductivity; enhancement of the conductivity is often seen in radiation measurements, as discussed in Chapter 5. The reason for this fast release follows from the way in which the DOS is charged when an electric field is applied (see Section 4.6). The applied field allows the HDIM to act like an enhanced charge storage system packing electrons into low-energy (near the CB) trap states and holding them there (a kind of nonlinear capacitive effect). These low-energy states release trapped charges very quickly when the applied field is removed; i.e., the QFL is time dependent and will drop quickly for early times. This behavior is responsible for the fast power law decay of the conductivity to the left of the vertical dashed line shown in Fig. 4.9. The vertical dashed line is the time at which the deep trapped charge distribution near ε_{max} begins to release it charge; we can also think of the deep state charge distribution as beginning to dominate the transport after this time. To the right of the vertical dashed line, we see that the conductivity levels off approaching its equilibrium (dark conductivity) value. The density of trapped energetically deep charge is much lower than the (early time) shallow counterparts; i.e., the QFL approaches the dark or equilibrium Fermi level. This has an important effect, since the internal field is largely due to shallow charges, which are larger in number (for early times) than the number of electrons in deep states. Thus, once the shallow charge distribution has dissipated, we are left with a low-charge concentration, low-field situation; i.e., with time, we move closer to a single electron approximation and the true or equilibrium material conductivity. Our estimation provides a value for the intrinsic material

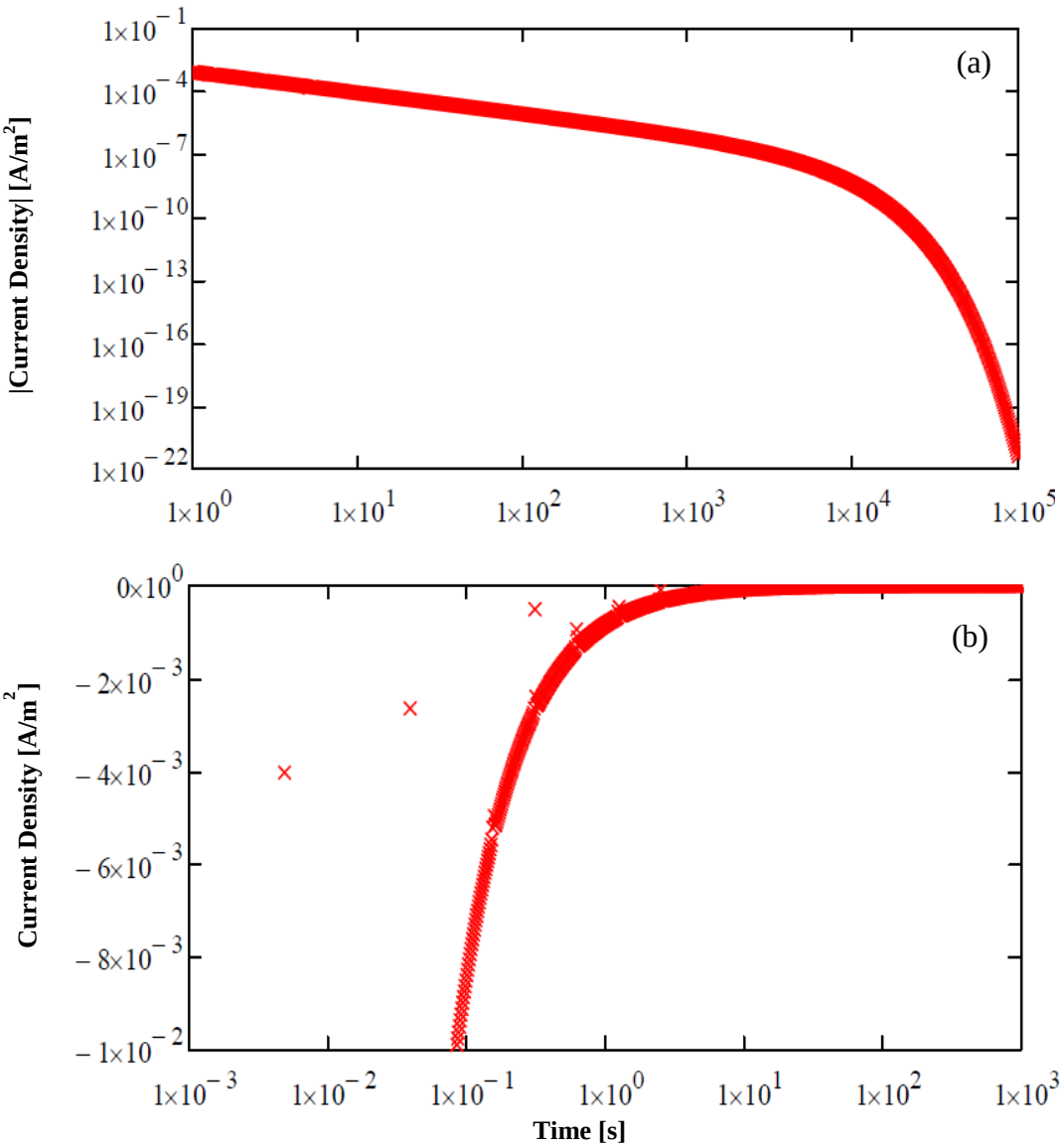

FIG 4.8. USU MPG CVC discharge model. Numerical estimations of the expected measured current density at the collecting (grounded) electrode. (a) Absolute value of the current density for a discharging HDIM. (b) Actual predicted current density for a discharging HDIM after the cessation of short timescale effects. The errors in the curve are seen as isolated red x's and missing points in the data curve; these result from the numerical calculation process.

conductivity (dark conductivity) of $\sigma_0 = 9 \times 10^{-17}[\Omega\ \mathrm{cm}]^{-1}$ shown in Fig. 4.9 as a horizontal dashed line. This value is in reasonable agreement with previous studies on LDPE (Montanari *et al.*, 2001, 2005; Dennison and Brunson, 2008; Brunson, 2009) which range from $\sim 1 \times 10^{-18}[\Omega\ \mathrm{cm}]^{-1}$ to $1 \times 10^{-15}\ [\Omega\ \mathrm{cm}]^{-1}$. Since the intrinsic material conductivity is obtained from the simplified model using material parameters from the fitted charging model (which are likely to be different due to field effects

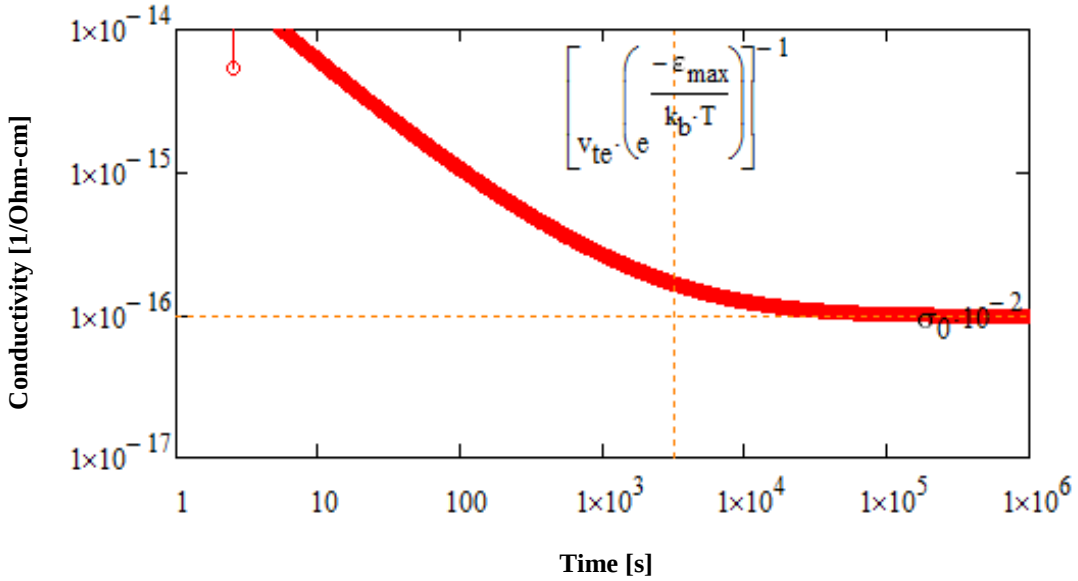

FIG 4.9. Time evolution of the material conductivity. The time-dependent conductivity can be estimated by taking the ratio of the time-dependent current density to the time-dependent internal electric field. The horizontal dashed line is the dark current conductivity and the vertical dashed line is the time at which the deep states begin to dominate the conductivity, i.e., the onset of dark current conduction. Note that a smaller section of the data is shown in this figure to highlight the low-conductivity limit.

caused by the much stronger applied field), we expect that our estimations will improve greatly with actual discharge data on LDPE and full numerical integration of the USU MPG CVC model.

4.9. Conclusion

The CVC section has presented a theoretical development for charge injection under application of an applied electric field, developed a charging model that includes the charge injection behavior, developed a discharging model, both with and without metal-interface behavior, validated to first order of the CVC charging model, and shown that the CVC discharging model will almost certainly yield accurate information about important physical material parameters, such as the conductivity. A preliminary analysis—performed in Section 4.8—provides confidence in the USU MPG CVC model and the results are shown to agree well with both the USU MPG SVP results (Chapter 5), as well as literature.

A concise discussion of the range of possible measurements and response regimes has been given, verifying the basic physical behavior. This was accomplished by extending the long timescale USU MPG CVC model with a simple phenomenological polarization model that can account for short timescale behavior (see Section 4.6). While the physical roots of this polarization model must be investigated further,

it does allow spacecraft designers the ability to predict short timescale behavior; thus the model can help mitigate breakdown events that occur when the material is near its degradation threshold. Chapter 4 has, therefore, presented a physically based set of models for the predication of charge redistribution in HDIM and mitigation of harmful spacecraft breakdown events that cover all timescales of interest to spacecraft designers.

The process of developing these models and applying them to USU MPG data has produced a new set of Mathcad^{TM} tools to describe the charging current density with field and time-dependent behavior; these are spacecraft engineering tools. These models and the data collected by the USU MPG CVC apparatus can and should be used in conjunction with the SCLC and VRH models of Chapters 2 and 3, respectively (refer to the introduction of this chapter). These models describe changes in the conductivity as a function of field and temperature for two physically different transport mechanisms, both of which are studied in the CVC system. These physical models in conjunction to the time-dependent models presented in this chapter offer a diverse theoretical platform upon which to study HDIM and connect the results to other USU MPG experiments.

Using the three major types of DOS (constant, exponential and Gaussian) together with the four bodies of theory (TAH, VRH, SCLC, and USU MPG CVC time-dependent charging and discharging models), a complete characterization of HDIM electron transport behavior, and a deep understanding of the physical make up, a complete set of engineering tools can be constructed.

All of these bodies of theory (TAH, VRH, SCLC, and time-dependent transport models like the USU MPG CVC) share the same set of physical transport equations discussed in Section 4.3. Numerically, the complete transport equations with the inclusion of injection terms can completely describe the behavior of any material in three dimensions as a function of time, injection behavior, internal and external electric field, and temperature. It is critical that full numerical models be developed and tested against data and analytical expressions. However, this project is beyond the scope of this work and is left for future work.

The goal of developing a simplified set of time-, electric field-, and temperature-dependent transport expressions for CVC has been accomplished. We have shown that the approximations used are reasonable and supported by results external to the USU MPG, that the models describe data on LDPE with high accuracy, and that the resulting physical parameters are consistent with both the literature and

previous USU MPG results. The remaining chapter is dedicated to the USU MPG Small Voltage Probe analysis, and shows similar agreement with both the CVC system and the literature.

CHAPTER 5

SURFACE VOLTAGE PROBE ANALYSIS

5.1. Introduction

The central theme of spacecraft charging requires a description of the interactions with the plasma environment and high-energy events that cause charging. Spacecraft materials accumulate negative or positive charge and potentials in response to interactions with the spacecraft environment. We are specifically concerned with the parts of the spacecraft that contain HDIM; thus, from this point on, when we use the word spacecraft material we mean HDIM. A material's electron emission, or electron yield, determines how much net charge accumulates and is, therefore, directly related to deposited charge and surface potential, as is evidenced by the much higher yields of typical HDIM when compared with materials of higher conductivity. Due to their higher mobility, incident electrons play a more significant role in the electron yield response than ion or photon fluxes and, therefore, in the resulting spacecraft charging. We, therefore, continue to constrain our discussion to electron fluxes and electron transport, as we have done throughout this work. This chapter develops the relationship between the surface potential and the charge distribution internal to or on the surface of an HDIM, and it also presents the connection to the electron yield of an HDIM

Largely, the goals of this chapter are approached through the development of theoretical models for the charging and decay of an HDIM leading to a surface potential. Specifically, we discuss surface voltage dependence due to a normally incident electron beam—allowing simulation of spacecraft environment conditions—on an HDIM as it charges up (electron beam on) and decays (electron beam off). This theoretical body is then compared to data taken using a small surface voltage probe (SVP) in the SEE test chamber (Hodges, 2013). These models will be referred to as the SVP charging and decay models. In Chapter 1 a discussion of six experimental configurations was presented (see Fig. 1.4). While all of the figures in Fig. 1.4 are relevant to the spacecraft charging problem, in this chapter we discuss only the physics associated with Fig. 1.4. (a) (ii). This chapter applies the transport equations—presented in Chapter 2—to the charging problem given by Fig. 1.4 (a) (ii); Fig. 1.4 (a) (iii) describes RIC

measurements, and while we will present a short and necessary discussion of RIC, it is largely left for future work (Gillespie, 2013).

We begin this chapter with an introduction to electron beam charging and the limitations and challenges that it presents. This discussion is used as a basis to argue that deposition of charge in the HDIM is—for high beam energies—the major factor in the resulting surface potentials. This discussion will include a short summary of secondary electron emission (SEE), radiation induced conductivity (RIC), and surface transport of charge. While these three mechanisms greatly complicate the physics of charge migration, deposition and continuity of charge, the associated discussion will show that—in large part—we can ignore the spatial region in which the difficult physics is occurring and treat the whole system like a simple parallel plate capacitor (or, in some cases, two simple parallel plate capacitors). This may seem an almost ridiculously simple assumption, but it will be seen that the surface potential predicted by SEE theory (Thomson, 2001; Hoffmann, 2010) is of the same form as that predicted by the charging equations; it will be shown that the surface potential equations of Hoffmann (2010) are nearly the linear first order approximations of the SVP charging theory. The assumption that we can treat the system as simple planes or blocks of charge allows the use of theoretical machinery developed in Chapter 4 to describe the charging of an HDIM under electron beam irradiation with very little modification.

Having introduced the problem and constraints, the development of the SVP charging model will be presented in Section 5.2. We start with an the assumption for high-energy electron beam charging discussed in Section 5.1 and the modifications to the transport Eqs. (2.6.8) through (2.6.13) to show that the assumptions made for the SVP model are consistent with the CVC charging model of Chapter 4. In Section 5.3 the SVP charging model is completed and fit to data from SVP measurements of electron beam charged Kapton-HN^{TM} and LDPE to extract relevant physical parameters.

Having developed the charging model, the focus of this chapter will be turned to the decay of the deposited charge body in Section 5.4. The development of the SVP decay model requires a great deal more development than that of the charging model, as we cannot rely on any information presented in Chapter 4. Section 5.4.1 develops the notion of a surface potential and Section 5.4.2 presents the detailed mathematics required to derive a closed form solution. Since the decay of charge occurs on extremely long timescales,

one is forced to consider what happens when the charge distribution reaches the rear collecting electrode, at which point the decay of surface potential will increase due to a new current path between the centroid of the charge body and the collecting electrode. This problem is addressed in Sections 5.4.3, 5.5.1, and 5.5.3, but is largely left for future work. Having developed a model for the surface potential decay, we again fit data from the SEE chamber on LDPE and Kapton-HN™. The agreement between experimental systems and the literature is found to be excellent. A short discussion of the physical parameters, condition of the data, fit to the data, and behavior of the model is presented.

5.2. Electron Beam Charging

Consider Fig. 5.1 in which an electron beam (a) is normally incident on an HDIM, which is grounded at the opposite side (the collecting rear electrode). Figure 5.1 is complex, and we will approach its discussion in a piecewise manor to make clear the important processes at work and the nature of the assumptions to be used in creating the SVP models. First, consider (a) and (b) and for the moment ignore the rest of the figure. Part (a) of the figure is the incident electron beam. Part (b) of the figure represents electrons that are ejected from the material; these electrons are called emitted electrons and there are two types. The first type of emitted electron is called a secondary electron (SE) and has an energy ≤ 50 eV by convention. The second type is called a backscattered electron (BSE) and has and energy ≥ 50 eV by convention. The emission of electrons for any material with an electron beam or energetic distribution of electrons is called secondary electron emission (SEE); thus, the reason why the chamber where the SVP data were taken is called the SEE chamber is now clear. We will not give a comprehensive discussion of SEE here as it has already been done very well by Thomson (2004) and Hoffmann (2010). We offer a brief synopsis taken from Hoffmann *et al.* (2008).

The electron-induced electron yield is characterized by the total yield, $\sigma_{yield}(\varepsilon_b) = (Q_{BSE} + Q_{SE})/Q_{TOT}$, where ε_b is the electron beam energy. The total yield is defined as the ratio of the emitted SE plus BSE electron flux to the incident electron flux. By convention, the SE yield, $\delta_{yield}(\varepsilon_b) = \frac{Q_{SE}}{Q_{TOT}}$, is the ratio for emitted electrons with energy less than or equal to 50 eV, and the BSE yield, $\eta_{yield}(\varepsilon_b) = \frac{Q_{BSE}}{Q_{TOT}}$, is the ratio for emitted electrons with energy greater than 50 eV to incident charge. The total yield is

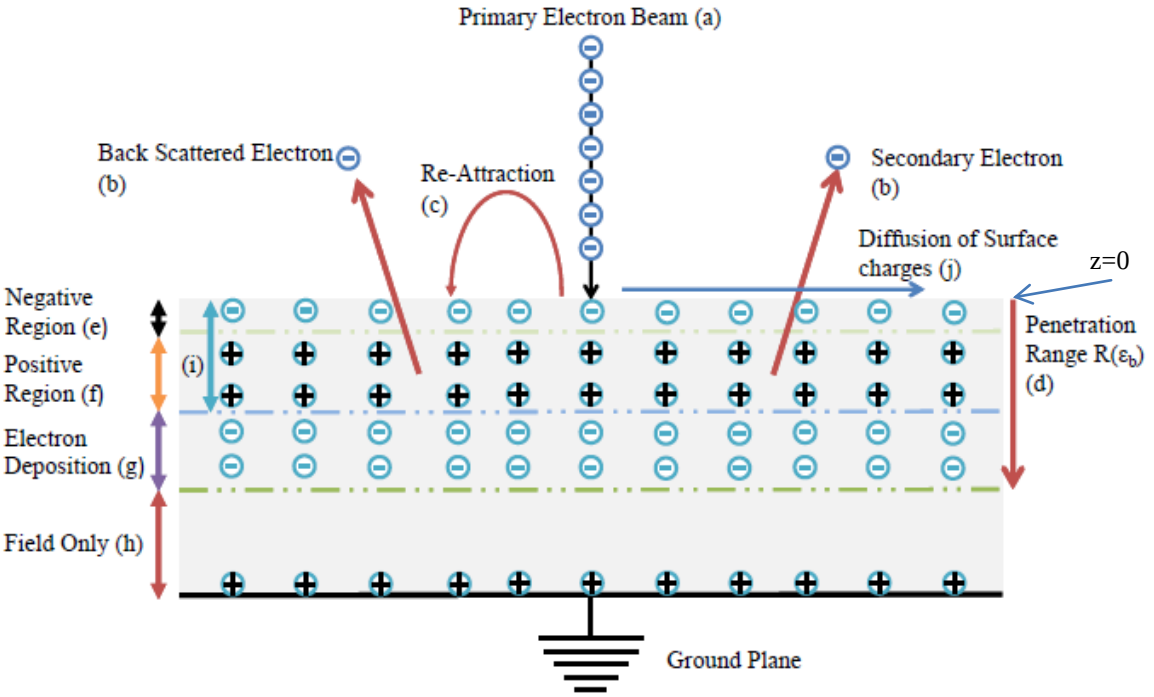

FIG 5.1. Basic electronic configuration for the SVP. Depicts important features in secondary electron emission that lead to a negative surface potential when the beam energy is greater than the second crossover energy. (a) Incident electron beam with energy, ε_b, and area, A. (b) A secondary electron (SEE) or backscattered electron (BSE) leaving the sample. (c) Re-attraction of a secondary to the surface; only occurs when there is a positive surface charge layer. (d) The range—as a function of beam energy—into the sample that the incident electrons will penetrate; region where electrons will be deposited. (e) Negative top layer caused by re-attraction of secondary electrons; the layer is positive for energies such that the yield is positive. (f) Positive region caused by the incident beam, leading to a net loss of electrons. (g) Electrons are trapped in localized states. (h) No electrons are deposited in this region, but an electric field due to the deposited charge is formed. (i) In this region radiation induced conductivity is active. (j) Diffusion of surface charge away from the incident beam center.

characterized by five parameters: the crossover energies ε_1 and ε_2 at which the total yield is one, the yield peak, $\sigma_{yeild}^{max}(\varepsilon_b^{max})$; the energy of the beam at the yield peak, ε_b^{max} (typically between 200 and 1000 eV for HDIM); and the rate at which the yield approaches the asymptotic limit or zero as the beam energy goes to infinity, $\varepsilon_b \rightarrow \infty$. Using the definitions for total, SE, and BSE one can write down a simple expression for the total yield, $\sigma_{yield}(\varepsilon_b) = \delta_{yield}(\varepsilon_b) + \eta_{yield}(\varepsilon_b)$; very often in the literature this is simply written as $\sigma = \eta + \delta$. In this dissertation, to avoid confusion with other parameters, we will use the explicit form above. The yield is characterized physically by three regions on a total yield versus beam energy plot. The first region is $0 < \varepsilon_b < \varepsilon_1$; in this range, the yield is always less than one as fewer electrons are emitted than incident, since electrons collect in surface traps on the surface of the material; this leads to net

negative charging. The second region occurs $\varepsilon_1 < \varepsilon_b < \varepsilon_2$; in this region, the yield is greater than one as more electrons are emitted than incident, yielding net positive charging. In this case, there is a positive surface layer due to release of loosely bound electrons near the surface of the material. In the final case, $\varepsilon_b > \varepsilon_2$, the yield is less than one and more complex picture develops in the HDIM, again with a net negative charging. This is shown in Fig. 5.1 and is the primary energetic region of interest for this dissertation. We will not consider the analysis for the first two cases where the beam energy is less than the second crossover energy. However, for the first case, the experiment is identical to Fig. 1.4 (a) (*i*), a time of flight measurement. There are a large number of authors whom have applied the transport equations and conducted measurement for this configuration: Rose (1963), Ghosh and Spear (1968), Pfister and Scher, (1977), Schmidlin (1977), Tiedje and Rose (1981), Orenstein *et al.* (1982), Arkhipov *et al.* (1983, 1984), Monroe (1986), Sessler (1987), Tyutnev *et al.* (2000, 2002b, 2006b), and Kao (2004), to name but a few. A main reason for this large body of literature regarding TOF measurements is its application to xerography and photoconduction in semiconducting materials. We will not consider the second case—where the energy is between or at the crossover energies—because the surface potential is generally quite small and the amount of charge on the surface of the HDIM is also small; thus, there is little application to the spacecraft charging problem. For details see Hoffmann (2010).

Returning to Fig 5.1, we now consider the formation of different charge layers given by (e), (f), (g), and (h). Consider the path of the incident primary electrons (PE) into the sample. As a PE enters the sample, it has a great deal of energy that is released in the material which, among other things, can liberate loosely bound electrons or give energy to free electrons; this creates a layer of positive charge, (f). Many of these electrons are emitted from the sample surface to be collected by the SEE measuring system, see Hoffmann (2010). However, a fraction of the emitted electrons have too little energy to escape the electric field created by the positive region, (f), and are re-attracted to the surface, (c). This action of re-attraction creates a negative charge layer on the surface of the material, (e). This negative surface layer is generally quite narrow. In order to give some idea of how small the negative surface layer might be, we first must consider how deep the PE can penetrate the sample. This is the range, $R(\varepsilon_b)$, shown in Fig. 5.1 as (d). The range is a function of the beam energy; the higher the energy, the deeper the PE will penetrate. We will not discuss the physics of the range, as an excellent theoretical model has already been developed by the USU

MPG (Wilson and Dennison, 2010; Wilson *et al.*, 2012). The range of PE in the material for the energies considered in this dissertation (between 2 keV and 10 keV) is about 1 μm to a few μm. The sample thicknesses are typically 25 to 30 μm; therefore, the range is typically a fraction of the sample depth. The negative surface layer depicted in Fig 5.1 (e) must be considerably smaller than this. This negative layer is expected to be on the order of a few 10's of nanometers, set by the range or inelastic mean free path of the lower energy SE. At the range, $R(\varepsilon_b)$, electrons are deposited into trapped states, creating a large negative charge distribution centered about $R(\varepsilon_b)$. This charge distribution is almost entirely responsible for the surface potential of the material; while the negative layer, (e), does contribute, it is very small when compared with the deposited charge distribution except near the crossover energies. The positive charge distribution, (f), is also usually very small and in fact PEA measurements on several HDIM suggest this is the case (Perrin, 2005; Griseri *et al.*, 2006; Le Roy *et al.*, 2008; Cornet *et al.*, 2008; Tzimas *et a*l., 2010). Why would one expect this to be true?

In order to answer this, a very complex set of physical phenomena must be described. These will not be discussed here at length; for more information, see Hoffmann (2010) and Thomson (2004). However, a simple discussion of Fig 5.1 can shed a great deal of light on why we should expect this to be true. First, consider the point of view of a PE as it enters the sample. The PE will have a great deal of energy to liberate other electrons from loosely bound states and—as discussed above—some will be ejected from the sample and others will enter the CB of the material causing an enhanced conductivity called radiation induced conductivity. RIC, impact ionization, scattering, local electric fields, and changes in the incoming PE distribution create a very dynamic region that will tend to minimize or relax the spatial extent of the positive charge distributions by allowing free electrons in the regions (e) and (f) to recombine with positive charge centers (Melchinger and Hofmann, 1995; Song *et al.*, 1997). RIC is an extremely well-studied subject and is one of the major applications of the transport equations; for more information, see Rose (1951), Sessler (1987), Kao (2004), Arkhipov (1993a), Melchinger and Hofmann (1995), and Weaver *et al.* (1977). Work on RIC by the USU MPG includes Dennison *et al.* (2003), Gillespie (2013), and Wilson *et al.* (2013).

Thus far, we have only discussed the top three charge layers in Fig. 5.1; little has been said about the region (h) or the action of radial diffusion in the sample. The radial transport of charge can occur by

diffusion, drift, dispersion, or hopping depending on the conditions of the experiment. On the surface of the material the electrons are expected to be in shallow trap states, and therefore, able to interact electrically. This can lead to a diffusive gradient away from the center of the impinging PEs'; this process is depicted in Fig 5.1 (j). Studies by Hodges (2013) have shown that this effect is minimal in Kapton-HN™. In the positive charge region, (f), the positive charges are the atomic or molecular centers left behind by liberated electrons and are, therefore, assumed immobile. The bulk charge distribution in region (g) is trapped in energetically deep states and, therefore, will only interact via conduction mechanisms whose mobility is on the order of the same transport processes moving charge toward the collecting electrode. Therefore, the spread of charge within the material in the radial direction is assumed to be negligible. The dynamics of this process again requires a significant theoretical development, and will therefore be left as future work. However, Baum *et al*. (1978) have approached this subject and presented a detailed analysis for the diffusion of surface charge.

The region in Fig 5.1 comprised by (e), (f), and (g) is very complex; however the net result of these processes can be characterized as a charge injection mechanism (Hodges, 2013). In Chapter 4 we brought together the theory of Wilcox (1971), Walden (1971), and Wintle (1974b), which develops a simple power law for the current density injected into the material as a function of time that characterized the complex processes operating at the material interface. This theory has been extended to include charge injection by particle beams in the formalism of Walden's injection mechanisms in (Hodges, 2013). Consider Fig. 5.1 once again. If we assume that the regions (e) and (f) comprise an effective electrode equivalent to a contacting front electrode, and that region (g) is just the injected trapped charge, then the SEE problem becomes a simple parallel plate capacitor with a rather complex injection mechanism. We need only know how many electrons are injected into the material, the injected current density. In fact, we have already developed the charge injection model, dependence of the trapped charge distribution, and a theoretical estimate for the observed current at the rear electrode in Chapter 4. In this chapter, the goal is the development of surface potential equations and not the current density collected at the rear electrode, though we will present it as modified for the SEE-SVP system.

Let us review the assumptions that were made in the last section: (1) there is little or no lateral displacement of the charge beyond the beam spot size; (2) the complex regions in Fig. 5.1 (e), (f), and (g)

can be modeled as a contacting electrode making the system act as a parallel plate capacitor; (3) the sheet of charge at R has a radial extent of $\sim 10^{-2}$m to $\sim 10^{-4}$m—given by the beam size—which is on the order of or larger than the sample depth $\sim 10^{-6}$ m. This allows one to approximate the deposited charge distribution as a plane of charge and the transport as a 1D problem. This approximation is useful in spacecraft charging as the distribution of incident PE in a space environment will be largely uniform over the sample, creating similar sheets of charge. Further assume that (4) the incident PE does not penetrate more than half way through the sample; RIC is likely to become a strong component and could cause charge to move upward toward the surface in a nonuniform way. This last condition should be tested against the models to establish limits on the use of the SVP model, as there is no literature or data known to the author that addresses these ideas. Assume that (5) the beam energy must be greater than the second crossover energy, above which there is no longer a significant spatial distribution of deposited charge. Finally, assume that (6) measurements do not exceed the transit time of charge across the sample to the rear electrode; this final condition was not mentioned above. If the electron beam is on for a very long time, a new conduction path may occur when the electron distribution completes transport across the sample and connects with the rear collecting electrode (ground plane in Fig. 5.1).

Having outlined the assumptions and physical picture, we now turn to the application of the necessary transport equations and the derivation of our charging and discharging models. For the charging models, the basic concept was taken from a set of models created for impact ionization studies and electron beam charging of electrets (Gross, 1964; Livingstone, 1973; DiMaria, 1975; Wintle, 1983, 1991, 1999, 2003; Nissan-Cohen, 1986; Sessler, 1987; Avini, 1987; Yang and Sessler, 1992; Song *et al.*, 1997; Liufu *et al.*, 1998; Sessler and Yang, 1999; Sessler *et al.*, 2004; Kao, 2004; Touzin, 2006; Cornet *et al.*, 2008; Wang, 2009; Fitting, 2010). For the decay models (which are far more prevalent), we have used the ideas in Toomer and Lewis (1980), Sessler (1987), Aragoneses *et al.* (2008), Watanabe *et al.* (1987), Chen (2010), Perrin (2005), Dissado and Fothergill (1992), Griseri *et al.* (2006), and Berlepsch (1985b).

5.3. Charging Models

The final result of Section 5.2 was that we can treat the SEE-SVP system as essentially a parallel plate capacitor. The theoretical framework to understand charge transport in HDIM when charge is

injected was developed in Chapter 4. As we show, little modification to the results of Chapter 4 is needed to predict the charging of an HDIM under electron beam irradiation. In Section 4.3, the transport equations are used to develop a simple model for the charging of an insulator due to injected electrons. Sections 4.3-4.6 present information essential before continuing with this chapter. Specifically, the key result of Section 4.3 is the charging equation,

$$\frac{dn_t(t)}{dt} = \frac{s_c J_s(t)}{q_e}[N_t - n_t(t)]. \tag{5.3.1}$$

Equation (5.3.1) is a differential equation that predicts the change in the trapped charge distribution, $n_t(t)$, as a function of time and total DOS, N_t, and a surface injection current density, $J_s(t)$. This equation has been used by many authors to investigate a wide array of charging and ESD phenomena. A few key authors are listed for the interested reader: electron emission (Sessler, 1987; Touzin, 2006; Cornet *et al.*, 2008; Fitting, 2010), capacitive methods (Kao, 2004), capacitive methods and ESD (Liufu, 1998), charging by radiation (Fowler, 1956), impact ionization and transport (Avini, 1987), capture and emission (DiMaria, 1975), ESD and charge trapping (Nissan-Cohen, 1986), trapping and detrapping dynamics (Nissan-Cohen, 1986), and photoconduction (Orenstein and Kastner, 1981). In this chapter, we apply Eq. (5.3.1) to obtain an expression for the current density at the rear electrode and surface potential due to irradiation. The solution of Eq. (5.3.1) is computed in Chapter 4; originally Eq. (4.3.15)

$$n_t(t) = N_t exp\left[\frac{-s_c\int_0^t J_s(\acute{t})d\acute{t}}{q_e}\right]\int_0^t exp\left[\frac{-s_c\int_0^{\acute{t}} J_s(\tilde{t})d\tilde{t}}{q_e}\right]\frac{s_c}{q_e}J_s(\acute{t})d\acute{t}. \tag{5.3.2}$$

Equation (5.3.2) describes the number of trapped electrons as a function of time. In order to solve this equation, one needs an expression for the injection current density, $J_s(z,t)$. The injection current density for the SVP system is not the same as for the CVC system of Chapter 4. This is suggested first by the depth dependence, z, which is not required in the CVC model, and results here from the fact that electrons penetrate into the sample with a range, *R*, which decreases as the trapped charge distribution grows. A comprehensive discussion of the dependence of $J_s(z)$ on the incident carrier penetration depth, *R*, is given in Touzin (2006). This spatial dependence is ignored here in order to arrive at a simple analytical expression for the injection current as a function of time. An investigation to connect the work of Walden (1971) (see Section 4.4) and Touzin (2006) is left as future work (see Hodges, 2013).

The derivation of Eq. (5.3.3), presented in Section 4.4, is the same, although the interpretation of the variables changes. The discussion of Section 4.4 developed a current density injection function, Eq. (4.4.10):

$$J_s(t) = J_0\left(1 + \frac{t}{\tau_{onset}}\right)^{-m} + J_{sat}. \tag{5.3.3}$$

The variable, J_0, is defined there as the initial current density provided by the battery to the HDIM under test, m was a positive power, τ_{onset} was the characteristic time for onset of the reduced injection current density, and J_{sat} was a saturation current density. The meaning of J_0 (in the SVP system) is not the same as it was in the CVC system. The initial current density must be scaled by the electron yield, since some of the PEs are emitted from the sample surface as SEs or BSEs. Therefore, as a first order approximation, we let $J_0 \rightarrow J_b\left(1 - \sigma_{yeild}\right)$, where J_b is the current density of the incident electron beam. The saturation current has a similar meaning in this context. In Chapter 4, J_{sat} was that conduction current density that existed after the trap filling process completed; or, stated another way, the part of the current created by electrons that made their way into the conduction band. The displacement current—due to the changing trapped charge generated electric field—will decrease with time, asymptotically approaching the saturation current. The SVP system can take data on both the conduction current during irradiation and the surface potential. Thus, this displacement current should be easy to characterize in the SEE-SVP system, unlike in the CVC system where control over the number of injection electrons does not exist. Making the correction to the injection current density function, Eq. (5.3.3) becomes

$$J_s(t) = J_b\left(\sigma_{yeild} - 1\right)\left(1 + \frac{t}{\tau}\right)^{-m} + J_{sat}. \tag{5.3.4}$$

A similar result to Eq. (5.3.4) has been found for coronal electrons charging of HDIM; using a very different formalism and Laplace transform methods; Ferreira and de Almeida (1997) has shown for an exponential DOS with dispersion parameter, $\alpha(T) = \frac{T_0^e}{T}$, the total injected current density for long times should be given by $J_s(t) = \frac{CV_0}{(\alpha(T)-1)!}t^{\alpha(T)-1}$. This equation bears a strong resemblance to Eq. (5.3.4). In fact, it suggests that there is a connection between the power, *m*, in Eq. (5.3.4) and the dispersion parameter, $\alpha(T)$. This connection has also been partially investigated by Wintle (1974b) and Hodges (2013), though their results are difficult to apply in this case. If a physically sound connection between *m*

and the DOS can be established, it will provide an excellent means by which to characterize a samples DOS type. An investigation of the connection between these two exponents is left as future work. Ferreira and de Almeida (1997) notes that for the full expression with dispersive character, there can be an increase in the current density when $\alpha > 1/2$. The effects of dispersion in the charging processes should be negligible as long as the dispersion is not too strong. Hytrel™ might be an exception (Hart *et al*., 2007). In this work, the description of charging current density and surface potential, studied by the USU MPG, involves only a nondispersive model. For a more detailed expression and inclusion of the dispersive regime (equivalent to including the energy dependence of the DOS) see Ferreira and de Almeida (1997), Sessler and Yang (1999), Gross (1974), Monroe (1983), Wintle (1999) and Montanari and Morshuis (2005).

The first step in creating a complete description of the charge build up that includes dispersive behavior is to extend Eq. (5.3.4) to include energy dependence. This is easily done using the transport equations Eqs. (4.3.6) and (4.3.7), as presented in Chapter 4 to obtain

$$\frac{dn_t(t)}{dt} = \frac{s_c J_s(t)}{q_e}[N_t - n_t(t)] - \nu_{te} \int exp\left[-\frac{\varepsilon}{k_b T}\right] n_t(\varepsilon, t) d\varepsilon. \tag{5.3.5}$$

In Eq. (5.3.5), $N_t = \int N_t(\varepsilon) d\varepsilon$ is the total DOS and ν_{te} is a attempt-to-escape factor. The last term on the RHS determines the release rate of trapped electrons at a specific energy integrated over the width of the DOS distribution. Inclusion of this term is equivalent to having a spread in the release times of the trapped electrons (i.e., there is a dispersion in the release times and, therefore, the electron transport). When dispersive transport is significant the inclusion of the last term is necessary. In general, dispersive transport occurs on timescales much longer than are required to charge up the sample. We, therefore, omit Eq. (5.3.5) from this discussion.

5.3.1. Charge Trapping

We begin with Eq. (5.3.2)—which gives the number of trapped electrons as a function of time—and the charge injection function, $J_s(t)$. Equation (5.3.2) was left in a general form in Section 4.3, so that we could develop an expression for the charge injection function; it is presented again here for reference:

$$n_t(t) = N_t exp\left[\frac{-s_c \int_0^t J_s(\acute{t}) d\acute{t}}{q_e}\right] \int_0^t exp\left[\frac{-s_c \int_0^{\acute{t}} J_s(\tilde{t}) d\tilde{t}}{q_e}\right] \frac{s_c}{q_e} J_s(\acute{t}) d\acute{t}.$$

Inserting Eq. (5.3.4) into Eq. (5.3.2) and completing the integration, an expression for the time-dependent density of trapped electrons is found to be

$$n_t(t) = N_t\left(1 - exp\left[\frac{s_c J_b\left(1-\sigma_{yield}\right)\tau_{onset}}{q_e(1-m)}\left(1 - \left[1 + \frac{t}{\tau_{onset}}\right]^{1-m}\right)\right]\right). \tag{5.3.6}$$

Equation (5.3.6) has the expected behavior for the density of trapped electrons as a function of time. At $t = 0$, Eq. (5.3.6) is zero and as $t \to \infty$ it gives N_t. (Recall that σ_{yeild} is less than 1 for the energies considered and that the power, m, is constrained to be between zero and one.) A simple time-dependent exponential is obtained when $m = 0$, consistent with case where the trap filling and release are on the same order (Wintle, 1974b); thus the equilibrium injection rate is reached in a time, $\tau_{onset}(m = 0) = \left(s_c J_b\left(1 - \sigma_{yeild}\right)/q_e\right)^{-1}$. Another possible explanation could be to consider the physics of the injection mechanism itself. For $m = 0$, there is essentially no injection time dependence and carriers go directly to trap states so that the DOS fills very quickly. For the case where $m \sim 1$, the time to charge up to equilibrium is nearly infinite; this is consistent with a long thermalization time of the injected carrier distribution, common in most HDIM (see Chapter 3). Applying the alternate explanation to the $m = 1$ case, the injection function is found to be dominant and carriers do not fill trapped states quickly. If we assume that the slow injection is caused by the DOS, then it would seem that only shallow trap states fill in the early time of thermalization, suggesting that the demarcation energy takes a very long time to descend into the DOS, indeed. These conjectures are left as future work. Once the trapped charge distribution—given by Eq. (5.3.6)—is known, a number of calculations can be done; these include time-dependent surface potential, time-dependent electric field in all parts of the sample, and conduction electron density.

Given Eq. (5.3.6) and the transport equations from Section 4.3, a simple model that describes the bulk transport of the injected electron distribution can be developed. Consider the simplified equation for the sum of the current densities (refer to Eq. (4.6.3) and the development that followed)

$$J_{tot}(t) = J_d(t) + J_p(t) + J_c(t). \tag{5.3.7}$$

Here the total current is the sum of the displacement, polarization, and conduction currents (or just drift current). As before, we do not consider polarization or diffusion as: (*i*) there is no strong polarizing electric field, and (*ii*) injected charges are strongly trapped, therefore, diffusion is negligible. The conduction current density is negligible—when compared to the effects of the change trapped charge

distribution—until equilibrium is established. Once the trapped states reach an equilibrium value and the current becomes nearly constant, one is observing only the conduction current density; this is equivalent to saying that the DOS is saturated and is, therefore, called the saturation current density, J_{sat}.

The majority of the time dependence in the observed current is due to the buildup of the trapped charge distribution. The change in the trapped charge distribution is directly related to the change in the electric field due to the trapped charge distribution, $\frac{\partial F_t(t)}{\partial t}$, and is a displacement current. Using Eq. (4.3.5) and eliminating the polarization and conduction current density components, the displacement current is given by

$$J_d(t) = -\epsilon_0 \epsilon_r \frac{\partial F_t(t)}{\partial t}. \tag{5.3.8}$$

Using Eq. (4.4.3), with the appropriate range equation and Eq. (5.3.8), an expression for the displacement current can be found:

$$J_d(t) = -q_e \frac{\partial n_t(t)}{\partial t}\big(d - R(\varepsilon_b)\big). \tag{5.3.9}$$

Using Eq. (5.3.6) an expression for the change in the trapped charge distribution can be found:

$$\frac{\partial n_t(t)}{\partial t} = \frac{s_c J_b (1-\sigma_{yield}) N_t}{q_e}(1 + t/\tau_{onset})^{-m} exp\left\{\frac{s_c J_b (1-\sigma_{yield})\tau_{onset}}{q_e(1-m)}\left(1 - \left(1 + \frac{t}{\tau_{onset}}\right)^{1-m}\right)\right\} \tag{5.3.10}$$

Equation (5.3.10) has the correct dimensions of carriers per unit area per unit time. Equation (5.3.10) and Eq. (5.3.9) give an expression for the displacement current due to the trapped charge distribution:

$$J_d(t) = J_b\left(1 - \sigma_{yield}\right) N_t s_c [d - R(\varepsilon_b)]\left(1 + \frac{t}{\tau_{onset}}\right)^{-m} exp\left\{\frac{s_c J_b (1-\sigma_{yield})\tau_{onset}}{q_e(1-m)}\left(1 - \left(1 + \frac{t}{\tau_{onset}}\right)^{1-m}\right)\right\}. \tag{5.3.11}$$

Here the product of the total DOS, capture cross section and length, $N_t s_c\big(d - R(\varepsilon_b)\big)$, is unitless, so that the dimensions of Eq. (5.3.11) are just current density, or charge per unit area. Equation (5.3.11) describes only the displacement current due to the changing trapped charge distribution. Using Eq. (5.3.7) for the sum of current densities and adding the saturation current density, J_{sat}, we arrive at the USU MPG charging model:

$$J_{tot}(t) = J_b\left(1 - \sigma_{yeild}\right) s_c N_t d\left[1 - \frac{R(\varepsilon_b)}{d}\right]\left(1 + \frac{t}{\tau_{onset}}\right)^{-m} \times exp\left\{\frac{s_c J_b (1-\sigma_{yield})\tau_{onset}}{q_e(1-m)}\left[1 - \left(1 + \frac{t}{\tau_{onset}}\right)^{1-m}\right]\right\} + J_{sat}$$

{USU MPG SVP Current Density Charging Model}. (5.3.12)

This model is not applied to data in this dissertation and its application must wait for future work. In the next section, the SVP surface potential equation is developed, which can be used in conjunction with Eq. (5.3.12) to study the nature of charge transport in HDIM responding to nonpenetrating electron beam radiation.

5.3.2. Surface Potential

We now want to make contact with the measured surface potential as a function of time that results from the charging process. Starting with (*i*) Poisson's equation, Eq. (4.3.2), for the trapped charge density, $q_e n_t$, and (*ii*) the assumption that the electric field due to the trapped charge distribution dominates the electric field at the surface of the HDIM, we find that

$$\epsilon_0 \epsilon_r \frac{dF_t(z,t)}{dz} = q_e n_t(z,t). \tag{5.3.13}$$

Since the movement of the charge distribution across the sample is much slower than the change in electric field due to the trapped charge distribution (Weaver *et al.*, 1977; Liufu, 1998; Griseri *et al.*, 2006; Dissado *et al.*, 2006), one can separate the spatial and time-dependent parts of Eq. (5.2.13) to obtain

$$\epsilon_0 \epsilon_r \frac{dF_t(z,t)}{dz} = q_e n_t(z) n_t(t). \tag{5.3.14}$$

Consider over what spatial range we should integrate this equation over to obtain the time-dependent field. The distribution of trapped carriers exists only in the region $R(\varepsilon_b) < z < d$, between the upper surface and the penetration depth (where $z = 0$ at the surface and $z = d$ at the collecting electrode). A very simple assumption is made here that the distribution of trapped carriers is uniform over this region. (This assumption is not consistent with Fig. 5.1, as it displays a much more realistic charge distribution.) This is not an accurate model and should be extended to represent the true spatial extent and character. An excellent starting point can be found in Touzin (2006), Sessler (1987), and Cazaux (2004). There are no trapped electrons in the region $R(\varepsilon_b) < z < d$ (e.g., there are no trapped charges in the region from $z = R(\varepsilon_b)$ to $z = d$). To simplify the integration, we assume a step function so that $n_t(z) = \Theta[\mathrm{z} - \mathrm{R}(\varepsilon_\mathrm{b})]\Theta(\mathrm{z} - d)$, which constrains the charge to the region of interest. Then

$$F_t(t) = \frac{q_e n_t(t)}{\epsilon_0 \epsilon_r} \int_0^{R(\varepsilon_b)} n_t(z) dz\,, \tag{5.3.15}$$

which upon integration gives

$$F_t(t) = \frac{q_e n_t(t)}{\epsilon_0 \epsilon_r} R(\varepsilon_b). \tag{5.3.16}$$

Equation (5.2.18) describes the electric field created by the deposited charge distribution. The field extends in the positive and negative z direction away from the trapped charge distribution in both directions. We now directly employ our assumption that the deposited charge distribution can be treated as a plane of charge with uniform spatial extent in the x and y directions, and positioned at $z = R(\varepsilon_b)$. Recall in Section 5.2 we discussed the assumptions, the key one being that we can treat the SVP system as a parallel plate capacitor in the region $R(\varepsilon_b) < z < d$. The physical picture for the SVP is exactly the same as that for the CVC system given by Fig 4.1. Parallel plate capacitors act largely as if they have uniform electric fields between their plates, assuming that the geometry does not change. To estimate the surface potential, however, we must make one very poor assumption; that the field between the plates is the same as that at the surface. This is not realistic, but has been applied by many authors see (Cazaux, 1999; Hodges, 2013). We seek a simple analytical model for the surface potential at $z = 0$. Then estimating the potential between the collecting electrode and our charge distribution follows from Eq. (5.3.16) and $[d - R(\varepsilon_b)]F_t(t) = V(t)$ to obtain

$$V_s(t) = \frac{q_e n_t(t)}{\epsilon_0 \epsilon_r}[d - R(\varepsilon_b)]R(\varepsilon_b) = \frac{q_e n_t(t) R(\varepsilon_b) d}{\epsilon_0 \epsilon_r}[1 - R(\varepsilon_b)/d]\,. \tag{5.3.17}$$

The accuracy of our calculation can be improved successively by selecting more realistic descriptions of the spatial extent of our charge distribution (i.e., (*i*) a delta function, which places the planar charge distribution at $z = R(\varepsilon_b)$, and (*ii*) a Gaussian distribution, which allows the charge to have some spatial extent in the z direction). The extension of Eq. (5.3.17) to more realistic charge distributions is left as future work. Equation (5.2.17) connects the number of trapped carriers and the energy-dependent range of electrons to the surface potential at the surface of the sample. For very early times, nearly all of the electrons will be absorbed into trapped states and $n_t(t) \approx n_{inj}(t)$, so that we may estimate the surface potential for short timescales. Recall the definition of current density, $J = Q/(A \times t)$. Then by setting $q_e n_t(t) d \approx \frac{q_e n_e(t) t R(\varepsilon_b)}{t} \approx J_0 t$, using this estimation with Eq. (5.3.17) suggests that the surface potential is $V_s(t) = \frac{J_0 t}{\epsilon_0 \epsilon_r} d\left[(1 - \frac{R(\varepsilon_b)}{d})\right]$ for very short times. One might ask what is meant by short

timescales? This equation is valid as long as the time-dependence of the potential is linear; even for a nonlinear system, there is some very short timescale where the potential will be approximately linear. We also know that the surface potential asymptotically approaches a constant value, given by Eq. (5.3.17). However, we still need a general nonlinear description of the surface potential to understand to what final value the material with charge and the shape of the surface potential curve for intermediate times.

Using Eq. (5.3.6), an extended expression for the surface potential can be written, which takes into account a changing charge injection function and the nonlinear nature of the charging process

$$V_s(t) = \frac{q_e N_t R(\varepsilon_b)}{\epsilon_0 \epsilon_r} d \left[(1 - \frac{R(\varepsilon_b)}{d})\right] \left\{1 - exp\left[\frac{s_c J_b (1-\sigma_{yield}) \tau_{onset}}{q_e (1-m)} \left(1 - \left[1 + \frac{t}{\tau_{onset}}\right]^{1-m}\right)\right]\right\}. \quad (5.3.18)$$

We have included the dependence of both the range, $R(\varepsilon_b)$, and the total yield, $\sigma_{yield}(\varepsilon_b)$, on the incident beam energy in Eq. (5.3.18) for completeness. This model can be extended to an incident energy and spatially-dependent model using the range function developed by Wilson and Dennison (Touzin, 2006; Cornet *et al.*, 2008; Wilson and Dennison, 2010; Fitting, 2010).

Equation (5.3.18) expresses the surface potential in terms of time, penetration range of the incident PEs, a DOS, SEE yield, the indecent beam energy, and beam current density. A very useful set of connections can be made through the work of Hoffmann (2010) and Thomson (2004) that primarily focused on electron emission and material charging. In particular, the total yield is approximated in Thompson as

$$\sigma_{yield}(t) = 1 + (\sigma_{initial} - 1) \exp(-C J_b t). \quad (5.3.19)$$

The variable, J_b, is the beam current density, C is a constant, and $\sigma_{initial}$ is the uncharged yield. Both Hoffmann and Thompson give expressions for the surface potential; Hoffmann greatly extends this discussion. The surface potential is given as

$$V_s(t) = \frac{Q_{accumulated}\left(1-\sigma_{yield}(t)\right) d}{A_{beam} \epsilon_0 \epsilon_r}. \quad (5.3.20)$$

Here, $Q_{accumulated}$ is the accumulated charge incident on the sample, and A_{beam} is the area of the incident electron beam on the sample. Using Eqs. (5.3.19) and (5.3.20), a time-dependent expression for the surface potential can be obtained:

$$V_s(t) = \frac{Q_{accumulated} d (1-\sigma_{initial}) \exp(-C J_b t)}{A_{beam} \epsilon_0 \epsilon_r}. \quad (5.3.21)$$

Equation (5.3.21) bears a strong resemblance to Eq. (5.3.18), but they come from very different theoretical perspectives. In addition, Eq. (5.3.21) is an approximation; it would seem clear that future work should investigate this connection. It is the belief of this author that once this connection is made clear, a great deal about the true nature of surface charging in HDIM under electron irradiation will be understood. In particular, a great deal was washed under the rug in Section 5.2 to present the concept that the SVP system acts largely like a simple parallel plate capacitor; while these are reasonable assumptions, the SEE theory presented in Thomson *et al.* (2004), Hoffmann (2010), and Hodges (2013) gives a great deal of theoretical detail regarding the physics of electron interactions in the region between the surface and the deposited charge distribution. In addition to these ideas, recent work has produced numerical models with what seems to be excellent predictive power using both the charge trapping equations presented in this work and the ideas of SEE; the interested reader should see Cornet *et al*. (2008), Fitting (2010), and Sessler (1987).

Despite the rather large number of approximations and exclusion of processes in the development of Eq. (5.3.18), it does rather well in determining the surface potential due to irradiation by an electron beam. It will be shown in the analysis section below this model provides values for physical parameters that are in reasonable agreement with the literature and previous applications.

5.4. Decay Model

In the first part of this chapter, the charging of an HDIM due to incident electrons is presented and models for the current density at the rear collecting electrode, along with the surface potential, are developed. In this section, the model for the decay of the deposited charge after the cessation of the electron beam is presented. Consider again Fig. 5.1 and how it will change when the electron beam is shut off. First, all the electron transport behavior in regions (e), (f), and (j) will cease and some of the charge imbalance will dissipate. The electron emission and RIC processes stop quickly—for modest beam energies and penetration depth—and largely the region above the deposited charge distribution will quickly come to equilibrium on a timescale much shorter than that required to dissipate the deposited charge. The measured current density at the rear collecting electrode and surface potential are then a direct result of changes in the trapped electron distribution, whether by release of electrons into the CB and subsequent re-

capturer forming a conduction current or by movement of the charge distribution toward the rear collecting electrode via the same detrapping and re-trapping processes. In order to estimate the material parameters and general form of the decay of deposited charge, we present a model originally developed by Toomer and Lewis (1980) and then extended by Aragoneses *et al.* (2008) using the work of Ferreira and de Almeida (1997) to include the effects of dispersive transport. The model of Aragoneses is extended in this dissertation, with an explicit derivation of all the physical parameters originally presented in Aragoneses *et al.* (2008) to which we add a physically motivated dispersion term. This surface potential decay model—from this point on called the SVP decay model—is based on simple injection into the conduction band states, bulk transport properties, and is governed by a simplified set of transport equations. The basic form and solution of the equations can be found in Orenstein *et al.* (1982), Berlepsch (1985b), Molinie (2005), Toomer and Lewis (1980), and Aragoneses *et al.*(2008).

The initial injection profile is a complicated trap controlled process, which has been modeled in the charging section of this chapter. We assume an initial surface voltage and develop the time-dependent surface potential decay based on the ideas of electron trapping, detrapping, and their effects on electron mobility. In the experiments conducted at USU, there is no externally applied electric field, and therefore, the transport of electrons to the collecting electrode for the trapped charge distribution is governed by the self-field between the collecting electrode and the deposited charge distribution. We leave the application of an externally applied field to future work.

The SVP decay model is derived for a single discrete energy level of bulk electron traps resulting from the disordered DOS [effectively a delta function (see Table 2.1)]. In order for the SVP decay model to be valid, the temperature cannot vary, so that the energy level of active traps responsible for the observed decay remains nearly constant. This last statement is equivalent to stating the trapped electron distribution will act as though there is a single energetic level in the DOS. In the analysis on LDPE by Toomer and Lewis (1980), there is often more than one term in the sum of possible states contributing to the observed decay, thus correcting for changes in the active region of the DOS. In our derivation, we will show why the Toomer equations worked and show that certain terms assumed to be simple constants in the Aragoneses treatment are, in fact, functions of temperature.

The derivation of the SVP decay model is more complex than that of the charging model, and we, therefore, give an outline of the derivation to guide the reader. First, we use Poisson's equation, the charge density, and continuity equation to get the rate of change in surface potential. Second, we introduce the trap controlled mobility that will allow the derivation of the final expression for the surface potential as a function of the time-dependent mobility; this completes the derivation of the Toomer and Lewis model. Third, we extend the form of the surface potential model due to Toomer to incorporate the dispersive mobility. This is done by solving the transport equations, showing equivalence to the solution of Toomer and finally correcting the theory with the new dispersive term. A discussion of the action of single level versus distributed level DOS is given and an estimation of the material conductivity presented.

5.4.1. Surface Potential Decay

In this section, a derivation connecting the surface potential, maximum (initial) charging potential, $V(t = 0) = V_0$, and the effective mobility is presented. The result of this derivation is an equation for the rate of change in the surface potential due to a time-dependent change in the effective mobility. The mobility is characterized as the ratio of carrier trapping time to the sum of the release and trapping time. That is, since the effective mobility is a trap-controlled process, we can understand the dynamics of the system by studying the effective mobility (sometimes called the trap-controlled mobility).

We begin with Poisson's equation (in a common form), the continuity equations, and derive a simple expression for the surface potential as a function of carrier mobility. Consider Poisson's equation, in one-dimensional geometry:

$$\frac{d^2}{dz^2}V_s(z,t) = -\frac{\rho_{tot}(z,t)}{\epsilon_0\epsilon_r}. \tag{5.4.1}$$

As it turns out, this expression is more useful if it can be cast in the form of a time-varying surface potential. Taking the derivative of both sides with respect to time and integrating twice in the spatial coordinate, z, over the thickness of the sample, we have

$$\frac{d}{dt}V_s(t) = -\frac{1}{\epsilon_0\epsilon_r}\int_0^d\int_0^z \frac{d}{dt}\rho_{tot}(\acute{z},\mathrm{t})d\acute{z}dz. \tag{5.4.2}$$

Consider the continuity equation with the current density replaced by $J_c(\mathrm{t}) = q_e n_e \mu_{trap}(t) F_t(z,t)$, where the internal electric field must be $F_t(z,t)$ as there are no other sources. Then, the continuity equation becomes

$$\frac{\mathrm{d}}{\mathrm{dt}}\rho_{\mathrm{tot}}(\mathrm{z},\mathrm{t}) = -q_e n_e \mu_{\mathrm{trap}}(t)\frac{\partial F_t(z,t)}{\partial \mathrm{z}}. \tag{5.4.3}$$

We have assumed that the mobility and density of charge carriers are not spatially-dependent. This assumption works because it is the mobility of the trapped charge distribution that determines the transport and has a spatial dependence that is very weak, when compared with the time dependence of the electric field. The position of the electric field does strongly influence the transport dynamics and cannot be ignored. In order to solve Eq. (5.4.3), we also need a definition for the trap controlled mobility:

$$\mu_{trap}(t) \equiv \frac{\mu_0 n_e(t)}{n_e(t)+n_t(t)}\,. \tag{5.4.4}$$

Further, the relationship of the charge density to the free and trapped electron distribution is

$$\rho_{tot}(x,t) = q_e\big(n_e(z,t) + n_t(z,t)\big). \tag{5.4.5}$$

By combining Eqs. (5.4.2) through (5.4.5), we obtain the following expression for the rate of change in the surface potential as a function of the trap-reduced mobility and electric field

$$\frac{d}{dt}V_s(t) = \mu_{trap}(t)\int_0^d F(z,t)\frac{dF_t(z,t)}{dz}dz. \tag{5.4.6}$$

Applying integration by parts, one gets

$$\frac{d}{dt}V_s(t) = \frac{\mu_{trap}(t)}{2}\big(F^2(d,t) - F^2(0,t)\big). \tag{5.4.7}$$

Equation (5.4.7) describes the connection between the electric fields at the collecting electrode and the surface of the sample, the trap-controlled mobility, and the temporal change in the surface potential. The field at the collecting electrode is zero, as that is the termination point for the field lines extending from the trapped charge distribution to the collecting electrode. To first order, the initial potential is $V_0 \approx F(d,0)/d$; this assumes that the depth of the charge distribution from the surface of the material, R, is much less than the sample thickness, d. The electric field in Eq. (5.4.7) clearly has a time-dependent component. The derivation of Eq. (5.4.7) is presented by many authors and in all of those papers the authors assume that the electric field time dependence can be ignored in favor of a constant electric field (Toomer and Lewis, 1980; Berlepsch, 1985b; Sessler, 1987; Molinie, 2005; Aragoneses *et al.*, 2008). There

is no clear way this author can see that this assumption is true. Ferreira and de Almeida (1997) state this assumption, and its basis, and develop a more complete solution for the surface potential, which differs only slightly from the solution we obtain. The solution of Ferreira is complex and requires a lengthy mathematical treatment; we therefore, use the simpler approach by the authors listed above, which retains all the important features of the model. Further, we use a secondary analysis to develop the dispersive transport term in our SVP decay mode, which was originally found by Ferreira and de Almeida (1997). It is true that the change in the electric field, and therefore the potential, is controlled by the time-dependent trap-controlled mobility. If one makes this assumption and further assumes that the product electric field times the mobility is controlled by the mobility, the following equation can be found using Eq. (5.4.7):

$$\frac{d}{dt}V_s(t) = \frac{-\mu_{trap}(t)}{2}\frac{{V_0}^2}{d^2}. \tag{5.4.8}$$

While this equation is clearly a first-order estimate, its interpretation is physically sensible and consistent with the work of Ferreira and de Almeida (1997). We should expect that the change in surface potential is controlled by a time- and field-dependent trap-controlled mobility. Toomer and Lewis (1980) take the surface DOS into account and the injection of charge adjusted by a ratio of surface to bulk states. This is done because in corona charging, many of the electrons will stay in surface states, which therefore has an impact on the decay. We assume perfect injection, and therefore, remove this analysis. For the beam energies involved—those greater than the second crossover energy—this should be a good assumption. However, for much lower energies and penetration depths, the distribution of energy states may need to be considered. In the analysis of LDPE data by Toomer and Lewis (1980), nearly perfect injection is assumed while using low-incident electron energies to charge the sample. We get reasonable agreement with their data (see analysis in this section), which offers limited support for this approximation.

5.4.2. Pre-transit Model

Equation (5.4.8) describes the rate of change in the surface potential as a function of time. Now a description of the trap-controlled mobility is needed to estimate the change in the surface potential. Consider the conductivity, which in turn is related to the time dependence of carriers in traps, and can be written as

$$\sigma_{material} = q_e n_e(t)\langle\mu(t)\rangle, \tag{5.4.9}$$

where $\langle\mu(t)\rangle$ is an (time) averaged mobility (Orenstein *et al.*, 1982). The problem has now been reduced to solving for the time-dependent mobility

$$\mu_{trap}(t) = \frac{\mu_0 n_e(t)}{n_e(t)+n_t(t)}. \tag{5.4.10}$$

The sum of the conduction carriers and the trapped carriers, $n_e(t) + n_t(t)$, is the total charge in the system, N_{inj}. As long as the charge body does not make contact with the grounded rear electrode, all the charge is basically still in the material, and using Eq. (5.4.10), we can write

$$\langle\mu(t)\rangle = \mu(t) = \frac{\mu_0 n_e(t)}{N_{inj}}. \tag{5.4.11}$$

Here, N_{inj} is the initial injected current density at the time when the electron beam was turned off. Now the problem is reduced to simply finding the number of carriers in the conduction band when recombination is not present, meaning that we do not have to include any positive charge distribution with which the electrons could recombine. This problem was solved for discrete and exponential DOS distributions by Orenstein *et al.* (1982), using the transport equations presented Section 2.6. In order to simplify the discussion, we need to write the transport equations in a slightly different form than was presented in Chapter 4. In the SVP decay model, recombination is ignored and it is assumed that the DOS is a delta function. Applying these assumptions to Eqs. (2.6.3) and (2.6.4), one gets

$$\frac{dn_e(t)}{dt} = N_{inj} - \alpha_{et}\, n_e(t)[N_t - n_t(t)] + \alpha_{te} N_e n_t(t), \tag{5.4.12}$$

and

$$\frac{dn_t(t)}{dt} = \alpha_{et}\, n_e(t)[N_t - n_t(t)] - \alpha_{te} N_e n_t(t)\,. \tag{5.4.13}$$

Recall from Section 2.5 that the frequencies at which electrons are captured and released are, respectively, $v_{et} = s_c v_T\big(N_t - n_t(t)\big) = \alpha_{et}\big(N_t - n_t(t)\big)$ and $v_{te} = s_c v_T N_e = \alpha_{te} N_e$. Inserting these definitions in Eqs. (5.4.12) and (5.4.13), we have

$$\frac{dn_t(t)}{dt} = -v_{te} n_t(t) + v_{et} n_e(t), \tag{5.4.14}$$

and

$$dn_c(t)/dt = +v_{te} n_t(t) - v_{et} n_e(t) + N_{inj}\delta\big(t_{beam\ off}\big). \tag{5.4.15}$$

The last term in Eq. (5.4.15) adds the initial injected charge at the instant the beam is turned off and the decay experiment begins. In order to solve this system of equations for the ratio of free electron density to

the total injected electron density and obtain an estimate of the trap controlled mobility, we employ the method of Laplace transforms to obtain

$$s\tilde{n}_t(s) = -\nu_{te}\tilde{n}_t(s) + \nu_{et}\tilde{n}_e(s), \tag{5.4.16}$$

and

$$s\tilde{n}_e(s) = +\nu_{te}\tilde{n}_t(s) - \nu_{et}\tilde{n}_e(s) + N_{inj}. \tag{5.4.17}$$

Here *s* is the Laplace integration variable. Some algebra yields the following solution:

$$\frac{\tilde{n}_e(s)}{N_{inj}} = \frac{1}{s\left(1+\frac{\nu_{et}}{\nu_{te}+\nu_{et}}\right)}. \tag{5.4.18}$$

The inverse Laplace transform of this equation is

$$\frac{n_e(t)}{N_{inj}} = \frac{\left(\nu_{te}+\nu_{et}e^{-(\nu_{te}+\nu_{et})t}\right)}{\nu_{te}+\nu_{et}}. \tag{5.4.19}$$

Substitution of Eq. (5.4.19) into the mobility expression Eq. (5.4.11) yields

$$\mu(t) = \mu_0\frac{\left(\nu_{te}+\nu_{et}e^{-(\nu_{te}+\nu_{et})t}\right)}{\nu_{te}+\nu_{et}}. \tag{5.4.20}$$

Equation (5.4.20) is the expression for the trap-controlled mobility obtained by Toomer and Lewis (1980), Berlepsch (1985b), and Aragoneses *et al.* (2008). In the work done by Toomer and Berlepsch, the solution was obtained by direct integration; in the case of Aragoneses *et al.* (2008) and Molinie (2005), it was found by Laplace transform. Having this expression now allows for the time integration of the rate of surface potential decay equation:

$$\frac{d}{dt}V_s(t) = -\frac{\mu_0}{2}\frac{\left(\nu_{te}+\nu_{et}e^{-(\nu_{te}+\nu_{et})t}\right)}{\nu_{te}+\nu_{et}}\frac{{V_0}^2}{d^2}, \tag{5.4.21}$$

which upon integration, yields

$$V_s(t) = V_0 - \mu_0\left(\frac{V_0}{2d^2(\nu_{te}+\nu_{et})}\right)^2\left(\nu_{te}t + \frac{\nu_{et}}{\nu_{te}+\nu_{et}}\left(1-e^{-(\nu_{te}+\nu_{et})t}\right)\right). \tag{5.4.22}$$

This is the model of Toomer, as it is presented in Aragoneses. Equation (5.4.22), however, only describes the drift component of the decay at a single trapping and detrapping level. The contribution of Aragoneses was to extend this model to include an expression for dispersive transport, using a model developed by Ferreira and de Almeida (1997). As it turns out, the analysis required to derive the dispersive term–for an exponential DOS–clarifies constants, which were not explained in the work of Aragoneses or

Ferreira. Further, having done the complete derivation of the dispersive component, one can extend the analysis to include the other DOS models presented in Chapter 2, Table 2.1.

In the previous analysis, it is assumed that the DOS acts at one level (a delta function DOS). We now lift this constraint to derive the expression for a dispersive surface potential behavior. The excitation rate when the beam is off is driven by thermal processes and local fields. For the present, we analyze only the thermally driven process (i.e., the low field limit). This means that the release frequency is now a temperature- and energy-dependent process. We further assume that a MB distribution can be employed to estimate the excitation rate or trapped electrons to the CB; in this case, the rate of release is given by

$$v_{te}(\varepsilon) = v_{te} exp[-\varepsilon/k_b T]. \tag{5.4.23}$$

An expression for the ratio of free electrons to total charge was found in Eq. (5.4.18); the same analysis can be applied to obtain a similar multiple discrete or continuous expressions (see Toomer and Lewis (1980) or Orenstein *et al.* (1982) for details). Toomer and Lewis (1980) suggest that we can modify Eq. (5.4.18) to include the effects of many discrete levels in the following way:

$$\frac{\tilde{n}_e(s)}{N_{inj}} = \frac{1}{s\left(1+\sum_i \frac{\nu^i_t C^i_{tot}}{\nu^i_r + \nu^i_t}\right)}. \tag{5.4.24}$$

In Eq. (5.4.24), the superscripts i are for the i^{th} trap and the value of C^i_{tot} is a ratio of total trapped carriers to those trapped at a particular level, i. There are many applications where the use and analysis of multiple discreet DOS is very useful; see Monroe (1986) and Schmidlin (1977) for a detailed discussion of the transition from multiple discreet states to a continuous distribution.

In HDIM, the amorphous nature of the material lends itself to a distributed set of traps or groups of distributed traps spread across the band gap. In a dispersive system, the distribution of states is exponential or Gaussian. Thus, we need a continuous energy-dependent description of the ratio, $\tilde{n}_c(s)/N_{inj}$, which can be obtained directly from the transport equations, Eqs. (2.6.3) and (2.6.4), or by letting the sum in Eq. (5.4.24) become an integral and assuming the energetic forms for the release and trapping rates (Orenstein *et al.*, 1982; Fritzsche, 1990) to obtain

$$\frac{\tilde{n}_e(s)}{N_{inj}} = \left\{s\left[1 + \int_0^\infty \frac{\alpha_{et}\, N(\varepsilon) d\varepsilon}{s + v_{te} exp[\varepsilon/k_b T]}\right]\right\}^{-1}. \tag{5.4.25}$$

In principle, this equation can be solved for any type of DOS profile (constant, exponential, or Gaussian) to determine the necessary ratio. This, however, is easier said than done and there are caveats to each type of solution. First, the upper limit of infinity is only good in the Gaussian and exponential integrations. For each of these DOS types, the falloff in DOS with energy is relatively fast in the gap. From the point of view of the DOS, integration of energies, even a small fraction of the gap energy away from their edges, is nearly equivalent to an infinite integration. For a constant DOS, one can only integrate down to the Fermi level as there is no dispersion in energy and no change in the energy dependence. We assume a normalized exponential expression for the DOS, and find the dispersive solution using

$$N(\varepsilon) = \frac{N_t}{k_b T_0^e} exp[-\varepsilon/k_b T_0^e], \tag{5.4.26}$$

and

$$\frac{\tilde{n}_e(s)}{N_{inj}} = \left(s + \alpha\alpha_{et} N_t \left(\frac{s}{v_0}\right)^{\alpha} \int_0^{\frac{v_{te}}{s}} \frac{u^{\alpha-1}du}{1+u}\right)^{-1}. \tag{5.4.27}$$

The limits of integration follow from the u substitution (Orenstein *et al.*, 1982). The integration of the interior term results in the hypergeometric expression (Abramowitz, 1965),

$$\int_0^{\frac{v_{te}}{s}} \frac{u^{\alpha-1}du}{1+u} = \frac{1}{\alpha}\left(\frac{\frac{v_{te}}{s}}{s}\right)^{\alpha} {}_2F_1\left[1, \alpha, \alpha+1, -\frac{v_{te}}{s}\right]. \tag{5.4.28}$$

In Eq. (5.4.28), ${}_2F_1$ is the hypergeometric function and $\alpha(T) \equiv \frac{T}{T_0^e}$, often referred to as the dispersion parameter (Rose, 1951; Schmidlin, 1977). Inserting this result back into Eq. (5.4.27), we get

$$\frac{\tilde{n}_e(s)}{N_{inj}} = \left(s + \alpha_{et} N_t {}_2F_1\left[1, \alpha, \alpha+1, -\frac{v_{te}}{s}\right]\right)^{-1}. \tag{5.4.29}$$

This equation cannot be solved in a closed form over all possible *s*. However, we can solve it in the limiting cases for very small and large *s*, which corresponds to long and short times. For large *s*, the hypergeometric function is simply one and we obtain

$$\frac{\tilde{n}_e(s)}{N_{inj}} = (s + \alpha_{et} N_t)^{-1}. \tag{5.4.30}$$

Taking the inverse Laplace transform of Eq. (5.4.30) we get

$$\frac{n_e(t)}{N_{inj}} = exp[-\alpha_{et} N_t t], \tag{5.4.31}$$

and replacing the $\alpha_{et} N_t$ with the simple trapping rate, we have

$$\frac{n_e(t)}{N_{inj}} = exp[-\nu_{et}t]. \tag{5.4.32}$$

Now, compare this result, with the Eq. (5.4.20) obtained for a simple single level discrete system shown below for reference:

$$\frac{n_e(t)}{N_{inj}} = \frac{(\nu_{te}+\nu_{et}e^{-(\nu_{te}+\nu_{et})t})}{\nu_{te}+\nu_{et}}. \tag{5.4.33}$$

The trapping rate, ν_{et}, of electrons from the CB to a trap state is always greater than or equal to the release rate, ν_{te}. In most cases the traps are deep—far from the CB—in the DOS, and the release rate is much smaller than the trapping rate; therefore, we can take the limit as the release rate goes to zero of Eq. (5.4.33) (i.e., $\nu_{te} \ll \nu_{et}$) and we recover Eq. (5.4.32). This approximation is consistent with traps in an exponential DOS that are energetically high in the DOS—far from the dark Fermi level—and far from the CB. Our solution for a distributed DOS is in agreement with that of a single level system when trapping is the dominant mechanism under these conditions.

Now consider what happens when s is very small, which corresponds to very long release times. We expect that this will yield behavior for a system that has a large dispersion in wait times. In this case, the hypergeometric function of Eq. (5.4.29) is approximately equal to $\left[\frac{sin[\alpha\pi]}{\alpha\pi}\right]^{-1}$. Performing the Laplace transform for the long time approximation of Eq. (5.4.29), one has

$$\frac{\tilde{n}_c(s)}{N_{inj}} = \left(s + \frac{\alpha\pi}{sin[\alpha\pi]}\alpha_{et}N_t\left(\frac{\nu_{te}}{s}\right)^{\alpha}\right)^{-1}. \tag{5.4.34}$$

This can only be done numerically; but with the approximation that $\frac{\alpha\pi}{sin[\alpha\pi]}\alpha_{et}N_t \gg s$ we have

$$\frac{\tilde{n}_e(s)}{N_{inj}} \cong \left(\frac{\alpha\pi}{sin[\alpha\pi]}\alpha_{et}N_t\left(\frac{\nu_{te}}{s}\right)^{\alpha}\right)^{-1}. \tag{5.4.35}$$

Application of the inverse Laplace transform to Eq. (5.4.35) gives us the long-term time-dependence of the decay

$$\frac{n_e(t)}{N_{inj}} \cong \frac{sin[\alpha\pi]}{\alpha\pi}\frac{\nu_{te}}{\nu_{te}}\left(\frac{1}{\nu_{te}t}\right)^{1-\alpha}. \tag{5.4.36}$$

Equation (5.4.36) is the ratio of free electron density to the total injected electron density. A useful change of variables allows one to write Eq. (5.4.36) as a function of the density of conduction and trapping states using $\frac{\nu_{te}}{\nu_{te}} = \frac{N_e}{N_t}$, where N_e is the density of conduction states within k_bT of the CB. This substitution

will allow for the estimation of the DOS ratio from data. Dispersive transport is often seen at low temperatures where hopping transport is active; when we are dealing with hopping transport, Eq. (5.4.36) holds, but the conduction states are then at the transport energy and the charge body is spread out in much deeper states (see Chapter 3).

In Section 5.4.2 we developed a relationship between the time rate of change in the surface potential and the trap-controlled mobility, which we repeat here for reference

$$\frac{d}{dt}V_s(t) = \frac{-\mu_{trap}(t)}{2}\frac{{V_0}^2}{d^2}. \tag{5.4.37}$$

Using Eq. (5.4.37) an expression for the surface rate of change for just the dispersive component is

$$\frac{d}{dt}V_s(t) = -\frac{\mu_0 sin[\alpha\pi]}{2\alpha\pi}\left(\frac{\nu_{te}}{\nu_{et}}\right)\left(\frac{1}{\nu_{te}t}\right)^{1-\alpha}\frac{{V_0}^2}{d^2}. \tag{5.4.38}$$

Equation (5.4.38) is then integrated to obtain

$$V_s(t) = -\frac{\mu_0 V_0 sin[\alpha(T)\pi]}{2d^2\alpha(T)^2\pi}\left(\frac{1}{\nu_{et}}\right)\left(\frac{1}{\nu_{te}t}\right)^{-\alpha(T)}\frac{{V_0}^2}{d^2}. \tag{5.4.39}$$

Equation (5.4.39) predicts the surface potential as a function of time, intrinsic mobility, μ_0, the dispersion parameter, α, the trapping and release rates, ν_{et} and ν_{te}, and the initial surface potential, V_0. Note, the temperature dependence of $V_s(t)$ is contained in the dispersion parameter, $\alpha(T)$.

We now make a simple assumption about the scalar nature of the surface potentials given by Eqs. (5.4.22) and (5.4.39). Equation (5.4.22) describes the decay of the surface potential, while the charge distribution is high in the density of states. In Section 3.1, the dynamic nature of the trapped charge distribution was discussed at length. In particular, the idea that the time spent in a trap went as the energetic depth in the DOS with respect to the CB edge was addressed; i.e., the deeper a trap in the DOS, the longer the time spent in those traps. For those electrons in very deep traps—in the band tail of the exponential distribution—the escape times are very long and distributed. The electric field due to electrons in deep traps will be nearly constant over a long period of time. For electrons in shallow states, the distribution of wait times will be a nearly single value; this results from the exponential nature of the DOS, causing a large number of electrons to be in states closer to the CB and fewer states in the deeper regions of the DOS resulting in a Fermi level that is high in the DOS. Electrons near the Fermi level are released and trapped quickly resulting in a fast changing potential. The timescales of the deep trap distribution and trap

distribution near the Fermi level suggest that we can approximate the total surface potential as the sum of potentials from two separate charge distributions. We, therefore, sum Eqs. (5.4.22) and (5.4.39) to obtain to SVP decay model for post electron beam charging

$$V_s(t) = V_0\left(1 - \frac{\mu_0 V(0)}{2d^2(\nu_{te}+\nu_{et})}\left(\nu_{te}t + \frac{\nu_{et}}{\nu_{te}+\nu_{et}}\left(1 - e^{-(\nu_{te}+\nu_{et})t}\right) - \frac{\mu_0 V(0) sin[\alpha\pi]}{2d^2\alpha^2\pi}\left(\frac{1}{\nu_{et}}\right)\left(\frac{1}{\nu_{te}t}\right)^{-\alpha}\right)\right). \quad (5.4.40)$$

This result is similar to that of Aragoneses *et al.* (2008), Toomer and Lewis (1980), and Ferreira and de Almeida (1997); there is one major notational difference. In the previous work, the temperature-dependent term $\gamma(T) \equiv \pi \frac{sin[\alpha(T)\pi]}{[\alpha(T)\pi]^2}\left(\frac{1}{\nu_{et}}\right)\left(\frac{1}{\nu_{te}}\right)^{-\alpha(T)}$ is defined giving

$$V_s(t) = V_0\left(1 - \frac{\mu_0 V_0}{2d^2(\nu_{te}+\nu_{et})}\left(\nu_{te}t + \frac{\nu_{et}}{\nu_{te}+\nu_{et}}\left(1 - e^{-(\nu_{te}+\nu_{et})t}\right) - \frac{\mu_0 V_0 \gamma(T)}{2d^2\alpha}(t)^{\alpha}\right)\right). \quad (5.4.41)$$

This expression is exactly the result presented by Aragoneses *et al.* (2008) and used to fit surface potential data for Kapton™ after coronal charging; we compare out results in Section 5.5. In our construction, we have identified the parameter γ(T), which was not done in the original paper, nor the theoretical work upon which the Aragoneses paper was based (Ferreira and de Almeida, 1997). Figure 5.2 shows the dependence of the function $sinc(\alpha\pi) \equiv \sin(\alpha\pi)/\alpha\pi$ on temperature—since the dispersion parameter, $\alpha(T)$, is a function of temperature—suggesting a distinct change in the type of temperature dependence at some critical dispersion value. In the original work by Ferreira and de Almeida (1997) the Scher waiting time distribution function (Scher *et al.*, 1980) was used to determine the decay in a dispersive system. The work of Scher and Montroll—while ground breaking, Zallen (1983) called it a phase transition from the anomalous to the obvious)—showed that the dispersion of waiting times lead to dispersive transport behavior (Zallen and Scher, 1971; Monroe, 1985; Blythe and Bloor, 2005). The work of Monroe (Rose, 1951, 1955, 1963; Tiedje and Rose, 1981; Monroe, 1983, 1985, 1986) and Schmidlin (1977) showed the exponential and later Gaussian DOS were responsible for the dispersive behavior. One of the criticisms of the Scher approach (Scher and Lax, 1973a, 1973b) was the lack of material-based parameters. In the construction of Ferreira and de Almeida (1997), this lead to the parameter product, ck, which was given no real interpretation. Equation (5.4.40) has the advantage of a complete characterization of the surface potential decay in terms of temperature dependence, dispersion parameter, and trapping and detrapping rates. The physical interpretation of dispersive transport is perhaps best explained in Tiedje and

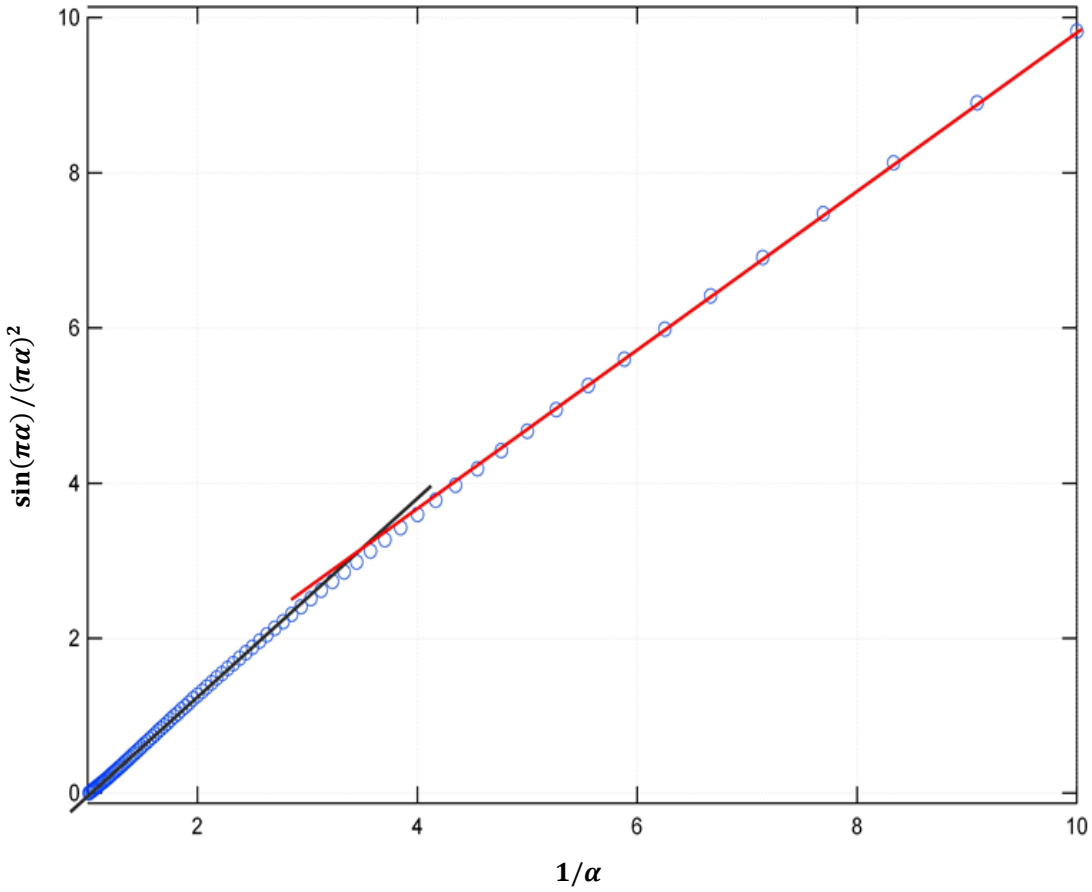

FIG 5.2. Dispersive surface potential decay parameter, $\gamma(T)$. This is equivalent to a 1/T plot and demonstrates the TAH-type behavior marked by the straight portions of the curve in the lower LHS of the plot (black line). We note that for very large dispersions, T << T_0, or very large α, there is a different type of behavior; see in the RHS of the plot (red line). This is the transition to low temperature $1/T^2$ behavior expected for VRH in an exponential DOS.

Rose (1981), Schmidlin (1977), Orenstein *et al.* (1982), and Kao (2004), where the derivation of the dispersive transport—in a photo excited system (Orenstein *et al.*, 1982)—was used to derive our result.

The reader may have realized that the decay of charge in the CVC system of Section 4.7 should be similar—if not exactly the same as—the SVP decay model given by Eq. (5.4.40). This follows from our assumptions about the charge distribution and geometry in the HDIM after electron beam charging; i.e., we assumed the SVP decay model acted like a parallel plate capacitor. These assumptions suggest that there should be a connection between Eq. (4.7.7) and Eq. (4.4.40) and there is. In the work of Ferreira and de Almeida (1997), an expression for the dependence of the potential, electric field, and current density at the collecting electrode for a corona charge HDIM are presented. The interested reader will find that a

mathematical formalism similar to that used to obtain the SVP decay model, Eq. (5.4.40), produces an expression that bears resemblance to Eq. (4.7.7) for the CVC decay model. This connection will not be discussed further in this dissertation and is left for future work; it seems obvious that this connection should exist and that it will allow a unified model of charge transport describing both the CVC and SVP surface potential decay experiments.

5.4.3. Post-Transit Model

In dispersive transport, the current decays linearly on a log-log plot until the charge distribution reaches the rear electrode, at which time it changes slope in a downward fashion (see Section 2.3.12). Thus, we would expect a major change in the surface potential decay profile, once the charge body makes contact with the rear electrode forming a new current path. The decay of the surface potential for times greater than the transit time has been derived in Ferreira and de Almeida (1997):

$$V_s(t) = \frac{d^2 t^{-\alpha(T)}}{2ck\Gamma[1-\alpha(T)]}\left(\frac{3}{2} - \mathrm{C}_{\mathrm{Euler}}\right), \tag{5.4.42}$$

where c and k are unspecified constants, C_{Euler} is called Euler's constant, and Γ is the gamma function. Ferreira suggests that the transit time should be

$$t_{transit} = \frac{\Gamma[1+\alpha(T)]}{{V_0}^2(ck)^2\Gamma[1-\alpha(T)]}\left(\frac{3}{2} - \mathrm{C}_{\mathrm{Euler}}\right). \tag{5.4.43}$$

Note again, that the temperature dependence of the surface potential and the transit time are contained in the dispersion parameter, $\alpha(T)$.

The decay after the transit time is expected to be a simple decreasing power law for any given temperature. As we will show, this is consistent with surface potential decay in LDPE after the transit time. An interesting comment can be made about this result. In the treatment of dispersive transport, the sum of the current slopes of the time dependence should be approximately -2. If we consider the sum of the slopes for the surface potential we get ~ 0. This is not surprising; it would seem that when dealing with the potential, the simple sum rule must be changed due to the derivative. We note that the sum of slopes for dV_s/dt does suggest the correct sum rule. It should be kept in mind when doing experiments that involve current measurement and surface potential measurement that we expect a different power law.

5.5. Analysis of LDPE and Kapton™

In this section, the theory developed Sections 5.3 and 5.4 will be applied to data taken on LDPE and Kapton™. This section is broken into four parts, charging for LDPE and Kapton™ and the decay for LDPE and Kapton™. The data used in this section were among the first experiments conducted on the SVP system developed by Hodges (2013). For a description of the experimental details, instrumentation error analyses, and additional results, see Hodges (2013). In each section we fit the requisite data, present the basic parameters, and give a brief discussion of their importance. The intent of this section is not to provide a detailed analysis of the data, but rather a proof of concept. Further, for each sample and charging regime we present only one data set, as there was only one data set at the time this dissertation was written. When analysis were preliminary in nature, the SVP system not fully characterized, and no additional data set over which the models can be tested were yet available, we find that the fitting of these data produced excellent agreement with the literature, thereby providing some confidence that, at least in part, the data itself were reasonable. All measurements were carried out with nearly identical experimental conditions. The system was charged incrementally at $1.1\ \mathrm{nA/cm^2}$ electron flux and a beam energy of $5000\ \mathrm{eV}$. For charging tests, surface voltage measurements were made by stopping the irradiation for 15 s, with an average irradiation time between measurements of 10 s. The internal pressure of the SEE SVP chamber was $\sim 10^{-8}$ Torr. The electron beam radius was estimated to be $0.8\ \mathrm{mm}$. The system temperature was not controlled, and thus, is approximated at room temperature, $\sim 20\ \mathrm{C^o}$. All data have been corrected to beam on and off time. However, during the two-year editing process of this dissertation and the thesis of Hodges, there have been significant changes to the data set. This includes a new data reduction procedure, changing the beam on/off times; for details of the data reduction process and improved fits, see Hodges (2013). While the results presented here are very good, the analysis must be redone.

5.5.1. Charging of LDPE

An LDPE sample with 27.4μm thickness was used. This sample had no charging history. The final data are presented in Fig. 5.3, with the charging model fit. Data fitting was done with *IGOR*™ *6.1,* using the USU MPG SVP charging model. In order to allow *IGOR*™ to effectively fit the data, Eq. (5.3.18) was reduced from

$$V_s(t) = \frac{q_e dN_t}{\epsilon_0 \epsilon_r}\left\{\left[\left(1 - \frac{R(\varepsilon_b)}{d}\right)\right]\right\} R(\varepsilon_b)\left[1 - exp\left\{\frac{s_c J_b (1-\sigma_{yield})\tau_{onset}}{q_e(1-m)}\left[1 - \left(1 + \frac{t}{\tau_{onset}}\right)^{1-m}\right]\right\}\right] \quad (5.5.1)$$

to the simplified form

$$V_s(t) = \mathrm{A}\left[1 - \exp\left\{-\left(\frac{\mathrm{B}\tau_{\mathrm{onset}}}{1-\mathrm{m}}\right)\left[1 - \left(1 + \frac{\mathrm{t}}{\tau_{\mathrm{onset}}}\right)^{1-\mathrm{m}}\right]\right\}\right]. \quad (5.5.2)$$

There are four free parameters in Eq. (5.5.2), but only τ_{onset} and m are not condensed into a general parameter. The decay onset time, τ_{onset}, and the quantity $(1 - m)$ are purposely separated from the other constants; this is done to avoid erroneous values due to the mixed dependence in Eq. (5.2.2). The quantities comprising the fitting parameter $A \equiv \frac{q_e dN_t}{\epsilon_0 \epsilon_r}$ are all known values, except the DOS N_t. The range, $R(\varepsilon_b)$, was predicted to be 1.1 μm at 5 keV, based on the models of Wilson and Dennison (2010). It is, therefore, easy to estimate the DOS from this expression. The same is true of the constant $B \equiv \frac{s_c J_b (1-\sigma_{yield})}{q_e}$, where only the capture cross section, s_c, in unknown; it also can be solved for easily once B is determined. The yield, $\sigma(\varepsilon_b)$, was predicted to be 0.3 electrons per incident electron, based on the measurements and models in Song *et al.* (1997). We assume the following parameters to estimate the DOS, N_t, and the capture cross section, s_c; the relative permittivity is $\epsilon_r = 2.8$, sample thickness, 27.4 μm, electronic charge, $q_e = 1.602 \times 10^{-19}$ C, and J_b = 0.8 nA/cm^2.

Equation (5.5.2) is fitted to the LDPE data and shown in Fig. 5.3 (black curve). Given the noise in the data, the fit is excellent. The residual shown at the top of the figure (red curve) is centered on zero and shows a consistent noise error of about 40V thought the data set. The results of the fit are summarized in Table 5.1. At worst, the fit suggests a 9% percent error and at best a 2 % percent error for early and late times, respectively. For the capture cross section, the agreement is excellent (see Chapter 2).

The estimated DOS is in modest agreement with literature (Montanari *et al.*, 2005; Brunson, 2009; Dennison *et al.*, 2009a). Often the DOS is predicted to be ~ 10^{18} cm^{-3}. The low result for the DOS obtained here is not surprising for the following reasons. First, the system had clearly not come to equilibrium, which would have given a higher value for the equilibrium surface potential, V_0; this is consistent with a partially filled DOS. It is also possible that the penetration range of the electrons was incorrectly estimated; this assumption should be checked against the USU MPG work on range equations (Wilson and Dennison, 2010; Hodges, 2013). The estimation may be improved if we consider that the range in the

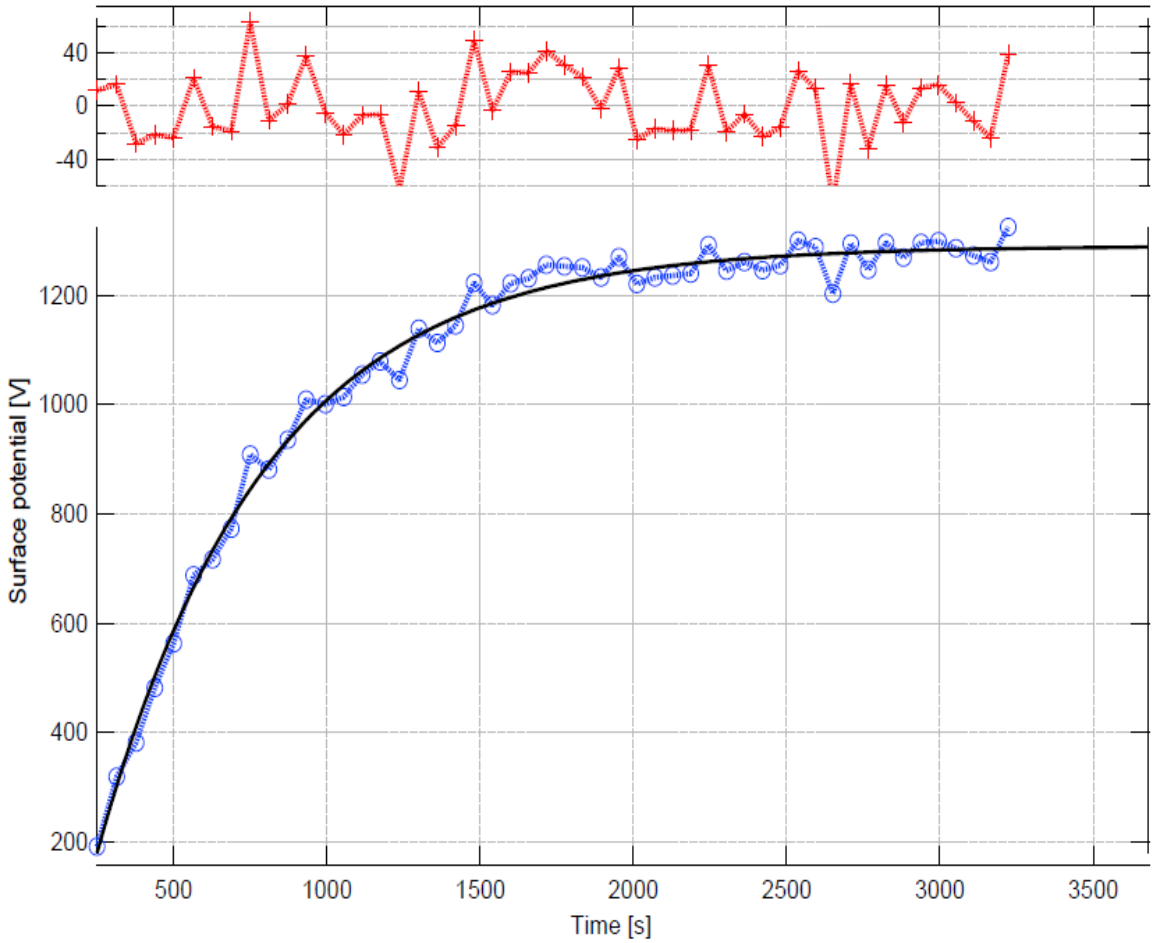

FIG 5.3. SVP electron beam charging model fit to LDPE. Surface potential charging of LDPE using a 5 keV, 0.8 nA/cm^2 flux electron beam. Data points are shown in (blue) and data are fit with the USU MPG SVP charging model (black curve) using Eq. (5.5.2). The red curve above is the residual between the LDPE data and the model. The residual is centered on zero and fluctuations are due entirely to noise in the data. At worst the fit suggests a 9% error (early times) and at best the error is 2 % error (long times).

TABLE 5.1. USU MPG SVP charging model data for LDPE.

ε_{beam} $[keV]$	$Fluence$ $[nA \cdot cm^{-2}]$	DOS $[cm^{-3}]$	s_c $[cm^2]$	V_0 $[V]$	τ_{min} $[s]$	m	σ $[\Omega^{-1}cm^{-1}]$	R $[m]$
5.0	0.8	$0.81 \times 10^{+17}$	5.2×10^{-13}	1.30×10^3	100	0.001	4.37×10^{-18}	1.1×10^{-6}

material is a distribution and the centroid is not at the maximum range, but rather closer to the sample irradiation surface. For a factor of 10 decreases in the range, the DOS would be estimated at $\sim 10^{17}$ cm^{-3}.

There are two important points to take away from this result. First, that our estimation of the DOS is strongly dependent on the effective range, and second that this estimation is in reasonable

agreement with the literature. Recall in Section 4.7 for the analysis of the CVC chamber, Fig. 4.5 suggested that the DOS was only filling to a fraction of its true value.

Finally, we estimate an effective conductivity using Ohms law as $J_b(\sigma_{yeild} - 1) = \frac{\sigma V_0}{R}$. This is a gross estimate as we have assumed knowledge of the electric field at the surface, which as stated earlier, we do not know. While the electric field at the surface cannot be zero, the concept of conductivity in the irradiated region is ill defined due to the complex nature of charge deposition and motion in this region. Keeping this in mind—and using our estimate—we find the conductivity for the charging process to be $\sim 4.74 \times^{-18}\ \Omega^{-1}\text{cm}^{-1}$, in good agreement with values found by (Brunson, 2009). Here we have used the range in place of the sample thickness as the charge distribution is situated at R from the surface; note that the conductivity may, in fact, be lower because we have used $J_b(\sigma_{yeild} - 1)$ in place of the actual injection current density.

A much better estimate of the conductivity can be found using the parameters from the surface potential fit and Eq. (5.3.12) for the current density that flows to the rear electrode. In this case, one could estimate the conductivity—using the material parameters—and apply Ohm's law over the region $0 < z < (d - R)$. Significant improvements to the estimation of the conductivity have been made in Hodges (2013).

In Table 5.1, the decay time, τ_{onset}, is listed with the subscript *min*; why is this? As it turns out, in order to get a good fit to the data, the decay time must be set to a large value—100 sec in this case—or the power parameter must be set to a very small value, $m = 0$. These numerical results tell us a great deal about the type of fit; i.e., it is nearly an exponential in form. In this case, a pure exponential was almost sufficient to fit the data; meaning that only a small contribution from the charge injection term is needed and the value of τ_{onset} nearly drops out of the equation, but not quite. This is why it is estimated at 100 s and the reason for the use of a different decay parameter. Physically this means that the relationship described by Eq. (5.3.1) between the trapped charge distribution and the injected current density is linear. For electron beam charging, the injection function is not expected to be very strong, as the electron beam deposits charge directly into the material. LDPE also has a higher mobility and conductivity (than does, say, Kapton™), a constant DOS, and does not exhibit dispersive behavior. As we will see in the next section regarding Kapton™, this pure exponential behavior is not always the case.

5.5.2. Charging of Kapton™

Kapton™ HN [DuPont] was chosen as the second test material in the SVP system. The fitting and analysis is largely the same as for LDPE, and thus we present only the results and a discussion of the parameters. Refer to Hodges (2013) for details. The data (blue), fit (black curve), and residual (red curve) are shown in Fig. 5.4. The residual again suggests the fit is quite good, with deviations due to experimental noise and measurement differences. The fit to Kapton™ is plotted on a log-log scale to highlight both the power law-like behavior and the slight deviation from the data in the first $10\ s$. Table 5.2 contains the results of the fit and the extracted material parameters. The test conditions for the Kapton™ sample were kept as close to the LDPE run as possible, with the exception that surface voltage is much higher, that the total yield, σ_{yeild}, is different from LDPE, and that the beam on and off times were different (Hodges, 2013). For Kapton™ Hoffmann (2010) has measured the total yield to be between 0.5 and 0.3 at the 5 keV incident energy; an average value has been used in our calculations of 0.4. The data fit is excellent after 10 s. (Recall that nearly 15 s is required to make a measurement; this likely causes errors for very short times.) The percent error between the fit and the data is bounded between 1% and 2%; the deviations in the residuals are again due to system noise and experimental errors, including current adjustments during the data runs.

The resulting DOS is slightly larger than for LDPE. However, the DOS is again lower than the predicted value $\sim 10^{18}\ \mathrm{cm}^{-3}$ (Breskin *et al.*, 1994; Fowler, 1955). This suggests that our assumption, that the value of N_t is only representative of a partially filled DOS, may be correct; in such a case, N_t only represents the maximum number of filled trapped states in the material at the equilibrium surface potential, V_0. Further, it should be noted that the Kapton™ measurements did not come to equilibrium, meaning that the DOS was not at its equilibrium value; allowing the system to come to equilibrium will provide a better estimate of the DOS. This must be investigated by subsequent researchers. An excellent method for studying the DOS is presented in Sessler's book, using thermally stimulated and photo-stimulated current methods (Sessler, 1987).

The capture cross section is in reasonable agreement with the values predicted in Chapter 2 and is not expected to vary a great deal from one HDIM to another.

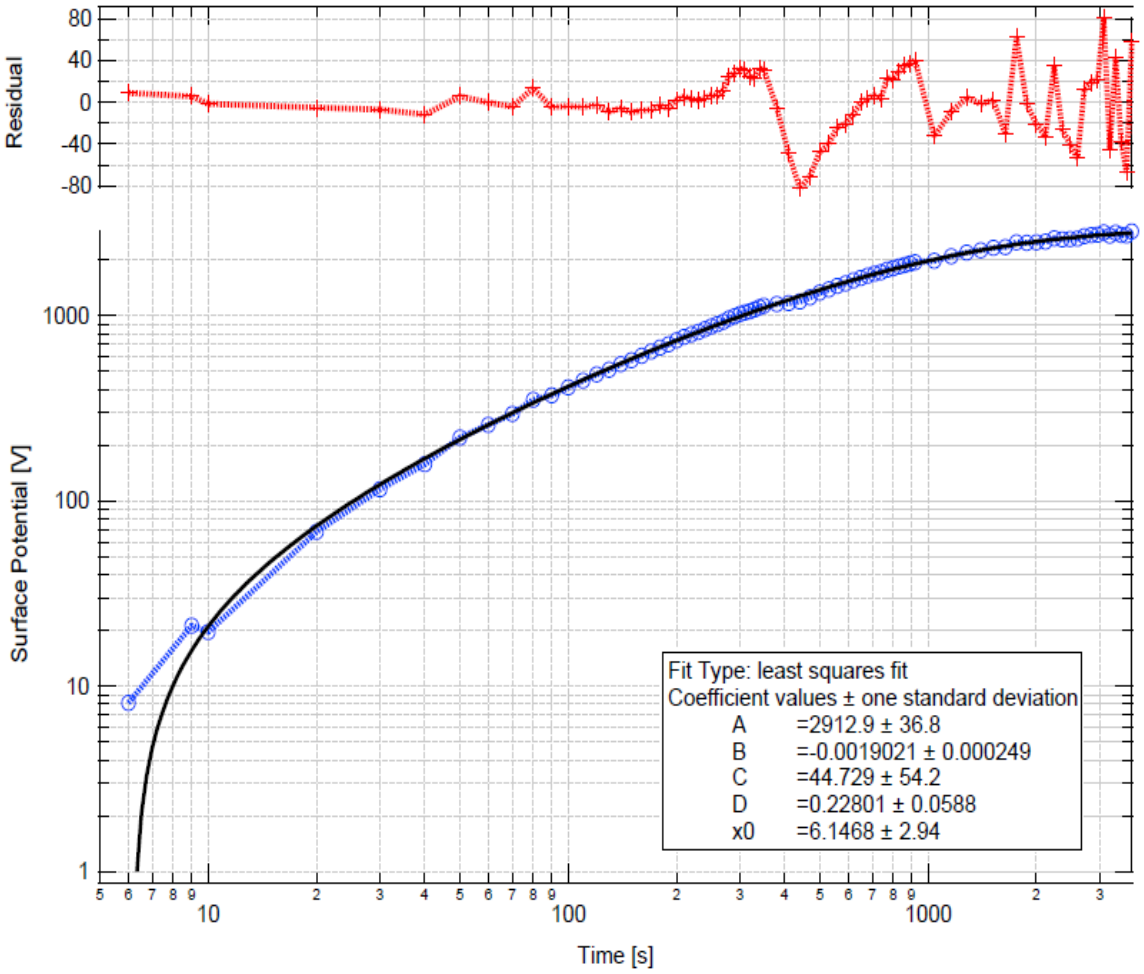

FIG 5.4. SVP electron beam charging model fit to Kapton™. Surface potential charging of Kapton using a 5 keV, 0.8 nA/cm^2 flux electron beam. Data points are shown in (blue) and data are fit with the USU MPG SVP charging model (black curve). The red curve above is the residual between the Kapton data and the model. The residual is near zero with fluctuations caused by both noise in the data and changes in the data collection process. Error for early times is estimated beyond 10 s—due to experimental difficulties—and is found to be less than 1% (best error case) and at worst the error is 2 % error (long times).

TABLE 5.2. USU MPG SVP charging model data for Kapton™.

ε_{beam} $[keV]$	$Fluence$ $[nAcm^{-2}]$	DOS $[cm^{-3}]$	s_c $[cm^2]$	V_0 $[V]$	τ_{min} $[s]$	m	σ $[\Omega^{-1}cm^{-1}]$	R $[m]$
5.0	0.8	$7.53 \times 10^{+17}$	6.35×10^{-13}	2.91×10^{3}	33.4	0.228	1.87×10^{-18}	1.1×10^{-6}

The parameters τ and m are considerably different for LDPE, and the shape of the data and fit to the data are also very different in appearance from the LDPE run. In Kapton™—a material expected to exhibit dispersive behavior—the power law injection term is active and necessary to get a good fit to the data; a simple exponential or even a double exponential will not provide a good fit. [Refer to Brunson

(2008) for an attempt to do this for LDPE data.] The surface potential is more than twice that found for LDPE, suggesting stronger trapping in Kapton™. Using the same method as for LDPE, we estimate the conductivity to be only slightly less than for LDPE. Typical estimates for the conductivity of Kapton™ are usually higher than for LDPE, in the $10^{-19}(\Omega\ \mathrm{cm})^{-1}$ range (Hoffmann, 2010).

5.5.3. Decay of LDPE

The decay of charge deposited in HDIM samples gives information about the strength of interaction of carriers with the material, trapping and detrapping rates, the intrinsic mobility, and—when present—the dispersion parameter. A detailed understanding of the material parameters is critical to understanding how long a deposited charge will require to dissipate. In Section 5.4.2, we presented the USU MPG SVP decay model, Eq. (5.4.40); it is presented below for reference

$$V_s(t) = V_0\left(1 - \frac{\mu_0 V_0}{2d^2(\nu_{te}+\nu_{et})}\left(\nu_{te}t + \frac{\nu_{et}}{\nu_{te}+\nu_{et}}\left(1 - e^{-(\nu_{te}+\nu_{et})t}\right) - \frac{\mu_0 V_0 \gamma(T)}{2d^2\alpha}(t)^{\alpha}\right)\right). \tag{5.5.3}$$

For review, V_0 is the initial surface voltage, ν_{te} is the release rate of carriers from traps, ν_{et} is the trapping rate, μ_0 is the intrinsic mobility, α is the dispersion parameter, d is of the sample thickness, and $\gamma(T)$ is a temperature-dependent parameter discussed in Section 5.4.2. Equation (5.5.3) can be written in a slightly simpler form to fit data

$$f(t) = V_0 - \frac{1}{2}\left(\frac{V_0}{d}\right)^2 \frac{\mu_0}{(\nu_{te}+\nu_{et})}\left[\nu_{te}t + \frac{\nu_{et}}{\nu_{te}+\nu_{et}}\{1 - exp[-(\nu_{te}+\nu_{et})t]\}\right] - {V_0}^2 C_5 t^{\alpha}, \tag{5.5.4}$$

where ; $C_5 \equiv \frac{\mu_0\gamma}{2d^2\alpha}$ has been condensed into a single constant for simplicity. There are five free parameters in the fit: $\nu_{te}, \nu_{et}, \mu_0, \alpha,$ and t. The values of $\nu_{te}, \nu_{et}, \mu_0,$ and α are estimated from the literature to provide a starting point for the fit. The details of the conditions under which the LDPE sample is charged is covered in Section 5.4.2 and will not be repeated here. Using Eq. (5.5.4), the decay of the deposited charge is fitted and the results are shown in Fig. 5.4 and Table 5.3. Figure 5.5 shows the LDPE data set in blue, the fit with Eq. (5.5.4) in black, and an additional fit in yellow. Parameters obtained from the fit using Eq. (5.5.4) are shown in Table 5.3. The second fit in yellow is necessary, as after this time the charge body has traversed the sample and made contact with the rear electrode. Notice that there is a vertical black line in the figure; this is the estimate of the transit time of the charge body as calculated for LDPE by Toomer and Lewis (1980). Also note that this transit time, $\tau_{transit}$, estimate is temporally situated at 1800

s. Since the data reduction used in this analysis does not take into account the time between measurements by the SVP probe—in an accurate way—the time spent by the charge in the material may exceed this expected value by a great deal, and our estimate of the transit time may be too small. A detailed analysis of this problem must be left as future work; however, a discussion of the post-transit decay is presented later in this section.

An important function of this model is the estimation of the charge decay time. The SVP decay model can be solved for *t* when the potential is zero, thus providing an estimate for the true decay time. This decay time should exceed the actual decay time because the SVP decay model assumes the charge distribution does not make contact with the rear electrode, at which time faster decay of the charge will begin to occur. The estimate of the decay time provides a simple way to estimate the conductivity of the material. Using the decay time versus resistivity plot as presented in Chapter 1 and found in Brunson (2009), we create a conductivity conversion formula,

$$\sigma_{dark} = \frac{\tau_{decay}\epsilon_0\epsilon_r}{10^{-13}Ohm-cm-sec}. \tag{5.5.5}$$

Using the data for LDPE obtained from the fit in Fig. 5.5 suggests that the decay time is $\sim 1.448 \times 10^4\ s$, which yields a conductivity of $\sim 4 \times^{-17}\ \Omega^{-1}cm^{-1}$. This is lower than the expected conductivity of $\sim 10^{-18}\ \Omega^{-1}\text{cm}^{-1}$ by a little more than a factor of ½, but consistent with our estimate from the charging fits in Section 5.5.1. The higher conductivity can be caused by a number of sources. For example, the charge distribution could have made contact with the collecting electrode during the measurement; the CVC results are for very long times, and it is possible that the short experimental time of the SVP measurement creates a disparity. As discussed above, for LDPE the deposited charge is expected to move a fair amount during the charging and discharging process, consistent with PEA measurements (Perrin, 2005; Griseri *et al.*, 2006; Chen, 2010). In these studies, the beam energy is about 8 keV, which is larger than the USU beam energy, but the flux is much lower at $50\ \text{pA/cm}^2$ versus $1.1\ \text{nA/cm}^2$ for the USU MPG experiments. This suggests, that while there may be fewer electrons deposited in the material during the charging process, those electrons will penetrate deeper into the material. The work of Griseri *et al.* (2006), Chen (2010), and Perrin (2005) is used to estimate an upper limit for the motion of the deposited charge moving toward the collecting electrode. The data suggest a charge body velocity of $0.17\ \mu\text{m/min}$.

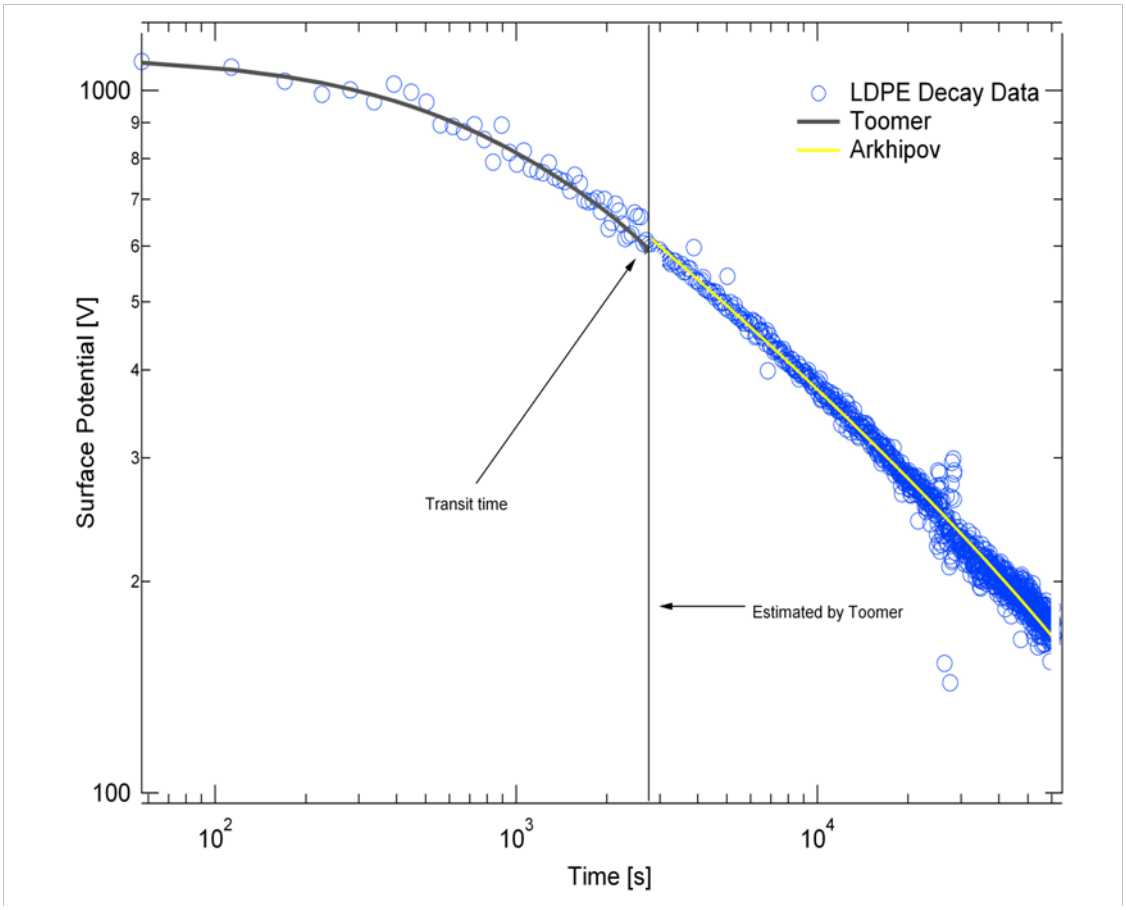

FIG 5.5. SVP decay model fit to LDPE. Data are shown in blue and fits are shown in black and yellow, respectively. The LDPE decay data fitted with the USU MPG SVP decay model for times less than the transit time (black curve) and a simple power law for times greater than the transit time (yellow curve).

TABLE 5.3. USU MPG SVP decay model data for LDPE .

$V_0[V]$	$Trapping\ rate\ v_{et}$ $[s^{-1}]$	$Release\ rate\ v_{te}$ $[s^{-1}]$	$Conductivity\ \sigma$ $[\Omega^{-1}cm^{-1}]$	$Trap\ energy$ $[eV]$
1168	$1.06 \times 10^{+3}$	2.13×10^{-4}	3.50×10^{-17}	-0.87

Assuming a small penetration depth of 1.1 μm , subtracting this from the sample depth, we obtain an estimate for the transit time of 10,000 s. The charge body would be expected to move completely across the sample in this time. This is slightly longer than the $\tau_{transit}$ time found by Toomer and Lewis (1980) of ~8000 s. However, the 10,000 s is a single estimate from a completely different type of measurement system. Further, the 10,000 s limit happens well within the time span of the data collected by the SVP on LDPE. The decay model we have presented is *only* good as long as the charge body does not contact the

rear of the sample. After the charge contacts the rear electrode, we must use the simple power law suggested by Ferreira and de Almeida (1997) and presented in Section 5.4.3.

We can now present a discussion of the double fit to the LDPE data shown in Fig 5.5 using the sum of the USU SVP decay model and a simple power law. The first curve is essentially the model of Toomer and Lewis (1980) as the dispersion parameter is found to be negligible; the power law term is zero for LDPE (no dispersion). This is expected since LDPE is thought to have a constant DOS. The form of the power law fit adapted from Ferreira and de Almeida (1997) is as follows:

$$f(t) = C_{coef} t^{pwr} + C_{offset}. \tag{5.5.6}$$

The fitted values that produce the yellow curve in Fig. (5.4) are: $C_{coef} = 9264\,V$, $pwr = -0.323$, and $C_{offset} = -97.98\,V$. While this power law gives a good fit to the data after the transit time, its solution for the time to decay yields a very surprising result. In the paper by Chen (2010), it is suggested that the decay will take ~ 15 days for complete charge leakage to occur, this is consistent with the estimate of the power law fit which suggests ~ 15.2 days for complete decay and a final dark conductivity of $3.4 \times 10^{18}\ \Omega^{-1}\text{cm}^{-1}$, which is quite large for LDPE. The USU MPG found that the dark current conductivity should be ~$1.8 \times 10^{18}\ \Omega^{-1}\text{cm}^{-1}$ (Brunson, 2009), which lies directly between our estimates for the conductivity using first the SVP decay model and second the power law model. A word of caution is required here; the interpretation of the models is suspect and the data is very preliminary. The SVP has errors in both the analysis and operation of the experiment itself. The application of models after the charge body contacts rear electrode should be scrutinized further, as it is not clear how the charge injection process, limits of the applied model, and decay of the local field affect the charge migration. Given those concerns, it is surprising that our fit has suggested a good agreement with the work of Chen (2010) and Perrin (2005) for LDPE on the long time decay, ~15 days, and that the conductivity is well characterized. Given that our understanding of the charge decay is paramount to the spacecraft equilibration process, it seems prudent to undertake a study of these effects after the charge body has contacted the rear electrode. This can be accomplished with higher incident beam energies, large fluxes, and longer wait times after the cessation of the electron beam. Since the model described for pre-transit describes over 63% of the total decay, it is a critical tool in understanding the fast response recovery of the spacecraft. Thus, in order to

understand this behavior in materials like LDPE, it is necessary to lower the beam energy and flux, thus allowing for longer times before the transit occurs.

From this point on, we concentrate on the pre-transit behavior and the associated fit using the USU MPG SVP decay model. The results of the fitting parameters and estimation of the upper limits for the conductivity are presented in Table 5.3. The trap energy is estimated using Eq. (5.4.23) and our calculated value, $\nu_{et}(\varepsilon) = 1.055 \times 10^{-3}\text{s}^{-1}$. This is inconsistent with the constant attempt-to-escape frequency estimated to be $\nu_{et} \sim 10^{12}$ s^{-1}; note, that the value of ν_{et} is found by analyzing the transport case, where the excitation rate, ν_{et}, is equal to the trapping rate, ν_{te} [see, for instance, Rose (1951) and Toomer and Lewis (1980)]. For reference and comparison, the data from Toomer and Lewis (1980) on LDPE is presented with the USU MPG data, (in gray) and has been included in Table 5.4. The agreement between the USU data and that of Toomer and Lewis is reasonable. We note there were a number of errors in the Toomer and Lewis (1980) paper. The trapping rates suggested by the Toomer and Lewis (1980) paper seem very high and may be an artifact of fitting their data over very short timescales; in fact, when adjusting the timescale in the USU fits, it was found that the exact number reported by Toomer and Lewis could be replicated, but only for short irradiation times. The short time fits yielded numbers for the release rate and trap rate consistent with Toomer and Lewis (1980); however, the mobility remained unaffected. For longer timescales, the release rate decreased as did the trapping rate, which became very small, $\sim 10^{-6}$ s^{-1}. In order to fit the data correctly, the transit time given by Toomer and Lewis (1980) must be used; this further suggests that this is a real problem with the current study. LDPE will require a consistent set of studies varying the flux and beam energy, plus a test system calibration, to determine proper application of this model. These studies should mirror the work of Toomer and Lewis (1980) and Aragoneses *et al.* (2008) in order to understand the complete picture.

Despite the difficulties in using the model and connecting our results with Toomer and Lewis, it is still clear that the model for both pre- and post-transit provide useful physical and predicative information about the decay of charge within LDPE. Though our estimates for the trapping rate and release rate are both an order of magnitude lower than those found by Toomer and Lewis, the overall agreement is still good. The fact that a single run on LDPE in a brand new experimental system yields results that are consistent with the literature is extraordinary. Further, when our results on LDPE are compared with the charging

TABLE 5.4. LDPE decay data comparison (USU MPG in grey).

$Temperature$ $[^oC]$	$V_0\ 10^3$ $[V]$	$Mobility\ 10^{-15}$ $[m^2/Vs]$	$Release\ rate\ 10^{-5}$ $[1/s]$	$Trap\ energy$ $[eV]$	$Trap\ rate\ 10^{-5}$ $[1/s]$
21	.950	4.2	2.4	1.0	48
	1.40	4.2	2.4	0.9	480
	2.60	4.2	5.7	0.9	1140
22	0.540	5.4	4.9	0.9	440
	0.848	5.4	12.6	0.9	680
	1.60	1.3	5.1	94	220
31	4.60	14	0.13	1.0	95
	1.25	16	1.1	0.1	250
	+1.67	16	1	0.1	320
21	-0.650	15	5.6	0.94	1200
	-0.950	15	7.0	0.93	1500
	-1.16	3.2	0.21	0.87	106
	-1.50	15	9.3	0.92	2000
	-2.10	15	21	0.90	4500
22	-0.410	120	4.6	0.94	7800
	-0.610	200	6.7	0.93	1900
	-0.910	35	2.1	0.96	4900
	-2.30	54	2.1	0.96	1600

After Toomer and Lewis (1980).

data, we find good agreement, as well. As we shall see, the agreement with Kapton™, (a material that the charge packet cannot cross quickly) is outstanding.

5.5.4. Decay of Kapton™

In this section, the model for decay given by Eq. (5.5.4) is used to fit Kapton™ decay data taken by Hodges (2013). The beam energy is the same as for LDPE outlined in Section 5.5.1, but the flux and beam on-off times differ somewhat Hodges (2013). The resulting fit is shown in Fig. 5.6; the USU data on Kapton™ are shown in blue and the fit as a green curve. In this case, the fit is quite good, given the noise in the data.

Note, there is what appears to be a doubling of the data in the y-axis direction. This is due to a repositioning error in the SVP system and has been addressed by Hodges (2012). The next anomaly is gap that begins around 9×10^4 s; this occurred when the sample carousel was rotated to observe another sample and then returned after some time to continue to take data on Kapton™. The data after this gap have been corrected for an offset error. The residual plot shows the two anomalies and a good deal of system noise; however, it is clear that the residual is centered about zero and—for the regions where there are no data anomalies—the error is bounded by 9% error for early times and 2% error for later times.

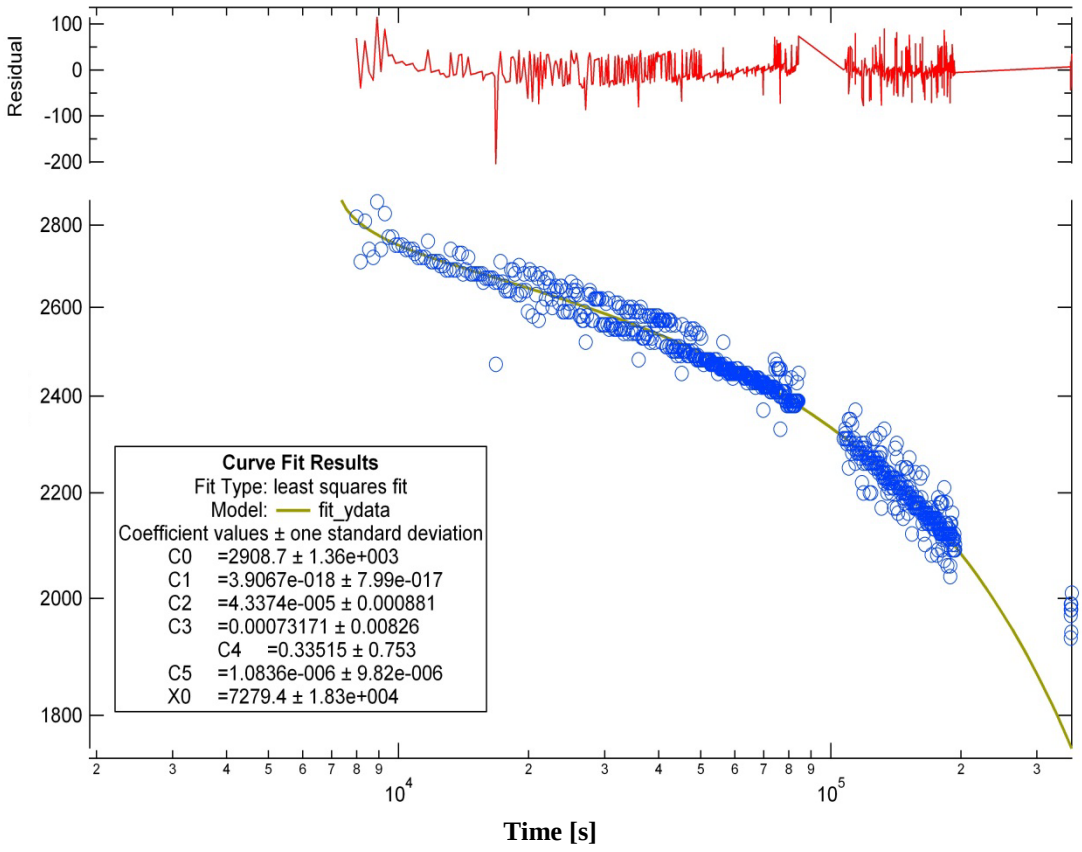

FIG 5.6. SVP decay model applied to data on Kapton™. Surface potential charging of LDPE using a 5 keV, 0.8 nA/cm^2 flux electron beam. Data points are shown in (blue) and data are fitted with the USU MPG SVP charging model (green curve). The red curve above is the residual between the LDPE data and the model. The residual is centered on zero and fluctuations are due entirely to noise in the data. At worst the fit suggests a 9% error (early times) and at best the error is 2 % error (long times).

TABLE 5.5 Kapton™ decay data comparison (USU MPG in grey).

$V_0[V]$	$\mu_0\ [m^2V^{-1}s^{-1}]$	$v_{te}\ [s^{-1}]$	$v_{et}\ [s^{-1}]$	$\gamma(T)$	α
983	2.03×10^{-17}	4.63×10^{-4}	6.36×10^{-4}	4.83×10^{-3}	9.40×10^{-1}
2018	2.02×10^{-17}	7.01×10^{-5}	2.34×10^{-4}	3.93×10^{-3}	1.29×10^{-1}
2827	6.98×10^{-17}	4.34×10^{-5}	7.32×10^{-4}	2.83×10^{-3}	3.35×10^{-1}
3011	2.13×10^{-17}	4.13×10^{-5}	5.05×10^{-4}	1.94×10^{-3}	6.87×10^{-1}

PEA data taken by Perrin (2005) suggest that the movement of the charge body in Kapton™ is significant, but may not be enough to penetrate the sample much beyond the expected range. Aragoneses *et al.* (2008) fit decay data from Kapton™ acquired using a CVC-type system (Aragoneses *et al.*, 2008); their fit appears to be in excellent agreement with data presented here. The data on Kapton™ exhibit the expected dispersive behavior, as evidenced by the nonzero power, α. This is in stark contrast to the behavior of LDPE, which needs no dispersion parameter to obtain a good fit. This result is also apparent in

Section 5.5.2 where the injection function has a nonzero power and is required to fit the charging data on Kapton™.

Table 5.5 includes the Aragoneses *et al.* (2008) results, together with the results of the USU SVP model fit to post-irradiated Kapton™ data (in grey). Using the decay time estimation technique employed in Section 5.5.3, a decay time of $\sim 1.6 \times 10^6$ s or ~ 18.5 days is found. This gives an estimated conductivity of $1.6 \times 10^{-19} \Omega^{-1} \mathrm{s}^{-1}$ in excellent agreement with the literature (Hoffmann, 2010). Inspection of Table 5.5 suggests immediately that we have good agreement between Aragoneses *et al.* (2008) and the USU estimation of the fitting parameters (i.e., the trapping rate, ν_{et}, detrapping rate, ν_{te}, gamma constant, $\gamma(\mathrm{T})$, and dispersion parameter, α). The only parameter that is not in very good agreement is the mobility, which deviates from the Aragoneses value by $\sim 50\%$. However, Aragoneses *et al.* (2008) state that their samples were tested in 40% to 50 % relative humidity—much higher than USU's samples. Further, recall that they used a CVC-type system to make the measurements. The USU samples are kept in a low humidity environment and prepared using a vacuum bakeout procedure to remove water and volatile polymer synthesis by products. The lower water concentration in the USU samples could easily account for the difference in mobility. To illustrate the level of agreement, two plots have been made from Table 5.5; values of V_0 are plotted versus the release rate and the dispersion parameter.

Figure 5.7 shows the dispersion parameter data versus starting surface potential, where the marker of V_0 on the plot indicates the USU data point. Not only does the dispersion parameter show strong field dependence, but the USU data point lies very closely along the curve. The field dependence of the dispersion parameter is not surprising. In Section 3.2, a discussion is presented illustrating the connection between the local field, the DOS, and the release rate (then called the thermal upward hopping rate, which applies in the TAH model, as well as the VRH model).

Next, the release rate, ν_{te}, versus V_0 is plotted in Fig. 5.8. Again the agreement is remarkable and there is a clear field dependence on the release rate parameter. This field dependence is predicted by the theory in Section 3.2. A discussion of the mobility and ν_{et} is not presented, as the data given in Aragoneses *et al.* (2008) and the USU MPG data taken together are insufficient to suggest a trend. In fact,

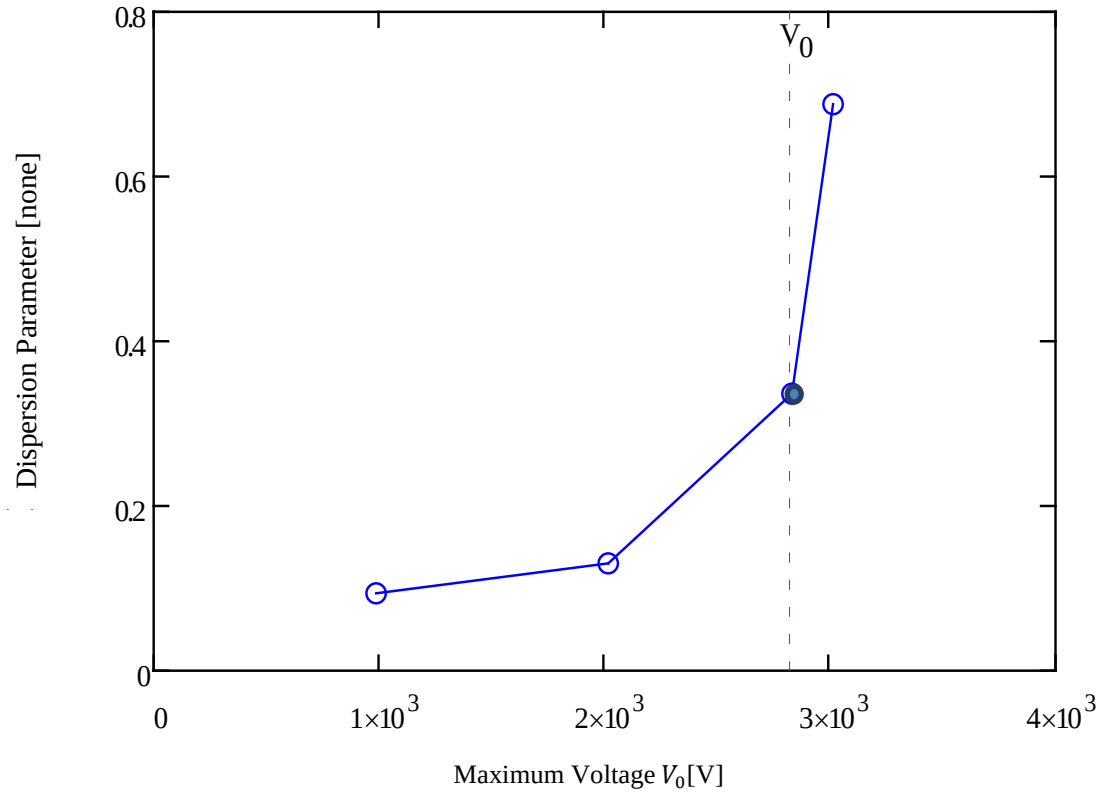

FIG 5.7. Comparison of dispersion parameter for USU data versus Aragoneses. This plot shows data from Aragoneses *et al*. (2008) (open circles) for the dispersion parameter versus V_0—initial surface potential—compared with the USU data (closed circle). The data point taken by the USU MPG falls predicable along the curve created. An increasing dispersion parameter is consistent with a field-induced disorder and enhanced dispersion.

we should not expect that the parameter, ν_{et}, would be affected by internal fields, as it has no known energetic dependence.

5.6. Conclusion

The data analysis section has brought to light a number of interesting features in both the charging and decay models and the data. First, our surface potential charging models seem to perform very well and predict reasonable values for the cross section, conductivity, and density of states. For the decay models for LDPE, we have found a clear case where the model limit is reached and a post-charge packet transit model is required to explain the behavior. In Kapton™ (a system that does not reach its transit time), we have excellent agreement with the literature and a model of dispersive transport, which handles the problems associated with an exponential DOS. This is in contrast to a system like LDPE whose DOS is

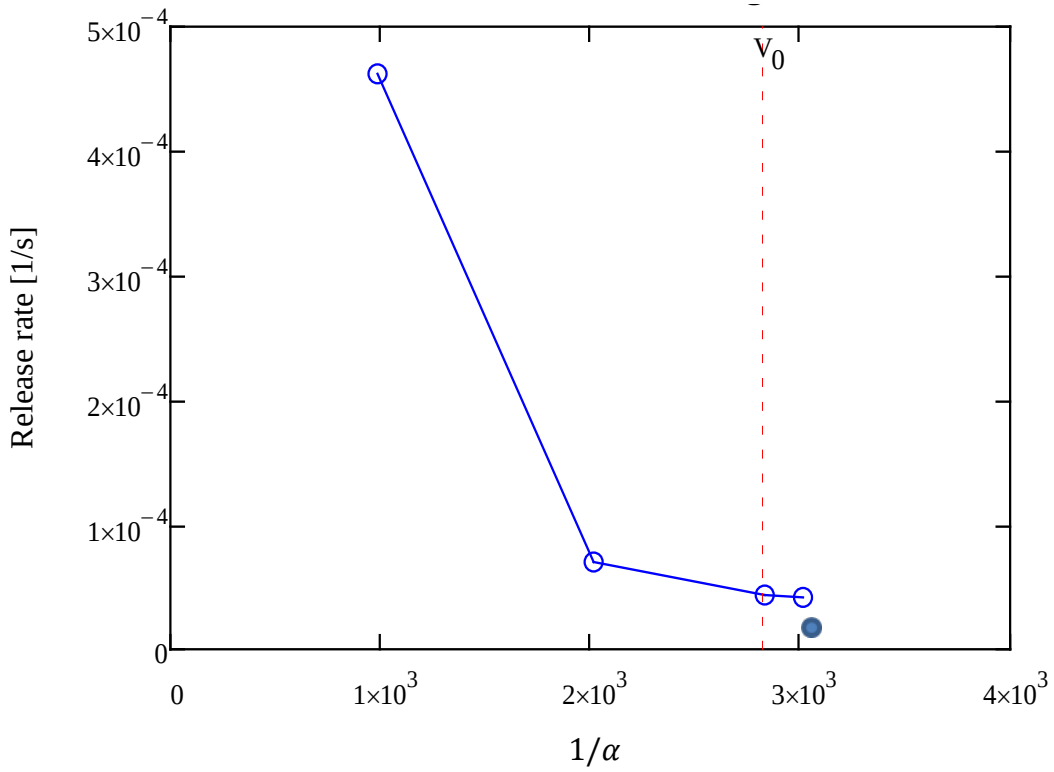

FIG 5.8. Comparison of dispersion electron release rate. Shown are data from [Aragoneses] (open circles) for the trapped electron release rate, ν_{te}, versus V_0—initial surface potential—USU SVP models prediction data (closed circle). The data point taken by the USU MPG falls predictably along the curve created using Aragoneses. A decreasing release rate parameter is consistent with an increasingly high internal field; which acts to lower the energy necessary for an electron to escape.

likely to change—due to degradation effects and defect creation—over the energy spectrum (Mizutani *et al.*, 2000) in a component-like way due to its semi-crystalline and amorphous nature. In fact, Mizutani *et al.* (2000) gives a table of activation energies, and the molecular regions within LDPE that are responsible; for $0.8\ to\ 1.0$ eV activation energies, it is suggested that the amorphous regions associated with defect structures are the primary active components. We obtained a value of 0.87 eV for our release rate activation energy, which seems to be in agreement. However, even for a system as complex as LDPE, we find reasonable agreement with literature within the pre-transit regime. Taking the data from the Toomer and Lewis (1980) table and creating plots for the release rate and trapping rate shows a strong dependence on the field (see Figs.5.7 and 5.8). The appearance of field dependence in the physical parameters makes a direct connection to the inclusion of field dependence described in Section 3.2. The results of this section clearly indicate that the dynamics of the high field regime are at work, and the system is controlled by the

interaction between the internal electric field, QFL (since the FL moves with time), and the demarcation energies (which govern the rate at which the DOS will fill up). A complete study on the dynamics of each material under a range of beam energies, temperatures, and fluxes will yield a great deal of information about these dynamics. These studies—in addition to concurrent studies on the surface potential, SEE, and CVC—will open doors to a deep understanding of the spacecraft charging phenomena.

CHAPTER 6

CONCLUSION

6.1. Introduction

This dissertation is a first step in bringing together, in a common language, a vast set of ideas that determine the behavior of many phenomena, including charge transport in HDIM. It provides an interpretation and methods for applications of the theoretical formalism set out in this dissertation, which are then applied to a specific set of experimental tests and results. The primary goal of this dissertation was the development of a single theoretical formalism that connects nearly all the major types of charging phenomena in HDIM to the specific nature of spacecraft charging using a comprehensive nomenclature. For spacecraft charging applications, the key idea is to understand how to apply this formalism and resulting theory in specific circumstances to mitigate spacecraft damage or failure. We, therefore, categorize the text methods applicable to spacecraft charging problem into six major configurations. These configurations were discussed in Chapter 1 and presented in Fig. 1.4. We summarize them here for reference:

(a) Nonpenetrating incident charge deposited on the surface of an insulator that is transported to a contacting metal surface through the bulk of the insulator or remains on the surface.

(b) Partially penetrating incident charge that penetrates into an insulator, and is then transported to a contacting electrode or remains within the insulator.

(c) Penetrating incident charge that passes through an insulator, generating a separation of positive and negative charge, enhancing the conductivity, and modifying the transport properties of the HDIM.

(d) Electrode-injected charge that is injected into the bulk of the HDIM using a contact interface such as a metal electrode, and subsequently undergoes transport to some other region of the HDIM.

(e) Polarization phenomena, or dielectric materials response to applied fields, caused by the application of an electric field leading to short timescale modifications of the exterior and/or interior fields of the HDIM.

(f) Electrostatic breakdown caused by the application of very high electric fields or large charged particle fluencies causing permanent damage to the HDIM.

These six configurations represent all the basic situations that a spacecraft material may encounter with regard to charge transport.

It is not surprising that the surface and bulk transport properties should determine movement of charge that is on the surface or internal to the material, establish electric fields internal and external to the HDIM, and provide information about the maximum fields that can be sustained, without permanently changing the material's structure. The level of difficulty in describing the charge transport comes largely from the fact that HDIM are—as the name implies—highly disordered, insulating, and subject to complex charge transport mechanisms. Over 100 years of research has been condensed and connected in this dissertation beginning with early work in radiation-induced currents and subsequent charge transport by Curie (1904); see Fowler (1956) and references therein, and references cited in this dissertation to the present day. The disordered nature of HDIM creates a situation in which transport of charge must be considered in terms of:

(*i*) Energy-dependent charge flux and fluence. (These are due to the local spacecraft environment.);

(*ii*) Temperature. (This often governs both the rate with which charge is transported and the type of conduction mechanism at work.);

(*iii*) Time. (Different configurations have different charging and discharging times, or equivalently trapping and release rates.);

(*iv*) Structural disorder. (This primarily determines the type, density, and energy depth of defects generated as localized states within the mobility gap.);

(*v*) Electrochemical structure. (The DOS and disordered chemical nature play an important role in the transport of charge.);

(*vi*) History of charging and discharging. (These include repeated stress—which can produce recoverable and irrecoverable defects—caused by external and internal fields, residual, or existing charge distributions.);

(*vii*) Types of transport. (There are several types of transport phenomena, e.g., TAH, VRH, diffusion, drift, and dispersion, as examples.);

(*viii*) Applied field, (These create changes in the internal structure that govern transport, can produce defects, and can lead to breakdown of the HDIM.);

(*ix*) Light and charged particle conditions. (Incident radiation can change the conductivity of the material via radiation induced processes.);

(*x*) Material shape. (Geometry determines the strength and direction of the electric fields.), and electrical configurations induced by bringing materials of different types in to contact with one another (e.g., work functions of different materials, Schottkey barriers, and diffusion of charges).

This extensive list highlights both the many areas of study that are part of this dissertation, but also the utility and required complexity of the single theoretical description presented in this dissertation, which allows all of these complex ideas to be connected and their physical actions understood. The great value of the connection between the macroscopic transport equations of Chapter 2 and the microscopic physics presented in Chapter 3 is in the realization that one can use the transport equations in nearly all applications to understand charge transport at both low and high temperatures. This is not to say that one can understand any and all transport phenomena through the transport equations; this is not true. However, for systems whose behavior acts in such a way that average or macroscopic behavior results—as is the case with HDIM—the approach is very effective.

This dissertation is a first step in completing the task of developing a complete understanding for how HDIM respond to their environment within a single theoretical formalism. In particular, this work has approached the problem of HDIM charging in the following consistent way. First, Chapter 2 uses the basic equations of electrostatics and electrodynamics-coupled with charge conservation and a basic understanding of charge trapping and release processes within HDIM to develop a set of one-dimensional transport equations under the condition that electrons are the majority carrier and all other carrier interactions can be ignored. Chapter 2 describes the transport equations governing what we call macroscopic transport. Second, (in Chapter 3) a detailed discussion of the nature of disorder, its interaction with injected charge, and its extension to the transport equation discussed in Chapter 2 was given. Chapters 4 and 5 present simple applications of the transport equations to USU MPG experimental data using a novel

approach. Specifically, the injection function concept is introduced and applied. The injection function is based on the DOS and interactions of injected charge at or near the surface upon which charge is incident. In large part, we have assumed simple geometries to make estimation of the physical quantities that determine charging and discharging characteristic easier. The reader should note that the applications in Chapters 4 and 5 to the USU MPG data from the CVC and SVP experiments were preliminary analyses, whose purpose was only to show the merit of the theoretical ideas presented in the first three chapters.

This dissertation has accomplished the main goals set out in the introduction. In this work, it has been shown that the connection between microscopic physics, macroscopic behavior, and the fundamental nature of spacecraft charging materials can be characterized by an average view of carrier dynamics generated by the interaction between the DOS of the material and the experimental configuration for the CVC and SEE-SVP test configurations. This average view leads to assumptions and insight into resulting phenomena that are embodied in the appropriate transport equations. The key point in the above discussion is that transport in HDIM is difficult to understand and—by extension—spacecraft charging is difficult to understand. In the sections that follow, a brief overview of each chapter is given and major points that are central to this work are highlighted. This chapter will close with a discussion of future work, additional insights, and some references for the interested reader.

6.2. Summary of Chapters 1 and 2

In Chapter 1, the basic problems facing the spacecraft charging community and research in HDIM as a whole are presented. The basic approach of this dissertation and six major experimental configurations are also outlined. In particular, Chapter 1 lays out the fundamental goals of this dissertation:

(a) Development of a theoretical framework in a common nomenclature that serves as a starting point for all of the experimental configurations discussed.

(b) Application of current theoretical models in charge transport to spacecraft charging problems.

(c) Extension of current USU MPG models to include a more complete description of charge transport in HDIM.

(d) Extension of current static charge models to explicitly include time dependence.

(e) Application of resulting models to contemporary USU MPG experimental systems.

(f) Generation of new USU MPG engineering design tools to assist spacecraft engineers to mitigate spacecraft charging.

These are the primary goals set forth and accomplished in this dissertation.

Chapter 2 lays the fundamental groundwork to understand how to unify charging in HDIM and develops a detailed set of transport equations that govern all the charge transport processes in the material bulk given the experimental configurations discussed in Chapter 1. These are, in fact, the key results of this dissertation. In order to develop a deep understanding of charge transport, Chapter 2, starts with a fundamental approach, introducing basic types of transport—such as drift and diffusion—and clearly highlighting the effects of disorder with respect to the better understood crystalline transport processes. The transport equations are supported in Chapter 2 by a detailed discussion of disorder in HDIM, its effects, nomenclature, and the many ways in which a distribution of charge can interact with that disorder. In particular, the transport equations represent the macroscopic average (mean field) behavior resulting from the DOS and complex carrier interactions within the HDIM. The discussion is simplified with the use of "six easy pieces of charge transport"—which are very simplified DOS diagrams using only the delta function DOS—that show carrier excitations and interactions (see Fig. 2.9). The discussion of the transport equations is supported by an explanation of space charge limited current and dispersive phenomena. These phenomena highlight two very important charge transport cases: in the case of SCLC—a charge transport process typically understood in the context of ordered systems—the theory is extended to include disordered materials; for the second case, dispersion—a charge transport process unique to disordered materials (not necessarily HDIM)—is presented. This juxtaposition of processes, one extended from ordered materials to disorder and the second uniquely disordered, highlight the need for understanding the nature of charge transport at the microscopic level. Said another way, just having the transport equations of Chapter 2 is not enough to understand the true nature of electron transport; a deep understanding of the movement of electrons at the microscopic level is required to interpret differing types of HDIM. The transport processes discussed in Chapter 2 are largely limited to transactions involving extended states and a single level of localized trap states with no energy dependence. (This is not true for the discussion of dispersion, as it serves as the transition discussion between Chapters 2 and 3.) This is not to say that the transport equations are limited to a single level DOS. The transport equations apply to any

type of DOS and any temperature. By contrast, the transport processes discussed in Chapter 3 involve distributions in energy of localized states, extending the transport equations to materials whose DOS covers many energies in the BG and allowing for a complete physical picture regarding carrier dynamics at all temperatures. In particular, we find that each HDIM has a unique type of DOS that dramatically changes the type of transport observed. Thus, Chapter 3 is dedicated to cementing the foundation upon which the transport equations of Chapter 2 are built.

6.3. Summary of Chapter 3

At the end of Chapter 2, a new process—called dispersion—was introduced; it was an exception to the simple mono-energetic delta function DOS that was used to assemble the transport equations. An understanding for the dispersion phenomena can only occur when the DOS is energetically extended in the BG. As it turns out, spatial disorder can also cause dispersion (Bässler, 1993). This meant that (*i*) a new physical description of the dynamics of the carriers in the trapped states was required, and (*ii*) a connection to the macroscopic or average behavior was needed. Because disordered materials have a high degree of complexity—both electronic and chemical—in their internal structure, the best that one can hope for is to understand the motion of charges in some average or statistical way; hence, such transport is often referred to as stochastic transport. As it turns out there is a tremendous body of research in this area generated by studies in photoconduction for disordered semiconductors. Chapter 3 develops the microscopic physical mechanisms that lead to average macroscopic behavior (specifically the conductivity, current density, surface potential, and electric field at the surface and interior to the HDIM), using a set of extended DOS to describe disorder in the material and to predict electron transport in HDIM.

The single electron approximation has been taken in this dissertation; however, it should be noted that in HDIMs, the influence of additional or internal carriers such as holes, excitons, and polarons are generally not significant. The case of holes only came into play as recombination centers or bipolar injection from a contact, which were neglected in this work. This assumption largely holds as electrons are the dominant form of carriers in USU MPG experiments. However, for certain types of contacts and many space environment conditions, positive species are injected simultaneously with electrons. For excitons and polarons, it is thought that due to their lifetime, the only contributions would be made via third party

interactions on timescales much shorter than the experimental times of interest; these are, therefore, neglected.

The development of the microscopic physical mechanisms was accomplished by considering an atomistic description of processes that can occur in the band gap and the effect that the disordered states have on charge trapping, detrapping, and recombination. All of these processes are shown to be controlled by the DOS; even charge generation can be affected by the nature of the DOS (see Section 4.4). Chapter 3 starts with an introduction to the microscopic concepts required to understand the effects the disordered states in the gap have on transport. These mechanisms that were considered were: hopping and hopping rates, demarcation energies, thermalization, transport energies, segregation times, Fermi levels, and thermalization times. These are all processes that are always active in determining the behavior of the observed localized state transport in any HDIM. In most cases, their effects are not seen directly, unless one is dealing with dispersive transport or low-temperature transport (generally referred to as hopping transport). In the literature, there has been a long-standing difficulty surrounding the concept of hopping transport. By definition, a hop is a jump between two localized states. Many authors confuse hopping transport with simple thermally activated trapping and detrapping, which is often called thermally activated hopping (TAH). TAH is often confused with a form of conduction where the electrons are released from trapped states and then enter the CB (the CB electrons may or may not be recaptured by adjacent trap sites). In a true thermally activated transport, the electron will never leave the localized DOS unless liberated from its trapped state purely by thermal processes to hop to the next available trap state never entering the CB. There is another form of hopping often confused with the process just defined as a true TAH. This hopping transport is called VRH and is fundamentally driven by low-temperature thermal process and a quantum mechanical interaction between localized states. In fact, in this type of hopping the range of the electron can vary—hence its name, variable range hopping. While the definition of each of these types of transport processes may seem mundane, they serve to highlight the very different ways in which the DOS—in a given HDIM—can drive the transport processes. It is exactly the machinery of Chapter 3 that allows the clear distinction of each of the processes. In addition, Chapter 3's results allow the extension of the trapping equations presented in Chapter 2 to low-temperature transport where TAH or VRH are the

dominant conduction mechanism. Without the tools of Chapter 3, it would be impossible to interpret the application of the transport equations when TAH or VRH are active.

Chapter 3 proceeds with a well-founded connection between the ideas for average atomistic systems (microscopic behavior) and macroscopic systems (measurable currents, voltages, and electric fields that result from microscopic behavior). In Section 3.2, insights into the validation and application of the transport energy, demarcation energy, thermalization time, and QFL were developed by interpreting macroscopic physical phenomena previously described by USU MPG VRH models via a concrete example, low-temperature VRH conductivity. This is in contrast to the high-temperature phenomena discussed in Section 2.7. In this example, the three parameter fit of the original USU model can be understood in terms of a simple two parameter model using the theoretical descriptions put forth in Section 3.1. Specially, the parameters σ_0^V ,T_V, and F_V for the VRH model can be expressed in terms of the carrier escape frequency, ν_0^i, and the segregation time, τ_{seg}. This is an important result because it connects the average macroscopic parameters of the USU MPG model with average microscopic parameters that describe the thermalization of trapped charge within the DOS. While this example only addresses the constant DOS, it clearly shows that the ideas presented in Section 3.1 provide predictive physical insight into current VRH models. Further, it connects details of averaging theory to a common interpretation originally developed by Mott and Twose (1961). An important next step in understanding the macroscopic description of VRH transport for the USU MPG experiments is the application of the macroscopic transport equations to the results discussed above. In Chapter 4 (see Section 4.4 and 4.6), only high-temperature data were used; therefore, the same equations should be applied to low-temperature data to test their predictive value. A discussion of VRH conductivity models for the exponential and Gaussian DOS is given in the final sections of Chapter 3, thus, providing a description of the hopping conductivity for HDIM. Chapter 3 provides a complete set of low-temperature, field-dependent conductivity models that will allow more accurate determination of spacecraft charging at low temperatures, where VRH is likely to be active. Of key interest is the fact that, when an HDIM's temperature drops low enough that its dominant method of transport is VRH, the conductivity—and hence ability to dissipate internal charge distributions—is severely reduced. Understanding these phenomena is critical to estimating the decay of charge in situations where the spacecraft is subjected to a high field or particle flux at low temperatures. Thus in Chapter 3, connections to

microscopic average behavior, macroscopic interpretation of those behaviors, and real examples leading to advances in spacecraft engineering have been developed.

Having developed the microscopic tools that allow for a complete physical picture of transport and a correct interpretation of the application of the transport equations in HDIM, the focus of this work was turned toward the derivation of models that describe charge transport in two of the six configurations presented in Chapter 1.

6.4. Summary of Chapter 4

It is paramount that this work developed concrete examples of the application of the transport equations to specific experimental systems used by the USU MPG and spacecraft designers in general. This is the focus of Chapter 4. The transport equations of Chapter 2 are applied to the CVC (parallel plate capacitor) system used to study the long-term effects of moderate to high electric fields on HDIM. One of the key points of this chapter was the use of a charge injection function, which provides a method to moderate the injected charge based on the electrode contact physics and the time-dependent internal charge distribution. The inclusion of the charge injection function in the transport equations and subsequent solution produced a completely new model for the measured current density at the collecting electrode due to charging of an HDIM in a CVC system. Further, it provided an estimation for the surface potential, electric field, and estimation of the dark current conductivity. The USU MPG did not have any previous models that described the time-dependent transport of charge and resultant current density.

The USU MPG CVC charging model can and should be used in conjunction with the models presented for SCLC (Section 2.7.1) and VRH transport (Sections 3.2.4, 3.2.6, and 3.2.7). Taken together, these models represent a comprehensive set of tools to characterize the behavior, dissipation, and mitigation of spacecraft charge problems. In particular a complete engineering tool for the estimation time-dependent current density has been developed using Mathcad^{TM}.

6.5. Summary of Chapter 5

The primary goals of this chapter were approached through the development of theoretical models for the charging and decay of an HDIM leading to a surface potential. Specifically, we discussed surface voltage dependence due to a normally incident electron beam—allowing simulation of spacecraft

environment conditions—on an HDIM as it charges up (electron beam on) and decays (electron beam off). The injection function approach of Chapter 4 was again used to describe the time-dependent injection of charge into an HDIM. Thus, using the same formalism with different physical interpretations to completely different experimental systems was shown to be related by the most obvious of common factors, the HDIM itself. Once developed, this theoretical body was then compared to data taken by using a small voltage probe (SVP) in the SEE system (Hodges, 2013). These models were referred to as the SVP charging and decay models.

The data analysis section brought to light a number of interesting features in both the charging and decay models and the data. First, our surface potential charging models seem to perform very well and predict reasonable values for the cross section, conductivity, and DOS. For the decay models in LDPE, we found a clear case where the model limit (The present model is limited to times before that deposited charge reaches the rear electrode,) is reached and a post-charging (beam off) transit model is required to explain the observed behavior. In Kapton™ (a system that does not reach its transit time during the experiments), we found excellent agreement with the literature and a model of dispersive transport that handles the problems associated with an exponential DOS. This is in contrast to a system like LDPE whose DOS is likely to change over the energy spectrum (Mizutani *et al.*, 2000) in a component-like way due to its semi-crystalline and amorphous nature. In fact, Mizutani *et al.* (2000) gives a table of activation energies and the corresponding molecular regions within LDPE responsible for such transitions.

For 0.8 eV to 1.0 eV activation energies, it is suggested that the amorphous regions associated with defect structures are the primary active components. We obtained a value of $0.873\ eV$ for our release rate activation energy, which seems to be in agreement with Mizutani. However, even for a system as complex as LDPE, we find reasonable agreement with literature within the pre-transit regime. Taking the data from the Toomer and Lewis (1980) table and creating plots for the release rate and trapping rate shows their strong dependence on the field. The appearance of field dependence in the physical parameters makes a direct connection to the inclusion of field dependence described in Section 3.2. The results of this section clearly indicate that the dynamics of the high field regime are at work, and the system is controlled by the interaction between the internal electric field, QFL (since the FL moves with time), and the demarcation energies (which govern the rate at which the DOS will fill up). A complete study on the dynamics of each

material under a range of beam energies, temperatures, and fluencies will yield a great deal of information about these dynamics. These studies—in addition to concurrent studies on the surface potential, SEE, and CVC—will open doors to a deep understanding of the spacecraft charging phenomena.

This dissertation has accomplished the goal set forth in Chapter 1 of developing a single, consistent theoretical framework for the study of charge transport, resultant electric fields, and dependence on local and internal electric fields, temperature, and incident energy of injected particles, particle flux, fluence, and time. This theoretical formalism has been shown to extend current theories and has allowed for the development of several new models for the study of charge transport, all of which are based on the transport equations from Section 2.6 and average microscopic tools introduced in Section 3.1. First, in Section 2.7.1 the complete SCLC theory as discussed in Section 2.7 in conjunction with the work of Kao, is used to show how SCLC behavior—originally developed for ordered materials—is extended to disordered materials; see Section 2.7.1. In Chapter 3, the original USU VRH model developed in Dennison *et al.* (2009a) is extended to include the average microscopic description. The USU VRH model is explained in terms of this new theoretical framework, leading to a reduction in the number of free parameters. In Chapter 4 a new model for the CVC system is developed using a combination of two methods, both of which are fundamentally based on the transport equations; this new model is the first of its kind to this author's knowledge. In Section 5.3, the developments made for charge injection are used to develop a new theory for the charging of HDIM under electron beam injection; this is also a new model though it is similar to a model that was incorrectly extended in Liufu *et al.* (1998). This approach is used to develop an expression for both the surface potential and current density of the collecting electrode, using the transport equations as a guide. In Section 5.4, a model originally developed by Toomer and Lewis, (1980) and extended by Aragoneses *et al.* (2008) using the work of Ferreira and de Almeida (1997) is developed from the transport equations; this leads to a complete description of the model in Aragoneses *et al.* (2008) which previously suffered from undetermined constants. Finally, the theoretical developments of Chapters 4 and 5 are fit to charging and decay data taken on LDPE and Kapton^{TM}. The agreement with the literature and across experimental platforms is modest, at worst, and in most cases, is excellent. In particular, in Section 5.5.4 regarding the decay of electron beam irradiated Kapton^{TM}, the agreement with the previous results in Aragoneses *et al.* (2008) is outstanding. This is particularly impressive as their data were taken on a

completely different type of apparatus that is essentially a CVC system. Further, the data on Kapton™ and LDPE were among the very first runs ever performed with the USU MPG SEE-SVP system.

To solidify the results of the CVC and SVP model validation, and subsequently the transport formalism presented in this dissertation, a set of fitting parameters is brought together in Table 6.1 and Table 6.2 showing LDPE and Kapton™, respectively (Sim, 2010). These parameters—the DOS, capture cross section, trapping and detrapping (or excitation) rates, conductivity, and mobility—are the most common predictors of a material's ability to dissipate charge, and therefore, are relevant to the spacecraft charging problem. Tables 6.1 and 6.2 are organized by experiment type (left column) and split into two sections, one for LDPE and one for Kapton™. All of these data come from USU MPG experiments; only a single data run was used for each of the experimental systems and material types, which must be improved and leaves our validation suspect. For LDPE, notice that in each of the columns, we get good agreement between experimental systems for all of the parameters where data are available. For Kapton™, data from RIC experiments originally conducted by Gillespie (2013) were fit with the transport equations to obtain the parameters used in this table. The application of the transport equations to RIC has been done by many authors and is discussed briefly in Section 5.2; for additional information, see Sim (2010). A more compete development of RIC in the formalism laid out in this dissertation has been written, but is not included here. The agreement between the different experimental systems is again good, with the exception of the detrapping parameter for RIC. Completion of the development, application, and interpretation of the RIC equations for the data sets described by Gillespie (2013) is left as future work; however, what is clear is that very useful information about material properties can be extracted using the formalism presented in this dissertation.

These results taken together with the theoretical formalism used to produce these models—in a single nomenclature—represents the totality of this dissertation. There is a tremendous amount of additional work to be done and to that end the final section of this dissertation is dedicated to a brief discussion of these areas future work.

TABLE 6.1 Cross-platform data for LDPE.

Experiment type	DOS N_t [cm^{-3}]	μ_0 10^{-15} [m^2Vs]	Cross section [cm^2]	Trapping rate [s^{-1}]	Detrapping rate [s^{-1}]	Conductivity [Ω^{-1} cm^{-1}]
SVP -Charge	$2.029 \times 10^{+17}$	N/A	1.498×10^{-14}	N/A	N/A	$\sim 2 \times 10^{-15}$
SVP – Decay	N/A	3.15×10^{-15}	N/A	1.055×10^{-3}	2.135×10^{-4}	$\sim 4.0 \times 10^{-}17$
CVC -Charge	3.08×10^{17}	1.256×10^{-15}	$1.209 \times 10^{}$	N/A	N/A	$\sim 1.0 \times 10^{-18}$
ESD	6.48×10^{18}	N/A	N/A	N/A	N/A	Curve

6.6. Future Work

There are numerous areas in this dissertation where future work is suggested. Some of these areas are in clarification and validation of theoretical concepts and ideas presented. In particular, the areas of RIC, SCLC, VRH, and ESD are all areas where the concepts presented in this dissertation can be used to extend the USU MPG understanding of charge transport, charge storage, and material breakdown in HDIM. A brief outline follows of major areas where extensions can be made.

Radiation induced conductivity is a key component in understanding the spacecraft charging problem. The transport equations of Chapter 2 should be applied to RIC; the interested reader should consult Rose (1951), Fowler (1955), Sessler (1987), Arkhipov (1993a), Weaver *et al.* (1977), Orenstein *et al.* (1982), Schmidlin (1977), Yahagi and Shinohara (2004), Dennison *et al.* (2009c), Tyutnev (1996), Gillespie (2013), and Sim (2010). In Chapter 5 a brief discussion of RIC was presented and its importance discussed. Further, the inclusion of the RIC equations will allow for a more complete analysis of present data taken on the USU MPG RIC system (Dennison *et al.*, 2009c; Gillespie, 2013). The use of the transport equations will allow for a determination of the dynamic response due to RIC of various HDIM that have been tested at USU, but as yet, remain unanalyzed with the exception of the equilibrium data analyzed for Tables 6.1 and 6.2. It will also allow for the cross checking of material parameters measured in the other USU systems and the literature.

Closely related to RIC is a set of experiments called time of flight (TOF). See Fig. 1.4 (a), (*i*). In this configuration, electrons are deposited on the surface of the sample and allowed to traverse the sample

TABLE 6.2 Cross platform data for Kapton-HN™

Experiment type	DOS N_t $[\mathbf{cm^{-3}}]$	μ_0 $\mathbf{10^{-15}}$ $[\mathbf{m^2Vs}]$	Cross section [cm^2]	Trapping rate $[\mathbf{s^{-1}}]$	Detrapping rate $[\mathbf{s^{-1}}]$	Conductivity $[\mathbf{\Omega^{-1}\,cm^{-1}}]$
SVP -Charge	$5.29 \times 10^{+17}$	N/A	1.29×10^{-14}	N/A	N/A	$\sim 3.85 \times 10^{-14}$
SVP – Decay	N/A	6.98×10^{-15}	N/A	7.32×10^{-4}	4.34×10^{-5}	$\sim 1.57 \times 10^{-}19$
CVC - Charge	4.27×10^{17}	5.00×10^{-14}	1.3×10^{-14}	3.33×0^{-6}	7.7×10^{-2}	$\sim 1.0 \times 10^{-18}$
ESD	5.17×10^{17}	N/A	1.5×10^{-13}	4.61×10^{-4}	2.58×10^{-5}	N/A

under the action of an applied electric field or a self-field. This experimental method is often used to estimate intrinsic values for material parameters; the mobility is the most common parameter to measure. The interested reader should consult Orenstein *et al.* (1982), Monroe (1986), Tyutnev *et al.* (2008c), and Sessler (1987). This type of measurement is very popular with researchers interested in photoconduction (sometimes confused with RIC). The TOF measurement has been performed under a different name by the USU MPG; the method was at that time called charge storage method [see (Swaminathan (2004)]. The transport equations are easily extended to include this method for both photo-induced surface charge and charge distributions deposited on the surface of the HDIM; the method presented in Swaminathan (2004) was the latter of the two.

The application of the SCLC theory is of critical importance to cross check results from the CVC charging model. In particular, in Section 2.7.1 models for the inclusion of the DOS in the SCLC models were discussed; this work is based on theories by Kao (2004), whose development of the subject is far better than that given in Chapter 2. Since the DOS is found to be critical in estimating the onset of different SCLS regimes and possibly breakdown phenomena (Montanari *et al.*, 2001), it is of great importance.

In Sections 3.2.4, 3.2.5, and 3.2.6 VRH models were discussed for the constant, exponential, and Gaussian DOS, respectively. While the model of Section 3.2.4 is an extension of the previous USU MPG VRH model, it remains untested. To this author's knowledge, the remaining two models have never been tested in HDIM. For HDIM known to have a given DOS and to exhibit VRH behavior in an attainable

temperature range, the verification of these models will provide an important verification of the theory presented in Chapter 3. The combination of the VRH models with time-dependent studies using the USU MPG CVC charging model will provide a pathway to study the extension of the transport equations to the low-temperature regime.

The extension of the transport equations and SCLC behavior to ESD is a critical component in the study and mitigation of spacecraft charging. These extensions to models in the formalism of this dissertation were completed during the writing of this dissertation, but are not included. The results of this investigation can be found in Sim and Dennison (2010), Sim (2010), and Ball (2012). Because this work is published elsewhere, no additional discussion will be given; the interested reader should consult Lewis (1990), Lewis *et al.* (1996), Lewis (2002), Crine *et al.* (1989a), Crine *et al.* (1989b), Crine *et al.* (1996), Dang *et al.* (1996), Blythe and Bloor (2005), Sessler (1987), Fothergill (1998), Kao (2004), Liufu (1998), and Avini (1987).

The next—and perhaps most easily accomplished—extension of this work is in the area of secondary electron emission (SEE). Several authors have made progress in applying some form of the transport equations to SEE [see, for instance Song *et al.* (1997), Cornet *et al.* (2008), and Fitting (2010)]. However, it is the opinion of this author all of these models suffer from fatal flaws. In particular, the model developed by Song uses RIC in place of a charge injection term; while RIC must be involved in the charge injection, RIC is not necessary to explain most of the observed phenomena. The models of Cornet *et al.* (2008) and Fitting (2010) are all numerical in nature and rely on a complex set of charge recombination mechanisms to explain the observed behavior. PEA measurement show quite clearly that charge injection by contact methods leads to a charge distribution that stays near the injecting electrode; thus, if an electron beam is incident on one side of the sample and the collecting electrode is on the other side, only a small region near the contacting electrode will have a positive charge distribution. It would seem difficult to explain how positive carriers can be involved in recombination processes anywhere but at the collecting electrode. In Section 5.3.2, a simple expression for the surface potential as a linear function of time and electron total yield was presented, in addition to a time-dependent expression for the total yield. These two results strongly suggest that a very general—and relatively simple—expression for the total yield can be obtained from the transport equations with careful inclusion of SEE theory. This can also be directly

related to a large body of literature on the mean energy loss of incident electrons to the material through the range models (Wilson and Dennison, 2010) and inelastic mean free path models. This work has been described in broad terms in Hodges (2013), but requires the detailed extensions available based of the theories of this dissertation.

Finally, the extension of the transport equations to model surface charge transport should be investigated to understand how charge redistributes on the surface of the spacecraft, in addition to the internal charge transport. This work has already been started by Toomer and Lewis (1980) and is an extension of the previous work used to develop the USU MPG SVP decay model. The new SVP system offers a powerful method for the study of surface charge transport, as shown in Hodges (2013).

For materials that have significant disorder—such as HDIM—the SCLC current density equations must be modified to reflect that disorder by including a description of the DOS. Three tables are shown, each describing a different piece of the SCLC behavior. These pieces are described in Section 2.7 and will not be discussed again here. For a complete discussion of regarding the physics and derivation of these equations see Kao (2004). In Table A.1, a list of the current density equations for various DOS types is shown. The parameter, θ (already described in Section 2.6), is characteristic of the effects the DOS will produce on the observed current density. Table A.3 shows expressions for θ for each of the DOS listed in Section 2.7. A new parameter called the effective sample depth, d_{eff}, is now included to account for the depth to which the charge distribution penetrates into the sample. The effective sample depth follows from the fact that in HDIM, the spatial distribution of traps—and for that matter conduction states—is disordered. Thus, the effective sample depth is a correction term based on the spatial distribution function, $S(x)$, of the injected charge. This spatial disorder term, like its energetic counterparts, can be a constant, exponential, or Gaussian; see Kao (2004) and references therein. Calculation of this parameter is not covered in this dissertation and presented only to alert the reader to the depth of information available in the discussion of SCLC behavior. In particular, the expression for m, l, d_{eff}, and θ are specific for each DOS, and therefore, carefully considered for each application. Further, each of these expressions has an accompanying set of voltage threshold equations, V_{Ω}, and V_{TFL}, that identify the various transition regions in Fig. (2.10).

REFERENCES

Abbott, J., and J. R. Dennison, 2005, "Methods for Determining Crossover Energies in Insulating Materials," in Utah State University Student Showcase, Logan, UT.

Abkowitz, M., 1986, "Comparison of the Drift Mobility Measured under Transient and Steady-State Conditions in a Prototypical Hopping System," Philos. Mag. Part B **53**, 193-216.

Abramov, V. N., Y. D. Pozhidaev, A. P. Tyutnev, V. S. Saenko, and A. V. Vannikov, 1987, "Mobility of Charge-Carriers in Polymers," Vysokomolekulyarnye Soedineniya Seriya A **29**, 260.

Abramowitz, M., 1965, *Handbook of Mathematical Functions: With Formulas, Graphs, and Mathematical Tables (Dover Books on Mathematics),* (Dover Publications, New York).

Alagiriswamy, A. A. and Narayan, K. S., 2002, "Relaxation Processes in Aromatic Polyimide," J. Phys. D **35**, 2850.

Ambegaokar, V., B. I. Halperin, and J. S. Langer, 1971, "Hopping Conductivity in Disordered Systems," Phys. Rev. B **4**, 2612.

Anderson, P. W., 1958, "Absence of Diffusion in Certain Random Lattices," Phys. Rev. **109**, 1492.

Anta, J. A., 2002, "Charge Transport Model for Disordered Materials: Applicaiton to Sensitized TiO_2," Phys. Rev. B **65,** 125324.

Apsley, N., and H. P. Hughes, 1974, "Temperature and Field-Dependence of Hopping Conduction in Disordered Systems," Philos. Mag. **30**, 963.

Apsley, N., and H. P. Hughes, 1975, "Temperature and Field-Dependence of Hopping Conduction in Disordered Systems, II, Philos. Mag. **31**, 1327.

Aragoneses, A., M. Mudarra, J. Belana, and J. A. Diego, 2008, "Study of Dispersive Mobility in Polyimide by Surface Voltage Decay Measurements," Polym. **49**, 2440.

Arkhipov, V. I., 1986, "Kinetics of Pair Recombination in Amorphous Materials," Fizika i Tekhnika Poluprovodnikov (Sankt-Peterburg) **20**, 556.

Arkhipov, V., 1993a, "Radiation-Induced Conductivity and Charge Storage in Irradiated Dielectrics," J. Appl. Phys. **26**, 1298.

Arkhipov, V. I., 1993b, "Non-Langevin Recombination in Disordered Deilectrics," J. Phys. D: Appl. Phys **26**, 1301.

Arkhipov, V. I., 1999, "Current Injection from a Metal to a Disordered Hopping System. II. Comparison between Analytic Theory and Simulation," Phys. Rev. B **59**, 7507.

Arkhipov, V. I., and G. J. Adriaenssens, 1995, "Thermally Stimulated Currents in Amorphous Semiconductors," J. Noncryst. Solids **181**, 274.

Arkhipov, V. I., and G. J. Adriaenssens, 1996, "Equilibrium Trap-Controlled Carrier Mobility in System of Randomly Fluctuating Localized States," Philos. Mag. Letters **73**, 263.

Arkhipov, V. I., and H. Bässler, 1994a, "A Random-Walk Model of Relaxations in Supercooled Melts," J. Noncryst. Solids **172-174**, 396.

Arkhipov, V. I., and H. Bässler, 1994b, "A Random-Walk Model of the Glass Transition and Relaxations in Supercooled Liquids," *Proc. 5th Conf. Hopping and Related Phenomena*, 161.

Arkhipov, V. I., H. Bässler, and D. V. Khramtchenkov, 1996a, "Random-Walk Approach to Dynamic and Thermodynamic Properties of Supercooled Melts, 2. Coupling of Structural Units and Susceptibility Spectra," Physical Chem. **100**, 5118.

Arkhipov, V. I., H. Bässler, and D. V. Khramtchenkov, 1997a, "Random Walk Approach to the Glass Transition and Relaxations in Super-Cooled Melts," Future Directions in Thin Film Science and Technology, in *Proc. Int. School on Condensed Matter Phys.*, 9th, Varna, Bulgaria, 1996, 40.

Arkhipov, V. I., E. V. Emelianova, and G. J. Adriaenssens, 2000, "Variable-Range Hopping within a Fluctuating Potential Landscape," J. *Phys.* Condensed Matter **12**, 2021.

Arkhipov, V. I., E. V. Emelianova, G. J. Adriaenssens, and H. Bässler, 2002a, "Equilibrium Carrier Mobility in Disordered Organic Semiconductors," J. Noncryst. Solids **299-302**, 1047.

Arkhipov, V. I., E. Emelianova, and H. Bässler, 2001a, "Equilibrium Charge Carrier Mobility in Disordered Hopping Systems," J. Opto. Adv. Mat. **3**, 601.

Arkhipov, V. I., E. V. Emelianova, and H. Bässler, 2001b, "Charge Carrier Transport and Recombination at the Interface between Disordered Organic Dielectrics," J. Appl. Phys. **90**, 2352.

Arkhipov, V. I., E. V. Emelianova, and H. Bässler, 2001c, "A Tandem Mechanism of Charge-Carrier Photogeneration in Disordered Organic Materials," Phys. Chem. Chem. Phys. Letters **340**, 517.

Arkhipov, V. I., E. V. Emelianova, P. Heremans, and G. J. Adriaenssens, 2002b, "Equilibrium Hopping Conductivity in Disordered Materials," J. Optoelectronics and Advanced Materials **4**, 425.

Arkhipov, V. I., E. V. Emelianova, P. Heremans, and H. Bässler, 2005a, "Analytic Model of Carrier Mobility in Doped Disordered Organic Semiconductors," Phys. Rev. B Condensed Matter and Materials Phys. **72**, 235202.

Arkhipov, V. I., I. I. Fishchuk, A. Kadashchuk, and H. Bässler, 2006, in *Charge Transport in Disordered Organic Semiconductors*, (Wiley-VCH Verlag Gmbh and Co., New York), p. 261.

Arkhipov, V. I., V. V. Gromov, M. N. Mamonov, A. G. Rozno, and A. I. Rudenko, 1987a, "Gamma-Ray Electrification of Dielectrics," Atomnaya Energiya **62**, 134.

Arkhipov, V. I., V. V. Gromov, M. N. Mamonov, A. G. Rozno, A. I. Rudenko, and M. N. Strikhanov, 1987b, "Electric-Field Relaxation Kinetics in Gamma Irradiated Polym. Dielectrics," Atomnaya Energiya **62**, 136.

Arkhipov, V. I., P. Heremans, E. V. Emelianova, G. J. Adriaenssens, and H. Bässler, 2002c, "Weak-Field Carrier Hopping in Disordered Organic Semiconductors: The Effects of Deep Traps and Partly Filled Density-of-States Distribution," J. Phys. Condensed Matter **14**, 9899.

Arkhipov, V. I., P. Heremans, E. V. Emelianova, G. J. Adriaenssens, and H. Bässler, 2003a, "Charge Carrier Mobility in Doped Semiconducting Polymers," Appl. Phys. Lett. **82**, 3245.

Arkhipov, V. I., P. Heremans, E. V. Emelianova, G. J. Adriaenssens, and H. Bässler, 2003b, "Equilibrium Trap-Controlled and Hopping Transport of Polarons in Disordered Materials," Phys. Chem., **288**, 51.

Arkhipov, V. I., P. Heremans, E. V. Emelianova, G. J. Adriaenssens, and H. Bässler, 2004, "Charge Carrier Mobility in Doped Disordered Organic Semiconductors," J. Noncryst. Solids **338-340**, 603.

Arkhipov, V. I., P. Heremans, E. V. Emelianova, and H. Bässler, 2005b, "Effect of Doping on the Density-of-States Distribution and Carrier Hopping in Disordered Organic Semiconductors," Phys. Rev. B **71**, 045214.

Arkhipov, V. I., M. Iovu, A. I. Rudenko, and S. D. Shutov, 1979, "An Analysis of the Dispersive Charge Transport in Vitreous 0.55 Arsenic Trisulfide:0.45 Antimony Trisulfide," Phys. Status Solidi (a) **54**, 67.

Arkhipov, V. I., M. S. Iovu, A. I. Rudenko, and S. D. Shutov, 1985a, "Kinetics of Nonequilibrium Recombination in Amorphous Semiconductors," Fizika i Tekhnika Poluprovodnikov (Sankt-Peterburg) **19**, 101.

Arkhipov, V. I., V. M. Login, and S. Ya. Shevchenko, 1985b, "Effect of Multiple Trapping on Photoreceptor Discharge Characteristics under the Condition of Surface Carrier Generation," Phys. Status Solidi (a) **89**, 293.

Arkhipov, V. I., and V. R. Nikitenko, 1993, "Quantum Efficiency of Geminate Recombination under Dispersive Transport Conditions," J. Noncryst. Solids **164-166**, 587.

Arkhipov, V. I., and V. R. Nikitenko, 1999, "Langevin-Recombination-Controlled Explosive Kinetics of Electroluminescence in Organic Semiconductors," Semiconductors (Translation of Fizika i Tekhnika Poluprovodnikov (Sankt-Peterburg) **33**, 862.

Arkhipov, V. I., V. R. Nikitenko, and A. P. Tyutnev, 1997b, "On the Frequency Dependence of Radiation-Induced Conductivity of Polymers within the Hopping Mechanism of Charge Carrier Mobility," Chem. Phys. Reports **16**, 387.

Arkhipov, V. I., V. R. Nikitenko, and A. P. Tyutnev, 1997c, "Radiation-Induced Dielectric Effect in Polymers," Chem. Phys. Reports **16**, 301.

Arkhipov, V. I., J. A. Popova, and A. I. Rudenko, 1983, "A Model of Trap-Controlled Recombination in Disordered Materials," Philos. Mag. B *Phys.* Condensed Matter Statistical Mechanics, Electronic, Optical and Magnetic Properties **48**, 401.

Arkhipov, V. I., J. Reynaert,Y. D. Jin, P. Heremans, E. V. Emelianova, G. J. Adriaenssens, and H. Bässler, 2003c, "The Effect of Deep Traps on Carrier Hopping in Disordered Organic Materials," Synthetic Metals **138**, 209.

Arkhipov, V. I., and A. I. Rudenko, 1979, "Anomalous Charge Transfer in Amorphous Semiconductors," Fizika i Tekhnika Poluprovodnikov (Sankt-Peterburg) **13**, 1352.

Arkhipov, V. I., and A. I. Rudenko, 1982a, "Behavior of Transient Photocurrent in Amorphous Semiconductors," Fizika i Tekhnika Poluprovodnikov (Sankt-Peterburg) **16**, 2068. (In Russian)

Arkhipov, V. I., and A. I. Rudenko, 1982b, "Dispersion Transport as a Method of the Spectroscopy of Localized States in Disordered Semiconductors," Tr. Vses. Konf. Fiz. Poluprovodn. **2**, 60. (In Russian)

Arkhipov, V. I., and A. I. Rudenko, 1982c, "Drift and Diffusion in Materials with Traps. II. Nonequilibrium Transport Regime," Philos. Mag. B *Phys.* Condensed Matter Statistical Mechanics, Electronic, Optical and Magnetic Properties **45**, 189.

Arkhipov, V. I., A. I. Rudenko, and S. D. Shutov, 1987c, "Transient Hopping Conductivity in Amorphous Semiconductors with Nonequilibrium Occupation of Localized States," J. Noncryst. Solids **97-98**, 129.

Arkhipov, V. I., A. P. Tyutnev, and V. R. Nikitenko, 1996b, "Mechanism of Charge Carriers Recombination in Polymers," Khimicheskaya Fizika **15**, 100. (In Russian)

Arkhipov, V. I., A. V. Vannikov, G. S. Mingaleev, Y. A. Popova, A. I. Rudenko, V. S. Saenko, and A. P. Tyutnev, 1984, "Transient Photocurrent Due to Step-Function Excitation in Disordered Materials - Computer-Simulation and Analytical Treatment," Phys. D-Appl. Phys. **17**, 1469.

Arnaout, M., 2010, "Contribution to Improving the Spatial Resolution of a Pulsed Electro Acoustic Cell Measurement," *Proc. IEEE Int. Conf. on Solid Dielectrics*, LAPLACE (Lab. plasma et conversion d'energie), Univ. de Toulouse, Toulouse).

Ashcroft, N., and N. D. Mermin, 1976, *Solid State Phys.* (Holt Rinehart and Winston, New York).

Auge, J. L., C. Laurent, D. Fabiani, and G. C. Montanari, 2000, "Investigating Dc Polyethylene Threshold by Space Charge. Current and Electroluminescence Measurements," Dielectr. Electr. Insul., IEEE Trans. **7**, 797.

Avini, E., 1987, "Trap Generation and Occupation in Stressed Gate Oxides under Spatially Variable Oxide Electric Field," Appl. Phys. Lett. **51**, 1857.

Ball, D., and J. R. Dennison, 2012, "An Electron Duel: Cathodoluminescence in Disordered Polymeric Materials," *National Council of Undergraduate Research*, Weber State University, Ogden, UT.

Baranovskii, S., and O. Rubel, 2006, "Charge Transport in Disordered Materials," Springer Handb. Electron. Photonic Mater., (Springer-Verlag, New York), 161.

Bässler, H., 1984, "Charge Transport in Molecularly Doped Polymers," Philos. Mag. Part B **50**, 347.

Bässler, H., 1993, "Charge Transport in Disordered Organic Photoconductors a Monte Carlo Simulation Study," Phys. Status Solidi (b) **175**, 15.

Batra I. P., B. H. Schechtman, and H. Seki, 1970, "Transient Space-Charge-Limited Currents in Photoconductor-Dielectric Structures," Phys. Rev. B, 2(3), 1592.

Baudoin, F., 2008, "Bipolar Charge Transport Model with Trapping and Recombination: An Analysis of the Current Versus Applied Electric Field Characteristic in Steady State Conditions," J. Phys. D-Appl. Phys. **41**, p. 025306.

Baum, E. A., Lewis, T. J., and Toomer, R., 1978, "The Lateral Motion of Charge on Thin Films of Polyethylene Terephthalate," J. Phys. D**11**, 963.

Berlepsch, H. V., 1985a, "Field-Dependent Injection in HDPE," Phys. Status Solidi (a) **92**, 285.

Berlepsch, H. V., 1985b, "Interpretation of Surface Potential Kinetics in HDPE by a Trapping Model," J. Phys. D**18**, 1155.

Blythe, T., and D. Bloor, 2005, *Electrical Properties of Polymers* (New York Press, New York).

Böer, K. W., 2002, *Survey of Semiconductor Physics* (Wiley, New York).

Böttger, H., and V. V. Bryksin, 1985, *Hopping Conduction in Solids* (VCH, Deerfield Beach, FL).

Breskin, A., R. Chechik, A. Gibrekhterman, I. Frumkin, L. Levinson, A. Notea, and B. Weingarten, 1994, "Secondary Electron Emission Gaseous Detectors for Fast X-Ray Imaging," Nucl. Instrum. Methods, A, **353**, 302.

Brunson, J., 2009, "Measurement of Charge Decay Time and Resistivity of Spacecraft Insulators Using Charge Storage Method and Application to Theoretical Modeling of Charging Behavior of Insulators," PhD Dissertation (Utah State University).

Brunson, J., and J. R. Dennison, 2005, "Comparison of Methods for Resistivity Measurements of Insulators," in *Proc. 10th Rocky Mountain NASA Space Grant Consortium NASA Fellowship Symposium*, Salt Lake City, UT.

Brunson, J., and J. R. Dennison, 2006, "E-Field Dependent Conduction in Low-Density Polyethylene," in *Proc. 11th Rocky Mountain NASA Space Grant Consortium NASA Fellowship Symposium*, Salt Lake City, UT.

Brunson, J., and J. R. Dennison, 2007, "Hopping Conductivity in Low-Density Polyethylene," in *Proc. 12th Rocky Mountain NASA Space Grant Consortium NASA Fellowship Symposium*, Salt Lake City, UT.

Brunson, J., and J. R. Dennison, 2008, "Temperature Dependent Hopping Conductivity Models for Low-Density Polyethylene," in *Proc. 13th Rocky Mountain NASA Space Grant Consortium NASA Fellowship Symposium*, Salt Lake City, UT.

Cazaux, J., 1999, "Some Considerations on the Secondary Electron Emission, δ, from e^- Irradiated Insulators," J. Appl. Phys. **85**, 1137.

Cazaux, J., 2004, "Charging in Scanning Electron Microscopy From Inside and Outside," Scanning **26**, 181.

Chen, G., 2010, "A New Model for Surface Potential Decay of Corona-Charged Polymers," J. Phys. D-Appl. Phys. **43**, 055405-055412.

Clerc, S., J. R. Dennison, R. Hoffmann, and J. Abbott, 2006, "On the Computation of Secondary Electron Emission Models," IEEE Trans. on Plasma Science **34**, 2219.

Cleve, B., B. Hartenstein, S. D. Baranovskii, M. Scheidler, P. Thomas, and H. Bässler, 1995, "High-Field Hopping Transport in Band Tails of Disordered Semiconductors," Phys. Rev. B, **51**, 16705.

Cornet, N., D. Goeuriot, C. Guerret-Piecourt, D. Juve, D. Treheux, M. Touzin, and H.-J. Fitting, 2008, "Electron Beam Charging of Insulators with Surface Layer and Leakage Currents," J. Appl. Phys. **103**, 13.

Crine, J. P., 2004a, "On the Interpretation of Some Electrical Aging and Relaxation Phenomena in Solid Dielectrics," in *Electrical Insulation and Dielectric Phenomena, 2004. CEIDP '04. 2004 Annual Report Conf. on Electrical Insulation and Dielectric Phenomena*.

Crine, J. P., 2004b, "Relations between Aging, Space Charge and Polarization of Polyethylene," in *Solid Dielectrics, 2004. ICSD 2004. Proc. 2004 IEEE Int. Conf. on Solid Dielectrics*.

Crine, J. P., 2005a, "Influence of Electro-Mechanical Stress on Electrical Properties of Dielectric Polymers," IEEE Trans. on Dielectr. Electr. Insul. **12**, 791.

Crine, J. P., 2005b, "On the Interpretation of Some Electrical Aging and Relaxation Phenomena in Solid Dielectrics," IEEE Trans. on Dielectr. Electr. Insul. **12**, 1089.

Crine, J. P., 2007, "A Molecular Model for the Electrical Aging of XLPE," in *Electrical Insulation and Dielectric Phenomena, 2007. CEIDP 2007. Annual Report--Conf. on Electrical Insulation and Dielectric Phenomena*.

Crine, J. P., C. Dang, and J. L. Parpal, 1996, "Electrical Aging of Extruded Dielectric Cables: A Physical Model," in *Electrical Insulation, 1996., Conf. Record of the 1996 IEEE Int. Symposium on Electrical Insulation*.

Crine, J. P., J. L. Parpal, and C. Dang, 1989a, "A New Approach to the Electric Aging of Dielectrics," in *Electrical Insulation and Dielectric Phenomena, 1989. Annual Report., Conf. on Electrical Insulation and Dielectric Phenomena*.

Crine, J. P., J. L. Parpal, and G. Lessard, 1989b, "A Model of Aging of Dielectric Extruded Cables," in *Conduction and Breakdown in Solid Dielectrics, 1989, Proc. 3rd Int. Conf. on Conduction and Breakdown in Solid Dielectrics,* Trondheim, Norway.

Curie, M., 1904, "Radium and Radioactivity," The Century Magazine 67, 461.

Dang, C., J. L. Parpal, and J.-P. Crine, 1996, "Electrical Aging of Extruded Dielectric Cables. Review of Existing Theories and Data," IEEE Trans. on Dielectr. Electr. Insul. **3**, 237.

Davies, D. K., 1969, "Charge Generation on Dielectric Surfaces," J. Phys. D **2**, 1533.

Davies, R., and J. R. Dennison, 1997, "Evolution of Secondary Electron Emission Characteristics of Spacecraft Surfaces," J. Spacecraft and Rockets **34**, 571.

Davis, E. A., 1985, *Amorphous Semiconductors,* M. H. Brodsky, Ed., Vol. 36 (Sringer-Verlag, New York).

Davis, V., D. Ferguson, D. Cooke, and M. Mandell, 2007, "NASCAP-2k Spacecraft-Plasma Environment Interactions Modeling: New Capabilities and Verification," AIAA 2007-1096, 45th AIAA Aerospace Sci. Meeting and Exhibit, Reno, NV.

Dekany, J., J. R. Dennison, and S. Hart, 2008, "Transient Conductivity of Kapton HN," in *American Physical Society Four Corner Section Meeting,* University of Texas-El Paso, El Paso, TX.

Dekany, J., and J. R. Dennison, 2009, "Time Dependent Conductivity of Spacecraft Materials," Utah State University Student Showcase, Logan, UT.

Dekany, J., A. M. Sim, J. Brunson, and J. R. Dennison, 2012, “Electron Transport Models and Precision Measurements in a Constant Voltage Chamber,” in *Proc.* 12*th Spacecraft Charging Technology Conf.*, Kitakyushu, Japan.

Dekany, J., A. M. Sim, J. Brunson, and J. R. Dennison, 2013, “Electron Transport Models and Precision Measurements with the Constant Voltage Conductivity Method,” accepted for publication in IEEE Trans. on Plasma Sci.

Dennison, J. R., 2010, “Effects on Spacecraft Charging of Modification of Materials by Space Environments” in *11th Proc. Spacecraft Charging Technology Conf.*, Albuquerque, NM.

Dennison, J. R., J. Brunson, P. Swaminathan, N. Green, and A. Frederickson, 2006a, "Methods for High Resistivity Measurements Related to Spacecraft-Charging," IEEE Trans. on Plasma Science **34**, 2191.

Dennison, J. R., and J. Brunson, 2008, "Temperature and Electric Field Dependence of Conduction in Low-Density Polyethylene," IEEE Trans. on Plasma Science **36**, 2246.

Dennison, J. R., J. Brunson, S. Hart, J. Gillespie, J. Dekany, C. Sim, and D. Arnfield, 2009a, "Engineering Tool for Temperature, Electric Field and Dose Rate Dependence of High Resistivity Spacecraft Materials,"Paper Number 092407**,** in *47th Am. Inst. of Aeronautics and Astronautics Meeting on Aerospace Sci.*, Orlando, FL.

Dennison, J. R., J. Gillespie, J. Hodges, R. C. Hoffmann, J Abbott, A. W. Hunt, and R. Spalding, 2009b, “Radiation Induced Conductivity of Highly-Insulating Spacecraft Materials,” in Application of Accelerators in Research and Industry, *Am. Inst.of Phys. Conf. Proc. Series*, Vol. **1099**, edited by Floyd D. McDaniel and Barney L. Doyle (Am. Inst. of *Phys.*, Melveille, NY), pp. 203-208.

Dennison, J. R., J. Gillespie, J. Hodges, R. Hoffmann, J. Abbott, A. Hunt, and R. Spalding, 2009c, "Radiation Induced Conductivity of Highly-Insulating Spacecraft Materials," in *Am. Inst. of Phys. Conf. Proc. Series*, Melveille, NY.

Dennison, J. R., J. L. Hodges, J. Duce, and A. Evans, 2009d, "Flight Experiments on the Effects of Contamination on Electron Emission of Materials," in *1st AIAA Atmospheric and Space Environments Conf.*, San Antonio, TX.

Dennison, J. R., C. Thomson, and A. Sim, 2004, "The Effect of Low Energy Electron and UV/Vis Radiation Aging on the Electron Emission Properties and Breakdown of Thin-Film Dielectrics," in *Proc. 8th 2004 IEEE Dielectrics and Electrical Insulation Society (DEIS) Int. Conf. on Solid Dielectrics (ICSD)*, Piscataway, NJ.

Dennison, J. R., C. D. Thomson, J. Kite, V. Zavyalov, and Jodie Corbridge, 2003, "Materials Characterization at Utah State University: Facilities and Knowledgebase of Electronic Properties of Materials Applicable to Spacecraft Charging," *Proc. 8th Spacecraft Charging Technology Conf.,* NASA Marshall Space Flight Center, Huntsville, AL.

Dennison, J. R., A. Sim, and C. D. Thomson, 2006b, "Evolution of the Electron Yield Curves of Insulators as a Function of Impinging Electron Fluence and Energy," IEEE Trans. on Plasma Science **34**, 2204-2218.

Dennison, J. R., A. Sim, J. Brunson, S. Hart, J. Gillespie, J. Dekany, C. Sim, and D. Arnfield, 2009e, "Engineering Tool for Temperature, Electric Field and Dose Rate Dependence of High Resistivity Spacecraft Materials," Paper Number AIAA-2009-0562, *Proc. 47th Am. Inst. of Aeronautics and Astronautics Meeting on Aerospace* Sci. Reno, NV.

DiMaria, D. J., 1975, "Capture and Emission of Electrons at 2.4-Ev-Deep Trap Level in SiO_2 Films," Phys. Rev. B **11,** pp 5023-5030.

Dissado, L. A., and J. C. Fothergill, 1992, *Electrical Degradation and Breakdown in Polymers* (P. Peregrinus, London).

Dissado, L. A., V. Griseri, W. Peasgood, E. S. Cooper, K. Fukunaga, and J. C. Fothergill, 2006, "Decay of Space Charge in a Glassy Epoxy Resin Following Voltage Removal," IEEE Trans. on Dielectr. Electr. Insul., **13**, 903.

Dunaev, A. F., V. S. Saenko, S. N. Makeev, N. I. Filatov, and E. D. Pozhidaev, 1992, "Pulsed Reactor Induced Conductivity in Polymers," Phys. Status Solidi (a) **130**, 391.

Elliott, S. R., 1990, "Physics of Amorphous Materials", 2nd ed., (Longman Scientificand Technical; John Wiley and Sons, New York).

Enis, T., 2002, "Dielectric Mixtures - Electrical Properties and Modeling," IEEE Trans. Dielectr. Electr. Insul. **9**, 809-828.

Esipov, S. E., 1991, "Multiple Trapping in Strong Electric Fields," Phys. Rev. B **44**, 7930.

Ferguson D. C., 2012, "New Frontiers in Spacecraft Charging," IEEE Trans. Plasma Phys., **40**, 139-143

Ferreira, G. F. L. and L. E. C. de Almeida, 1997, "Space-Charge Transport in Disordered Media," Phys. Rev. B **56**, 11579.

Fishchuk, I. I., V. I. Arkhipov, A. Kadashchuk, P. Heremans, and H. Bässler, 2007, "Analytic Model of Hopping Mobility at Large Charge Carrier Concentrations in Disordered Organic Semiconductors. Polarons Versus Bare Charge Carriers," Phys. Rev. B **76**, 045210.

Fitting, H. J., 1975, "The Energy Loss of Transmitted and Backscattered Electrons," Physical D: Appl. Phys. **8**, 1480.

Fitting, H. J., 2010, "Time-Dependent Start-up and Decay of Secondary Electron Emission in Dielectrics," J. Appl. Phys. **108,** 033711.

Fitting, H. J., H. Glaefeke, and W. Wild, 1979, "Creation Energies for Secondary Electrons," Kristall und Technik **14**, K13.

Fothergill, J. C., 1998, "Space Charge in Solid Dielectrics," edited by L. A. Dissado (The Dielectrics Society, London).

Fowler, J., 1956, "X-Ray Induced Conductivity in Insulating Materials," Proc. Royal Society London. Series A, Mathematical and Physical Sciences (1934-1990) **236**, 464.

Fowler, J. F., 1955, "X-Ray Induced Conductivity in Insulating Materials," PhD Dissertation, (University of London).

Fraser, D. A., 1983, *The Physics of Semiconductor Devices* (Clarendon Press ; Oxford University Press, New York).

Frederickson, A. R., P. B. McGrath, and P. Leung, 1989, "Radiation-Induced Electrical Insulator Breakdown," Annual Report., *Conf.* on Electrical Insulation and Dielectric Phenomena, 210, 10.

Frenkel, J., 1938, "On Pre-Breakdown Phenomena in Insulators and Electronic Semi-Conductors," Phys. Rev. **54**, 647.

Fritzsche, H., 1990, *"Transport, Correlation and Structure Defects,"* in Advances in Disordered Semiconductors (World Scientific, Singapore).

Fromhold, A. T. J., 1990, "Theorems Relating to Space-Charge Retardation and Enhancement of Current Transort in Solids," J. Appl. Phys **67**, 4370.

Frubing, P., D. Blischke, R. Gerhard-Multhaupt, and M. S. Khalil, 2001, "Complete Relaxation Map of Polyethylene: Filler-Induced Chemical Modifications as a Dielectric Probes," J. Phys. D **34**, 3051.

Garrett, H. B., 1981, "The Charging of Spacecraft Surfaces," Reviews of Geophysics and Space Physics **19**, 577.

Garrett, H. B., I. Jun, and A. A. Shapiro, 2007, "Interstellar Space Missions: Ultra-Reliability Requirements and Engineering Issues," in *45th AIAA Aerospace Sci. Meeting and Exhibit*, Reno, NV.

Gaur, M., 2008, "Thermally Stimulated Discharge Current and Fractional Polarization Studies in Polyimide (Kapton-H) Samples," Indian J. Pure & Appl. Phys. **46**, 118.

Gaur, M., 2010, "Space Charge Analysis in Polyimide (Kapton-H) Samples," J. Therm. Anal. Calorim. **101**, 1079.

Ghosh, P. K., and W. E. Spear, 1968, "Electronic Transport in Liquid and Solid Sulfur," Proc. Phys. Soc., London, Solid State Phys. **[2]1**, 1347.

Giacometti, J. A., G. F. L. Ferreira, and B. Gross, 1985, "Negative Charge Transport in Fluoroethylenepropylene by the Constant Current Method," Phys. Status Solidi A: Appl. Research **88**, 297.

Gill, W. D., 1972, "Drift Mobilities in Amorphous Charge Transfer Complexes of Trinitrofluorenone and Poly-N-Vinylcarbazole," J. Appl. Phys. **43**, 8.

Gillespie, J., 2013, "Measurements of the Temperature Dependence of Radiation Induced Conductivity in Polymeric Dielectrics," MS Thesis (Utah State University).

Grant, A. J., and E. A. Davis, 1974, "Hopping Conduction in Amorphous Semiconductors," Solid State Commun. **15**, 563.

Griseri, V., 2009, "Behavior of Dielectrics in a Charging Space Environment and Related Anomalies in Flight," IEEE Trans. on Dielectr. Electr. Insul. **16**, 685-689.

Griseri, V., K. Fukunaga, T. Maeno, C. Laurent, L. Levy, and D. Payan, 2004, "Pulsed Electro-Acoustic Technique Applied to in-Situ Measurement of Charge Distribution in Electron-Irradiated Polymers," IEEE Trans. on Dielectr. Electr. Insul. **11**, 891.

Griseri, V., C. Perrin, K. Fukunaga, T. Maeno, D. Payan, L. Levy, and C. Laurent, 2005, "Analysis of Electron Behaviour in Polymeric Films During Electronic Irradiation," Annual Report *Conf.* on Electrical Insulation and Dielectric Phenomena, p. 645.

Griseri, V., C. Perrin, K. Fukunaga, T. Maeno, D. Payan, L. Levy, and C. Laurent, 2006, "Space-Charge Detection and Behavior Analysis in Electron Irradiated Polymers," IEEE Trans. on Plasma Science **34**, 2185.

Gross, B., 1964, *Charge Storage in Solid Dielectrics* (Elsevier, Amsterdam).

Gross, B., 1974, "Charge Dynamics for Electron-Irradiated Polymer-Foil Electrets," J. Appl. Phys. **45**, 2841.

Gross, B., 1978, "Charge Storage and Transport in Solid Dielectrics. (the Case of Irradiated Polymers)," Annual Report - Conf. on Electrical Insulation and Dielectric Phenomena, 55, Vol 1.

Gross, B., 1980, "Radiation-Induced Charge Storage and Polarization Effects [in Dielectrics]," Topics in Appl. Phys. **33**, 217.

Gross, B., and L. De Oliveira, 2003, "Transport of Excess Charge in Electron-Irradiated Dielectrics," J. Appl. Phys. **45**, 4724.

Gross, B., J. Dow, and S. Nablo, 2003a, "Charge Buildup in Electron-Irradiated Dielectrics," J. Appl. Phys. **44**, 2459.

Gross, B., R. Faria, and G. Ferreira, 1981a, "Radiation-Induced Conductivity in Teflon Irradiated by X Rays," J. Appl. Phys. **52**, 571.

Gross, B., R. Gerhard-Multhaupt, A. Berraissoul, and G. Sessler, 1987, "Electron-Beam Poling of Piezoelectric Polymer Electrets," J. Appl. Phys. **62**, 1429.

Gross, B., J. A. Giacometti, and G. F. L. Ferreira, 1981b, "Charge Storage and Transport in Electron-Irradiated and Corona-Charged Dielectrics," IEEE Trans. on Nuclear Science **NS28**, 4513.

Gross, B., and S. V. Nablo, 1967, "High Potentials in Electron-Irradiated Dielectrics," J. Appl. Phys. **38**, 2272.

Gross, B., and L. Nunes De Oliveira, 1974, "Transport of Excess Charge in Electron-Irradiated Dielectrics," J. Appl. Phys. **45**, 4724.

Gross, B., G. Sessler, and J. West, 1977, "Location of Charge Centroid in Electron-Beam-Charged Polymer Films," J. Appl. Phys. **48**, 4303.

Gross, B., G. Sessler, and J. West, 2003b, "Charge Dynamics for Electron-Irradiated Polymer-Foil Electrets," J. Appl. Phys. **45**, 2841.

Halperin, B. I., and M. Lax, 1966, "Impurity-Band Tails in the High-Density Limit. I. Minimum Counting Methods," Phys. Rev. **148**, 722.

Hart, S. R., , J. Brunson, and J. R. Dennison, 2007, “Electric-Field-Induced Hopping Conductivity in Polymers,” *Bull. Am. Phys. Soc.* **52**(1) Part II,. Am. Phys. Soc. March Meeting 2007, Denver, CO.

Hastings, D., and H. Garrett, 1996, *Spacecraft-Environment Interactions* (Cambridge Atmospheric and Space Science Series, New York).

Hertel, D., and H. Bässler, 2008, "Photoconduction in Amorphous Organic Soilds," Chem. Phys. Chem. **9**, 666.

Hertel, D., A. A. Ochse, V. I. Arkhipov, and H. Bässler, 1999, "Recent Advances in Charge Transport in Random Organic Solids: The Case of Conjugated Polymers and Discotic Liquid Crystals," J. Imaging Science and Technology **43**, 220.

Hodges, J., 2013, "*In Situ* Electric Field Measurements," MS Thesis (Utah State University).

Hodges, J. L., A. M. Sim, J. Dekany, G. Wilson, A. Evans, and J. R. Dennison, 2013, "*In Situ* Surface Voltage Measurements of Layered Dielectrics," submitted to IEEE Trans. on Plasma Sci..

Hoffmann, R., 2010, “Electron-Induced Electron Yields of Uncharged Insulating Materials” MS Thesis, (Utah State University).

Hoffmann, R., J. R. Dennison, C. D. Thomson, and J. Albretsen, 2008, "Low-Fluence Electron Yields of Highly Insulating Materials," IEEE Trans. on Plasma Science **36**, 2238.

Ieda, M., 1984, "Electrical Conduction and Carrier Traps in Polymeric Materials," IEEE Trans. on Electrical Insulation **E1-19**, 162-178.

Ieda, M., T. Mizutani, and Y. Suzuoki, 1980, "TSC and TL Studies of Carrier Trapping in Insulating Polymers," Memoirs of the Faculty of Engineering, Nagoya University, Japan **32**, 2.

Ieda, M., G. Sawa, and S. Kato, 2003, "A Consideration of Poole-Frenkel Effect on Electric Conduction in Insulators," J. Appl. Phys. **42**, 3737.

Ieda, M., G. Sawa, and K. Kitagawa, 1972, "Electrical Conduction of Irradiated Polyethylene After Annealing," Annu. Rep. Conf. Elec. Insul. Dielec. Phenomena, 338-345.

Ieda, M., and Y. Suzuoki, 1997, "Space Charge and Solid Insulating Materials: In Pursuit of Spacecharge Control by Molecular Design," IEEE Electrical Insulation Magazine **13**, 10.

Iwamoto, M, 1995, "Transient Current Across Insulating Films with Long-range Movements of Charge Carriers," J. Appl. Phys. **79**, 7936.

Jackson, J. D., 1998, *Classical Electrodynamics*, 3rd ed. (Wiley, New York).

Kao, K. C., 1976, "Theory of High-Field Electric Conduction and Breakdown in Dielectric Liquids," IEEE Trans. on Electrical Insulation **EI11**, 121.

Kao, K. C., 2004, *Dielectric Phenomena in Soilds* (Elsevier Academic Press, San Diego).

Karkin, A.,V. Arkhipov, V. Marchenko, and B. Goshchitskii, 1979, "Electrical Resistivity of V_3Si and Nb_3Sn Under Neutron Radiation," Physica Status Solidi (a) 54, K53.

Kastner, M. A., and D. Monroe, 1982, "The Relationship between Transient and Steady-State Photoconductivity in Amorphous Semiconductors," Sol. Energy Mater. **8**, 41.

Kite, J., 2007, "Secondary Electron Production and Transport Mechanisms by Measurement of Angle-Energy Resolved Cross Sections of Secondary and Backscattered Electron Emission," PhD Dissertation (Utah State University).

Kite, J., J. R. Dennison, W. Y. Chang, and R. E. Davies, 2000, "Effects of Evolving Surface Contamination on Spacecraft Charging," in *Am.Phys. Soc. Four Corner Sectional Meeting*, Fort Collins, CO.

Le Roy, S., V. Griseri, G. Teyssedre, and C. Laurent, 2008, "Simulation of Charge Build up and Transport in Electron Beam Irradiated Organic Dielectrics: Comparison to Space Charge Measurements," in *Electrical Insulation and Dielectric Phenomena, 2008. CEIDP 2008 Annual Report Conf. on Electrical Insulation and Dielectric Phenomena*.

Leach, R., and M. Alexander, 1995, "Failures and Anomalies Attributed to Spacecraft Charging," NASA STI/Recon Technical Report N **96**, 11547.

Legendijk, A., B. van Tiggelen, and D. S. Wiersma, 2009, "Fifty Years of Anderson Localization," Phys. Today **62**.

Lewis, T. J., 1990, "Charge Transport, Charge Injection and Breakdown in Polymeric Insulators," J. Phys. D **23**, 1469.

Lewis, T. J., 2002, "Polyethylene under Electrical Stress," IEEE Trans. on Dielectrics and Electrical Insulation **9**, 717-729.

Lewis, T. J., J. P. Llewellyn, M. J. Van Der Sluijs, J. Freestone, and R. N. Hampton, 1996, "A New Model for Electrical Ageing and Breakdown in Dielectrics," Paper No. 430, in *7th Int. Conf. on Dielectric Materials, Measurements and Application*.

Li, L., 2007, "Tempurature and Field-Dependence of Hopiing Conduction in Organic Semiconductors," Microelectronics J. **38**, 47.

Liu, R., 1993, "Pulsed Electro-Acoustic Method for Measurement of Space Charge Distribution in Power Cables under Both DC and AC Electric Fields," J. Phys. D-Appl. Phys **26**, 986.

Liufu, D., 1998, "High-Field Induced Electrical Aging in Polypropylene Films," J. Appl. Phys. **83**.

Liufu, D., X. S. Wang, D. M. Tu, and K. C. Kao, 1998, "High-Field Induced Electrical Aging in Polypropylene Films," J. Appl. Phys. **83**, 2209.

Livingstone, A. W., 1973, "Impact Ionization of Deep Impurities in Zinc Selenide," J. Phys. C **6**, 3491.

Maeno, T., 2004, "Open-Pea System for Space Charge Measurment in Dielectrics under Irradition," *IEEE Int. Conf. on Solid Dielectrics*, Tokyo Japan, 944-946, Vol 1.

Mandell, M., I. Katz, and M. Hilton, 2001, "NASCAP-2k Spacecraft Charging Models: Algorithms and Applications, in 2001: A Spacecraft Charging Odyssey," *Proc. 7th Spacecraft Charging Technology Conf.* (The Netherlands), **23**, 499.

Many, A., and G. Rakavy, 1962, "Theory of Transient Space-Charge-Limited Currents in Solids in the Presence of Trapping," Phys. Rev. **126**, 1980.

Marianer, S., 1992, "Effective Tempurature of Hopping Electrons in a Strong Electric Field," Phys. Rev. B **46**, 13100-13103.

McKelvey, J., 1993, *Solid State Physics for Engineering and Materials Science* (Krieger Pub. Co. Malabar, FL).

Melchinger, A., and S. Hofmann, 1995, "Dynamic Double Layer Model: Description of Time Dependent Charging Phenomena in Insulators under Electron Beam Irradiation," J. Appl. Phys. **78**, 6224.

Miller, A., and E. Abrahams, 1960, "Impurity Conduction at Low Concentrations," Phys. Rev. **120**, 745.

Mizutani, T., H. Semi, and K. Kaneko, 2000, "Space Charge Behavior in Low-Density Polyethylene," IEEE Trans. Dielectr. Electr. Insul., **7**, 503.

Mizutani, T., Y. Suzuoki, and M. Ieda, 1977, "Thermally Stimulated Currents in Polyethylene and Ethylene–Vinyl-Acetate Copolymers," J. Appl. Phys. **48**, 2408.

Molinie, P., 2005, "Measuring and Modeling Transient Insultor Response to Charging: The Contribution of Surface Potential Studies," IEEE Trans. Dielectr. Electr. Insul. **12**, 939-950.

Monroe, D., 1983, "Generalizations of Multiple Trapping," Philos. Mag. B **47**, 605.

Monroe, D., 1985, "Hopping in Exponential Band Tails," Phys. Rev. Lett. **54**, 146.

Monroe, D., 1986, "Effect of a Defect Level on Multiple Trapping: Exact Results," Solid State Commun. **60**, 435.

Monroe, D., 1987, "Band-Edge Conduction in Amorphous Semiconductors," in *Disordered Semiconductors*, edited by M.A. Kastner, G.A. Thomas, and S.R. Ovshinsky (Plenum, New York), p. 705.

Monroe, D., J. Orenstein, and M. Kastner, 1981, "Density of States in the Gap of a-As_2Se_3 by Photocurrent Transient Spectroscopy," J. Phys. C, **42-4**, 559.

Monroe, D., Y. H. Xie, E. A. Fitzgerald, and P. J. Silverman, 1993, "Transport in High-Mobility Germanium-Silicon ($Si_{1-X}Ge_x$) Heterostructures Grown by Molecular-Beam Epitaxy," Mater. Res. Soc. Symp. Proc. **281**, 449.

Montanari, G., I. Ghinello, A. Motori, S. Gubanski, and D. Das Gupta, 1998, "Searching for Short-Term Techniques for the Inference of Electricalthreshold of PET DC Conductivity Measurements," IEEE Trans. on Dielectr. Electr. Insul. **5**, 148.

Montanari, G., G. Mazzanti, F. Palmieri, A. Motori, G. Perego, and S. Serra, 2001, "Space-Charge Trapping and Conduction in LDPE, HDPE and XLPE," J. Phys. D **34**, 2902.

Montanari, G. C., C. Laurent, G. Teyssedre, A. Campus, and U. H. Nilsson, 2005, "From LDPE to XLPE: Investigating the Change of Electrical Properties. Part I. Space Charge, Conduction and Lifetime," IEEE Trans on Dielectr. Electr. Insul. **12**, 438.

Montanari, G. C., and P. H. F. Morshuis, 2005, "Space Charge Phenomenology in Polymeric Insulating Materials," IEEE Trans. on Dielectr. Electr. Insul. **12**, 754.

Mott, N. F., 1961, "The Theory of Impurity Conduction," Adv. Phys. **10**, 107.

Mott, N. F., 1973, "Transport in Disordered Materials," Phys. Rev. Lett. **31**, 466.

Mott, N. F., 1977, "Electronic Processes in Glasses," Struct. Noncryst. Mater., Proc. Symp. 101-107.

Mott, N. F., 1981, "Conduction near a Mobility Edge," J. de Physique, Colloque, *Proc. Ninth Int. Conf. on Amorphous and Liquid Semiconductors*, 42(C4), pp. 27 -31.

Mott, N. F., 1984, "The Conductivity near a Mobility Edge," Philos. Mag. B **49**, L75.

Mott, N. F., and E. A. Davis, 1971, *Electronic Processes in Non-Crystalline Materials,* (Clarendon Press, Oxford).

Mott, N. F., and E. A. Davis, 1979, *Electronic Processes in Non-Crystalline Materials*, 2nd ed. (Oxford University Press, New York).

Mott, N. F., and R. W. Gurney, 1964, *Electronic Processes in Ionic Crystals* (Dover Publications, New York).

Mott, N. F., and W. D. Twose, 1961, "The Theory of Impurity Conduction," Adv. Phys. **10**, 107.

Mozer, A. J., 2005, "Time-Dependent Mobility and Recombination of the Photoinduced Charge Carriers in Conjugated Polymer/Fullerene Bulk Heterojunction Solar Cells," Phys. Rev. B **72**, 035217.

Muller, R. S., 1963, " A Unified Approach to the Theory of Space-Charge-Limited Currents in an Insulator with Traps," Solid–State Electron. **6**, 25.

Nath, R., and M. Perlman, 1989, "Steady-State Bulk Trap-Modulated Hopping Conduction in Doped Linear Low-Density Polyethylene," J. Appl. Phys. **65**, 4854.

Nikolaenkov, D. V., V. I. Arkhipov, and V. R. Nikitenko, 2003, "Temperature Dependence of Hopping Conductivity of Disordered Materials with Accounting for the Temporal Fluctuations of the Energy of Localized States," Khimicheskaya Fizika **22**, 88.

Nissan-Cohen, Y., 1986, "Trap Generation and Occupation Dynamics in Si02 under Charge Injection Stress," J. Appl. Phys **60, 2024**.

Noolandi, J., 1977a, "Equivalence of Multiple-Trapping Model and Time-Dependent Random Walk," Phys. Rev. B **16**, 4474.

Noolandi, J., 1977b, "Multiple-Trapping Model of Anomalous Transit-Time Dispersion in a-Selenium," Phys. Rev. B **16**, 4466.

Noolandi, J., 1977c, "Theory of Anomalous Dispersion in a-Selenium," Solid State Commun. **24**, 477.

Noolandi, J., 1977d, "Theory of Charge Transport in Amorphous Materials," *Amorphous Liq. Semicond., Proc. Int. Conf.*, 224.

Noolandi, J., 1979, "Stochastic Hopping Versus Multiple-Trapping: The Current State of Theory and Experiment," *Annu. Rep., Conf. Electr. Insul. Dielectr. Phenom.*, 79.

Novikov, L. S., 1999, "Contemporary State of Spacecraft/Environment Interaction Research," Radiat. Meas. **30**, 661.

Novikov, L. S., S. A. Bednyakov, I. K. Ermolaev, N. N. Pilyugin, N. D. Semkin, and K. E. Voronov, 2006, "Ground-Based Tests of Thin-Film Structures and Protective Shields," Eur. Space Agency, [Spec. Publ.] **SP-616**, 50.

Novikov, L. S., V. N. Mileev, E. N. Voronina, L. I. Galanina, A. A. Makletsov, and V. V. Sinolits, 2009, "Radiation Effects on Spacecraft Materials," Poverkhnost, 32, pp 199-214.

Novikov, Y. A., and A. V. Rakov, 1995, "Mechanisms of Secondary Electron Emission of a Relief Surface," J. Moscow Phys. Soc. **5**, 229.

Orenstein, J., and M. Kastner, 1979, "Time-Resolved Optical Absorption and Mobility of Localized Charge Carriers in a-Arsenic Selenide," Phys. Rev. Lett. **43**, 161.

Orenstein, J., M. Kastner, and D. Monroe, 1980, "Time-Resolved Measurements of Photo-Induced Optical Absorption and Photocurrent in Amorphous Arsenic Selenide (As_2Se_3)," J. Noncryst. Solids **35-36**, 951.

Orenstein, J., and M. A. Kastner, 1981, "Thermalization and Recombination in Amorphous Semiconductors," Solid State Commun. **40**, 85.

Orenstein, J., and M. A. Kastner, 1982, "Photocurrent Transient Spectroscopy: Measurement of the Density of Localized States in a-Arsenic Selenide (As_2Se_3[3]). Reply to Comments," Phys. Rev. Lett. **48**, 1229.

Orenstein, J., M. A. Kastner, and V. Vaninov, 1982, "Transient Photoconductivity and Photoinduced Optical Absorption in Amorphous Semiconductors," Philos. Mag., B **46**, 23.

Pai, D., and B. Springett, 1993, "Physics of Electrophotography," Rev. Mod. Phys. **65**, 163.

Perrin, C., 2005, "Space Charge Analysis in Polymers Irradiated by a Quasi-Monoenergetic Electron Beam," *Proc. 2005 Int. Symposium on Electrical Insutation Materials*, Tokyo Japan.

Pfister, G., and H. Scher, 1977, "Electronic Transport in Disordered Solids," *Amorphous Liq. Semicond., Proc. Int. Conf*, (Edinburgh, Scottland), **7**, 197.

Pivrikas, A., 2005, "Charge Carrier Transport and Recombination in Bulk-Heterojunction Solar-Cells," Proc. *Organic Light-Emitting Materials and Devices IX* **5938**, 132.

Pollak, M., 1972, "A Percolation Treatment of DC Hopping Conduction," J. Noncryst. Solids. **11**.

Poole, H., 1916, "On the Dielectric Constant and Electrical Conductivity of Mica in Intense Fields," Philos. Mag. **32**, 112.

Poole, H. H., 1917, "The Temperature Variation of the Electrical Conductivity of Mica," Philos. Mag. (1798-1977) **34**, 195.

Pope, M., 1982, *Electronic Processes in Organic Crystals* (Oxford University Press, New York).

Raikh, M. E., S. D. Baranovskii, and B. I. Shklovskii, 1990, "Dimensional Quantization Amorphous Hydrogenated Silicon Quantum-Well Structures: The Alloy Model," Phys. Rev. B: **41**, 7701.

Reynaert, J., D. Cheyns, D. Janssen, R. Muller, V. I. Arkhipov, J. Genoe, G. Borghs and P. Heremans, 2005, "Ambipolar Injection in a Submicron-Channel Light-Emitting Tetracene Transistor with Distinct Source and Drain Contacts," J. Appl. Phys. **97**, 114501.

Ritter, A.L. J. R. Dennison, and R. Jones, 1984, "The Spectral Momentum Density of Amorphous Carbon from (e,2e) Spectroscopy," Phys. Rev. Lett. **53**, 2054-2057.

Rose, A., 1951, "An Outline of Some Photoconductive Processes," RCA Review **12**, 362.

Rose, A., 1955, "Space-Charge-Limited Currents in Solids," Phys. Rev. **97**, 1538.

Rose, A., 1961, "A Probe for the Defect Structure of Solids," *Proc. Int. Conf. on Semiconductor Phys.*, 458.

Rose, A., 1963, *Concepts in Photoconductivity and Allied Problems,* Vol. 19 (Interscience Publishers, New York).

Rose, A., and M. A. Lampert, 1959, "Photoconductor Performance, Space-Charge Currents, and the Steady-State Fermi Level," Phys. Rev. **113**, 1227.

Rudenko, A. I., and V. I. Arkhipov, 1978, "Trap-Controlled Transient Current Injection in Amorphous Materials," J. Noncryst. Solids **30**, 163.

Rudenko, A. I., and V. I. Arkhipov, 1979, "A Model of Anomalous Charge-Transport Behavior in Amorphous Materials," Philos. Mag. B *Phys.* Condensed Matter Statistical Mechanics, Electronic, Optical and Magnetic Properties **39**, 465.

Rudenko, A. I., and V. I. Arkhipov, 1982a, "Drift and Diffusion in Materials with Traps," Philos. Mag. Part B **45**, 209.

Rudenko, A. I., and V. I. Arkhipov, 1982b, "Drift and Diffusion in Materials with Traps. I. Quasiequilibrium Transport Regime," Philos. Mag. B Phys. Condensed Matter Statistical Mechanics, Electronic, Optical and Magnetic Properties **45**, 177.

Rudenko, A. I. and V. I. Arkhipov, 1982c, "Drift and Diffusion in Materials with Traps. III. Analysis of Transient Current and Transit Time Characteristics," Philos. Mag. B *Phys.* Condensed Matter Statistical Mechanics, Electronic, Optical and Magnetic Properties **45**, 209.

Sah, C.-T., 1991, *Fundamentals of Solid-State Electronics* (World Scientific, Singapore; River Edge, NJ).

Scher, H., 1977, "Hopping, Multiple-Trapping and Trap-Controlled Hopping," *Amorphous Liq. Semicond., Proc. Int. Conf.*, 209.

Scher, H., S. Alexander, and E. Montroll, 1980, "Field-Induced Trapping as a Probe of Dimensionality in Molecular Crystals," *Proc. National Academy of Sci.* **77**, 3758.

Scher, H., and M. Lax, 1973a, "Stochastic Transport in a Disordered Solid. I. Theory," Phys. Rev. B **7**, 4491.

Scher, H., and M. Lax, 1973b, "Stochastic Transport in a Disordered Solid. II. Impurity Conduction," Phys. Rev. B **7**, 4502.

Scher, H., and E. Montroll, 1975, "Anomalous Transit-Time Dispersion in Amorphous Solids," Phys. Rev. B **12**, 2455.

Schiff, E. A., 1981, "Trap-Controlled Dispersive Transport and Exponential Band Tails in Amorphous Silicon," Phys. Rev. **24, 6189**.

Schmidlin, F. W., 1977, "Theory of Trap-Controlled Transient Photoconduction," Phys. Rev. B Solid State **16**, 2362.

Schmidlin, F. W., 1980, "Kinetic Theory of Hopping Transport. I. The Formalism and Its Relationship to Random Walks," Philos. Mag. B Phys. Condensed Matter Statistical Mechanics, Electronic, Optical and Magnetic Properties **41**, 535.

Sessler, G., 1987, *Electrets,* G. M. edited by Sessler, Vol. 33 (Springer-Verlag, New York).

Sessler, G., M. Figueiredo, and G. Ferreira, 2004, "Models of Charge Transport in Electron-Beam Irradiated Insulators," IEEE Trans. on Dielectr. Electr. Insul. **11**, 192.

Sessler, G., and J. West, 1976, "Trap-Modulated Mobility of Electrons and Holes in Teflon Fep," J. Appl. Phys. **47**, 3480.

Sessler, G., and G. Yang, 1999, "Charge Dynamics in Electron-Irradiated Polymers," Brazilian J. Phys. **29**, 233.

Shklovskii, B. I., 1984, *Electronic Properties of Doped Semiconductors* (Springer-Verlag, New York).

Shklovskii, B. I., A. L. Efros, and I. Y. Yanchev, 1971, "Activation Energy of Hopping Conduction," Pis'ma Zh. Eksp. Teor. Fiz. **14**, 348.

Shklovskii, B. I., H. Fritzsche, and S. D. Baranovskii, 1989, "Electronic Transport and Recombination in Amorphous Semiconductors at Low Temperatures," Phys. Rev. Lett. **62**, 2989.

Shockley, W., 1950, "Holes and Electrons," Phys. Today **3**, 16.

Shockley, W., 1951, "New Phenomena of Electronic Conduction in Semiconductors," in *Semiconducting Materials* (Butterworth Scientific Publication, London), p. 26.

Shockley, W., 1976, *Electrons and Holes in Semiconductors, with Applications to Transistor Electronics* (R. E. Krieger Pub. Co., Malabar, FL).

Sim, A., 2010, "A Unified Model of Charge Transport in Insulating Materials," *Rocky Mountain Space Grant Consortium Conf. Proc.*, Logan, UT.

Sim, A., J. R. Dennison, and C. Thomson, 2005, "Evolution of the Electron Yield Curves of Insulators as a Function of Impinging Electron Fluence and Energy," in *Proc. 9th Spacecraft Charging Technology Conf.*, Epochal Tsukuba, Japan.

Sim, C., and J. Dennison, 2010, "Evaluation of the Temperature and Time Dependence of Electrostatic Breakdown," Utah State University Undergraduate Research and Creative Opportunities Grant.

Sim, C., A. M. Sim, J. R. Dennison, and M. Stromo, 2012, "Defect-Driven Dynamic Model of Electrostatic Discharge and Endurance Time Measurements of Polymeric Spacecraft Materials,"*Proc.* 12*th Spacecraft Charging Technology Conf.*, Kitakyushu, Japan.

Song, Z. G., C. K. Ong, and H. Gong, 1997, "Secondary and Backscattered Electron Yields of Polymer Surface under Electron Beam Irradiation," Appl. Surf. Sci. **119**, 169.

Spiegel, M., 1971, *Schaum's Outline of Calculus of Finite Differences & Differential Equations*, edited by M. R. Spiegel, (McGraw-Hill Companies, New York).

Swaminathan, P., 2004, "Measurement of Charge Storage Decay Time and Resistivity of Spacecraft Insulators," MS Thesis (Utah State University).

Tahira, K., 1985, "Anomalous Photocurrent Transient in Polyethylene," J. Appl. Phys D **18**.

Teyssedre, G., and C. Laurent, 2005, "Charge Transport Modeling in Insulating Polymers: From Molecular to Macroscopic Scale," IEEE Trans. on Dielectr. Electr. Insul. **12**, 19p.

Teyssedre, G., C. Laurent, A. Aslanides, N. Quirke, L. A. Dissado, G. C. Montanari, A. Campus, and L. Martinotto, 2001, "Deep Trapping Centers in Crosslinked Polyethylene Investigated by Molecular Modeling and Luminescence Techniques," IEEE Trans. on Dielectr. Electr. Insul. **8**, 744.

Teyssedre, G., C. Laurent, G. C. Montanari, A. Campus, and U. H. Nilsson, 2005, "From LDPE to XLPE: Investigating the Change of Electrical Properties. Part II. Luminescence," IEEE Trans. on Dielectr. Electr. Insul. **12**, 447-454.

Teyssedre, G., C. Laurent, G. Perego, and G. Montanari, 2009, "Charge Recombination Induced Luminescence of Chemically Modified Cross-Linked Polyethylene Materials," IEEE Trans. on Dielectr. Electr. Insul. **16**, 232.

Teyssedre, G., D. Mary, and C. Laurent, 2003, "Electroluminescence and Photoluminescence of UV-Aged Poly(Ethylene-Naphthalate) Films," Proc. IEEE Science, Measurement and Technology, **150**, 83.

Thomson, C., 2001, "Experimental Investigation of Snapover: The Sudden Increase of Plasma Current Drawn to a Positive Biased Conductor When Surrounded by a Dielectric," MS Thesis (Utah State University).

Thomson, C., 2004, "Measurements of the Secondary Electron Emission Properties of Insulators," PhD Dissertation (Utah State University).

Thomson, C., J. R. Dennison, and R. Curruth, 2002, "Experimental Studies of the Secondary Electron Emission Properties of Dielectrics," in *NASA Graduate Student Researchers Program Conf.*, NASA Marshall Space Flight Center, Huntsville, AL.

Thomson, C. D., V. Zavyalov, J. R. Dennison, and J. Corbridge, 2004, "Electron Emission Properties of Insulator Materials Pertinent to the *Int.* Space Station," NASA Conf. Publication **2004-213091**, 83.

Thouless, D. J., 1974, "Electrons in Disordered Systems and the Theory of Localization," Phys. Reports **13**, 93.

Tiedje, T., 1980, "A Physical Interpretation of Dispersive Transport in Disordered Semiconductors," Solid State Commun. **37**, 49.

Tiedje, T., B. Abeles, D. L. Morel, T. D. Moustakas, and C. R. Wronski, 1980, "Electron Drift Mobility in Hydrogenated Amorphous Silicon," Appl. Phys. Lett. **36**, 695.

Tiedje, T., and A. Rose, 1981, "A Physical Interpretation of Dispersive Transport in Disordered Semiconductors," Solid State Commun. **37**, 49.

Tiedje, T., A. Rose, and J. M. Cebulka, 1981, "A Physical Interpretation of Dispersive Transport in Amorphous Silicon Hydride," *AIP Conf. Proc.* **73**, 197.

Toomer, R., and T. J. Lewis, 1980, "Charge Trapping in Corona-Charge Polyethylene Films," J. Phys. D **13**, 1343.

Touzin, M., 2006, "Electron Beam Charging of Insulators: A Self-Consistent Flight-Drift Model," J. Appl. Phys. **99**.

Treadgold, R. H., 1966, *Space Charge in Solids* (Elsevier Publishing Company, New York).

Tyutnev, A. P., 1996, "Radiation-Induced Conductivity of Polymers: A Review," High Energy Chemistry **30**, 1.

Tyutnev, A. P., G. S. Mingaleev, A. V. Vannikov, A. F. Dunaev, V. S. Saenko, and V. S. Likhovidov, 1983a, "Kinetics of Radiation-Induced Conductivity in Some Polymers," Phys. Status Solidi (a) **75**, 385.

Tyutnev A. P., V. N. Abramov., P. I. Dubenskov, V. S. Saenko, E. D. Pozhidaev, and A. V. Vannikov, 1985a, "Doping Effects in Transient Radiation-Induced Conductivity of Polymers," Phys. Status Solidi (a) **91**, 715.

Tyutnev A. P., V. N. Abramov, V. S. Saenko, P. I. Dubenskov, A. V. Vannikov, and E. D. Pozhidaev, 1985b, "Radiation-Induced Conductivity in Foamed Dielectrics," Phys. Status Solidi (a) **88**, 673.

Tyutnev A. P., S. G. Boev, V. N. Abramov, E. A. Kuzmenkov, and A. V. Vannikov, 1990, "Track Effects in Radiation Induced Conductivity of Polymers," Phys. Status Solidi (a) **121**, 205.

Tyutnev A. P., P. I. Dubenskov, V. S. Saenko, and A. V. Vannikov, 1984a, "Radiation-Induced Conductivity of Poly- (N-Vinylcarbazole) and Poly - (N-Epoxypropylcarbazole)," Phys. Status Solidi (a) **84**, 585.

Tyutnev, A. P., R. S. Ikhsanov, V. S. Saenko, and E. D. Pozhidaev, 2006a, "Theoretical Analysis of the Rose-Fowler-Vaisberg Model," Polymer Science Series A **48**, 1196.

Tyutnev, A. P., R. S. Ikhsanov, V. S. Saenko, and E. D. Pozhidaev, 2007, "Theoretical Analysis of the Rose-Fowler-Vaisberg Model: Dipolar Conductivity," Polymer Science Series A **49**, 861.

Tyutnev, A. P., R. S. Ikhsanov, V. S. Saenko, and E. D. Pozhidaev, 2008a, "Numerical Simulation of Annealing of Dose Effects in Radiation-Induced Conductivity of Polymers," Polymer Science Series A **50**, 212.

Tyutnev, A. P., R. S. Ikhsanov, V. S. Saenko, and E. D. Pozhidaev, 2008b, "Theoretical description of the prompt component of pulsed radiation-induced conductivity in polymers in terms of the ion pair mechanism of radiolysis," High Energy Chem. **42**, 266.

Tyutnev, A. P., Y. Kundina, V. S. Saenko, and E. D. Pozhidaev, 2003, "Charge Carrier Transport in Disordered Solids: Dispersive Versus Gaussian," High Performance Polymers **15**, 77.

Tyutnev, A. P., Y. F. Kundina, V. S. Saenko, and E. D. Pozhidaev, 2002a, "On the Transport of Excess Charge Carriers in Polymers," Polymer Science Series B **44**, 77.

Tyutnev, A. P., D. N. Sadovnichii, and S. G. Boev, 1996, "Chemical Aspects of the Radiation-Induced Conductivity in Polymers," Acta Polymerica **47**, 119.

Tyutnev, A. P., V. S. Saenko, V. N. Abramov, V. P. Sichkar, A. I. Kaepechin, E. D. Pozhidaev, and A. V. Vannikov, 1985c, "Dose Effects in Transient Radiation-Induced Conductivity in Polymers," Phys. Status Solidi (a) **89**, 311.

Tyutnev, A. P., V. S. Saenko, A. F. Dunaev, E. D. Pozhidaev, and A. V. Vannikov, 1984b, "Temperature Dependence of Transient Radiation-Induced Conductivity in Polymers," Phys. Status Solidi (a) **85**, 591.

Tyutnev, A. P., V. S. Saenko, A. I. Karpeurin, G. S. Mingaleev, V. I. Arkhipov, A. I. Rudenko, and A. V. Vannieov, 1984c, "Radiation-Induced Conductivity in Polymers under Continuous Irradiation," Phys. Status Solidi (a) **83**, 365.

Tyutnev, A. P., V. S. Saenko, Y. F. Kundina, A. N. Doronin, V. F. Zinchenko, and E. D. Pozhidaev, 2002b, "Radiation-Induced Injection Conductivity of Polymers," High Energy Chemistry **36**, 300.

Tyutnev, P., S. Saenko, S. Ikhsanov, V. N. Abramov, and E. D. Pozhidaev, 2008d, "Generation of Excess Charge Carriers in Molecularly Doped Polymers by Electron-Beam Irradiation," High Energy Chemistry **42**, 29.

Tyutnev, A. P., V. S. Saenko, E. D. Pozhidaev, and A. F. Akkerman, 1982, "Transient Radiation-Induced Conductivity in Polymers," Phys. Status Solidi (a) **73**, 81.

Tyutnev, A. P., V. S. Saenko, and E. D. Pozhidaev, 2006b, "Universal Technique for Studying Electron Transport in Polymers," Polymer Science Series B **48**, 251.

Tyutnev, A. P., V. S. Saenko, E. D. Pozhidaev, and R. S. Ikhsanov, 2008c, "Time of Flight Results for Molecularly Doped Polymers Revisited," J. Phys.-Condensed Matter **20**, 215-219.

Tyutnev, A. P., V. S. Saenko, E. D. Pozhidaev, and V. A. Kolesnikov, 2005, "Charge Carrier Transport in a Molecularly Doped Polymer: Dispersive Versus Gaussian," High Performance Polymers **17**, 175.

Tyutnev, A. P., V. S. Saenko, E. D. Pozhidaev, and V. A. Kolesnikov, 2006c, "Charge Carrier Transport in Polyvinylcarbazole," J. Phys.-Condensed Matter **18**, 6365.

Tyutnev, A. P., V. S. Saenko, A. V. Vannikov, Y. F. Kundina, and E. D. Pozhidaev, 2000, "Electron Transport of Holes in Molecularly Doped Polycarbonate and Its Radiation-Induced Conductivity," High Energy Chemistry **34**, 80.

Tyutnev, A. P., V. S. Saenko., A. V. Vannikov, and G. S. Mingaleev, 1983b, "Radiation-Induced Conductivity in Polyethylene," Phys. Status Solidi (a) **78**, 689.

Tyutnev, A. P., V. S. Saenko., A. V. Vannikov, and V. E. Oskin, 1984d, "Radiation Induced Dielectric Effect in Polymers," Phys. Status Solidi (a) **86**, 363.

Tzimas, A., Rowland, S. M., Dissado, L. A., Fu, M., and Nilsson, U. H.,2010, "The Effect of DC Poling Duration on Space Charge Relaxation in Virgin XLPE Cable Peelings," J. Phys. D: Appl. Phys.**43**, 215401.

Vissenberg, M. C. J. M., 1998, "Theory of the Field-Effect Mobility in Amorphous Organic Transistors," Phys. Rev. **57**, 12964-12968.

Vukmirovic, N., and L. Wang, 2010, "Carrier Hopping in Disordered Semiconducting Polymers: How Accurate is the Miller-Abrahams Model?," (Lawrence Berkeley National Laboratory, Computational Research Division), internal publication and personal communication.

Walden, R. H., 1971, "A Method for the Determination of High-Field Conduction Laws in Insulating Films in the Presence of Charge Trapping," J. Appl. Phys **43**, 1178.

Wang, J., 2009, "Surface Charging of Polyimide Based on Radiation-Induced Conductivity Model," Protection of Materials and Structures from Space Environment, *Proc. 9th Int. Conf.*, Toronto, Canada.

Watanabe, H., N. Yoshimura, S. Katoh, and N. Kobayashi, 1987, "Microdischarges on an Electron Gun under High Vacuum," J. Vac. Sci. Technol. A: Vacuum, Surfaces, and Films **5**, 92.

Weaver, L., J. Shultis, and R. Faw, 1977, "Analytic Solutions of a Model for Radiation-Induced Conductivity in Insulators," J. Appl. Phys. **48**, 2762.

Wilcox, P., 1971, "A Dielectric Loss Model Based on Interfacial Electron Tunneling," Can. J. Phys. **50**, 912-924.

Wilson, G., and J. R. Dennison, 2010, "Approximation of Range in Materials as a Function of Incident Electron Energy," in *Proc. 11th Spacecraft Charging and Technology Conf.*, Albuqueruqe, NM.

Wilson, G., A. Evans, J. Dekany, and J. R. Dennison, 2012, "Charging Effects of Multilayered Dielectric Spacecraft Materials: Surface Voltage, Discharge and Arcing," in *Proc.* 12*th Spacecraft Charging Technology Conf.*, Kitakyushu, Japan.

Wilson, G., A. Evans, J. Dekany, and J. R. Dennison, 2013, "Charging Effects of Multilayered Dielectric Spacecraft Materials: Surface Voltage, Discharge and Arcing," accepted for publication in IEEE Trans. on Plasma Sci.

Wintle, H., 1974a, "Absorbtion Current, Dielectric Constant, and Dielectric Loss by Tunneling Mechanism," J. Appl. Phys **44**, 2514.

Wintle, H., 1974b, "Absorbtion Currents and Steady Currents in Polymer Dielectrics," J. Noncryst. Solids **15**, 471-486.

Wintle, H., 1983, *Conduction Processes in Polymers*, Vol. IIA (American Society for Testing and Materials, Baltimore, MD).

Wintle, H., 1991, "Models for the Decay of Radiation-Induced Conduction," IEEE Trans. on Electrical Insulation **26**, 26.

Wintle, H., 1999, "Charge Motion and Trapping in Insulators: Surface and Bulk Effects," IEEE Trans. on Dielectr. Electr. Insul. **6**, 1.

Wintle, H. J., 2003, "Charge Motion in Technical Insulators: Facts, Fancies and Simulations," IEEE Trans. on Dielectr. Electr. Insul. **10**, 826-841.

Wysocki, S., 1995, "The Energy Distribution Function of Excess Electrons Trapped in the Pulse Irradiated Low Density Polyethylene (LLPE)," Radiation. Phys. Chem. **45**, 79.

Yahagi, K., and K. Shinohara, 2004, "Effect of Carrier Traps in Polyethylene under Gamma-Ray Irradiation," J. Appl. Phys. **37**, 310.

Yang, G., and G. Sessler, 1992, "Radiation-Induced Conductivity in Electron-Beam Irradiatedinsulating Polymer Films," IEEE Trans. on Electrical Insulation **27**, 843.

Zallen, R., 1983, *The Physics of Amorphous Solids* (Wiley, New York).

Zallen, R., and H. Scher, 1971, "Percolation on a Continuum and the Localization-Delocalization Transition in Amorphous Semiconductors," Phys. Rev. B **4**, 4471.

Zatekin, V. V., V. S. Kulikauskas, L. S. Novikov, V. P. Petukhov, V. N. Chernik, P. N. Chernykh, Y. O. Bakhvalov, N. G. Aleksandrov, and T. N. Smirnova, 2008, "Use of Rutherford Backscattering and X-Ray Fluorescence Analysis to Study Polyimide Films from the Mir Orbital Space Station," Poverkhnost, Vol. 3, pp. 23-26.

Zhang, G., W. Zhao, and Z. Yan, 2002, "Analysis of Insulator Surface Charging Due to Charge Injection and Secondary Electron Emission in Vacuum," *20th Int. Symposium on Discharges and Electrical Insulation in Vacuum*, Tours, France, p. 622.

APPENDIX

TABLES FOR DOS TYPES IN SCLC BEHAVIOR

TABLE A.1 List of SCLC DOS-dependent equations.

Case	Single Carrier Injection SCLC current density
Trap-free	$J = \frac{9}{8}\epsilon_0\epsilon_r\,\mu_e\frac{V^2}{d^3}$
Delta Function DOS	$J = \frac{9}{8}\epsilon_0\epsilon_r\,\mu_e\theta_{delta}\frac{V^2}{{d_{eff}}^3}$ For all trap depths.
Exponential DOS	$J = (q_e)^{1-l}\mu_e N_c\left(\frac{2+\alpha}{1+\alpha}\right)^{(1+\alpha)/\alpha}\left(\frac{1}{1+\alpha}\frac{\epsilon_0\epsilon_r}{N_t^e}\right)^{1/\alpha}\frac{V^{(1+\alpha)/\alpha}}{{d_{eff}}^2}$ $\alpha = \frac{T}{T_0^e}$ For all trap depths
Gaussian DOS	$J = \frac{9}{8}\epsilon_0\epsilon_r\mu_e\theta_{gaussian}\frac{V^2}{{d_{eff}}^2}$ For Shallow Traps. $J = {q_e}^{1-m}\mu_e\left(\frac{2m+1}{m+1}\right)^{m+1}\left(\frac{m}{m+1}\frac{\epsilon_0\epsilon_r}{N_t^G}\right)^{m}\frac{V^{m+1}}{{d_{eff}}^2}$ For Deep Traps.
Constant DOS	$J = 2q_e\mu_e N_c g_e\frac{V}{d_{eff}}exp\left[\frac{-\epsilon_{up}-\epsilon_{low}}{k_bT}\right]exp\left[\frac{2\epsilon_0\epsilon_r V}{q_e N_t^c k_b T {d_{eff}}^2}\right]$ where ϵ_{up} and ϵ_{low} are the upper and lower energy bounds of the DOS considered and g_e is called the degeneracy factor. For all trap depths.

After Kao (2004).

TABLE A.2 SCLC critical parameters.

DOS	V_Ω	V_{TFL}
Delta	$\frac{8}{9}\frac{q_e n_e {d_{eff}}^2}{\theta_\delta \epsilon_0 \epsilon_r}$	$\frac{q_e (N_t - n_t) {d_{eff}}^2}{2\epsilon_0 \epsilon_r}$
Constant	$\frac{q_e N_t^c k_b T {d_{eff}}^2}{2\epsilon_0 \epsilon_r}\left[ln\left[\frac{n_e}{2 g_e N_{cb}}\right] - \frac{(\varepsilon_{high} - \varepsilon_{low})}{k_b T}\right]$	$\frac{q_e N_t^c (\varepsilon_{high} - \varepsilon_{low}) {d_{eff}}^2}{2\epsilon_0 \epsilon_r}$
Exponential	$\frac{q_e {d_{eff}}^2}{\epsilon_0 \epsilon_r} N_t^e(\varepsilon_f^0)\left(\frac{n_e}{N_c}\right)^\alpha (1 + \alpha)\left(\frac{1+\alpha}{2+\alpha}\right)^{\alpha+1}$	$\frac{q_e {d_{eff}}^2}{\epsilon_0 \epsilon_r}\left[\frac{9}{8}\frac{\left(N_t^e(\varepsilon_f^0)\right)^{1/\alpha}}{N_c}(1 + \alpha)\left(\frac{1+\alpha}{2+\alpha}\right)^{\left(\frac{\alpha+1}{\alpha}\right)}\right]^{\frac{\alpha}{\alpha-1}}$
Gaussian Shallow Traps	$\frac{8}{9}\frac{q_e n_e {d_{eff}}^2}{\theta_G \epsilon_0 \epsilon_r}$	Approaches the Delta function DOS value for very small energy distributions ε_G; i.e., it is indistinguishable.
Gaussian Deep Traps	$\frac{q_e {d_{eff}}^2}{\epsilon_0 \epsilon_r} N_t^G(\varepsilon_t)\left(\frac{n_e}{N_c}\right)^{1/m}\left(\frac{1+m}{m}\right)\left(\frac{1+m}{2m+1}\right)^{\frac{m+1}{m}}$	$\frac{q_e {d_{eff}}^2}{\epsilon_0 \epsilon_r}\left[\frac{9}{8}\frac{\left(N^G(\varepsilon_t)\right)^m}{N_c}\left(\frac{m+1}{m}\right)^m\left(\frac{m+1}{2m+1}\right)^{1/(m+1)}\right]$

After Kao (2004).

TABLE A.3 Correction fucntions.

DOS	θ_i	d_{eff}
Delta	$\frac{g_e N_c}{N_t^d} exp\left[-\frac{\varepsilon_t}{k_b T}\right]$	$\left[\frac{3}{2}\int_0^d \left(\int_0^t \left(\theta_\delta + S(x)\right) dx\right)^{1/2} dt\right]^{2/3}$
Constant	Since theta is an energetic parameter it does not appear when the DOS is constant.	$\left[2\int_0^d \left(\int_0^t \left(S(x)\right) dx\right) dt\right]^{1/2}$
Exponential Where $N_t\left(\varepsilon_f^0\right)$ is the DOS evaluated at the Fermi level	$\frac{N_c}{N_t^e\left(\varepsilon_f^0\right)} exp\left[-\frac{\varepsilon_f^0}{k_b T}(1-\alpha)\right]$	$\left[\frac{2+\alpha}{1+\alpha}\int_0^d \left(\int_0^t \left(S(x)\right) dx\right)^{\alpha/(1+\alpha)} dt\right]^{(1+\alpha)/(2+\alpha}$
Gaussian Shallow Traps $\varepsilon_t > \varepsilon_f^0$	$\frac{g_e N_c}{N_t^G} exp\left[-\frac{\varepsilon_t}{k_b T} + \frac{1}{2}\left(\frac{\varepsilon_G}{k_b T}\right)^2\right]$	$\left[\frac{2+m}{1+m}\int_0^d \left(\int_0^t \left(S(x)\right) dx\right)^{m/(1+m)} dt\right]^{(1+m)/(2+}$
Gaussian Deep Traps $\varepsilon_t < \varepsilon_f^0$	$\frac{g_e N_c}{N_t^G(\varepsilon_t)} exp\left[-\frac{\varepsilon_f^0}{k_b T}\left(\frac{m-1}{m}\right)\right]$	$\left[\frac{2m+1}{1+m}\int_0^d \left(\int_0^t \left(S(x)\right) dx\right)^{m/(1+m)} dt\right]^{\frac{m+1}{2m+1}}$
	$m \equiv \sqrt{\left[1+\frac{2\pi{\varepsilon_G}^2}{(4k_b T)^2}\right]}$	

After Kao (2004).

CURRICULUM VITAE

Alec M Sim
Assistant Professor of Physics
Irvine Valley College

EDUCATION:

Bachelor of Science
Physics
June 2003

Master of Science
Physics
University of Kentucky
December 2008

Doctor of Philosophy
Physics
Dissertation: "Unified Model of Charge Transport in Insulating Polymeric Materials"
Utah State University
December 2013

SCHOLARSHIPS, FELLOWSHIPS, AND AWARDS:

Excellence in Teaching Award (IVC)	2012
NASA-CIPAIR Grant Co-Principle Investigator (COD)	2011-Present
Rocky Mountain Space Grant Consortium Fellowship	2008-2010
Sigma Pi Sigma, (Physics Honor Society) (USU)	2009-Present
Kentucky Kernel	2008-Present
Outstanding Graduate Poster APS Four Corners Meeting	2009
Fred Keller Scholarship (CSUSB)	2003
Undergraduate Honors (CSUSB), *Cum laude*	2003
NASA-FAR, FACULTY AWARDS RESEARCH Scholarship (CSUSB)	2002-2003
Computer Science, Engineering and Mathematics Scholarships (CSUSB)	2000-2002
Sigma Xi, (Scientific Research Society)	2001-Present
CSUSB Society of Physics Students Chapter President	1998-2000

TEACHING AND RESEARCH EXPERIENCE:

Assistant Professor of Physics, Irvine Valley College Dr. Lianna Zhao	2011-Present
Temporary Professor of Physics, College of the Desert Dr. Doug McCntyre	2011
Teaching Assistant, Utah State University Dr. J. R. Dennison	2008-2010
Research Assistant, Utah State University Dr. J. R. Dennison	2008-2010
Teaching Assistant, University of Kentucky Dr. Gang Cao	2006-2008
Research Assistant, University of Kentucky	2006-2008

Dr. Gang Cao
Adjunct Physical Science Instructor, Morehead State University 2005
Dr. Antoni Carnevali
Summer Instructor, Utah State University 2004
Dr. J.R. Dennison
Teaching Assistant, Utah State University 2003-2005
Dr. J.R. Dennison

Class Instruction Developed, implemented, and taught courses at the introductory physics, intermediate, advanced levels. Courses taught include, introduction to physical science (liberal arts level), introduction to physics (liberal arts level), College physics I and II (Algebra based), Physics for Scientists and Engineers I, II, III, (Calculus based). In addition, I have taught advanced courses on LabVIEW programming, computer interface programming, and electronic design, Co-taught courses at the graduate level, and advanced undergraduate level. Other subjects include geology, astronomy, chemistry, (non-lab), mathematics, and biological systems.

Laboratory Instruction Taught labs at all levels from freshman to graduate for a total of seven years at three universities and two colleges, Utah State University, University of Kentucky, Morehead State University, College of the Desert, and Irvine Valley College.

Mentorship Mentored many students at the undergraduate level in analysis, experimental design, computer programming, and development of theory. Projects include the development of analysis programs to process data for high vacuum capacitive long term measurements on highly insulating materials, error analysis techniques in low current measurements, electrostatic breakdown studies and development of theoretical models, Honors Transfer Council of California (HTCC) abstract submission and project mentorship 2012-2013 (Irvine Valley College). All completed efforts have resulted in publications and presentations (see presentations). In addition, please see work at Irvine Valley College and College of the Desert.

Theory and Modeling Developed a consistent theoretical framework that allowed for the characterization of physical parameters across a wide array of experimental systems involved in the testing of electron transport processes. Through experimental validation, material characterization and cross platform analysis analytical models have been developed that accurately determine highly insulating polymeric material behavior.

Instrument Design and Fabrication Designed and built a high sensitivity anemometer system for the study of nonlinear dynamics in semi fluid systems. Developed a computer automated system to control acquisition of anemometry data, positioning control system, and automated analysis. Developed a high sensitivity anemometer amplifier which included DAQ interfacing and GPIB instrument control.

Instrument Design and Fabrication Designed and built a high sensitivity laser micrometer system for the study of nonlinear dynamics of cantilever mounted piezo-electric actuators.

Instrumentation and Design Built and maintained a high magnetic field low temperature inductance, resistance, and capacitance measurement system.

Electron Yield and Spectroscopy Developed a computer automated system for acquisition of secondary electron emission spectrum and assisted in the development of a UHV system to measure electron yield of insulating materials using a pulse technique.

Data Acquisition and Analysis Utilized LabVIEW, Igor, Matlab and MathCad to write data acquisition and analysis programs used in labs at the USU Materials Physics Group, University of Kentucky, and California State University San Bernardino.

PUBLICATIONS:

Alec M. Sim and JR Dennison, "Comprehensive Theoretical Framework for Modeling Diverse Electron Transport Experiments in Parallel Plate Geometries," Paper Number, AIAA-2013-, *5th AIAA Atmospheric and Space Environments Conf.*, San Diego, CA, June 24-27, 2013, in preparation.

Justin Dekany, Alec M. Sim, Jerilyn Brunson, and JR Dennison, "Electron Transport Models and Precision Measurements in a Constant Voltage Chamber," accepted for publication in *IEEE Trans. on Plasma Sci.*, 2012, 10 pp.

Joshua L. Hodges, Alec M. Sim, Justin Dekany, Gregory Wilson, Amberly Evans, and JR Dennison "*In Situ* Surface Voltage Measurements of Layered Dielectrics," accepted for publication in *IEEE Trans. on Plasma Sci.*, 2012, 10 pp.

Amberly Evans Jensen, Gregory Wilson, Justin Dekany, Alec M. Sim and JR Dennison "Low Temperature Cathodoluminescence of Space Observatory Materials," accepted for publication in *IEEE Trans. on Plasma Sci.*, 2012, 6 pp.

Justin Dekany, Alec M. Sim, Jerilyn Brunson, and JR Dennison, "Electron Transport Models and Precision Measurements in a Constant Voltage Chamber," *Proc.* 12*th Spacecraft Charging Technology Conf.*, (Kitakyushu, Japan, May 14-18, 2012), 12 pp.

Joshua L. Hodges, Alec M. Sim, Justin Dekany, Gregory Wilson, Amberly Evans, and JR Dennison "*In Situ* Surface Voltage Measurements of Layered Dielectrics," *Proc.* 12*th Spacecraft Charging Technology Conf.*, (Kitakyushu, Japan, May 14-18, 2012), 13 pp.

Amberly Evans, Gregory Wilson, Justin Dekany, Alec M. Sim and JR Dennison "Low Temperature Cathodoluminescence of Space Observatory Materials," *Proc.* 12*th Spacecraft Charging Technology Conf.*, (Kitakyushu, Japan, May 14-18, 2012), 8 pp.

Alec Sim and J.R Dennison, "Unified Model of Charge Transport in Insulating Polymeric Materials," *Proc. 15th Rocky Mountain NASA Space Grant Consortium NASA Fellowship Symposium*, (Logan, UT, May 1 2010), 10 pp.

JR Dennison, Alec Sim, Jerilyn Brunson, Steven Hart, Jodie Gillespie, Justin Dekany, Charles Sim and Dan Arnfield, "Engineering Tool for Temperature, Electric Field and Dose Rate Dependence of High Resistivity Spacecraft Materials Paper Number," AIAA-2009-0562, *Proc. 47th American Institute of Aeronautics and Astronomics Meeting on Aerospace Sci.*, 2009.

J.R. Dennison, Alec Sim and Clint Thomson, "Evolution of the Electron Yield Curves of Insulators as a Function of Impinging Electron Fluence and Energy," *IEEE Transaction on Plasma Science*, **34**(5*)* October 2006, 2204-2218.

Alec Sim, J.R. Dennison and Clint Thomson, "Evolution of the Electron Yield Curves of Insulators as a Function of Impinging Electron Fluence and Energy," *Proc. 9th Spacecraft Charging Technology Conf.*, (EPOCHAL TSUKUBA, TSUKUBA, April 4-8, 2005), 19 pp.

Tim Usher and Alec Sim, "Nonlinear dynamics of piezoelectric high displacement actuators in cantilever mode", J. Appl. Phys. **98**, 064102 (2005).

J.R. Dennison, C.D. Thomson, Jodie Corbridge, Alec Sim and Jonathan Abbott, "Final Report: Electronic Properties *Int.* Space Station Materials," 100 pages, (Boeing Corporation, Houston, TX, June, 2004).

Prasanna Swaminathan, A.R. Frederickson, J.R. Dennison, Alec Sim, Jerilyn Brunson and Eric Crapo, "Comparison of Classical and Charge Storage Methods for Determining Conductivity of Thin Film

Insulators," *Proc. 8th Spacecraft Charging Technology Conf.,* (NASA Marshall Space Flight Center, Huntsville, Al, October 2003), 15 pp.

PRESENTATIONS:

Alec M. Sim and JR Dennison, "Comprehensive Theoretical Framework for Modeling Diverse Electron Transport Experiments in Parallel Plate Geometries," Paper Number, AIAA-2013-, *5th AIAA Atmospheric and Space Environments Conf.*, San Diego, CA, June 24-27, 2013.

Dale C. Ferguson, Jeremy-Murray Krezan, David Barton, JR Dennison, and Stephen Gregory and Alec Sim, "On the Feasibility of Detecting Spacecraft Charging and Arcing by Remote Sensing," Paper Number, AIAA-2013-, *5th AIAA Atmospheric and Space Environments Conf.*, San Diego, CA, June 24-27, 2013.

Zheng Chuen Wong, Alec Sim, Roy McCord, "Calibrating Spectrometers in an Efficient Manor", Honors Transfer Counsel *Conf.*, Irvine, CA, March 17th, 2013.

Josh Pham and Alec Sim, "Panacea for Cancer: Is Proton Therapy the Go-To Method of Treatment for All Cancers?", Honors Transfer Counsel *Conf.*, Irvine, CA, March 17th, 2013.

Zheng Chuen Wong, Alec Sim, Roy McCord, "Calibrating Spectrometers in an Efficient Manor", Southern California *Conf.* on Undergraduate Research, Channel Islands, CA, November 17th, 2012.

Christopher Ramirez, Kurt Kloesel, Alec Sim, Timothy Usher, "Aircraft Integrated Research Vehicle Optimal Loading Test-Stand (AIRVOLT)", Southern California *Conf.* on Undergraduate Research, Channel Islands, CA, November 17th, 2012.

Jeff Hamilton, Alec Sim, Ilknur Erbas-White, Jack Appleman, "Is the fear of Nuclear Energy as a source of power Justified?", Southern California *Conf.* on Undergraduate Research, Channel Islands, CA, November 15th, 2011.

Charles Sim, Alec Sim, JR Dennison, Matthew Stormo, "Defect-Driven Dynamic Model of Electrostatic Discharge and Endurance Time Measurements of Polymeric Spacecraft Materials," 2012 Sigma Pi Sigma Quadrennial Congress, Orlando, FL, November 8-10, 2012.

Charles Sim, Alec Sim and JR Dennison, "Electric Field Dependence of the Time to Electrostatic Breakdown in Insulating Polymers," National Council of Undergraduate Research, Weber State University, Ogden, UT, March 29-31, 2012.

Amberly Evans, Gregory Wilson, Justin Dekany, Alec M. Sim and JR Dennison "Low Temperature Cathodoluminescence of Space Observatory Materials," 12*th Spacecraft Charging Technology Conf.*, Kitakyushu, Japan, May 14-18, 2012, poster presentation.

Justin Dekany, Alec M. Sim, Jerilyn Brunson, and JR Dennison, "Electron Transport Models and Precision Measurements in a Constant Voltage Chamber," 12*th Spacecraft Charging Technology Conf.*, Kitakyushu, Japan, May 14-18, 2012, poster presentation.

JR Dennison and Alec M. Sim, "Unified Density of States Based Model of Electron Transport and Emission of Spacecraft Materials," 12*th Spacecraft Charging Technology Conf.*, Kitakyushu, Japan, May 14-18, 2012, poster presentation.

Charles Sim, Alec M. Sim, JR Dennison and Matthew Stromo, "Defect-Driven Dynamic Model of Electrostatic Discharge and Endurance Time Measurements of Polymeric Spacecraft Materials," 12*th Spacecraft Charging Technology Conf.*, Kitakyushu, Japan, May 14-18, 2012, poster presentation.

Joshua L. Hodges, Alec M. Sim, Justin Dekany, Gregory Wilson, Amberly Evans, and JR Dennison "*In Situ* Surface Voltage Measurements of Layered Dielectrics," 12*th Spacecraft Charging Technology Conf.*, Kitakyushu, Japan, May 14-18, 2012, poster presentation.

Douglas Ball, Alec Sim, Josh Hodges, Ryan Hoffman and JR Dennison, "Electron Induced Luminescence of Insulating Polymeric Materials," American Physical Society Four Corner Section Meeting, Weber State University, Ogden, UT, Oct 15-16, 2010.

Alec Sim and JR Dennison, "A Unified Model of Charge Transport in Highly Insulating Materials," American Physical Society Four Corner Section Meeting, Weber State University, Ogden, UT, Oct 15-16, 2010.

Charles Sim, Alec Sim, Douglas Ball and JR Dennison, "Temperature and Endurance Time of Electrostatic Field Strengths of Polymeric Spacecraft Insulators," American Physical Society Four Corner Section Meeting, Weber State University, Ogden, UT, Oct 15-16, 2010.

Alec Sim and JR Dennison, "Charge Dynamics in Insulting materials" *Proc. 15th Rocky Mountain NASA Space Grant Consortium NASA Fellowship Symposium*, Logan, UT, May 1 2010.

Alec Sim and JR Dennison, "Parameterization of Temperature, Electric Field, Dose Rate and Time Dependence of Low Conductivity Spacecraft Materials Using a Unified Electron Transport Model," 11*th Spacecraft Charging Technology Conf.*, Albuquerque, NM, Sept 20-24, 2010.

Charles Sim, Alec Sim, Douglas Ball and JR Dennison, "Temperature and Endurance Time of Electrostatic Field Strengths of Polymeric Spacecraft Insulators," 11*th Spacecraft Charging Technology Conf.*, Albuquerque, NM, Sept 20-24, 2010.

Alec Sim with JR Dennison, " A Unified Theoretical Approach to Modeling Materials Properties for Spacecraft Charging," *Proc. 15th Rocky Mountain NASA Space Grant Consortium NASA Fellowship Symposium*, (Logan, UT, May 12 2010).

Justin Dekany, JR Dennison and Alec Sim, "Reduction and Characterization of Error in Low Current Measurements," American Physical Society Four Corner Section Meeting, Colorado School of Mines, Golden, CO, Oct 23-24, 2009.

Alec Sim and JR Dennison, "Charge Dynamics in Disordered Insulating Materials," American Physical Society Four Corner Section Meeting, Colorado School of Mines, Golden, CO, Oct 23-24, 2009.

JR Dennison, Ryan Hoffmann, Jennifer A. Roth, and Alec Sim, "Effects of Radiation Induced Conductivity on Samples Charged by Particle Beams," American Physical Society Four Corner Section Meeting, University of Texas-El Paso , El Paso , TX, Oct 17-18, 2008.

JR Dennison, Jerilyn Brunson, Ryan Hoffman, Jonathon Abbott, Clint Thomson and Alec Sim, "*Measurements of Electrical and Electron Emission Properties of Highly Insulating Materials*," Air Force Office of Scientific Research Workshop On Multifunctional Materials, Keystone III Workshop 2005, Keystone Hotel and *Conf.* Center, CO, 21 – 26 Aug 2005.

Alec Sim, J.R. Dennison and Clint Thomson, "Evolution of the Electron Yield Curves of Insulators as a Function of Impinging Electron Fluence and Energy," Invited Talk, *9th Spacecraft Charging Technology Conf.,* Epochal Tsukuba, Tsukuba, Japan April 4-8, 2005.

Alec Sim, J.R. Dennison and Clint Thomson, "Effects of Incident Electron Fluence And Energy On The Electron Yield Curves And Emission Spectra of Dielectrics," *Bull. Am. Phys. Soc.* 50(1) Part II, (2005). American Physical Society March Meeting 2005, Mar 21-25, 2005, Los Angeles, CA.

JR Dennison, C. D. Thomson, and Alec Sim, "The effect of low energy electron and UV/VIS radiation aging on the electron emission properties and breakdown of thin-film dielectrics," 8th IEEE Dielectr. Electr. Insul. Society (DEIS) *Int. Conf.* on Solid Dielectrics (ICSD), Jul 5-9, 2004, Toulouse, France.

Timothy D. Usher, Alec Sim, Gevale Ashford, Gilberto Camargo, and Adalia Cabanyog," Modeling and Applications of New Piezoelectric Actuator Technologies" California State University, San Bernardino, 5500 University Parkway, San Bernardino, CA 92407, USA, SPIE *Conf.* 2004.